



Immune dysfunction in the skin disease hidradenitis suppurativa

Barry Moran MSc

School of Biochemistry and Immunology

A thesis submitted to Trinity College Dublin
as completion of the degree of Doctor of Philosophy

2020

Supervisor: Professor Jean Fletcher

Joint Supervisor: Professor Kingston Mills

Declaration of authorship

I declare that this thesis has not been submitted as an exercise for a degree at this or any other university and it is entirely my own work.

I agree to deposit this thesis in the University's open access institutional repository or allow the library to do so on my behalf, subject to Irish Copyright Legislation and Trinity College Library conditions of use and acknowledgement.

A handwritten signature in black ink, appearing to read 'Barry Moran', is written over a horizontal line.

Barry Moran

14337320

Abstract

Hidradenitis suppurativa (HS) is a chronic, relapsing, inflammatory skin disease. Painful lesions and boils present at hair follicles of the inframammary fold, genitals, groin, buttocks and perianal areas. Severe cases progress to dermal tunnelling and scarring, with ruptured cysts resulting in a bloody, foul-smelling discharge. HS affects patients' physical, mental, social and economic wellbeing and is significantly associated with low quality of life scores.

The cellular pathogenesis in HS is poorly understood and there is an urgent need for improved therapeutics. Immune dysregulation has been shown to play a major role, and so detailed characterisation of the immune cell component is invaluable.

To study the immune cells within HS patient blood and skin, this study utilised state-of-the-art technologies including imaging cytometry, high-parameter flow cytometry and single cell RNA sequencing.

This thesis has for the first time identified multiple B cell, T cell and myeloid cell subsets present at significantly enriched levels in HS lesional skin. It identified CD1c⁺ dendritic cells (cDC2) as the cellular source of the potent immune mediators IL-1 β , IL-18, IL-23 and the activated NLRP3 inflammasome. Importantly, it demonstrated a substantial polyfunctional CD4 T cell population, dramatically skewed towards IL-17 production, leading to a Th17 cell: Treg cell imbalance. Finally, it showed this balance restored, and a reduction in the polyfunctional IL-17⁺ T cells, upon anti-TNF treatment.

These data suggest that Th17 cells play a key role in HS pathogenesis and that their activation is likely driven by mediators produced by CD1c⁺ dendritic cells in HS lesional skin. Systemic inflammation is apparent given that HS patient blood and even clinically normal skin have significant inflammation. This study underscores the rationale for therapeutic suppression of the IL-17 pathway and suggests novel targets.

Acknowledgements

Firstly, I would like to thank my supervisor Professor Jean Fletcher. Given her formidable expertise in translational immunology, Jean was always the one I wanted to do this project with and I'm so glad she took me on. She is unwaveringly sincere, intuitive, fair, kind and wise. I always leave a chat with Jean feeling much the better for it. It has been a pleasure from day one and I look forward to many more years working together.

To Professor Kingston Mills for his co-supervision, support and mentorship. To my mind, Kingston is the smartest person in any room. But what really sets him apart is his pragmatism and sense of what is really the right and fair thing to do in almost every situation. A rock of wisdom and a great ongoing advocate and influence in my career.

To the Fletcher and Mills labs for all their friendship, help and scientific support. To Drs Deborah Cluxton, Jamal Sulaimani and in particular Dr Andreea Petrasca who always selflessly lends a hand and keeps the whole lab in order. To the newbie Conor Smith who arrived in perfect time to add much needed RNA-Seq expertise, always helping out with a smile on his face. He is becoming an exceptional scientist. And to Dr Sharee Basdeo for being fun and ever-patient, getting me reacquainted with pipettes, tissue culture and the likes in the early days.

To the staff and students of the School of Biochemistry and Immunology and the broader Trinity Biomedical Sciences Institute for all their collegiality and friendship along the way. In particular to Professor Cliona O'Farrelly for providing the necessary push and encouragement at the start and Mr Liam McCarthy and Professors Ed Lavelle and Gavin Davey for giving me the backing of the School.

To the patients and healthy volunteers who donated samples for these studies. To the clinical collaborators in St Vincent's University Hospital, Tallaght Hospital and St Michael's Hospital, namely Professors Brian Kirby, Anne-Marie Tobin, Des Winter and Mrs Margaret O'Donnell, and Drs Alex Zaborowski, Roz Hughes, Catriona Gallagher, Anna Malara and Jana Musilova. To Dr Karsten Hokamp in TCD for his invaluable bioinformatics wizardry. To AbbVie collaborators, in particular Dr Will Housley and Ms

Heidi Renshaw. To Professor Aurelie Fabre and Drs Achilleas Floudas, Cathal Harmon and Conor Finlay for helpful input to the project. And in particular a very special thanks to Dr Cheryl Sweeney, a great friend and colleague, for first whetting our interest in HS.

To the British Skin Foundation and the TCD Dean's Initiative for providing much needed funding for the project. To Kate Easten and Ian Gerrard from BD, and Al Stewart during his time with eBioscience, for going above and beyond to provide additional support so I could get this work done with limited resources.

To my Mam and Dad for instilling in me a sense of fun, curiosity and confidence; and to never take myself too seriously. I miss Dad every day. To my sister, brothers and their families for always making me laugh and feel loved. And my great friends for that vital release of a laugh, chat or a pint whenever needed.

Lastly, to my wife Sophie, son Will and daughter Lucy. My favourite people in the world, and the best distractions through the hard times and the foremost reasons to persevere. Sophie, you have been my rock through it all and this project very much feels like a joint achievement with you. I am forever grateful and I love you always.

Contents

Declaration of authorship	ii
Abstract	iii
Acknowledgements	iv
Tables	xii
Figures	xiii
Author publications (thesis)	xviii
Author publications (other).....	xix
Abbreviations	xxii
1 Introduction.....	2
1.1 The innate immune system	2
1.1.1 Macrophages.....	3
1.1.2 Neutrophils.....	3
1.1.3 Eosinophils.....	4
1.1.4 Basophils.....	4
1.1.5 Mast cells.....	5
1.1.6 Dendritic cells	5
1.1.7 Innate lymphoid cells	6
1.1.8 iNKT cells	6
1.1.9 MAIT cells	7
1.1.10 $\gamma\delta$ T cells	7
1.2 The adaptive immune system	8
1.2.1 B cells.....	8
1.2.2 T cells.....	10
1.2.3 Cytotoxic T cells.....	13
1.2.4 Helper T cells	13

1.2.5	Th cell subsets.....	14
1.3	IL-17.....	19
1.4	Skin immunity.....	22
1.5	IL-17 in the skin	28
1.5.1	Tc cells.....	28
1.5.2	iNKT cells.....	28
1.5.3	MAIT cells.....	29
1.5.4	Innate lymphoid cells.....	29
1.5.5	$\gamma\delta$ T cells.....	29
1.5.6	Mast cells	30
1.5.7	Neutrophils	30
1.6	Hidradenitis suppurativa.....	31
1.6.1	Symptoms	31
1.6.2	Prevalence.....	33
1.6.3	Impact	33
1.6.4	Classification	34
1.6.5	Risk factors.....	35
1.6.6	Pathogenesis.....	38
1.6.7	Immune dysregulation in HS.....	41
1.6.8	Treatments.....	42
1.7	Working hypothesis	46
1.8	Aims.....	46
2	Materials and Methods.....	48
2.1	Materials	48
2.1.1	PBMC preparation	48
2.1.2	Complete IMDM preparation	48

2.1.3	T cell stimulation	48
2.1.4	Other materials	49
2.1.5	Cytometry antibodies	49
2.2	Methods.....	51
2.2.1	Patient recruitment.....	51
2.2.2	Isolation and cryopreservation of PBMC	51
2.2.3	Cell counting.....	52
2.2.4	Complete media selection and preparation	52
2.2.5	Single cell preparation from skin biopsy	54
2.2.6	T cell stimulation with PMA and ionomycin	57
2.2.7	Surface staining for flow cytometry	57
2.2.8	Intracellular and intranuclear staining for flow cytometry.....	57
2.2.9	Cytometer set up.....	60
2.2.10	Cytometric analysis	64
2.2.11	Statistical analysis.....	64
2.2.12	SPICE analysis	64
2.2.13	Illustrations.....	64
2.2.14	Imaging flow cytometry	65
2.2.15	Histology slide preparation	67
2.2.16	scRNA-Seq	67
2.2.17	scRNA-Seq data analysis.....	68
3	Phenotypic and transcriptomic characterisation of hidradenitis suppurativa skin	72
3.1	Introduction.....	72
3.2	Aims	75
3.3	Clinical details	76
3.4	Results.....	80

3.4.1	Increased frequency of leukocytes and T cells in the lesional skin of HS patients compared with healthy control skin.....	80
3.4.2	Increased frequency of B cells in the lesional skin of HS patients compared with healthy control skin	84
3.4.3	Increased frequency of DC, but not dermal macrophages, in the lesional skin of HS patients compared with healthy control skin	87
3.4.4	Increased frequency of activated and resting neutrophils in the lesional skin of HS patients compared with healthy control skin	93
3.4.5	Increased frequency of an NK cell-enriched population in the lesional skin of HS patients compared with healthy control skin	98
3.4.6	Histological analysis of HS skin highlights a heterogeneous inflammatory profile	102
3.4.7	scRNA-Seq analysis reveals multiple immune cell clusters present in HS skin	106
3.4.8	scRNA-Seq analysis showed clear differences in gene expression between HS lesional skin and healthy control skin	120
3.5	Discussion.....	126
3.5.1	Myeloid cells in HS lesional skin	126
3.5.2	ILC and NK cells in HS lesional skin	128
3.5.3	B cells in HS lesional skin	129
3.5.4	T cells in HS lesional skin.....	130
4	Hidradenitis suppurativa is characterised by T cell dysregulation	134
4.1	Introduction	134
4.2	Aims.....	137
4.3	Clinical details.....	138
4.4	Results	142
4.4.1	Similar frequency of T cells in the peripheral blood of HS patients and healthy controls	142

4.4.2	A minor increase in the proinflammatory T cell profile characterises HS patient peripheral blood	148
4.4.3	Reduced frequency of Treg cells in HS patient peripheral blood	154
4.4.4	Substantial increase in the number of T cells in HS lesional skin	161
4.4.5	T cells in HS patient skin display a marked proinflammatory profile, characterised by Th17 associated cytokines.....	168
4.4.6	HS patient lesional skin exhibited a significant increase in Treg cells	178
4.4.7	Frequency of T cells in the skin remained unchanged in HS patients treated with anti-TNF therapy.	184
4.4.8	The proinflammatory profile of T cells in the skin was reduced in HS patients undergoing anti-TNF therapy.....	189
4.4.9	Similar frequency of Treg cells in the skin of HS patients undergoing anti-TNF therapy compared with treatment naïve patients	195
4.4.10	Reduction in T cell polyfunctionality in HS patients undergoing anti-TNF therapy	198
4.5	Discussion	204
5	General discussion.....	212
5.1	Introduction	212
5.2	Implications for HS therapy	217
5.3	Limitations	220
5.4	Future directions	221
6	Appendix.....	225
6.1	HS classifications.....	225
6.2	Quality of RNA sequencing data is within normal parameters	228
6.3	Differential gene expression reveals a distinct transcriptional profile for each identified cell cluster	230

6.4	Cell cluster locations of genes markedly up- and down-regulated expressed in HS compared with healthy control skin.....	231
7	Bibliography	237

Tables

Table 1.1 IL-17 cytokines and their receptors, cellular sources, target cells and functions.	21
Table 1.2 APC subsets in healthy skin.	26
Table 1.3 Relevant biological therapeutics targeting autoimmune and inflammatory disease.	45
Table 2.1 Cytometric fluorochrome panel for immunophenotyping skin samples.	61
Table 2.2 Cytometric fluorochrome panel for analysis of PMA/I stimulated T cells in PBMC and skin samples.	62
Table 2.3 Cytometric fluorochrome panel for analysis of unstimulated T cells in PBMC and skin samples.	63
Table 2.4 Fluorochrome panel for imaging flow cytometry.	66
Table 3.1 Clinical details for HS patient group 1.	78
Table 3.2 Clinical details for healthy control group 1.	79
Table 3.3 Cell cluster frequency.	110
Table 4.1 Clinical details for HS patient group 2.	139
Table 4.2 Details for healthy control group.	140
Table 4.3 Clinical details for anti-TNF therapy HS patient group.	141
Table 6.1 The Hurley classification of HS (A) and the HS severity index (B).	225
Table 6.2 The Sartorius System classifying severity of HS.	226
Table 6.3 The HS Physician’s Global Assessment (A) and the International Hidradenitis Suppurativa Severity Score System (B).	227
Table 6.4 Quality of RNA sequencing data is within normal parameters (1 of 2).	228
Table 6.5 Quality of RNA sequencing data is within normal parameters (2 of 2).	229

Figures

Figure 1.1 Differentiation of CD4 effector T cell subsets.	15
Figure 1.2 Structure and immune cell components of healthy human skin.	27
Figure 1.3 Schematic of HS patient inflammatory sites.	32
Figure 1.4 HS pathogenesis.....	40
Figure 2.1 cIMDM is the optimal medium for T cell stimulation.....	53
Figure 2.2 Classification of epitope damage during skin dissociations protocols.	56
Figure 2.3 Workflow for intracellular cytokine analysis.	59
Figure 2.4 Workflow for histology and scRNA-Seq.....	70
Figure 3.1 CD45 ⁺ cells were enriched in HS lesions compared with healthy control skin.	82
Figure 3.2 T cells were enriched in HS lesional compared with healthy control skin. ...	83
Figure 3.3 B cells were enriched in HS lesional compared with healthy control skin. ...	85
Figure 3.4 Plasmablasts and plasma cells were enriched in HS lesional compared with healthy control skin.	86
Figure 3.5 Gating strategy for dermal macrophages and DC populations in the skin....	89
Figure 3.6 CD64 ⁺ SSC ^{int} cells in HS lesional skin included multiple DC populations.	90
Figure 3.7 Representative images of CD64 ⁺ HLA-DR ⁺ cells.....	91
Figure 3.8 Significant enrichment of DC, but not dermal macrophages, in HS skin compared with healthy control skin.....	92
Figure 3.9 Neutrophils were enriched in HS lesional compared with healthy control skin.	95
Figure 3.10 Representative images of CD64 ^{lo} HLA-DR ^{lo} neutrophils.....	96
Figure 3.11 Both activated and resting neutrophils were enriched in HS lesional compared with healthy control skin.....	97
Figure 3.12 NK cells were enriched in HS lesional compared with HS uninvolved skin.	100
Figure 3.13 Non-TBnk lymphocytes were enriched in HS lesional skin samples compared with healthy control skin.	101
Figure 3.14 Histology illustrates immune cell infiltration in HS lesional skin.....	104

Figure 3.15 Histology illustrates minimal immune cell infiltration in healthy control skin.	105
Figure 3.16 UMAP plot identified 30 unique cell clusters within HS patient lesions and healthy control skin.....	109
Figure 3.17 scRNA-Seq expression profiles for genes associated with CD4 T cell clusters within HS patient lesions and healthy control skin.....	111
Figure 3.18 scRNA-Seq expression profiles for genes associated with Th17 cell clusters within HS patient lesions and healthy control skin.....	112
Figure 3.19 scRNA-Seq expression profiles for genes associated with CD8 T cell, NK cell and ILC clusters within HS patient lesions and healthy control skin.....	113
Figure 3.20 scRNA-Seq expression profiles for genes associated with B cell clusters within HS patient lesions and healthy control skin.....	114
Figure 3.21 scRNA-Seq expression profiles for genes associated with myeloid cell clusters within HS patient lesions and healthy control skin (I).	115
Figure 3.22 scRNA-Seq expression profiles for genes associated with myeloid cell clusters within HS patient lesions and healthy control skin (II).	116
Figure 3.23 UMAP plot visualising cell clusters within HS patient lesional skin.	117
Figure 3.24 UMAP plot visualising cell clusters within healthy control skin.....	118
Figure 3.25 UMAP plot overlaying cell populations of HS patient lesional skin with healthy control skin.....	119
Figure 3.26 UMAP plots for each individual HS patient lesions and healthy control skin sample.	122
Figure 3.27 Principal component analysis and differential gene expression for HS patient lesions compared with healthy control skin.	123
Figure 3.28 Volcano plot highlights gene expression fold change for HS patient lesions compared with healthy control skin.	124
Figure 3.29 scRNA-Seq pathway analysis for HS patient lesions compared with healthy control skin.....	125
Figure 4.1 Plots representing the gating strategy to identify CD4 and CD8 T cells in peripheral blood.....	144
Figure 4.2 Representative plots validating the gating strategy to identify CD4 T cells in peripheral blood.....	145

Figure 4.3 Similar frequency of CD3, CD8 and CD4 T cells in healthy control and HS patient peripheral blood.....	146
Figure 4.4 Increased frequency of CLA expressing CD8 and CD4 T cells in peripheral blood from HS patients v healthy controls.	147
Figure 4.5 Cytokine profile of CD8 T cells in HS patient and healthy control peripheral blood.....	150
Figure 4.6 Cytokine profile of CD4 T cells in HS patient and healthy control peripheral blood.	151
Figure 4.7 Similar frequency of CD161 expression on CD8 and CD4 T cells in HS patient versus healthy control peripheral blood.	152
Figure 4.8 Frequency of Th subsets Th17, Th1, ex-Th17 and transitioning ex-Th17 unchanged in HS patient compared with healthy control peripheral blood.	153
Figure 4.9 Plots representing the gating strategy to identify Treg cells in peripheral blood.	156
Figure 4.10 Representative dot plots validating the gating strategy to identify Treg cells.	157
Figure 4.11 Decreased frequency of Treg cells, and an increased ratio of Th17 cells to Treg cells, in HS patient compared with healthy control peripheral blood.	158
Figure 4.12 Frequency of CLA and CD161 expression on Treg cells unchanged in HS patient versus healthy control peripheral blood.....	159
Figure 4.13 Frequencies of CD39 and CTLA-4 expression on Treg cells unchanged in HS patient versus healthy control peripheral blood.....	160
Figure 4.14 Plots representing the gating strategy to identify CD4 and CD8 T cells in skin samples.	163
Figure 4.15 Representative plots validating the gating strategy to identify CD4 T cells.	164
Figure 4.16 Increased number of CD45 ⁺ cells and CD3 T cells in HS lesional compared with healthy control skin.	165
Figure 4.17 Similar frequency of CD8 and CD4 T cells in HS patient compared with healthy control skin.	166
Figure 4.18 Reduced frequency of CLA expression on CD8 and CD4 T cells in the lesional skin of HS patients compared with healthy control skin.	167

Figure 4.19 Representative dot plots for CD8 T cell cytokine expression in healthy control and HS patient skin.....	171
Figure 4.20 CD8 T cells in HS patient skin secrete multiple proinflammatory cytokines.	172
Figure 4.21 Representative dot plots for CD4 T cell cytokine expression in healthy control and HS patient skin.....	173
Figure 4.22 CD4 T cells in HS patient skin secrete multiple proinflammatory cytokines.	174
Figure 4.23 No association between CD4 T cell cytokine expression in HS patient skin and body mass index.....	175
Figure 4.24 Increased frequency of CD161 ⁺ T cells in HS patient skin.....	176
Figure 4.25 Frequency of T helper subsets in HS patient and healthy control skin.	177
Figure 4.26 Plots representing the gating strategy to identify Treg cells in skin samples.	180
Figure 4.27 Increased frequency of Treg cells, and an unbalanced ratio of Th17 cells to Treg cells, in HS patient lesional skin compared with healthy control skin.....	181
Figure 4.28 Frequency of CLA expression unchanged, but significant increase in CD161 expression, in Treg cells in HS patient lesional skin compared with healthy control skin.	182
Figure 4.29 Frequencies of CD39 and CTLA-4 expression unchanged in Treg cells in HS patient lesional skin compared with healthy control skin.	183
Figure 4.30 Similar number of CD45 ⁺ cells and CD3 T cells in the skin of treatment naïve HS patients compared with those treated with anti-TNF.....	186
Figure 4.31 Similar frequency of CD8 and CD4 T cells in the skin of treatment naïve HS patients compared with those treated with anti-TNF.	187
Figure 4.32 Similar frequency of CLA expression on CD8 and CD4 T cells in the skin of treatment naïve HS patients compared with those treated with anti-TNF.....	188
Figure 4.33 CD8 T cell cytokine expression in the skin of treatment naïve HS patients compared with those treated with anti-TNF.	191
Figure 4.34 CD4 T cell cytokine expression in the skin of treatment naïve HS patients compared with those treated with anti-TNF.	192

Figure 4.35 Frequency of CD161 expression on CD8 and CD4 T cells in the skin of treatment naïve HS patients compared with those treated with anti-TNF.	193
Figure 4.36 Frequency of Th subsets in the skin of treatment naïve HS patients compared with those treated with anti-TNF.	194
Figure 4.37 Frequency of Treg cells, and ratio of Th17 cells to Treg cells, in the skin of treatment naïve HS patients, or those treated with anti-TNF.	196
Figure 4.38 Frequency of CLA, CD161, CD39, and CTLA-4 expression on Treg cells in the skin of treatment naïve HS patients, or those treated with anti-TNF.	197
Figure 4.39 Increased cytokine polyfunctionality of CD8 T cells in the skin of treatment naïve HS patients compared with those treated with anti-TNF.	201
Figure 4.40 Increased cytokine polyfunctionality of CD4 T cells in the skin of treatment naïve HS patients compared with those treated with anti-TNF.	203
Figure 5.1 Proposed mechanism of immune dysfunction in HS.	216
Figure 5.2 Therapies targeting the IL-17 pathway in HS.	219
Figure 6.1 Differential gene expression reveals a distinct transcriptional profile for each identified cell cluster.	230
Figure 6.2 UMAP plots for markedly upregulated genes primarily in plasmablasts and plasma cells.	231
Figure 6.3 UMAP plots for markedly upregulated genes primarily in myeloid subsets.	232
Figure 6.4 UMAP plot for markedly upregulated genes primarily in Th17 cells.	233
Figure 6.5 UMAP plot for markedly downregulated genes primarily in T cells and myeloid subsets.	234
Figure 6.6 UMAP plot for markedly downregulated genes primarily in pDC.	235

Author publications (thesis)

CD1c⁺ dendritic cells are the cellular source for IL-1 β , IL-23 and the NLRP3 inflammasome in hidradenitis suppurativa patient skin

B Moran, CM Smith, A Zabarowski, M Ryan, J Karman, RW Dunstan, K Smith, J Musilova, KHG Mills, K Hokamp, M O'Donnell, B Kirby, DC Winter, WJ Housley, JM Fletcher
Manuscript in preparation.

IL-17 in inflammatory skin diseases psoriasis and hidradenitis suppurativa (Review)

JM Fletcher*, **B Moran**, A Petrasca, CM Smith

* corresponding author

Clin Exp Immunol. 2020 May 7. doi: 10.1111/cei.13449.

Enrichment of polyfunctional IL-17-producing T cells in paradoxical psoriasis skin lesions

B Moran, C Gallagher, AM Tobin, JM Fletcher

J Invest Dermatol. 2020 May;140(5):1094-1097. doi: 10.1016/j.jid.2019.10.010.

Enrichment of plasma cells in the peripheral blood and skin of patients with hidradenitis suppurativa

J Musilova*, **B Moran***, CM Sweeney, A Malara, A Zaborowski, R Hughes, DC Winter, JM Fletcher#, B Kirby#

* joint first author # joint corresponding author

J Invest Dermatol. 2020 May;140(5):1091-1094.e2. doi: 10.1016/j.jid.2019.08.453.

Hidradenitis suppurativa is characterized by dysregulation of the Th17:Treg cell axis, which is corrected by anti-TNF therapy

B Moran, CM Sweeney, R Hughes, A Malara, S Kirthi, AM Tobin, B Kirby, JM Fletcher

J Invest Dermatol. 2017 Nov;137(11):2389-2395. doi: 10.1016/j.jid.2017.05.033.

Author publications (other)

Dimethyl fumarate modulates the Treg:Th17 cell axis in psoriasis patients

J Sulaimani, D Cluxton, J Clowry, A Petrasca, O Molloy, **B Moran**, CM Sweeney, N McNicholas, C McGuigan, B Kirby, JM Fletcher
Br J Dermatol. 2020 May 21. doi: 10.1111/bjd.19229.

A population of pro-inflammatory T cells co-express $\alpha\beta$ and $\gamma\delta$ T cell receptors

SC Edwards, CE Sutton, K Ladell, EJ Grant, JE McLaren, F Roche, P Dash, N Apiwattanakul, W Awad, K Miners, SJ Lalor, JC Ribot, S Baik, **B Moran**, A McGinley, V Pivorunas, L Dowling, M Macoritto, J Paez-Cortez, A Slavin, G Anderson, B Silva-Santos, K Hokamp, RM McLoughlin, PG Thomas, DA Price, KHG Mills
J Exp Med. 2020 May 4;217(5):e20190834. doi: 10.1084/jem.20190834.

Low density granulocytes in ANCA vasculitis are heterogenous and hypo-responsive to anti-myeloperoxidase antibodies

A Ui Mhaonaigh, AM Coughlan, A Dwivedi, J Hartnett, J Cabral, **B Moran**, K Brennan, SL Doyle, K Hughes, R Lucey, A Floudas, U Fearon, S McGrath, S Cormican, A De Bhailis, EJ Molloy, G Brady, MA Little
Front Immunol. 2019 Nov 7;10:2603. doi: 10.3389/fimmu.2019.02603.

Differential regulation of human Treg and Th17 cells by fatty acid synthesis and glycolysis

D Cluxton, A Petrasca, **B Moran**, JM Fletcher
Front Immunol. 2019 Feb 4;10:115. doi: 10.3389/fimmu.2019.00115.

Enriched CD141+ DCs in the joint are transcriptionally distinct, activated, and contribute to joint pathogenesis

M Canavan, AM Walsh, V Bhargava, SM Wade, T McGarry, V Marzaioli, **B Moran**, M Biniecka, H Convery, S Wade, C Orr, R Mullan, JM Fletcher, S Nagpal, DJ Veale, U Fearon
JCI Insight. 2018 Dec 6;3(23):e95228. doi: 10.1172/jci.insight.95228.

Guidelines for the use of flow cytometry and cell sorting in immunological studies

A Cossarizza, HD Chang, A Radbruch, A Acs, D Adam,, **B Moran**,, Zimmermann J (231 authors)
Eur J Immunol. 2019 Oct;49(10):1457-1973. doi: 10.1002/eji.201970107.

Ex-Th17 (nonclassical Th1) cells are functionally distinct from classical Th1 and Th17 cells and are not constrained by regulatory T cells

SA Basdeo, D Cluxton, J Sulaimani, **B Moran**, M Canavan, C Orr, DJ Veale, U Fearon, JM Fletcher
J Immunol. 2017 Mar 15;198(6):2249-2259. doi: 10.4049/jimmunol.1600737.

Polyfunctional, pathogenic CD161+ Th17 lineage cells are resistant to regulatory T cell-mediated suppression in the context of autoimmunity

SA Basdeo, **B Moran**, D Cluxton, M Canavan, J McCormick, M Connolly, C Orr, KHG Mills, DJ Veale, U Fearon, JM Fletcher

J Immunol. 2015 Jul 15;195(2):528-40. doi: 10.4049/jimmunol.1402990.

Remote access technology offers tremendous possibilities to the cytometry community

B Moran, A Blanco-Fernández, R Gardner, J Tigges, V Toxavidis, J Daley

Cytometry Part A 83 (12), 1062-1065. doi: 10.1002/cyto.a.22409

Functionalization of carbon nanoparticles modulates inflammatory cell recruitment and NLRP3 inflammasome activation

M Yang, K Flavin, I Kopf, G Radics, CHA Hearnden, GJ McManus, **B Moran**, I Villalta-Cerdas, LA Echevoyen, S Giordani, EC Lavelle

Small. 2013 Dec 20;9(24):4194-206. doi: 10.1002/sml.201300481.

Blocking retinoic acid receptor- α enhances the efficacy of a dendritic cell vaccine against tumours by suppressing the induction of regulatory T cells

KC Galvin, L Dyck, NA Marshall, AM Stefanska, KP Walsh, **B Moran**, SC Higgins, LS Dungan, KHG Mills

Cancer Immunol Immunother. 2013 Jul;62(7):1273-82. doi: 10.1007/s00262-013-1432-8.

Alveolar macrophages contribute to respiratory tolerance by inducing FoxP3 expression in naive T cells

MM Coleman, D Ruane, **B Moran**, PJ Dunne, J Keane, KHG Mills

Am J Respir Cell Mol Biol. 2013 Jun;48(6):773-80. doi: 10.1165/rcmb.2012-0263OC.

The immunoregulatory role of CD4+FoxP3+CD25- regulatory T cells in lungs of mice infected with Bordetella pertussis

MM Coleman, CM Finlay, **B Moran**, J Keane, PJ Dunne, KHG Mills

FEMS Immunol Med Microbiol. 2012 Apr;64(3):413-24. doi: 10.1111/j.1574-695X.2011.00927.

Pneumolysin activates the NLRP3 inflammasome and promotes proinflammatory cytokines independently of TLR4

EA McNeela, A Burke, DR Neill, C Baxter, VE Fernandes, D Ferreira, S Smeaton, R El-Rachkidy, RM McLoughlin, A Mori, **B Moran**, KA Fitzgerald, J Tschopp, V Pétrilli, P W Andrew, A Kadioglu, EC Lavelle

PLoS Pathog. 2010 Nov 11;6(11):e1001191. doi: 10.1371/journal.ppat.1001191.

CD39+ Foxp3+ regulatory T Cells suppress pathogenic Th17 cells and are impaired in multiple sclerosis

JM Fletcher, R Lonergan, L Costelloe, K Kinsella, **B Moran**, C O'Farrelly, N Tubridy and KHG Mills

J Immunol. 2009 Dec 1;183(11):7602-10. doi: 10.4049/jimmunol.0901881.

CD11c+ CD8 α + dendritic cells promote protective immunity to respiratory infection with *Bordetella pertussis*

PJ Dunne, **B Moran**, RC Cummins, KHG Mills

J Immunol. 2009 Jul 1;183(1):400-10. doi: 10.4049/jimmunol.0900169.

Hepatitis C virus-specific Th17 cells are suppressed by virus-induced TGF- β

AG Rowan, JM Fletcher, EJ Ryan, **B Moran**, JE Hegarty, C O'Farrelly, KHG Mills

J Immunol. 2008 Oct 1;181(7):4485-94. doi: 10.4049/jimmunol.181.7.4485.

ADAP is required for normal α IIb β 3 activation by VWF/GP Ib-IX-V and other agonists

A Kasirer-Friede, **B Moran**, J Nagrampa-Orje, K Swanson, ZM Ruggeri, Schraven B, Neel BG, Koretzky G, Shattil SJ

Blood. 2007 Feb 1;109(3):1018-25. doi: 10.1182/blood-2006-05-022301.

A role for PKC θ in outside-in α IIb β 3 signalling

A Soriani, **B Moran**, M De Virgilio, T Kawakami, A Altman, C Lowell, K Eto, SJ Shattil

J Thromb Haemost. 2006 Mar;4(3):648-55. doi: 10.1111/j.1538-7836.2006.01806.x.

Megakaryocytes derived from human embryonic stem cells: a genetically tractable system to study megakaryocytopoiesis and integrin function

M Gaur, T Kamata, S Wang, **B Moran**, SJ Shattil, AD Leavitt

J Thromb Haemost. 2006 Feb;4(2):436-42. doi: 10.1111/j.1538-7836.2006.01744.x.

PTP-1B is an essential positive regulator of platelet integrin signalling

EG Arias-Salgado, F Haj, C Dubois, **B Moran**, A Kasirer-Friede, BC Furie, B Furie, BG Neel, SJ Shattil

J Cell Biol. 2005 Aug 29;170(5):837-45. doi: 10.1083/jcb.200503125.

The contribution of genetic factors to thrombotic and bleeding outcomes in coronary patients randomised to IIb/IIIa antagonists

DC Shields, AP Fitzgerald, PA O'Neill, C Muckian, D Kenny, **B Moran**, CP Cannon, CE Byrne, DJ Fitzgerald

Pharmacogenomics J. 2002;2(3):182-90. doi: 10.1038/sj.tpj.6500100.

Abbreviations

ACPA	anti-citrullinated protein antibodies
ADCC	antibody-dependent cell-mediated cytotoxicity
AF	Alexa Fluor
APC	antigen presenting cells
AS	ankylosing spondylitis
BCR	B cell receptor
BMI	body mass index
BSA	bovine serum albumin
CCL	chemokine (C-C motif) ligand
CD	cluster of differentiation
CD	Crohn's disease
cDC	conventional dendritic cells
cIMDM	complete Iscove's Modified Dulbecco's Medium
CLA	cutaneous leukocyte antigen
CLP	common lymphoid progenitor cells
Con	healthy control group samples
CTLA-4	cytotoxic T-lymphocyte-associated protein 4
CTLs	cytotoxic T lymphocytes
DAMP	damage associated molecular pathogen
DC	dendritic cells
dDC	dermal dendritic cells
DMSO	dimethyl sulfoxide
EMA	European medicines agency
Fc block	Fc receptor binding inhibitor
FCS	foetal calf serum
FDA	food and drug administration (US)
FGFR2	fibroblast growth factor-receptor 2
FixVia eF506	Fixable Viability Dye eFluor™ 506
FoxP3	forkhead box P3
FSC	forward scatter channel

g	gram
g	standard gravity
GM-CSF	granulocyte-macrophage colony-stimulating factor
h	hours
H&E	haematoxylin and eosin
hi	high expression
HiSCR	hidradenitis suppurativa clinical response score
HLA DR	human leukocyte antigen – DR isotype
HS	hidradenitis suppurativa
HS L	HS lesional skin
HS P	HS perilesional skin
HS U	HS uninvolved skin
I	ionomycin
IDO	Indoleamine 2, 3-Dioxygenase
Ig	immunoglobulin
IFN	interferon
IL	interleukin
IMDM	Iscove's Modified Dulbecco's Media
int	intermediate expression
J	joint segment
JAK	Janus kinase
LC	Langerhans cells
LD	live/dead viability marker
LN	lymph nodes
lo	low expression
LPS	lipopolysaccharide
MAIT cells	Mucosal associated invariant T cells
MALT	mucosal associated lymphoid tissue
MAPK	mitogen-activated protein kinase
MHC I / II	major histocompatibility complex class I / class II
mins	minutes
ml	millilitre

μl	microlitre
mm	millimeter
μm	micrometer
MMP	matrix metalloproteinase
MS	multiple sclerosis
NALT	nasal associated lymphoid tissue
NETs	neutrophil extracellular traps
NF-κB	nuclear factor kappa-light-chain-enhancer of activated B cells
NK cells	natural killer cells
NLRP	Nucleotide-binding oligomerization domain, Leucine rich Repeat and Pyrin domain containing
nm	nanometer
ns	not significant
OCRL1	inositol-5-phosphatase 1
ORS	outer root sheath
PAMP	pathogen associated molecular pathogen
PB	plasmablasts
PB	permeabilization buffer (1X)
PBMC	peripheral blood mononuclear cells
PBS	phosphate buffered solution
PC	plasma cells
PCA	principal component analysis
pDC	plasmacytoid dendritic cells
PFS	periodic fever syndromes
PG	pyoderma gangrenosum
PLZF	promyelotic leukemia zinc finger
PMA	phorbol-2-myristate-13-acetate
PMA/I	phorbol-2-myristate-13-acetate and ionomycin
PMT	photomultiplier tube
RA	rheumatoid arthritis
ROR-γt	retinoic acid-related orphan receptor gamma
RPMI	Roswell Park Memorial Institute media

RT	room temperature
scRNA-Seq	single cell RNA sequencing
SD	standard deviation
SEM	standard error of the mean
SLE	systemic lupus erythematosus
SLO	secondary lymphoid organs
Sn	setons
SNP	single-nucleotide polymorphism
ssDNA	single stranded DNA
SSC	side scatter channel
STATs	signal transducers and activators of transcription
T-bet	T-box expressed in T cells
Tc cells	cytotoxic T cells
Tcm cells	central memory T cells
TCD	Trinity College Dublin
TCR	T cell receptor
Tem cells	effector memory T cells
Temra cells	effector T cells re-expressing CD45ra
TGF- β	transforming growth factor beta
Th	T helper
TIP-DC	TNF and inducible nitric oxide synthase producing DC
TLR	toll-like receptor
Tmm	migratory memory T
TNF	tumour necrosis factor
TRAF6	tumour necrosis factor receptor (TNFR)-associated factor 6
Treg cells	regulatory T cells
Trm cells	resident memory T cells
TSLP	thymic stromal lymphopoetin
UMAP	uniform manifold approximation and projection
v	versus
V	variable segment

Chapter 1

Introduction

1 Introduction

1.1 The innate immune system

The body has a number of strategies that defend against infection, from anatomical barriers to innate and adaptive defences. Initially the skin, respiratory, genitourinary and gastrointestinal tracts act as physical barriers through their epithelial cells which form tight junctions, creating a protective seal (Murphy et al., 2016). Internal epithelia produce mucus, which prevent microorganisms from binding to the surface, and these microbes can then be expelled by mechanisms such as peristalsis and ciliary movement. Most epithelial surfaces produce a variety of antimicrobial proteins and enzymes as well as being colonised by commensal bacteria, or microbiota, which can further prevent invasion. The complement cascade, a system of about thirty different circulating proteins, bind to infectious agents and can cause cell lysis, as well as elicit recruitment of phagocytic immune cells.

Pathogens unhindered by these physical and chemical barriers will next interact with the cellular branch of the innate immune system. This tier is considered broadly specific and is usually induced by common molecular components unique to microbes, such as bacterial lipopolysaccharides (LPS), single stranded viral RNA and fungal β -glucan. Once triggered, innate immune cells may act directly to kill the invading microbe or produce mediators that drive an immune response in other cells.

Cells of the immune system have many variable yet overlapping roles; innate cells interact with and support the adaptive system (Section 1.2). Most immune cells develop from pluripotent haematopoietic stem cells in the bone marrow, with granulocytes, dendritic cells and most macrophages arising from the common myeloid progenitor cell. However, tissue resident macrophages such as alveolar macrophages, microglia, Kupffer cells and Langerhans cells, are derived from erythro-myeloid progenitor cells originating in the yolk sac (Gomez Perdiguero et al., 2015). The common lymphoid progenitor (CLP) cell in the bone marrow acts as a precursor to some innate and adaptive cells.

1.1.1 Macrophages

Macrophages are mononuclear cells found in almost all tissues; their primary function to patrol for, then phagocytose, pathogens and cellular debris. They may circulate in the blood in their immature form as monocytes, before migrating into tissue where they differentiate. Monocytes and resting macrophages express very little MHC II or co-stimulatory molecules on their cell surface, but this is markedly enhanced upon activation. Macrophages, along with neutrophils and dendritic cells amongst others, initiate their immune response through pathogen recognition receptors (PRR). PRR recognise microbial molecular signatures, branded pathogen-associated molecular patterns (PAMPs), expressed on pathogenic, non-self, cells. Molecules from stressed or dying cells, known as alarmins or damage-associated molecular patterns (DAMPs), can trigger a similar response. The inflammasome complex is found in a host of innate cells and is one of the most important PRR. It elicits activation of caspases and conversion of pro-IL-1 β to its active form IL-1 β . NLRP3 is the best characterised inflammasome, its basal expression of NLRP3 markedly increases upon recognition of PAMPs or DAMPs (Zahid et al., 2019).

Beyond their phagocytic role, macrophages play a role in orchestrating the adaptive immune response and antigen presentation to T cells. Macrophages do not migrate to lymph nodes but can locally amplify effector T cell responses. They can promote T cells to produce interferon (IFN) - γ which then enhances the macrophage response in a feed-forward loop (Murphy et al., 2016).

Macrophages may be polarised and play a pro-inflammatory, killing role as M1 (classically activated) macrophages, or anti-inflammatory, healing role in the case of M2 (alternatively activated) macrophages (Mills et al., 2000). Rather than two distinct subsets (M1 and M2), it is likely that there is a spectrum of macrophage function, with M1 and M2 describing either pole of this functionality (Ley, 2017).

1.1.2 Neutrophils

Neutrophils, though short-lived, are the most abundant immune cell in the blood. They are not generally found in healthy tissue, but their production increases massively upon

an immune event, whereupon they travel to sites of infection and inflammation. They are the first responders, destroying microbes and damaged cells through phagocytosis, degranulation of intracellular lytic granules as well as the release of neutrophil extracellular traps (NETs). NETs are web-like extracellular fibres, composed of lytic granule proteins, with chromatin acting as the major structural component (Brinkmann et al., 2004) They are secreted by neutrophils 3-8 hours after activation (Papayannopoulos, 2018). NETs trap and neutralise pathogens and prevent microbial dissemination. Phagocytosis may be enabled through opsonisation, where extracellular bacteria, coated with antibody, are phagocytosed via antibody binding to Fc receptors on the neutrophil surface. Similarly, both macrophages and neutrophils express complement receptors, which recognise complement-bound microbes.

1.1.3 Eosinophils

Eosinophils are much less abundant granulocytes than neutrophils in the circulation, primarily residing along the respiratory, gut and genitourinary connective tissue where they defend against extracellular microbes. When recruited and activated by protein or lipid mediators from mast cells or effector T cells, they release toxic granules that, as well as killing pathogens, may damage host tissues during allergic reactions (Luna-Gomes et al., 2013). Further, they can produce various mediators and cytokines which can recruit immune cells and further potentiate the immune response.

1.1.4 Basophils

Basophils are the least common granulocyte in the blood, accounting for <1% of circulating granulocytes, but are the only circulating cell containing histamine. They are the largest granulocyte and play a role in host defence to large extracellular pathogens. They are activated either through their PRR upon PAMP recognition, or via crosslinking of FcεR1 receptor-bound immunoglobulin (Ig) E (Buckland, 2020). Like mast cells, once activated they release granules containing histamine, heparin and serotonin, promoting inflammation and Th2 differentiation (Section 1.2.5.2)

1.1.5 Mast cells

Originally believed to be tissue-infiltrating basophils, mast cells are now known to have separate cell precursors, and are distinguished from basophils by the absence of cluster of differentiation (CD) 123 (Franco et al., 2010). They are long-lived tissue-resident cells found primarily in the skin, mucosal tissue and connective tissue surrounding blood vessels. They exit the bone marrow in an immature state, maturing in the tissue. Their mode of activation and effector function are similar to that of basophils. As well as defence against parasites, both mast cells and basophils are noted for their role in allergy and anaphylaxis

1.1.6 Dendritic cells

Dendritic cells (DC) comprise myeloid DC (mDC) and plasmacytoid DC (pDC). Upon bone marrow production and egress, DC travel through the blood stream to reside in tissues, actively sampling their environment for danger. They are abundant in tissues at the external interface, such as the gastrointestinal tract, nose, lungs and skin. PRR activation upon PAMP recognition matures the DC, driving it to ingest particles or microbes by micropinocytosis and phagocytosis, and process the pathogen antigens internally. Expression of the chemokine receptor CCR7 promotes mature DC trafficking to its closest (draining) lymphoid tissue to present antigens in the MHC complex to naïve T cells, hence acting as a mediator between the innate and adaptive immune systems (Section 1.2.5 and Figure 1.1). In addition, DC have the unique ability to phagocytose bacteria- or viruses (independent or within an infected host cell), or tumour cells, and “cross-present” its antigens by MHC I to naïve CD8 T cells (Gutiérrez-Martínez et al., 2015).

Unlike mDC, pDC do not express CD11c and have no major involvement in antigen presentation. Instead, they are primarily implicated in early defence against viruses, expressing toll-like receptor (TLR) 7 and TLR9, and producing high levels of anti-viral type I interferons (Murphy et al., 2016).

1.1.7 Innate lymphoid cells

There are a number of cells that develop in the bone marrow from the CLP cell but lack specific antigen receptors that define T and B cells. These are innate lymphoid cells (ILC) and include ILC1, ILC2, ILC3 and natural killer (NK) cells. ILC are largely tissue-resident effector cells that serve to amplify an immune response, acting more swiftly than adaptive cells. They are preferentially located at barrier surfaces. ILC are primarily activated by cytokines produced by activated innate immune cells. They are the innate counterpart to T cells (Section 1.2.4), with ILC1, ILC2 and ILC3 mirroring CD4 T helper type 1 (Th1) cells, Th2 and Th17 cells respectively, while NK cells are the CD8 T cell counterpart (Vivier et al., 2018). NK cells are larger than T and B cells and release cytotoxic granules to kill target cells. In addition, via Fc receptors on their cell surface, NK cells can target and destroy antibody-coated cells through antibody-dependent cell-mediated cytotoxicity (ADCC).

1.1.8 iNKT cells

Invariant NKT (iNKT) cells are derived in the thymus, and constitute only 0.1–1% of T cells in the circulation (Haygreen, 2020). Although many appear to remain in the thymus, iNKT cells migrate to mucosal surfaces and peripheral lymphoid tissue, and have been reported in the liver, skin and lymph node (LN) (Doisne et al., 2009). They express an invariant $\alpha\beta$ -T cell receptor (TCR) as well as some NK cell markers. Rather than engaging with antigens presented by MHC molecules as do conventional ($\alpha\beta$ -TCR) T cells (Section 1.2.2.1), iNKT cells' TCR interacts with glycolipids presented by CD1d, an MHC I-like molecule (Krovi et al., 2018).

iNKT cells are “innate-like” adaptive lymphocytes, unique in that they express proteins associated with memory cells despite being antigen naïve. They have a defined effector function upon leaving the thymus and mount an immune response to infection within minutes to hours as opposed to days in the case of adaptive lymphocytes. CD1-binding lipid antigens have been identified on commensal intestinal bacteria and it appears iNKT cells play an important role in regulating mucosal immunity. Like ILC, iNKT cell subpopulations are believed to parallel their T cell counterparts. Although yet to be confirmed in humans, iNKT cell subsets iNKT1 (PLZF^{lo}T-bet⁺), iNKT2 (PLZF^{hi}GATA-3^{hi}) and

iNKT17 (PLZF^{int}ROR- γ t⁺) subsets have been identified in the mouse (Coquet et al., 2008; Y. J. Lee et al., 2013).

1.1.9 MAIT cells

Mucosal associated invariant T (MAIT) cells are intraepithelial effector lymphocytes which express a semi-invariant TCR, restricted by the MHC-related protein 1 (MR1) (Chiba et al., 2018). MR1 is found in the endoplasmic reticulum of all cells, where it may egress to the cell surface, ligate to B vitamin metabolites common to pathogenic bacteria and yeast, and interact with the MAIT cell TCR (Salio et al., 2020). MAIT cells, like conventional T cells, undergo TCR rearrangement and positive selection in the thymus (Section 1.2.2.1). Similar to cytotoxic T cells, most MAIT cells (~ 85%) express CD8 on their cell surface, produce proinflammatory cytokines such as IFN- γ and tumour necrosis factor (TNF) and may directly lyse their target cell. The CD8⁻ MAIT cell subpopulation comprises of double negative (CD4⁻CD8⁻) MAIT cells, which are phenotypically and transcriptionally distinct, but are derived from this principal CD8⁺CD4⁻ MAIT cell pool (Dias et al., 2018). Unlike conventional T cells, MAIT cells gain effector capability prior to thymic egress and respond much more rapidly (Napier et al., 2015).

MAIT cells are abundant in humans and have been identified in a variety of sites including peripheral blood, LN, lung, liver, rectum, small intestine, and skin. They may represent up to 20% of CD8 T cells in the lung, and 20% of total T cells in the liver (Gold et al., 2015). They have been implicated in protective immunity, being oncolytic in cancer but playing a pathogenic role in inflammatory diseases such as obesity, inflammatory bowel disease (IBD) and multiple sclerosis (MS) (Rudak et al., 2018; Salio et al., 2020).

1.1.10 $\gamma\delta$ T cells

$\gamma\delta$ T cells constitute up to 10% of total T cells and arise in the thymus from the same CLP as conventional, $\alpha\beta$ -TCR T cells (Section 1.2.2.1), but undergo γ -chain gene rearrangement to develop a $\gamma\delta$ -TCR. $\gamma\delta$ T cells are considered “unconventional” T cells which straddle innate and adaptive immunity. They can rearrange TCR genes and

develop a memory phenotype, but do not require MHC molecules and can mount an immune response within hours. Upon thymic egress, mature $\gamma\delta$ T cells do not express CD4 or CD8, and like iNKT and MAIT cells, migrate primarily to epithelial and mucosal sites, and to a lesser degree lymphoid organs.

Human $\gamma\delta$ T cells comprise the V δ 1 and V δ 2 subsets, with V δ 1 T cells predominating in the thymus and peripheral tissues, recognising mostly uncharacterised stress-related antigens. V δ 2 T cells make up the majority of $\gamma\delta$ T cells in the blood, and primarily recognise phosphorylated antigens. Both subsets may progress to play a direct, cytotoxic role, killing target cells, or an indirect role, activating other immune cells through cytokines such as IFN- γ , IL-4 and IL-17 (Lawand et al., 2017).

1.2 The adaptive immune system

T cells (i.e. $\alpha\beta$ T cells) and B cells make up the cells of the adaptive immune system. B cells (or B lymphocytes) mediate the production of antigen-specific Ig, whilst T cells carry out the cell-mediated responses. Lymphocyte precursors develop in the bone marrow from haematopoietic stem cells which differentiate into multipotent progenitor cells, then onto the CLP cells. B cells develop in the bone marrow, whereas T cell development occurs in the thymus.

1.2.1 B cells

1.2.1.1 *B cell development*

B cells begin in the foetal liver, and develop in the bone marrow throughout life (Roghani, 2020). Ig gene rearrangement of D (diversity region) to J (joint segment) and V (variable region) of the heavy and light Ig chains allows progression of pro-B cells to late pro-B cells, then large B cells, then small pre-B cells and on to immature B cells with IgM surface expression (Murphy et al., 2016). Immature B cells with a strong affinity to self-antigen may be rescued by subsequent gene rearrangement yielding a new receptor (receptor editing). If this new receptor is still self-reactive, the B cell will die by apoptosis (clonal deletion).

Those immature B cells that do not recognise self-antigen exit the bone marrow to the periphery, migrating to the secondary lymphoid organs (SLO) to differentiate into mature B cells, expressing IgD as well as IgM. The SLO comprise of the spleen and LN, as well as the mucosal associated lymphoid tissue (MALT), nasal associated lymphoid tissue (NALT), tonsils, adenoids and Peyer's patches of the small intestine.

1.2.1.2 B cell activation

In the case of B cell activation via T cells, T and B cells reside close to each other in the SLO; T cells in the T cell zone, B cells in the primary lymphoid follicles. Non-phagocytic macrophages and follicular DC (fDC) also reside here, trapping opsonised antigen. B cells sample antigens for up to a day, whereupon activated B cells are then distributed along the T cell zone: B cell zone interface. The B cell receptor (BCR; a B cell surface bound Ig) binds to antigen, eliciting a signalling cascade similar to the TCR on the T cell surface (Section 1.2.2.2). The B cell is a professional antigen presenting cell, and can endocytose antigen via the BCR and process it intracellularly, subsequently presenting antigen peptides via MHC II to Th cells. Cytokines produced by the Th cell act on the B cell to enhance its survival and proliferation, as well as regulating the type of antibody produced (Murphy et al., 2016). Antigen-stimulated B cells which do not interact with their cognate Th cells apoptose within 24 hours.

Two to three days after the Th cell encounter, B cells proliferate and differentiate to form a primary focus in the SLO. At this point, some of the activated B cells develop into antibody synthesising plasmablasts. Plasmablasts, short-lived cells that have begun to secrete antibody, continue to divide and permit T cell interaction. They still have high levels of BCR and MHC II on their surface, primarily produce IgM and offer some early protection. Some of the mature B cells travel to the primary lymphoid follicle to form a germinal centre, where they account for most of the cells, although follicular Th (Tfh) cells may constitute up to 10%. Dynamic cell division occurs here as the immune response proceeds. These B cells undergo somatic hypermutation, where point mutations accumulate at the Ig variable region, producing similar B cell clones. Most mutations have a negative impact and these cells are eliminated by apoptosis due to insufficient Tfh cell binding. This process ensures B cell expansion does not overwhelm

the lymphoid tissue. Where the mutation enhances antigen affinity, this leads to positive selection and these clones will be selectively expanded, undergoing additional rounds of division.

Ig class switching occurs next, whereby cytokines secreted by Tfh cells direct B cells to switch production to different isotypes. For instance, IFN- γ induces IgG3 and IgG2a, TGF- β induces IgG2b and IgA. Different Ig classes have differing distribution and function; for example, IgM is found primarily in the blood and is very efficient at complement activation, whereas IgA functions primarily as a neutralising antibody in secretions lining the respiratory and intestinal tract.

1.2.1.3 B cell function

Most B cells that survive this somatic hypermutation and class switching go on to become plasma cells, producing large amounts of antibody. These cells no longer proliferate, lose their surface-bound Ig and are not induced by antigen. Some of these plasma cells migrate to the bone marrow where they can become very long lived, producing high-affinity, class-switched antibody.

A smaller percentage of B cells that survive the germinal centre differentiate into memory B cells, residing in tissue (Meng et al., 2017). These are antigen-experienced, slow-dividing cells that may persist for decades. They express surface bound Ig but do not secrete antibody. Upon reinfection with the same antigen, the memory B cell will rapidly proliferate and differentiate into plasma cells, thus mounting a swift, specific response. A small cohort of reactivated memory B cells may re-enter the germinal centre to undergo additional somatic hypermutation and class switching. This induction of memory B cells is the principal response employed in prophylactic vaccinations.

1.2.2 T cells

1.2.2.1 T cell development

T cells develop from CLP which migrate to the thymus. In the thymic cortex, CLP progress to CD44⁺Kit⁺ double-negative (DN) 1 cells; double-negative insofar as they do not express CD4 or CD8. Gene rearrangement (D_{β} to J_{β}) of the β -TCR chain progresses the

DN1 cells to DN2 and DN3 stages. V to DJ β -TCR rearrangement then leads to a complete β -TCR chain, with DN4 cells proliferating rapidly. Eventually the proliferation abates, and these cells now express CD4 and CD8 on their cell surface. These small double positive ($CD4^+CD8^+$) cells now undergo α -chain gene rearrangement (V to J_α), with most double-positive cells successfully producing a functional $\alpha\beta$ -TCR (Murphy et al., 2016).

From this point, thymocytes with a TCR that recognise self-MHC complex molecules are selected for survival (positive selection), the others (70-90%) dying by apoptosis. Thymocytes with TCR that have a strong affinity for MHC: self-antigen complexes are triggered to die by apoptosis (negative selection). This negative selection subsequently occurs for single positive ($CD4^+$ or $CD8^+$) thymocytes in the thymic medulla. Ultimately, approximately 98% of thymocytes are eliminated through this positive and negative selection process, the surviving cells exiting the thymus as mature naïve T cells. Cells with TCR that upon positive selection had preferentially recognised MHC I complex molecules develop as mature naïve T cells expressing CD8 (CD8 T cells), those preferential to MHC II complexes develop as CD4 T cells.

In addition to the conventional CD4 and CD8 T cells, some small subpopulations emerge, including iNKT cells (Section 1.1.8), MAIT cells (Section 1.1.9), and $\gamma\delta$ T cells (Section 1.1.10). In addition, thymically-derived regulatory T (tTreg) cells are a CD4 T cell subset that arise from the same $\alpha\beta$ -TCR double-positive thymocytes as CD4 and CD8 T cells. During their maturation, they upregulate CD25 and the transcription factor FoxP3. Their TCR repertoire is thought to have a high affinity for MHC: self-peptide complexes.

1.2.2.2 T cell activation

Mature, naïve T cells egress to the circulation travelling to the SLO. They recirculate between the blood and SLO via the lymphatics, interacting with thousands of DC at the SLO in a day, until they engage their cognate antigen. Upon antigen recognition, naïve T cells cease to migrate, undergo highly proliferative clonal expansion and differentiate into effector T cells of different functional classes (Murphy et al., 2016).

This T cell priming (activation) is characterised by three signals. The initial step is the specific binding of the antigen-loaded MHC molecule on an APC to the TCR on the T cell (signal 1; Figure 1.1). TCR binding on a CD8 T cell is to MHC I and is stabilised by the co-receptor CD8; with CD4 T cell binding to MHC II, stabilised by CD4. The co-stimulatory molecules CD80 and CD86 on the APC then bind to CD28 on the T cell (signal 2); without signal 2 a T cell becomes anergic. Once a T cell is activated, it differentiates into an effector T cell and undergoes rapid cell division driven by autocrine IL-2. This T cell differentiation process is dependent on the cytokine combinations in their microenvironment (signal 3). Whereas all CD8 T cells differentiate into cytotoxic T cells (Tc cells/ CTLs; Section 1.2.3), CD4 T cells differentiate into several effector T cell subsets with differing immune functions (Figure 1.1; Section 1.2.5).

Once activated, effector T cells can now exit the SLO and travel into tissues, particularly to sites of infection, or to B cell follicles within the SLO (Section 1.2.1.2). They bind potential target cells transiently, and upon antigen recognition form a tighter bond to enable their effector function (Sections 1.2.3 and 1.2.4).

1.2.2.3 Memory T cells

Following the resolution of an adaptive immune response, the vast majority of the clonally expanded effector cells die by apoptosis, with a small cohort surviving as memory T cells. They revert to a more stable, resting state but upon reinfection with the same pathogen will mount a much swifter and greater response than naïve T cells.

Memory T cell subsets include effector memory T (Tem) cells, central memory T (Tcm) cells, and the more recently identified resident memory T (Trm) cells. Tem cells patrol the periphery, and traffic directly to the re-infected tissue to exert effector function. Tcm cells recirculate between the blood and SLO; upon re-infection they are reactivated in the SLO, proliferating at high rates to become Tem cells. Another memory T cell population is described as effector T cells re-expressing CD45RA (Temra) cells, given their CD45RA⁺CCR7⁻ phenotype. The function of Temra cells is unclear, although they seem to have a more cytotoxic potential, even within the CD4 T cell compartment. They

appear to play a role in protection against viruses such as dengue virus and other viral pathogens (Tian et al., 2017).

Trm cells reside in tissues, primarily at barrier sites such as the lungs, nose, gastrointestinal tract and skin, and do not show evidence of activation (Steinbach et al., 2018). They are long-lived and provide potent local immunosurveillance. Whereas Trm cells in the mouse are identified based on the expression of CD69 and CD103, human Trm cells are distinguished by the presence of CD69 alone; with CD103 expression limited to a subset of CD8 Trm cells (Kumar et al., 2017).

1.2.3 Cytotoxic T cells

CD8 effector T cells (cytotoxic T lymphocytes [CTLs] or cytotoxic T [Tc] cells) function to directly kill tumour cells or cells infected with bacteria or viruses. They are serial killers, moving on from one target cell to another. They may be primed by mature DC in the absence of CD4 effector T cells (Section 1.1.6), though for most viral infections CD4 effector T cells further stimulate the APC via CD40 engagement and the CD8 T cell through IL-2 expression (Gao et al., 2016).

Tc cells carry out their killing by triggering apoptosis in their target cell, ensuring microbes are not released to infect other cells (Murphy et al., 2016). This triggered apoptosis is performed in three ways; first by secreting cytokines, the classical ones being IFN- γ and TNF, which drive anti-tumour and anti-microbial responses. Second, through release of the cytotoxic granules perforin, granzyme and granulysin. Together, these enable protein cleavage within the target cell with resultant apoptosis (Wissinger, 2020). Third, through the transmembrane protein Fas ligand (FasL), expressed on the Tc cell surface. FasL binds Fas, expressed on the target cell, leading to trimerisation with consequent caspase-driven apoptosis.

1.2.4 Helper T cells

Upon activation, CD4 T cells differentiate into diverse helper T (Th) cell subsets, depending on the differing cytokine cocktails in their milieu (Figure 1.1). They orchestrate or enhance a specific immune response as opposed to direct cell killing in

the case of Tc cells. Whereas MHC I is expressed on virtually all cells (except for mature red blood cells), MHC II is principally only expressed on professional APC (macrophages, DC and B cells).

1.2.5 Th cell subsets

The variation observed in Th cell subsets is elicited by different classes of microbes and the subsets are defined by the cytokines they secrete. Beyond their protective role, most are implicated in autoimmune and inflammatory diseases. Although various Th cell subsets may develop during an immune response, usually one will predominate, particularly in autoimmunity, allergy or persistent infection. In reality, Th cell subsets may well be fluid rather than distinct, with cells polarising to differing characteristics and roles depending on the conditions. Indeed, many highly activated T cells may be described as polyfunctional, expressing multiple diverse pro-inflammatory cytokines simultaneously. Nevertheless, it is helpful to characterise Th cells based on their observed roles.

1.2.5.1 *Th1 cells*

Th1 cells express the transcription factor T-bet and are induced by IL-12 and IFN- γ . They signal through the signal transducers STAT1 and STAT4, and express IFN- γ as their signature cytokine. Their primary function is to eradicate microbial infections that manifest within macrophages. IFN- γ drives phagocytosis and chemokine secretion, activates macrophages, increases antigen presentation and TLR expression on innate cells and promotes IgG class switching (Raphael et al., 2015). When Th1 cells recognise antigens expressed on the macrophage cell surface, the secreted IFN- γ acts to enhance microbicidal activity through macrophage and B cell recruitment, and this IFN- γ drives further Th1 cell activation in an autocrine loop.

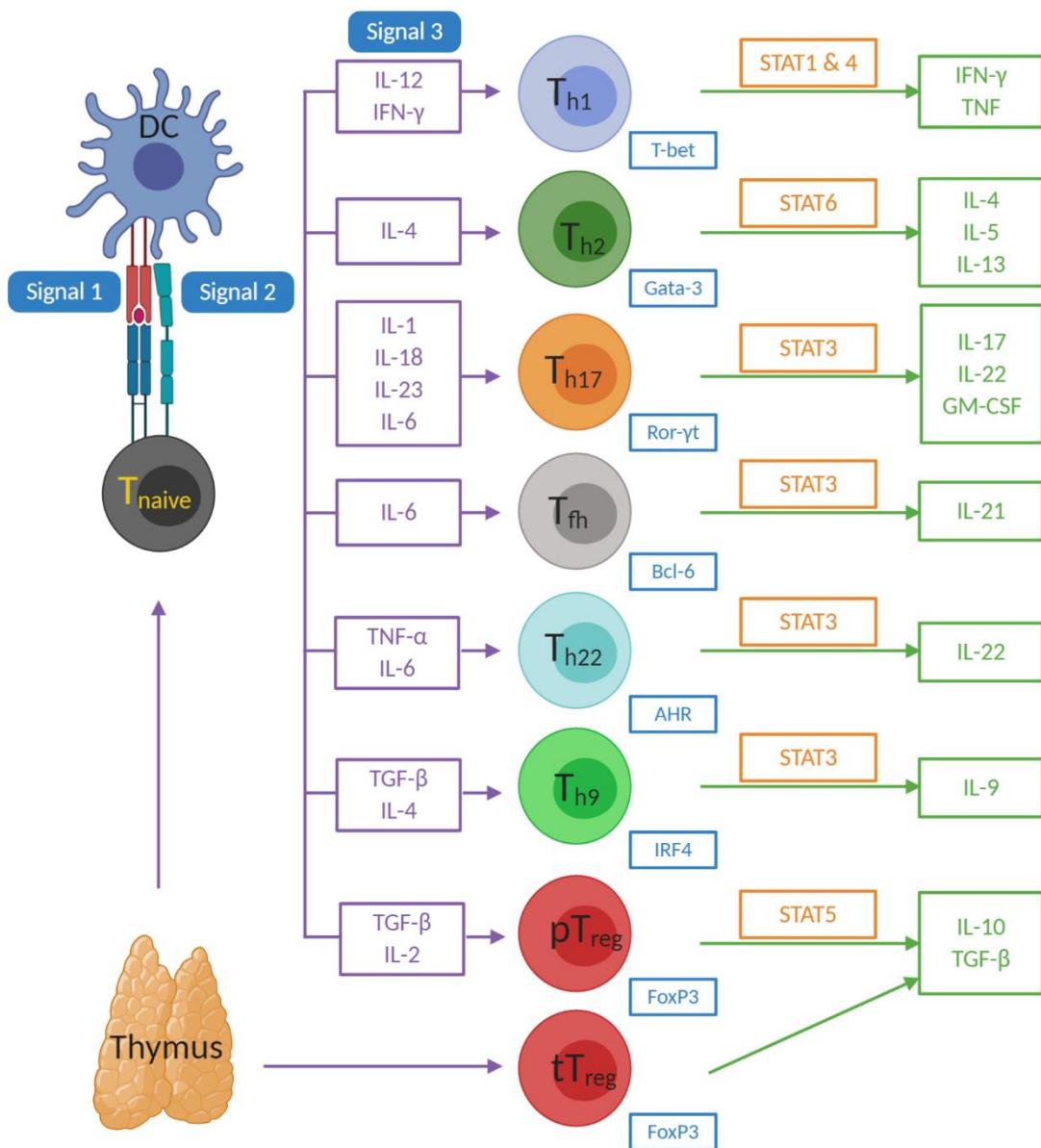


Figure 1.1 Differentiation of CD4 effector T cell subsets.

Upon engaging an infectious agent, DC may become activated via their PRR and phagocytose the pathogen, presenting antigens via the MHC class II pathway. Naïve T cell activation is initiated through engagement of this antigen: MHC II complex with the T cell TCR (signal 1), along with co-stimulation through CD28 (T cell) and CD80/86 (APC) binding (signal 2). Upon activation, Th cells undergo clonal expansion and differentiate into one of seven effector subsets (Th1, Th2, Th17, Tfh, Th22, Th9 and pTreg cells) depending on the cytokines present in their microenvironment (signal 3). Signalling induced by these polarising cytokines activates specific STATs and transcription factors which direct the function of the Th cell type, including production of their signature cytokines. Peripheral Treg (pTreg) cells have a similar phenotype and function to thymic-derived Treg (tTreg) cells.

1.2.5.2 *Th2 cells*

Th2 cells require IL-4 and differentiate via expression of the transcription factor GATA3 through STAT6. This drives secretion of the Th2 associated cytokines IL-4, IL-5 and IL-13, as well as IL-9 and IL-10 (Raphael et al., 2015). As with IFN- γ in Th1 cells, IL-4 promotes development of its own lineage through established positive and negative feedback loops. Th2 cells function to control infections of extracellular pathogens such as helminths. This drives the production of eosinophils, mast cells and IgE. Th2 cells induce B cell class-switching to produce IgE in such pathogen infections as well as in allergy (Murphy et al., 2016).

1.2.5.3 *Tfh cells*

Tfh cells remain within the lymphoid tissue and play a unique role supporting B cell development of class-switched antibodies in the germinal centre (Section 1.2.1.2). They are not associated with any particular immune response and may develop alongside Th1, Th2 or Th17 cells. Hence they can contribute to eradicating most pathogen types (Murphy et al., 2016). They are driven by IL-6, producing high levels of IL-21 via the regulator Bcl-6, and are identified principally by expression of the chemokine CXCR5. Tfh cells signal through STAT3 and STAT5.

1.2.5.4 *Th22 cells*

Although the cytokine IL-22 is associated with Th1, Th2 and in particular Th17 cells, there are also a population of CD4 T cells that express IL-22 but not the other Th cell signature cytokines. This subset has been classed as Th22 cells (S. Eyerich et al., 2009; Trifari et al., 2009). They develop in the presence of TNF and IL-6, with signal transduction via Jak1, Tyk2 and STAT3 (Wolk et al., 2011). They may be under the control of the aryl-hydrocarbon receptor (AhR) transcription factor (Trifari et al., 2009). Th22 cells are characterised by the expression of the chemokine receptors CCR4 and CCR10 (K. Eyerich et al., 2015). They act primarily on epithelial cells and hepatocytes, functioning in antimicrobial defence, barrier maintenance and protecting against excessive damage. Langerhans cells have been shown to play a role in dermal Th22 cell differentiation in the skin (Fujita et al., 2009).

1.2.5.5 *Th9 cells*

IL-9 was originally considered a Th2 cytokine, but is now associated with a distinct subset, termed Th9 cells. Their development is dependent on TGF- β , IL-4 and IL-21 under the control of STAT3 (Zhang et al., 2019), and they promote Treg cell survival, enhancing Treg cell suppressive function. Despite this role and their expression of the potent anti-inflammatory IL-10, they are thought to play a pathogenic role in asthma, systemic lupus erythematosus (SLE) and neuropathology (Raphael et al., 2015).

1.2.5.6 *Treg cells*

Unlike tTreg cells, peripheral or inducible Treg (pTreg, iTreg or Th3) cells require antigen recognition and develop from naïve T cells in the SLO. They act as the brakes for the immune response, suppressing inflammation and inhibiting inappropriate immune responses. pTreg cells are activated in the presence of TGF- β but the absence of IL-6, whereas Th17 cells are activated by both TGF- β and IL-6. In the absence of pathogens, IL-6 production by innate cells should be low, favouring differentiation of the Treg cell (Murphy et al., 2016). Treg cells are defined by their production of IL-10 and TGF- β , their expression of CD25 and the transcription factor FoxP3, as well as little or no expression of the T cell activation marker IL-7 receptor α (CD127).

Type 1 Treg (Tr1) cells are antigen-specific peripheral Treg cells that do not constitutively express FoxP3 nor IL-2. They play a role in inducing and maintaining peripheral tolerance. Their potent suppression is through IL-10 and TGF- β , and they express low levels of IFN- γ . Along with expressing suppressive cytokines, they have a cytotoxic role and can control inflammation by downregulating MHC II and lysing myeloid APC via perforin and granzyme-B (Magnani et al., 2011).

1.2.5.7 *Th17 cells*

Th17 cells are triggered in response to extracellular fungal or bacterial infection, leading to neutrophil recruitment as well as B cell class switching to IgG2 and IgG3. Th17 cells have been implicated in a number of inflammatory diseases and appear to be key mediators of autoimmunity (Langrish et al., 2005). Signature cytokines include IL-17A, IL-22 and GM-CSF, and the cells act to stimulate epithelial cells in the skin,

gastrointestinal, respiratory and urogenital tracts to produce antimicrobial peptides, cytokines and chemokines. Many cytokines have been implicated in their differentiation, in particular IL-1, IL-6, IL-18, IL-23 and TGF- β . IL-23, the crucial Th17 activating cytokine, is a heterodimer of p19 and p40, with the p40 subunit shared with IL-12, the key driver of Th1 cells. Th17 cells require STAT3, and their differentiation is via the transcription factor ROR- γ T. All human Th17 cells appear to express CCR6 and originate from CD161⁺ CD4 T cells, with CD161 considered a pan-marker for Th17 cells (Cosmi et al., 2008).

1.2.5.8 *Th17 cell plasticity*

Human Th17 cells appear to be highly plastic and may be further divided into subgroups. These subpopulations are likely extremes in a continuous spectrum of Th17 cell phenotype and function but are convenient in classifying cell states. For example, ex-Th17 cells (extinguished Th17, or non-classical Th1 cells) describe a subset of T cells that develop from the Th17 cohort (Annunziato et al., 2007). They occur when Th17 cells switch from expressing IL-17 to IFN- γ . Although the in vivo process is incompletely understood, it occurs ex vivo in the presence of IL-12 rather than IL-23 (Lexberg et al., 2010). Like Th17 cells, ex-Th17 cells express the surface marker CD161, the chemokine receptor CCR6, and the IL-23 receptor (IL-23R). The Th1 cell associated chemokine receptor CXCR3 is increased in ex-Th17 cells compared with Th17 cells (Maeda et al., 2019). Ex-Th17 cells are functionally distinct from Th17 or Th1 cells; being more polyfunctional and resistant to Treg cell suppression (Basdeo et al., 2017). Cells expressing both IL-17 and IFN- γ , as well as CD161, may be characterised as transitioning exTh17 cells (or Th17/1 cells) (Nistala et al., 2010).

It is likely that not all IL-17⁺ T cells play a pathogenic role; with IL-1 β driving inflammatory Th17 cells producing IL-17 and IFN- γ but not IL-10 (Zielinski et al., 2012). Alternatively, Th17 cells over-stimulated with antigen downregulate IL-17 production but upregulate IL-10, exerting a more tissue-protective and immunosuppressive role. It has been reported that pathogenic Th17 cells may be limited to those expressing CXCR3 or the multi-drug transporter MDR1 (Lam et al., 2016).

1.3 IL-17

IL-17A was first cloned in 1993, with other structurally similar proteins identified in the early 2000s. The IL-17 family of cytokines consists of six proteins, IL-17A to F; IL-17A being the archetypal member (Table 1.1). It is clear that IL-17 cytokines not only play a role in host defence against pathogens, but also in autoimmunity. IL-17A, C, E and F are the most characterised and are all implicated in autoimmune inflammation. IL-17A and IL-17F, which are often co-expressed, may be secreted not only by Th17 cells, but also to a lesser degree by Tc cells (Cheuk et al., 2017; Cheuk et al., 2014), ILC3 (M. B. M. Teunissen et al., 2014), iNKT cells (Venken et al., 2019) and $\gamma\delta$ T cells (Cai et al., 2011; Laggner et al., 2011). There is also controversial evidence regarding the ability of myeloid cells to express IL-17 family cytokines (Lin et al., 2011; Noordenbos et al., 2016; Tamassia et al., 2018) (Section 1.5).

By contrast, IL-17C is expressed primarily by epithelial cells and keratinocytes in response to cytokine and TLR activation (Gomez Perdiguero et al., 2015; Johansen et al., 2011). Meanwhile, IL-17E (IL-25) is produced in the skin by keratinocytes, and is more associated with Th2 cell responses and allergy than autoimmunity. The role of IL-17B is currently unclear; perhaps playing a role in joint pathogenesis, and its expression is associated with poor prognosis in some cancers. IL-17B is produced by neutrophils, B cells, neurons and stromal cells, though not by activated T cells. Similarly, IL-17D is poorly expressed by activated immune cells but has been identified in tissue such as skeletal muscle, brain, adipose, heart and lung (Brembilla et al., 2018).

The IL-17 receptors are generally understood to be comprised of heterodimers of IL-17RA together with ligand-specific subunits (IL-17RB to E) and are ubiquitously expressed on epithelial cells (Yao et al., 1997). Homodimers or heterodimers of IL-17A and IL-17F bind to a receptor composed of the RA and RC subunits, albeit with differing affinities (Wright et al., 2008) (Table 1.1). Recently, mouse and primary human keratinocyte studies demonstrated that IL-17RD may also partner with IL-17RA and directly bind IL-17A, thus proposing a second functional receptor for IL-17A (Su et al., 2019). This was observed only in IL-17A, not for IL-17F or the IL-17A/F heterodimer. IL-17C is recognised by a receptor consisting of RA and RE subunits, whilst IL-17E signalling

is mediated via a receptor of RA and RB subunits (Yao et al., 1997). In contrast to this heterodimer model, a new study has demonstrated an IL-17RC homodimer that anchors IL-17F, thus suggesting the possibility of an IL-17RA-independent IL-17 signalling pathway (Goepfert et al., 2020). IL-17B signals through an unidentified receptor containing IL-17RB. The receptor for IL-17D currently remains unknown. All IL-17 receptors recruit Act1 as an adaptor molecule for downstream signalling via TRAF6, MAP-kinase and NFκB (Gaffen, 2009).

For the purpose of this thesis, unless stated otherwise, IL-17 represents IL-17A.

IL-17 cytokine	IL-17R subunits	Sources	Target Cells	Role in host defence and health	Role in disease
IL-17A homodimer	RA+RC [1, 2]	Th17 cells [6, 7], Tc17 cells [8], $\gamma\delta$ T cells [9, 10, 11], iNKT cells [9], ILC3 [12, 13]	Keratinocytes, epithelial cells, fibroblasts [14]	Defence against extracellular bacterial and fungal infections, barrier maintenance, wound healing [14]	Pathogenic in chronic inflammation, autoimmunity & some cancers [14]
	RA+RD [3]				
IL-17F homodimer	RA+RC [2]	Th17 cells [6, 7], Tc17 cells [8], $\gamma\delta$ T cells [9, 10, 11], iNKT cells [9], ILC3 [12, 13]	Keratinocytes, epithelial cells, fibroblasts [14]	Defence against extracellular bacterial and fungal infections, barrier maintenance, wound healing [14]	Pathogenic in chronic inflammation, autoimmunity & some cancers [14]
	RC+RC [4]				
IL-17A+F heterodimer	RA+RC [2, 5]				
IL-17C homodimer	RA+RE [2]	Keratinocytes, epithelial cells, cutaneous neurons [14, 15, 16, 16]	Autocrine effects on keratinocytes, epithelial cells, neurons [14]	Microbial defence, barrier maintenance, epithelial repair, cutaneous neuroprotection [14]	Pathogenic in inflammatory skin diseases including psoriasis [17, 18], atopic dermatitis [19], HS [18]
IL-17E homodimer (IL-25)	RA+RB [2]	Keratinocytes, endothelial cells, epithelial cells, Th2 cells, macrophages, myeloid cells, ILC2 [14, 20]	Epithelial cells, fibroblasts, endothelial cells, Th2 cells, Th9 cells, iNKT cells, ILC2, [20]	Defence against helminths, promotes Th2 cell- mediated immunity [14]	Pathogenic in allergy (Xu et al., 2017) psoriasis (Xu et al., 2018)
IL-17B homodimer	RB+? [2]	Neutrophils, B cells, neurons, stromal cells, epithelial cells, chondrocytes [21, 22]	Epithelial cells, fibroblasts, macrophages [22, 23]	Protective against <i>Citrobacter rodentium</i> Infection [22]	Pathogenic in inflammatory arthritis [23], gastric and breast cancers [21], lung fibrosis [24], protective against colitis and asthma [22]
IL-17D homodimer	unknown	Skeletal muscle, brain, adipose, heart and lung tissue [21]	Endothelial cells [21], DC [25] macrophages [26]	Protective against viral infection and tumours [21]	Pathogenic in sepsis [26], pathogenic role in certain intracellular infections [25]

Table 1.1 IL-17 cytokines and their receptors, cellular sources, target cells and functions.

Table references: 1 (Yao et al., 1997), 2 (Gaffen, 2009), 3 (Su et al., 2019), 4 (Goepfert et al., 2020), 5 (Wright et al., 2008), 6 (Langrish et al., 2005), 7, (Harrington et al., 2005), 8 (Cheuk et al., 2014), 9 (Venken et al., 2019), 10 (Laggner et al., 2011), 11 (Cai et al., 2011), 12 (M. B. M. Teunissen et al., 2014), 13 (Bernink et al., 2019), 14 (McGeachy et al., 2019), 15 (Ramirez-Carrozzi et al., 2011), 16 (Johansen et al., 2011), 17 (Johnston et al., 2013), 18 (Navrazhina et al., 2020), 19 (Guttman-Yassky et al., 2018), 20 (Xu & Dong, 2017), 21 (Brembilla et al., 2018), 22 (Reynolds et al., 2015), 23 (Yamaguchi et al., 2007), 24 (Yang et al., 2019), 25 (Y. Lee et al., 2019), 26 (Yan et al., 2020).

1.4 Skin immunity

The skin is the largest organ of the body, providing structural integrity, restricting water loss, regulating temperature, and acting as a barricade to exclude microbes, allergens and chemicals. In addition, it forms an active barrier, serving as the first line in immunological protection.

Human skin consists of two major components, the outer epidermal layer anchored to the loose connective tissue of the dermis (Figure 1.2) (Kashem et al., 2017). The epidermis comprises the outermost stratum corneum, then the stratum granulosum, the spinous cell layer and finally the basal layer (stratum basale) (Pasparakis et al., 2014). The stratum basale forms rete ridges, epidermal extensions projecting into the lower dermis. The impermeable stratum corneum, consisting of rows of corneocytes (essentially flattened, denucleated keratinocytes), is interspersed with sweat ducts and hair follicles. These appendages lack the stratum corneum and consist of live keratinocytes lining the cavity. They serve as an outside-in channel for small-molecules and drugs, as well as inside-out channel for water expulsion. Numerous species of commensal bacteria (microbiota) cover the skin and openings. As well as keratinocytes and corneocytes, melanocytes are also located in the epidermis, primarily in the stratum basale.

The pilosebaceous unit makes up the hair follicle with the attached sebaceous gland and connecting muscle (arrector pili). The hair follicle begins at the surface of the epidermis, running deep into the dermis. The infundibulum is the upper portion, running from the epidermal surface to the opening of the sebaceous gland. Next is the isthmus, from this gland-opening to the lower portion, the bulge. The bulge is the area of insertion of the arrector pili muscle, which is connected to the dermis. Below these three regions are the inferior segment, including the bulb, which encompass the follicular matrix and capillary-containing dermal papilla. Surrounding the hair shaft is the internal root sheath, then the outer (external) root sheath (ORS), both of which cease at the isthmus area. Epidermal stem cells line the ORS (Orvain et al., 2020). The hair follicle is immunoprivileged, with follicular keratinocytes expressing anti-inflammatory cytokines such as IL-10 and TGF- β , and downregulating expression of MHC I (Kabashima et al., 2019).

Where this immune privilege fails, T cell responses against the skin microbiota may progress to an autoimmune response, such as that reported in alopecia areata (Kang et al., 2010).

In the skin there is a well-orchestrated interplay between epithelial, stromal and immune cells in order to coordinate host defence and maintain tissue homeostasis. 90-95% of cells in the healthy epidermis are keratinocytes, and although their primary function is maintaining a physical barrier, they also play a role in innate immunity. They express a number of PRR and have been shown to produce various cytokines such as thymic stromal lymphopoietin (TSLP), IL-1 family members and TNF (Carmi-Levy et al., 2011). Interestingly, keratinocyte chemokines differ depending on their location within the epidermis, and keratinocytes in the hair follicle infundibulum express chemokine (C-C motif) ligand (CCL) 20, CCL2 in the isthmus, and CCL8 around the hair bulge (Kabashima et al., 2019).

Langerhans cells (LC), a subset of professional APC, reside amongst keratinocytes in the epidermis (Figure 1.2). LC were originally considered a DC subset; though more recent developmental studies have revealed them as monocyte-derived tissue-resident macrophages that acquire a more DC like phenotype in the skin (Ginhoux et al., 2006; Hoeffel et al., 2012). LC can extend their dendrites through keratinocyte tight junctions to engage antigen from the stratum corneum (Kubo et al., 2009). Upon an inflammatory event, LC can migrate to the T cell zone of the draining LN within three to four days to further a T cell response. CD8⁺ Trm cells are the other immune cell regularly found in healthy human epidermis (Pasparakis et al., 2014). Both LC and CD8 Trm cells are primarily based within the stratum granulosum and spinous cells layers.

Both CD4 and CD8 T cells are found in the skin, usually in the form of Trm cells, and predominantly around hair follicles. Whereas CD8 Trm cells are in the epidermis, CD4 Trm are found primarily in the dermis. Treg cells are also resident in the dermis, largely close to the ORS bulge area, and they likely contribute to the immunosuppressive qualities of the hair follicle (Kabashima et al., 2019).

The dermis tends to be much thicker than the epidermis. Fibroblasts are the dominant cell here, playing a role in wound and fibrotic tissue repair. Sweat glands and pilosebaceous units stem through this profuse extracellular matrix comprising of collagen and elastin fibres with an intermeshing lymph, blood and neural network (Kabashima et al., 2019). Immune cells present in the homeostatic dermis include dermal DC (dDC), macrophages, mast cells, ILC and NK cells, with a small number of neutrophils, monocytes and Trm cells patrolling for pathogens. These cells are readily recruited via the dynamic vascular system.

The dermis contains Trm cells and APC that are typically found across all non-lymphoid tissues. dDC are closely related to conventional DC (cDC) subsets located in lymphoid tissues (Kashem et al., 2017). Upon antigen uptake, as well as migrating to the draining LN, dDC can activate tissue-resident and infiltrating T cells in the skin in both the steady state and during inflammation to direct the immune response (Ho et al., 2019).

Dermal cDC express MHC II and low levels of CD11c, and can be subdivided into CD141⁺ DC and CD1c⁺ DC (Table 1.2). Their murine homologs are classified as cDC1 and cDC2 respectively, and so for simplicity CD141⁺ DC will herein be annotated as cDC1, CD1c⁺ DC as cDC2.

cDC1 are a relatively rare population, expressing CD141, XCR1, CLEC9A and IRF8, and appear to be more efficient than cDC2 at antigen cross-presentation (Gutiérrez-Martínez et al., 2015). Blood cDC1 express the skin homing receptor cutaneous lymphocyte antigen (CLA) in contrast to dermal cDC1 which are CLA⁻ (Kashem et al., 2017). Dermal cDC1 rapidly migrate to the deep T cell zones of draining LN and constitute 20-40% of LN resident DC.

cDC2 are the most populous dDC and are characterised by their expression of CD1c, CD11b and IRF4. cDC2 are not only found in the skin but in most lymphoid and non-lymphoid tissue. In inflammation, cDC2 may be derived from peripheral blood monocytes and be the precursors to so-called LC-like cells, driven by keratinocyte expression of TSLP and TGF- β (Martinez-Cingolani et al., 2014).

Dermal macrophages in humans are positive for MHC II, CD11c, CD14 and FXIIIa. Though vastly superior at phagocytosis, they are much less potent in regard to T cell activation when compared with LC and dDC (Tamoutounour et al., 2013). They comprise both the short-lived, non-autofluorescent, blood monocyte-derived macrophages as well as the long-lived, highly autofluorescent skin-resident macrophages. The high autofluorescence is due in part to the melanin granules within this macrophage subset.

Additional populations appear to home to the skin and play a local role in skin inflammation. In psoriasis, a population of TNF and inducible nitric oxide synthase-producing DC (TIP-DC) are found, as well as IL-20⁺IL-23⁺ DC (Pasparakis et al., 2014). CD1a⁺ inflammatory dendritic epidermal cells (IDEC) have been identified in lesional skin of atopic eczema and other skin inflammatory diseases, residing in the lower layer of the epidermis (Otsuka et al., 2018). Both TIP-DC and IDEC are MHC II^{hi}CD11c^{hi}.

pDC are absent, or present in very low numbers, in healthy skin but may be recruited during skin inflammatory episodes (Kashem et al., 2017). Unlike mDC, pDC are derived from both myeloid and lymphoid precursors (Rodrigues et al., 2018) and do not express CD11c. They may be identified by their expression of CD123, CD303 (BDCA-2) and CD304 (BDCA-4). Morphologically, they are more comparable to plasma cells or B cells rather than mDC.

There are a number of murine dermal APC that have yet to have human homologs identified, such as the migratory XCR1⁻CD11b⁻ dDC, and the so called monocyte derived (mo-) DC, though these may reside within the human dermal macrophage population (Kashem et al., 2017).

APC subsets					
	LC	CD141 ⁺ DC	CD1c ⁺ DC	pDC	CD14 ⁺
Annotation	LC	cDC1	cDC2	pDC	Dermal macrophages
Location	Epidermis		Dermis		
MHC II	+	+	+	+	+
CD11c	low	low	+	-	+
CD1a	++	-	+*	-	-
CD14	-	-	-	-	+
CD1c	+	-	+	-	+/-
CD303	-	-	-	+	-
CD304	-	+	+/-	+	-
CD141	-	++	-/+	-/+	-
XCR1	-	+	-	-	-
CLEC9A	-	+	-	-	-
CD207 (Langerin)	++	-	-/+*	-	-
CD326 (EpCAM)	+	-	-	-	-
CD324 (E-cadherin)	+	-	-	-	-
CD11b	low	-	+	-	+
CX3CR1	+	-	+	-	+
CD172 α (SIRP α)	+	-	+	-	+

Table 1.2 APC subsets in healthy skin.

Marker expression on human skin APC subsets.

* migratory skin DC.

Adapted from Kashem et al., 2017.

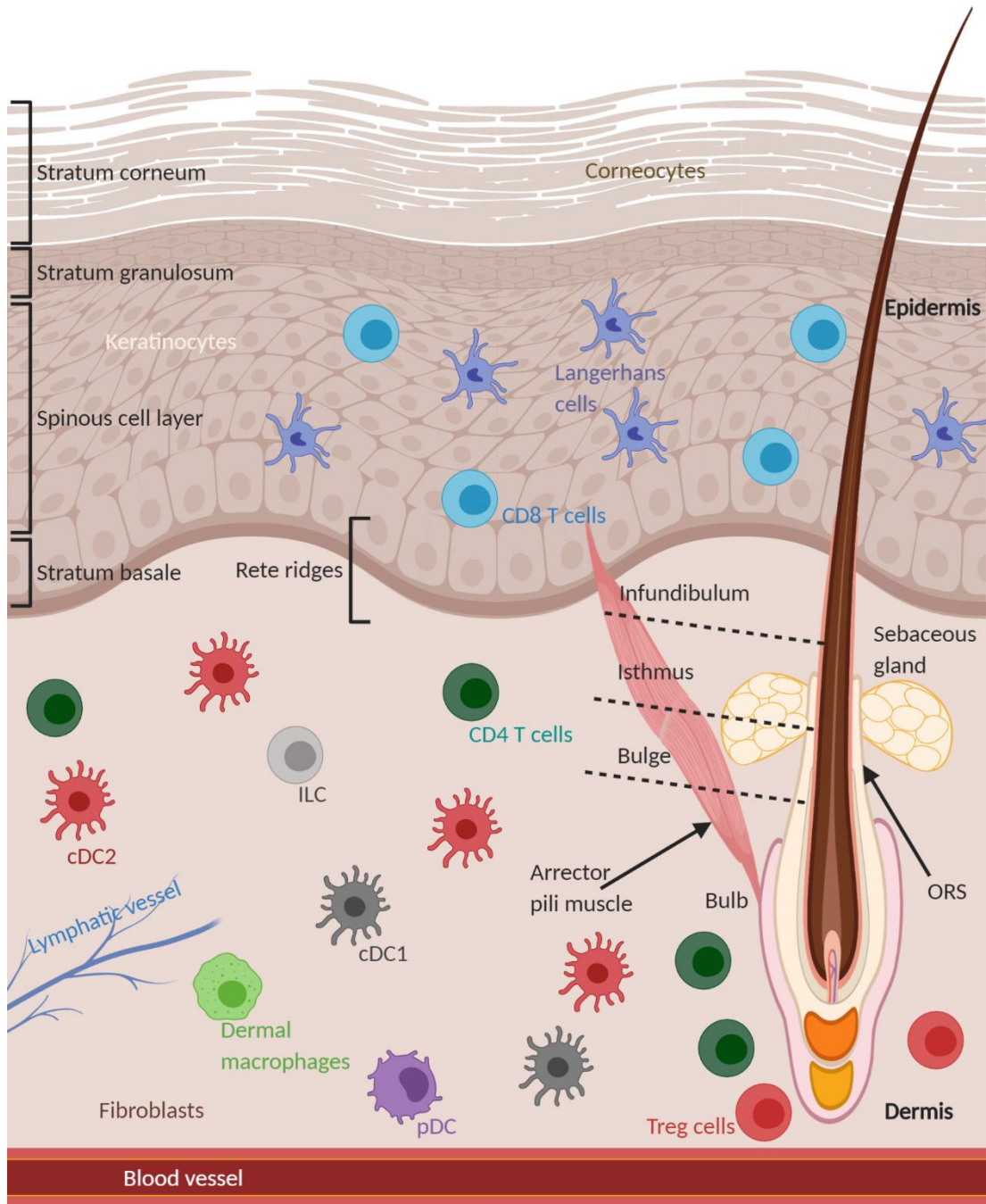


Figure 1.2 Structure and immune cell components of healthy human skin.

Human skin consists of two major components, the thick dermis below the thinner epidermis, where rete ridges project down into the dermis. Immuno-privileged hair follicles extend from the dermis, the hair shaft protruding through the epidermis. Resident immune cells in the dermis include Langerhans cells and CD8 Trm cells, with a more diverse array in the dermis, including CD4 Trm cells, ILC, DC and macrophages.

1.5 IL-17 in the skin

Th17 cells appear to be the primary cellular source of IL-17A in the skin. However, other cells have been shown to produce IL-17 under varying conditions.

1.5.1 Tc cells

IL-17 producing Tc cells (Tc17) have been identified in the skin, with CD49a⁻ CD8⁺ Trm cells shown to be the IL-17 producing subset (Cheuk et al., 2017). Tc17 cells have been implicated in skin disease, with highly responsive Tc17 cells expressing IL-17A and IL-22 observed in psoriasis epidermal tissue, including clinically resolved disease (Cheuk et al., 2014). Teunissen and colleagues implicate Tc17 cells in psoriasis, and identify them as the major CD8⁺ cell producing IL-17 in psoriatic skin (M. B. Teunissen et al., 2014). In paradoxical psoriasis, where psoriasis-like lesions develop in patients undergoing anti-TNF treatment, Tc17 cells appear to be even more prominent in the lesional skin of patients (Moran et al., 2020). Recently, treatment with biologics targeting the IL-17 pathway (secukinumab, ustekinumab or guselkumab) for the condition lichen planus, an inflammatory disorder of the skin and mucous membranes, showed clear clinical improvement, with a reduction in Tc17 levels in patient skin (Solimani et al., 2019).

1.5.2 iNKT cells

Although subsets of iNKT cells have been shown to produce IL-17 in various organs of the mouse including the skin (Coquet et al., 2008; Doisne et al., 2009), there have been relatively few human studies. Li et al showed increased levels of these cells in mouse models of type 1 diabetes, but no evidence in patient peripheral blood mononuclear cells (PBMC) (S. Li et al., 2014). An iNKT cell subset of human PBMC was shown to express CD161 and produce IL-17, in combination with IFN- γ , upon stimulation with TGF- β , IL-1 β and IL-23 (Moreira-Teixeira et al., 2011). More recently, IL-17 producing iNKT cells were identified in healthy and spondylarthritis patients' PBMC, and shown to be enriched in the inflamed joints of these patients (Venken et al., 2019).

1.5.3 MAIT cells

MAIT cells have been implicated in a number of inflammatory and autoimmune diseases. CD161⁺ MAIT cells secreting IL-17 upon phorbol myristate acetate and ionomycin (PMA/I) activation have been identified (Dusseaux et al., 2011). There was an enrichment in the synovial fluid of ankylosing spondylitis (AS) patients, and those MAIT cells had an amplified IL-17 phenotype (Gracey et al., 2016). They were shown to produce more IL-17 and less IL-10 in the adipose tissue of obese patients compared with healthy controls (Carolan et al., 2015). MAIT cells have been suggested to be present in the skin at levels similar to that in PBMC (J. Li et al., 2017) and were abundant in psoriatic skin, producing both IL-17A and F (Cole et al., 2019), albeit much less frequent than Tc17 cells (M. B. Teunissen et al., 2014).

1.5.4 Innate lymphoid cells

ILC3 express IL-17 and are the ILC equivalent to Th17 cells. An increase in IL-17 producing ILC3 in psoriasis patient skin and blood has been reported when compared with normal controls or atopic dermatitis patients (Villanova et al., 2014), with the proportions of ILC2 and ILC1 remaining unchanged (M. B. M. Teunissen et al., 2014). Given the appropriate cytokine milieu, ILC can readily transdifferentiate into other ILC subsets (Almeida et al., 2016). ILC2 trans-differentiation to IL-17-producing ILC3-like cells has recently been described, with skin homing IL-17 producing ILC2 identified in peripheral blood (Bernink et al., 2019). The authors contest that the IL-17⁺ ILC3 in psoriatic lesions are derived from ILC2 expressing the skin homing receptor CCR10.

1.5.5 $\gamma\delta$ T cells

TCR- $\gamma\delta$ T ($\gamma\delta$ T) cells are rare in healthy human skin although IL-17 producing $\gamma\delta$ T cells have been associated with elements of skin disease. In the mouse, $\gamma\delta$ T cells in the epidermis produce IFN- γ and IL-13, and are known as dendritic epidermal T cells (DETC), whereas in the dermis they are highly polarised towards producing IL-17, expressing either V γ 4 or V γ 6 TCRs (Papotto et al., 2017). In murine models of psoriasis, $\gamma\delta$ T cell-derived IL-17 mobilises granulocytes and promotes tissue damage via IL-17RA (Cai et al., 2011), whilst IL-22 acts on keratinocytes to induce upregulation of inflammatory genes

(Cibrian et al., 2016). In humans, there have been much fewer studies that suggest a pathogenic role for $\gamma\delta$ T cells in the skin. The V δ 2 subset was reported to produce IL-17 and implicated in psoriasis (Laggner et al., 2011; Papotto et al., 2017). Going further, Cai et al. suggested that IL-23 responsive $\gamma\delta$ T cells are the primary IL-17 producers in human psoriatic skin (Cai et al., 2011). IL-17-producing V γ 9V δ 2 T cells have been reported in the synovial fluid of psoriatic arthritis patients (Guggino et al., 2016) but there appear to be no other human studies demonstrating pathogenic IL-17⁺ $\gamma\delta$ T cells in the skin.

1.5.6 Mast cells

IL-17 producing mast cells have been described in humans, with its release via degranulation or extracellular trap formation (Lin et al., 2011). These have been linked to a favourable outcome in bladder cancer (Dowell et al., 2017), but a poor prognosis in hepatocellular carcinoma (Tu et al., 2016). More so than IL-17, mast cells have been shown to be a major source of IL-22 in patients with psoriasis and atopic dermatitis (Mashiko et al., 2015). However, it has more recently been contended that human mast cells from primary tissue may not in fact produce IL-17, but rather capture exogenous IL-17 into intracellular granules, then subsequently release it (Noordenbos et al., 2016).

1.5.7 Neutrophils

Along with mast cells, neutrophils were previously reported as the dominant IL-17-producing cells in human skin (Lin et al., 2011), and a major source of IL-17 in the lesional skin of hidradenitis suppurativa (HS) patients (Lima et al., 2015). However, it is still controversial as to whether human neutrophils actually express IL-17 at all. A recent, thorough study sampled highly purified neutrophils from blood and skin from suspect diseases, using multiple detection techniques and stimulation conditions (Tamassia et al., 2018). No evidence of IL-17A, IL-17B or IL-17F RNA or protein was detected. As neutrophils express large amounts of the receptor IL-17RA, it is possible that neutrophils sequester extracellular IL-17 via their receptors, accounting for false-positive cases.

1.6 Hidradenitis suppurativa

1.6.1 Symptoms

HS, also known as acne inversa or Verneuil's disease, is a recurrent, inflammatory, follicular skin disease that commonly affects the apocrine-bearing skin (armpits, inframammary fold, genitals, groin, buttocks and perianal areas; Figure 1.3). Typical acute lesions or boils can arise quickly and present as painful, erythematous nodules, with associated fever (Jemec, 2012). Unlike other chronic skin conditions, HS results in pus formation and irreversible tissue damage and scarring. Rupture of HS lesions can lead to a bloody, suppurative, foul-smelling discharge.

The average lesion lasts 7 days, with a median of 2 per month, and 62% of patients report persistent, painful inflammatory lesions (Hoffman et al., 2017). In advanced stages, the lesions may become more numerous and upon rupture, sinus tracts may form with resulting fibrotic and cribriform (sieve-like) scar formation. This leads to dermal contractures and hardening of the affected skin (Martorell et al., 2015). These sinus tracts may join together to form cords and dermal tunnels, with chronic suppuration and hypertrophic scarring. This fibrotic scarring in the groin and axilla leads to restricted and painful movement, and paired with odorous, bloody discharges manifests in significantly low quality of life scores affecting patients' mental, social and economic wellbeing.

HS patients may have systemic complications, with many sufferers having cardiovascular and metabolic complications associated with obesity, as well as IBD and depression (Sabat et al., 2020).

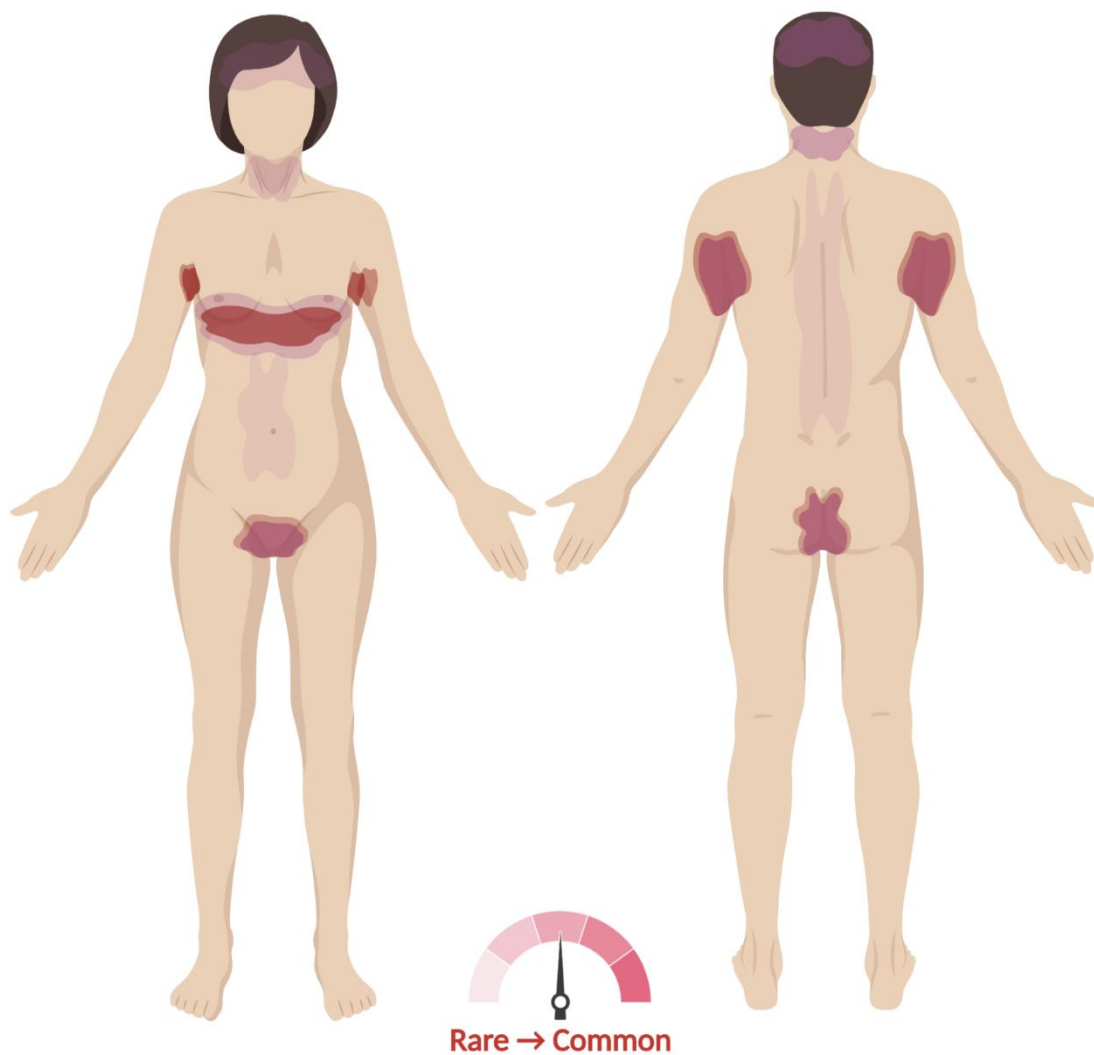


Figure 1.3 Schematic of HS patient inflammatory sites.

HS is a chronic inflammatory skin disease that commonly affects the apocrine-bearing skin. Lesions and boils most commonly affect the groin, perianal, axilla and inframammary skin folds.

1.6.2 Prevalence

HS is a chronic disease, most commonly arising at mid-teens, frequently persisting in the patient through middle and old age. It may be considered as an uncommon, but not rare, disease. Widely varying prevalence has been claimed, from 0.006% in a US epidemiological study (Vazquez et al., 2013), to 1% in the French general population (Revuz et al., 2008), and up to 4% in female patients attending a sexual health clinic (Jemec et al., 1996a). A recent large-scale retrospective analysis of over 48 million patients in the US found an overall prevalence of 0.10%; 0.14% for women and 0.058% for men (Garg et al., 2017).

This overall variability is not surprising, in part due to differing susceptibility in distinct populations. For example, HS appears to disproportionately affect African-Americans (Vaidya et al., 2017; Vlassova et al., 2015), at up to 3 times the rate of the general population (Garg et al., 2017). In addition, despite its characteristic clinical presentation, it is extraordinarily under-diagnosed. General practitioners, who may have no experience of the disease, are usually the first point of contact and so it is frequently misdiagnosed. Patients may also be reluctant to present for examination given the unpleasantness of the symptoms. Hence there is an average of seven years from onset of symptoms to diagnosis (Margesson et al., 2014).

The female to male ratio is 3:1 in HS (Garg et al., 2017), with onset in females frequently at menarche. Some female patients report flares with their menstrual cycle, suggesting a hormonal component, though studies have been inconclusive (Hoffman et al., 2017).

HS is also associated with low socioeconomic status which may be tied with prevalent lifestyles such as smoking or obesity (Deckers et al., 2016) (Section 1.6.5), though this may be more a consequence of the symptoms and subsequent low quality of life (Wertenteil et al., 2018).

1.6.3 Impact

Patients with HS suffer with a wide range of social and psychological consequences of the disease. These effects are associated with low socioeconomic status, with a recent

Australian study showing that HS patients were more likely to have a lower income or be unemployed compared with non-HS individuals (Calao et al., 2018). This economic burden may well be driven by additional sick days from work compared with the general public, from an additional 2.7 work days (Jemec et al., 1996b) up to 18.4 days annually per patient (Tzellos et al., 2019).

Strong negative emotions characterise the disease, including sadness and anger due to the lesional appearance, along with shame of its malodour. There is worry in patients that the treatments will not be successful and that the patient will have to suffer for decades (Esmann et al., 2016). Patients fear that others would be disgusted upon seeing their condition. Further, their pain can leave them with a feeling of powerlessness over their bodies, exacerbated by a sense that their pain severity is not fully appreciated by others. Patients frequently present with symptoms similar to that of social anxiety, including fears of being perceived negatively by others and so avoiding social interactions (Keary et al., 2019). Perhaps unsurprisingly, it has been reported that HS patients have a significantly reduced quality of sexual life, irrespective of genital lesions (Alavi et al., 2018).

The impact of depression and isolation has been shown to be more severe in HS than other dermatological patients and correlates with disease severity (Onderdijk et al., 2013). Interestingly, one study found that quality of life and depression was more associated with illness perception rather than actual disease severity (Pavon Blanco et al., 2019). In any case, it is clear that HS takes a substantial toll on patients' emotional and psychological wellbeing and should be managed and supported accordingly.

1.6.4 Classification

HS classifications of severity are essential in order to direct treatment options. There are a number of staging systems used by clinicians in classifying HS, although no apparent gold standard (Napolitano et al., 2017). The simplest and most widely used one to classify severity is the Hurley Classification System (Table 6.1A). However, it is perhaps limited given it is a static scale that does not reverse upon treatment. Other metrics include the HS Severity Index (Table 6.1B) (Grant et al., 2010), the modified Sartorius

System (Table 6.2) (Sartorius et al., 2009) and the HS Physician’s Global Assessment (PGA; Table 6.3A) (Kimball et al., 2012; Zouboulis et al., 2015). More recently, the European Hidradenitis Suppurativa Foundation Investigator Group proposed the International Hidradenitis Suppurativa Severity Score System (IHS4) as a simple, dynamic, consensus-driven method (Table 6.3B) (Zouboulis et al., 2017).

A modified version of the Hurley system has also been proposed (Prens et al., 2019). Termed the “refined Hurley classification”, it essentially subdivides both Hurley stage I and II into A (mild), B (moderate) and C (severe), thus creating 7 subgroups in total. Its aim is to create a more detailed form of HS classification and ultimately refine treatment strategies. It is yet to be seen if this new scoring system is robustly adopted.

Finally, rather than as an initial classification, the Hidradenitis Suppurativa Clinical Response (HiSCR) is a clinical endpoint to assess treatment effectiveness. It is defined as a greater than 50% reduction in inflammatory lesion count with no increase in abscesses or draining fistulae when compared to baseline (Kimball et al., 2014).

1.6.5 Risk factors

1.6.5.1 *Smoking*

An association with cigarette smoking has been observed in most epidemiological studies of HS, with up to 90% of patients having smoked tobacco (Sartorius et al., 2009), and the risk of developing HS is twice that in smokers (Garg, Papagermanos, et al., 2018). Smoking is also linked to Crohn’s disease (CD), an autoimmune disease associated with HS (Parkes et al., 2014). Although a triggering effect, smoking may not be a driver of HS disease severity (Canoui-Poitrine et al., 2009). The contributory reasons are unclear, though the pathogenic effects of smoking such as neutrophil chemotaxis, down-regulation of antimicrobial peptides, stimulation of *Staphylococcus aureus* bacteria, and keratinocyte production of TNF may play a role (Hana et al., 2007). Interestingly, neutrophil NET dysfunction has been linked with smoking, with cigarette smoke exposed mice more prone to NET formation but defective in NET degradation, and displaying more pDC activation (Qiu et al., 2017).

The AhR is a ligand dependent transcription factor expressed in Th22 and Th17 cells and is reported to play a role in IL-17 and IL-22 production (Veldhoen et al., 2008). Chemical components in cigarette smoke act as AhR ligands and have been linked with induction of Th17 cells (Quintana et al., 2008). AhR ligands can also drive production of Treg cells so there may be a complex interplay between Th17 and Treg cells upon AhR ligation, dependent on physiological conditions (Apetoh et al., 2010). A recent study of rheumatoid arthritis (RA) patients undergoing anti-TNF therapy showed smoking enhanced TNF-induced NF- κ B activation through AhR signalling, with production of IL-1 β and IL-6 (Nii et al., 2019). This IL-1 β and IL-6 increase in current smokers may have led to the observed ineffective therapeutic response in this cohort, leading to treatment discontinuation.

Cigarette smoke has also been associated with citrullination, where the non-encoded amino acid citrulline is created by posttranslational modification from arginine (Schellekens et al., 1998). Smoking is hypothesised to induce citrullination in the lungs, ultimately driving generation of anti-citrullinated protein antibodies (ACPA). These ACPA are associated with development of RA, and indeed expression of ACPA is incorporated into RA classification (Klareskog et al., 2011). It is conceivable that similar mechanisms may be contributing to the pathogenesis in HS, and citrullinated proteins and their autoantibodies have been identified in HS lesional skin (Byrd et al., 2019).

Rather than a pathogenic role, it has also been suggested that the apparent risk of smoking may in fact simply be correlative, and more a case that having such a horrible disease makes one more likely to smoke (Saleem et al., 2018).

1.6.5.2 Obesity

Obesity is associated with HS, with studies reporting an average body mass index (BMI) of 31 in people with HS (G. Kelly et al., 2015; Reddy et al., 2019). This likely contributes to the pathology rather than causation; multiple large moist skin folds driving enhanced friction leading to follicular occlusion. Obesity is also associated with thickening of the skin (acanthosis), which may play a role in follicular occlusion and intensifying subsequent inflammation.

Obesity in itself is characterised by low grade inflammation, and the risk of developing obesity related conditions is related to the degree of obesity, as well as the anatomical distribution of visceral fat (Pereira et al., 2014). Adipose tissue has its own active immune system, populated with macrophages, B cells, T cells, and ILC which may exacerbate HS (Boulenouar et al., 2017; Lynch et al., 2012). Macrophages are four-fold more populous in the adipose tissue of obese patients (Weisberg et al., 2003), and macrophages within the adipose tissue of obese HS patients have been shown to express IL-1 β and TNF (Melnik et al., 2013). Further, adipokines, the signalling molecules produced in adipose tissue, have been shown to be dysregulated in HS, with anti-inflammatory adiponectin reduced, and proinflammatory resistin and leptin increased, in HS (Malara et al., 2018). Miller et al. found a significant association between obesity and HS, particularly so between diabetes mellitus and HS (I. M. Miller et al., 2014).

1.6.5.3 Bacterial infections

A range of bacterial strains have been associated with HS lesions, potentially playing a role in triggering the disease along with its progression. However, the role of infection in HS pathogenesis is still controversial. Bacterial cultures of HS lesions have only yielded normal skin commensals, mostly *Staphylococcus* and *Corynebacterium* species (Ring et al., 2015). In fact, the authors found a reduction in bacterial aggregates (biofilm) in perilesional HS skin compared with that of healthy controls. More recently, the authors concluded that biofilm formation was more a consequence of HS inflammation rather than causative, due to inflammation-derived keratinous debris, enlarged hair follicles and sinus tract formation (Ring et al., 2017).

Further, despite efficacy of antibiotics such as rifampicin, clindamycin or tetracycline in early stage treatment for HS, the symptoms of HS frequently return. Such antibiotics also work as T cell immunomodulators (Saunte et al., 2017), which is the likely therapeutic value here. For example, doses of tetracycline that do not inhibit bacterial growth can still be immunomodulatory by inhibiting bacterial products that stimulate inflammation (Perret et al., 2014). Tetracycline has various non-antibiotic anti-inflammatory properties; acting primarily by limiting matrix metalloproteinase (MMP) synthesis by inflammatory cells as well as inhibiting the MMP produced.

1.6.5.4 Genetics

Inheritable risk factors also appear to play a role in HS pathogenesis. Overall assessment of genetic influences is complicated by the large-scale under-reporting and variable severity. Nonetheless, multiple HS familial studies in a number of different countries and ethnicities have linked mutations in the genes for the γ -secretase complex, particularly PSEN1 and NCSTN. In particular, Chinese (Wang et al., 2010), English (Pink et al., 2011), French (Miskinyte et al., 2012), Japanese (Y. Nomura et al., 2013) and African-American families (Pink et al., 2013). As γ -secretase catalyses the intramembrane proteolysis of Notch receptors, attenuated Notch signalling in the skin is implicated (T. Nomura, 2020). In mice, Notch1/Notch2 knockouts exhibit epidermal cysts and hyperkeratosis with follicular occlusion, mirroring the *Psen1*⁻/*Psen2*⁻ mice phenotype (Pan et al., 2004). In any case, Notch and γ -secretase mutations are only seen in a very small subset of HS patients, suggesting additional, unidentified genes also predispose to HS, emphasising the multifactorial nature of the condition (Liu et al., 2016).

Other gene mutations associated with HS include a missense mutation in the connexin-26 gene (Montgomery et al., 2004), FGFR2 (Higgins et al., 2017) and OCRL1 (Marzuillo et al., 2018). An increased copy number of the genes DEFB103 and DEFB4 is also reported to be a risk factor (Giamarellos-Bourboulis et al., 2016). In relation to immune regulation genes, a single nucleotide polymorphism (SNP) in the TNF gene was found to be related to a more severe phenotype (Savva et al., 2013), as was a SNP in IL-12Rb1 (Giatrakos et al., 2013).

Given the evidence thus far, it is likely that there are multiple genes contributing to a predisposition to HS, or linked to the age of onset or disease severity, but environmental factors and aberrant immune regulation are more impactful to HS pathogenesis.

1.6.6 Pathogenesis

Although HS pathogenesis is still uncertain, it clearly originates at the hair follicle. It most likely initiates with hyperkeratosis, then follicular dilation and occlusion, followed by cyst formation. Once the cyst ruptures, a potent immune response ensues, with immune cell influx and associated inflammation (Figure 1.4).

Follicular occlusion may initially be driven by a genetic predisposition to keratinisation of the infundibulum, or exogenous factors such as the microflora, smoking, obesity and/or mechanical stress. Keratinocytes derived from HS patients' follicular ORS have been shown to have a proinflammatory phenotype when compared with healthy controls, with aberrant production of CXCL10 (IP-10) and CCL5 (RANTES) (Hotz et al., 2016). These keratinocytes, upon PRR stimulation, produce IL-1 β , driving the production of TNF, IL-6 and IL-8. These initial occurrences may contribute to follicular plugging, leading to cyst formation.

In fact, the ORS in HS patient skin has recently been shown to have an increased number of proliferating progenitor cells with a loss of quiescent ORS stem cells (Orvain et al., 2020). The replication fork speed was increased by 2-3 fold in HS patient ORS stem cells relative to healthy control ORS, a phenomenon which induces DNA replication stress and genomic instability (Maya-Mendoza et al., 2018). The resultant accumulation of endogenous cytoplasmic ssDNA and micronuclei induces IFN synthesis through the IFI16-STING pathway, which establishes chronic inflammation.

Rupture of the dilated hair follicle likely scatters its contents intradermally, including keratin fibres, dermal detritus, and multiple DAMPs and PAMPS (van der Zee et al., 2012). This may then trigger multiple immune pathways such as IL-17/IL-23, the NLRP3 inflammasome and TLR activation (Vossen et al., 2018). This subsequently involves a diverse immune cell infiltrate and skin structural alterations, leading to cyst formation.

The final stage leading to severe HS is chronic inflammation and sinus tract formation. Fibrotic factors and proliferating epithelial strands, which continuously propel the immune system, result in scarring and tunnelling. These cavities may join together, or burrow to distal areas. Such tracts are very hospitable to biofilms, again driving inflammation and the characteristic suppurative, malodorous discharge. Globally, this uncontrolled inflammation may elicit a systemic response and prompt the early inflammatory events again in distant susceptible regions.

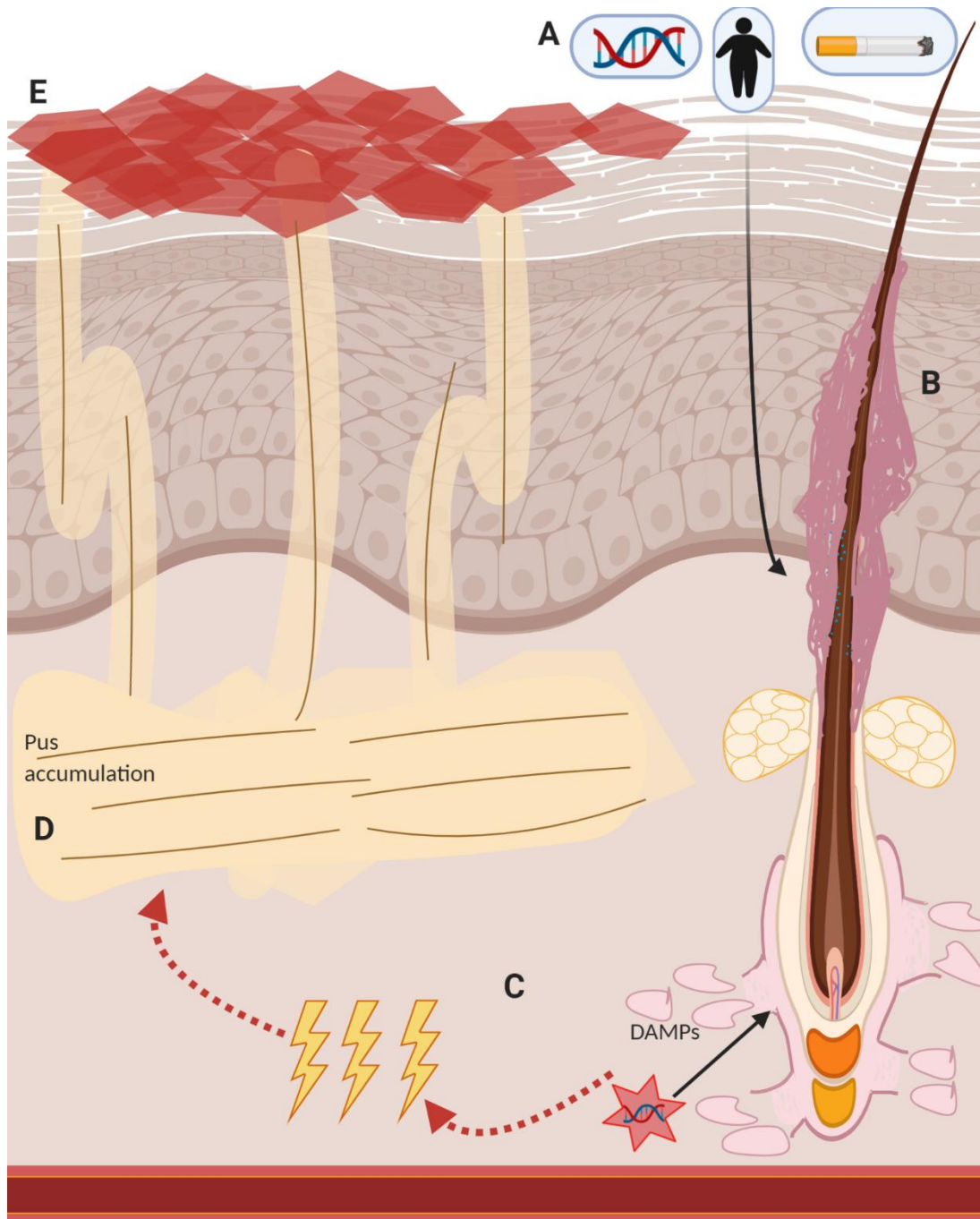


Figure 1.4 HS pathogenesis.

HS pathogenesis is likely triggered by some underlying endogenous (obesity, genetic predisposition) or exogenous (smoking, bacterial infection) risk factor (A) and is characterised by hyperkeratosis and follicular dilation and release of ORS DAMPs (B), leading to cyst formation. Upon follicular cyst rupture, DAMPs are released, driving a potent immune response (C). Chronic inflammation leads to sinus tract formation and tunnelling (D), with inflammatory lesions (E).

1.6.7 Immune dysregulation in HS

A homeostatic immune system is maintained through the balance of the pro-inflammatory and tolerogenic tiers of the immune system. However, a numerical or functional disparity in this equilibrium can lead to immune dysregulation. Where pro-inflammatory responses are unhindered, allergy and autoimmunity can prevail. In many cases the aetiology of autoimmune conditions is unknown, but may be associated with some infections, environmental triggers and genetic predispositions. They are categorised as organ-specific or systemic diseases and may be mediated by self-antibodies and Tc cells, but always require Th cell involvement. Autoimmune diseases involve both innate and adaptive responses, whereas autoinflammatory diseases are associated with over-activation of innate responses exclusively.

It is now accepted that dysregulated immune responses play a role in HS pathogenesis, given the association of HS with various autoimmune conditions. Further, the disease is characterised by numerous proinflammatory cytokines being aberrantly expressed. Immune-modifying therapies have proven very successful in patients with moderate to severe disease and are now an established intervention (Section 1.6.8).

HS has been linked to the autoimmune skin disease pyoderma gangrenosum (PG) and forms part of the PG, acne, suppurativa hidradenitis (PASH) triad, with IL-1 β and IL-17 induction observed in both conditions (G. Kelly et al., 2015; Marzano et al., 2014; Marzano et al., 2010).

An association between HS and IBD has been proposed in numerous studies (Church et al., 1993; van der Zee et al., 2010). In particular, the autoimmune condition CD seems to be linked, with a cross-sectional study reporting that HS was significantly associated with CD but not ulcerative colitis (Shalom et al., 2016). Both HS and CD have a similar age of onset and have been linked to smoking, and a recent, large-scale study showed that HS patients are three-times more likely to develop CD (Garg, Hundal, et al., 2018). However, there is little evidence as yet to show a common cellular or molecular pathogenesis to both diseases, although a 2015 study showed for the first time a prevalence of CD161⁺

T cells in patients with both conditions, along with the same T cell clones identified in the PBMC, gut and HS lesion (Giudici et al., 2015).

Irregular cytokine levels have been observed in HS patient skin and PBMC, with elevated levels of IL-1 β , IL-23 and IL-17 having been reported in HS lesions, (Hotz et al., 2016; G. Kelly et al., 2015; Lima et al., 2015; Schlapbach et al., 2011; van der Zee et al., 2012; van der Zee et al., 2011; Wolk et al., 2011). In addition, increased amounts of serum IL-17 has been observed in HS patients (Matusiak et al., 2017). Elevated TNF and IL-10 have also been reported (G. Kelly et al., 2015; van der Zee et al., 2011), with reduced levels of IL-22 (Wolk et al., 2011). More recently, those of the IL-1 family such as IL-6, IL-36 and IL-38 have been implicated, with levels of IL-1 β and IL-36 increased in HS skin compared to healthy controls, whereas IL-38 was higher in perilesional HS skin but lower in the lesion (Di Caprio et al., 2017; Hessam et al., 2018; Witte-Handel et al., 2019).

1.6.8 Treatments

HS is frequently under-reported and then often misdiagnosed, and so early presentation to a specialist dermatologist is unlikely. In any case, therapeutic interventions are varied and frequently unsatisfactory (Alikhan et al., 2009). Medical direction may include lifestyle changes such as weight loss, smoking cessation, and wearing loose clothing. Topical creams such as acne washes may bring some relief, while antibiotics are usually prescribed and can quell infection and arrest new breakouts.

The anti-diabetes treatment metformin, as well as the chemotherapeutic drug methotrexate, have had success in suppressing flares, although the mechanisms for both are unclear. Likewise, the contraceptive pill and retinoids have had reported benefits (A. K. Clark et al., 2017).

Lesions and dermal tunnelling may warrant surgical intervention; examples being laser surgery, de-roofing (turning deep tracts into scars), incision and drain, or excision and skin graft (Alharbi et al., 2012). A novel technique with less severe morbidity is the placement of setons; non-absorbable nylon sutures guided through the lesion and tied externally (Lajevardi et al., 2015). The compression created along with the local

inflammatory reaction of adjacent tissues initiates fibrosis, and is an established intervention in anal fistulae (M. E. Kelly et al., 2014).

Biologics are showing promise in treating HS (Table 1.3). The TNF inhibitor adalimumab (Humira™/ Hefiya™) is a monoclonal antibody directed towards soluble and membrane-bound TNF, and is the only FDA- and EMA- approved treatment for moderate to severe HS (Section 6.1). Early studies showed a significant reduction in HS severity (I. Miller et al., 2011); with phase III trials confirming optimal dosage and reporting significantly higher clinical response rates at 12 weeks compared with placebo (Kimball et al., 2016).

Infliximab (Remicade™) is a chimeric monoclonal antibody that binds TNF and prevents its downstream effects. It is licenced for the treatment of RA, AS, ulcerative colitis, psoriatic arthritis, psoriasis and CD, and its efficacy in HS was first noted when CD patients being treated with infliximab had improvement in their HS (Katsanos et al., 2002; Martinez et al., 2001). To date, only one randomised clinical trial has been performed, with relatively low numbers reaching the primary endpoint (Grant et al., 2010). However, infliximab may be a preferable treatment for cases of more severe, recalcitrant HS, with or without CD (van Rappard et al., 2012). Other TNF inhibitors have had mixed results, with promising clinical trial results from infliximab (Remicade™; NCT00795574), but disappointing outcomes for etanercept (Enbrel™; NCT00107991) (Maarouf et al., 2017).

IL-17A blockade therapies hold promise. Secukinumab (Cosentyx™) is still undergoing trials (NCT03099980) but appears positive through case reports (Thorlacius et al., 2018). However, surprising adverse reactions have been reported (Marasca et al., 2019), whereby a psoriasis patient developed HS following secukinumab treatment in an apparently paradoxical manner; similar to reactive conditions reported in anti-TNF therapies (Conrad et al., 2018; Moran et al., 2020). A trial for the IL-17A and IL-17F dual-targeting bimekizumab has completed Phase II (NCT03248531), anecdotally yielding promising results. Ustekinumab (Stelara™) inhibits both IL-12 and IL-23 as it binds to their p40 subunit, hence potentially constraining both Th1 and Th17 responses. Studies show clinically meaningful improvement (NCT01704534) (Blok et al., 2016). However,

similar to the secukinumab event above, there has also been a case report of a psoriasis patient treated with ustekinumab developing HS (Gkini et al., 2018).

The IL-1 α inhibitor bermekimab (Xilonix™) and IL-1 receptor A (IL-1Ra) antagonist anakinra (Kinerit™) both appear to have reached satisfactory endpoints in clinical trials for moderate to severe HS (NCT02643654 and NCT01516749 respectively). Intriguingly, there is a case report of CD20 blockade via Rituximab (Rituxin™) completely ablating HS in a patient with chronic active antibody-mediated rejection following a kidney transplant (Takahashi et al., 2018). Likewise, rituximab has been shown to inhibit proinflammatory cytokines in a HS explant model (Vossen et al., 2019).

Trials for other likely targets have yielded disappointing results. For example, a 2016 trial for IFX-1, which is directed against complement C5a, as yet has no results posted (NCT03001622), suggesting unsatisfactory outcomes. Similar for the 2016 trial of apremilast (Otezla™), a phosphodiesterase 4 inhibitor (NCT02695212).

Target	Name	Brand name	Manufacturer	Main indications
TNF	Adalimumab	Humira™, Hefiya™	Abbvie	RA, CD, UC, PsO), PsA, AS, uveitis, JIA, HS
TNF	Infliximab	Remicade™	Janssen	RA, CD, UC, PsO, PsA, AS, HS*
TNF-R	Etanercept	Enbrel™	Amgen	RA, CD, UC, PsO, PsA, AS
IL-1 α	Bermekimab	Xilonix™	XBiotech	CRC*, PsO*, AD*, HS*
IL-1Ra	Anakinra	Kinerit™	SOBI	RA, NOMID, HS*
IL-1 β	Canakinumab	Ilaris	Novartis	JIA, PFS
IL-17A	Ixekizumab	Taltz™	Lilly	PsO, PsA
IL-17A	Secukinumab	Cosentyx™	Novartis	PsO, PsA, AS, HS*
IL-17A & IL-17F	Bimekizumab		UCB	PsO, PsA, AS, HS*
IL-17-R	Brodalumab	Kyntheum™	Leo Pharma	PsO, HS*
IL-12 & IL-23	Ustekinumab	Stelara™	Janssen	CD, PsO, PsA, HS*
IL-23	Guselkumab	Tremfya™	Janssen	PsO, HS*
IL-23	Tildrakizumab	Ilumya™	Sun Pharma	PsO
IL-23	Risankizumab	Skyrizi	Abbvie	CD, UC, PsO, PsA, AD
CD20	Rituximab	Rituxan™, Mabthera™	Roche	RA, V, SLE

Table 1.3 Relevant biological therapeutics targeting autoimmune and inflammatory disease.

AD: atopic dermatitis, AS: ankylosing spondylitis, CD: Crohn's disease, CRC: colorectal cancer, HS: hidradenitis suppurativa, JIA: juvenile idiopathic arthritis, NOMID: neonatal-onset multisystem inflammatory disease, PFS: periodic fever syndromes, PsA: psoriatic arthritis, PsO: plaque psoriasis, RA: rheumatoid arthritis, SLE: systemic lupus erythematosus, UC: ulcerative colitis, V: vasculitis. * undergoing clinical trials, not approved.

1.7 Working hypothesis

HS is a poorly understood chronic inflammatory skin disease with unsatisfactory treatments, characterised by aberrant immune responses. Identifying the key cellular players and their transcriptional, phenotypic and functional profile will contribute to the understanding of HS pathology and may propose novel targets and therapeutics.

1.8 Aims

To identify the key immune cells involved in HS pathogenesis and analyse their function and interplay to uncover new therapeutic options, or to underscore existing ones.

1. Assess the immune cell profile in HS skin.

Using optimal dissociation techniques, single immune cells from lesional HS skin and healthy control skin will be characterised to confirm and quantify immune cell populations. Tissue sample characterisation will involve:

- single cell gene expression analysis via scRNA-Seq
- histological imaging
- flow and imaging cytometry

2. Characterise T cell function in HS patients.

T cells, in particular Th17 cells, have been implicated in HS. The aim of this strand of the study is to establish the frequency and role of T cells in the blood and skin of HS patients.

T cell characterisation will involve:

- flow cytometric analysis of blood and skin samples
- intracellular cytokine analysis of T cell subsets
- comparison with samples from anti-TNF treated HS patients

Chapter 2

Materials and Methods

2 Materials and Methods

2.1 Materials

2.1.1 PBMC preparation

Product	Company
PBS (phosphate buffered saline)	Sigma Aldrich
Lithium heparin phlebotomy tubes	BD Biosciences
DMSO (dimethyl sulfoxide)	Sigma Aldrich
Lymphoprep	Fresenius Kabi

2.1.2 Complete IMDM preparation

Product	Company
Iscove's Modified Dulbecco's Medium (IMDM)	Sigma Aldrich
Foetal calf serum (FCS)	BioSera
L-Glutamine–Penicillin–Streptomycin solution (PSG)	Sigma Aldrich

2.1.3 T cell stimulation

Product	Company
Phorbol 12-myristate 13-acetate (PMA)	Sigma Aldrich
Ionomycin (I)	Sigma Aldrich
Brefeldin A	Sigma Aldrich

2.1.4 Other materials

Product	Company
123count eBeads Counting Beads	Thermo Fisher Scientific
Brilliant stain buffer	BD Biosciences
Bovine serum albumin (BSA)	Sigma Aldrich
Collagenase from Clostridium histolyticum Type 1A	Sigma Aldrich
CryoStor™ cell cryopreservation media	Stem Cell Technologies
Fc Block	BD Biosciences
Fixable Viability Dye eFluor™ 506 (FixVia eF506)	Thermo Fisher Scientific
FoxP3 Staining Kit	eBioscience
Hoechst 33342	Thermo Fisher Scientific
SYTOX™ Blue dead cell stain	Thermo Fisher Scientific
Trypan Blue	Sigma Aldrich
Whole Skin Dissociation Kit, human	Miltenyi Biotec

2.1.5 Cytometry antibodies

Antibody	Fluorochrome	/50 µl	Supplier	Clone
all anti-human				
CD3	BV650	1.25	BD Biosciences	UCHT1
CD3	BV711	1.25	BD Biosciences	UCHT1
CD4	PE-CF594	1.25	BD Biosciences	L200
CD8	APC-eF780	1.25	eBioscience	SK1
CD14	BV786	1.25	BD Biosciences	M5E2
CD16	PerCP-Cy5.5	1.25	BD Biosciences	3G8

CD19	BV711	2.5	BioLegend	HIB19
CD20	APC	8	BD Biosciences	2H7
CD25	PE-Cy7	2.5	eBioscience	BC96
CD38	AF488	1.25	BioLegend	HIT2
CD39	PerCP-eF710	2.5	eBioscience	eBioA1
CD45	AF700	1.25	eBioscience	HI30
CD45	APC-Cy7	2	BioLegend	2D1
CD64	BV421	1.25	BD Biosciences	10.1
CD123	BV605	1.25	BD Biosciences	7G3
CD127	APC-eF780	2.5	eBioscience	eBioRDR5
CD161	PE-Cy5	5	BD Biosciences	551138
CLA	BV421	1.25	BD Biosciences	HECA-452
CTLA-4	BV786	1.25	BD Biosciences	BN13
FoxP3	PE	1.25	eBioscience	236A/E7
GM-CSF	PE	1.25	BioLegend	BVD2-21C11
HLA-DR	PE	1.25	BD Biosciences	G46-6
IFN- γ	BV605	1.25	BD Biosciences	B27
IL-2	PE-CF594	1.25	BD Biosciences	5344.111
IL-10	BV786	0.625	BD Biosciences	JES3-9D7
IL-17	AF488	1.25	BioLegend	BL168
IL-22	PE-Cy7	1.25	eBioscience	22URT1
Ki67	A488	1.25	BD Biosciences	B56
TCR- $\gamma\delta$	BV650	1.25	BD Biosciences	B1
TNF	PerCP-Cy5.5	1.25	eBioscience	Mab11

2.2 Methods

2.2.1 Patient recruitment

All studies were reviewed and approved by the St. Vincent's Healthcare Group Ethics and Medical Research Committee, Dublin. Patients were recruited during dermatology or surgical consultation at St Vincent's Hospital Dermatology Department and St Michael's Hospital Surgical Theatres respectively. Healthy control samples were donated by volunteers at St Vincent's Hospital Dermatology Department, St Vincent's Private Hospital Plastic and Reconstructive Surgery Clinic, and Trinity Biomedical Sciences Institute. The project was discussed with all patients and they were presented with a patient information leaflet and consent form. In particular, it was clearly explained to them that participation would not affect their medical care in any way. All patients and healthy volunteers provided full informed consent. Patient and healthy control clinical information is detailed in the relevant sections of this thesis.

2.2.2 Isolation and cryopreservation of PBMC

Blood was collected by a trained, authorised phlebotomist into lithium heparin tubes, kept at room temperature (RT, 22°C), and processed within 24 hours (h). Blood was diluted 1:1 with sterile PBS, and 25 ml diluted blood was carefully layered over 17.5 ml Ficoll-Hypaque (Lymphoprep; density 1.077g/ ml) per tube. PBMC were isolated by density-gradient centrifugation at 800 g for 20 minutes (min) at RT, ensuring the brake was off. The white interface layer containing the PBMC was removed using a Pasteur pipette, at 10 – 15 ml per tube, transferred to a fresh tube, resuspended to 50 ml in sterile PBS, and then centrifuged at 600 g for 10 min. The supernatant was then removed, the pelleted cells resuspended to 50 ml sterile PBS, and centrifuged at 300 g for 10 min. This supernatant was then discarded and the PBMC pellet resuspended in cold, heat-inactivated (at 56°C for 30 minutes) FCS, and cells counted (see 2.2.3). An equal volume of 2X freezing mix (20% dimethyl sulfoxide [DMSO] in FCS) was then added dropwise, with aliquots of $2.5 - 5 \times 10^6$ cells added to cryovials and frozen immediately in CoolCell freezing containers at -80°C (at a rate of -1°C per min). Cryovials were transferred to liquid nitrogen tanks after 24 h for long term storage.

2.2.3 Cell counting

Cells in suspension were diluted in Trypan Blue, and visualised under a microscope using a haemocytometer; dead cells stain dark blue in Trypan Blue. Viable (clear) cells in one or more squares (containing the 16 sections) of the haemocytometer were counted, and the total number of cells were calculated using the formula as follows:

$$\text{Total cells} = \text{cells counted per square} \times \text{dilution factor} \times 10^4 \text{ cells per ml}$$

Where microparticle beads of a known concentration (e.g. 123count eBeads counting beads) were added to samples before cytometric analysis, cell counts were calculated using the following formula:

$$\text{Absolute count (cells/}\mu\text{l)} = \frac{(\text{cell count} \times \text{bead volume})}{(\text{eBeads count} \times \text{cell volume})} \times \text{eBead concentration}$$

2.2.4 Complete media selection and preparation

Complete Roswell Park Memorial Institute medium (cRPMI) is an established culture medium for the maintenance and stimulation of T cells. However, there is evidence that cRPMI contains too little Ca^{2+} for maximal ionomycin stimulation and that cIMDM is more suitable (Zimmermann et al., 2015). In order to determine the optimal media to use for subsequent experiments, PBMC were treated with PMA and ionomycin (PMA/I) and Brefeldin A in the presence of cIMDM or cRPMI media. CD4 and CD8 T cell cytokine detection via intracellular cytokine staining was then performed. T cells stimulated in cIMDM yielded an approximately 100% increase in TNF and 25% increase in IFN- γ production when compared with cRPMI (Figure 2.1). IL-2 production in CD4 and CD8 T cells also displayed a two-fold increase when stimulated in cIMDM (data not shown). No difference in frequency of CD3, CD4 or CD8 T cells was noted between either media conditions. Hence cIMDM was selected for use in all successive experiments.

To prepare complete IMDM (cIMDM) 500 ml IMDM was supplemented with 50 ml heat-inactivated FCS and 5 ml PSG.

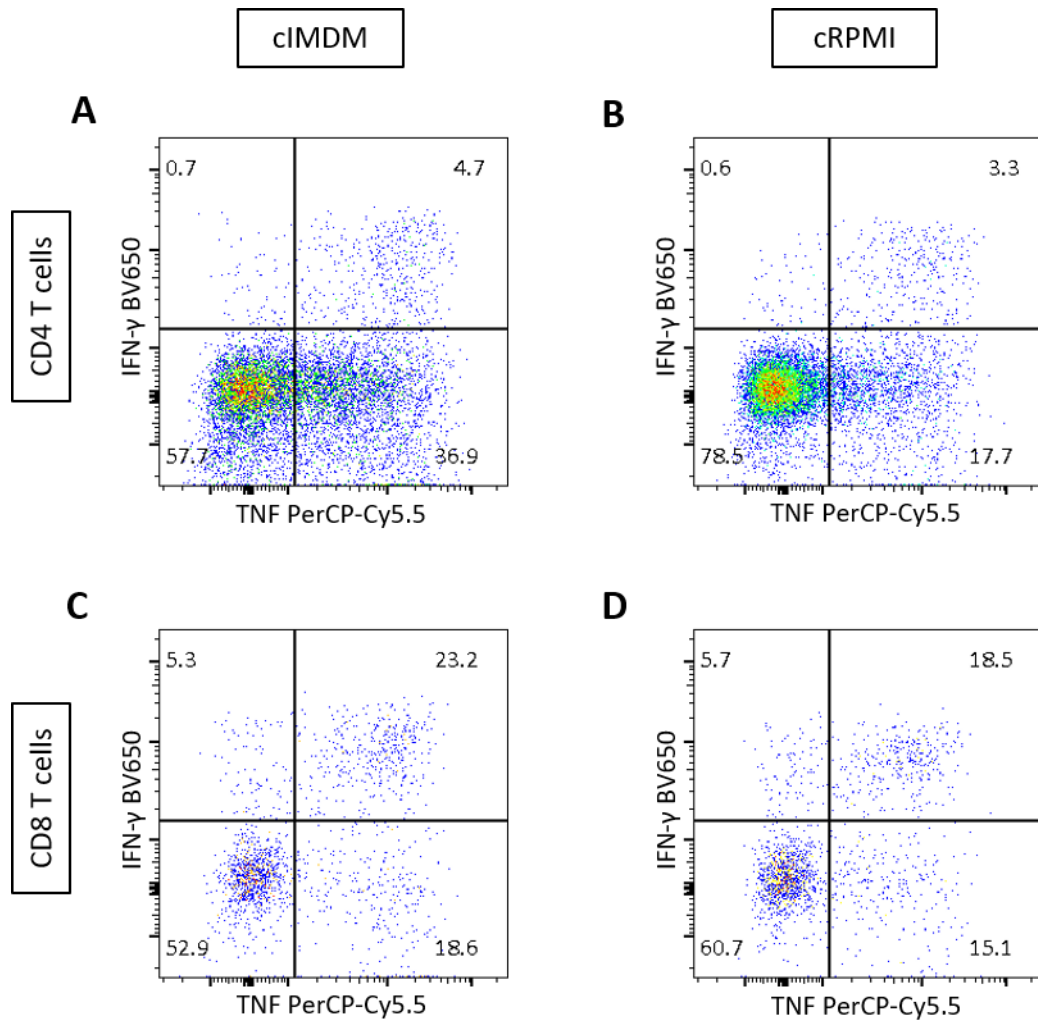


Figure 2.1 cIMDM is the optimal medium for T cell stimulation.

PBMC from a healthy donor were treated with PMA/I and Brefeldin A for 5 h, stained for surface and intracellular markers, and analysed by flow cytometry. Representative dot plots display TNF and IFN- γ expression. Plots **A** and **B** are gated on CD4 T cells, plots **C** and **D** are gated on CD8 T cells. Plots **A** and **C** were stimulated in cIMDM, **B** and **D** in cRPMI medium. Approximately 100% more TNF and 25% more IFN- γ were detected when PBMC were stimulated in cIMDM rather than cRPMI medium. Plots are representative of three experiments.

2.2.5 Single cell preparation from skin biopsy

2.2.5.1 Protocol I

(applicable to chapter 3; Phenotypic and transcriptomic characterisation of hidradenitis suppurativa skin)

Human skin (a 3 or 6 mm biopsy, excised surgical tissue from HS seton intervention, or excess tissue from breast reduction surgery) was placed in a dry, sterile tube for transfer to TCD. The sample was cut in half (approximately), and one half preserved in a vial of 10% formalin for subsequent histopathology analysis (Section 2.2.15). The remainder was weighed, then processed into a single cell preparation using the Miltenyi Biotec Whole Skin Dissociation Kit.

The samples for the Whole Skin Dissociation Kit were washed in PBS, then diced with a scalpel into approximately 1 mm pieces. 435 µl of Buffer L was transferred into an empty gentleMACS C tube. Enzyme P (12.5 µl) was then added only when cell yield was a priority (i.e. samples for single cell RNA sequencing [scRNA-Seq]), given its potency as a dissociating agent with subsequent damage to some cell surface proteins (Figure 2.2). Hence Enzyme P was omitted when epitope integrity took precedence (i.e. samples for phenotypic analysis only). 50 µl of Enzyme D and 2.5 µl of Enzyme A were then added and the solution gently mixed.

The skin sample was then added (maximum size of 6 mm biopsy approximately per gentleMACS C tube) and incubated in a water bath at 37°C for 3 h, followed by addition of 500 µl cold cIMDM. The gentleMACS C tube was then inserted into the mechanical gentleMACS Dissociator and the program h_skin_01 run (this gently rotates and macerates the sample for 37 seconds). Following the cycle, the sample was centrifuged briefly to collect the sample at the bottom of the tube, and then passed through a 70 µm filter into a 50 ml tube. To help filter the biopsy, the plunger of a 1 ml syringe was used to disrupt the tissue through the mesh filter. The filter was then washed through with 4 ml cold IMDM. Next, the filtered sample was centrifuged at 300 g for 10 min at 4°C, and the sample then resuspended in an appropriate volume of PBS. With regard to cells for subsequent scRNA-Seq, 90% of the sample was resuspended in CryoStor

cryopreservation media, added to cryovials and frozen immediately in CoolCell freezing containers at -80°C (at a rate of -1°C per min). Cryovials were transferred to liquid nitrogen tanks after 24 h. The remaining 10% of the sample was used for same day flow cytometric analysis (Section 2.2.7).

2.2.5.2 Protocol II

(applicable to chapter 4; Hidradenitis suppurativa is characterised by T cell dysregulation)

Human skin was biopsied (6 mm) by the clinician and placed in a dry, sterile tube for transfer to TCD. The biopsy was then diced with a scalpel into approximately 1 mm pieces and transferred into a 5 ml tube with 3 ml collagenase solution (5 mg/ml collagenase A1, in PBS with 1% FCS). The sample was incubated in a water bath at 37°C for 3 h; then passed through a 70 µm mesh filter. To help filter the biopsy, the plunger of a 1 ml syringe was used to disrupt the tissue through the mesh filter. PBS was used to wash the cells through, and the tube then centrifuged at 300 g for 5 min. The pellet was resuspended in cIMDM.

Protocol II is almost certainly a less optimal procedure than Protocol I. However, as this aspect of the project commenced with this procedure, it was pertinent to maintain the same method throughout this trial for consistency and controlled comparisons.

	A	B	C	D	E
	gMACS + P 3 hours	gMACS - P 3 hours	gMACS + P 16 hours	Collagenase 3 hours	Collagenase 16 hours
Yield	Good	Fair	Fair	Poor	Bad
CD3	Good	Good	Good	Good	Fair
CD4	Poor	Good	Bad	Bad	Bad
CD8	Poor	Good	Bad	Fair	Bad
CD11c	Fair	Good	Bad	Fair	Poor
CD14	Good	Good	Bad	Bad	Bad
CD16	Poor	Poor	Poor	Poor	Good
CD19	Good	Good	Poor	Fair	Bad
CD20	Poor	Good	Bad	Good	Bad
CD38	Fair	Good	Bad	Bad	Bad
CD45	Good	Good	Fair	Good	Fair
CD64	Fair	Good	Bad	Fair	Poor
CD123	Fair	Good	Bad	Poor	Bad
CD161	Poor	Good	Bad	Good	Bad
HLA-DR	Good	Good	Fair	Good	Fair

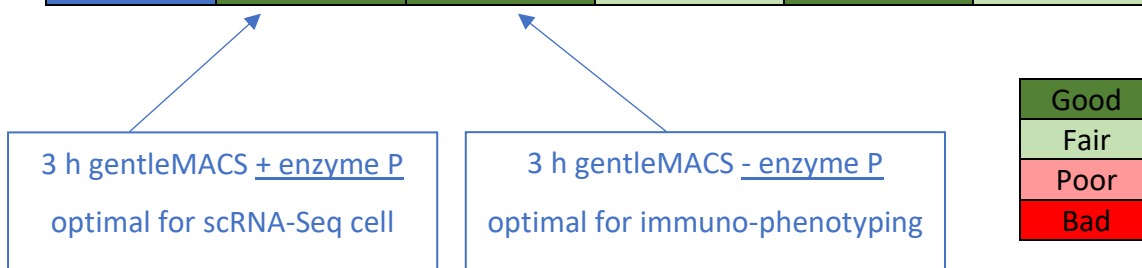


Figure 2.2 Classification of epitope damage during skin dissociations protocols.

Schematic shows empirical observation of effect of skin dissociation protocols on cell yield and epitope damage. Columns show differing treatments; 3 h gentleMACS incubation including Enzyme P (Protocol 2; **A**), 3 h gentleMACS incubation excluding Enzyme P (**B**), 16 h gentleMACS incubation including Enzyme P (**C**), 3 h Collagenase A1 incubation (Protocol 1; **D**) and 16 h Collagenase A1 incubation (**E**). Cell yield efficiency and epitope integrity are expressed in heat-map form from deep green (optimal marker detection) to deep red (bad /no expression detected).

2.2.6 T cell stimulation with PMA and ionomycin

For intracellular cytokine analysis, PBMC or dissociated skin cells were treated with 50 ng/ml PMA and 500 ng/ml ionomycin (PMA/I) in the presence of the protein transport inhibitor Brefeldin A (5 µg/ml) in cIMDM. Samples were then placed in an incubator at 37°C for 16 h. Unstimulated controls were treated with Brefeldin A (5 µg/ml) alone in the absence of PMA/I.

2.2.7 Surface staining for flow cytometry

Cells were treated as appropriate (e.g. rested, stimulated), after which 2 ml PBS was added and cells centrifuged at 300 g for 5 min, and the supernatant discarded. 50 µl FixVia eF506 in PBS (1:1000) was added, incubated in the dark at RT for 15 min, along with 2 µl Fc block where appropriate to minimise Fc receptor “non-specific” antibody binding. 2 ml PBS was added, and cells centrifuged at 300 g for 5 min, and the supernatant discarded. The cell pellet was resuspended in 50 µl PBS containing antibodies targeting surface membrane proteins. A master mix was prepared when multiple antibodies were used. Where more than one BD Horizon Brilliant™ fluorochrome was used, Brilliant stain buffer was added to the mix. Samples were incubated in the dark at RT for 15 min before adding 2 ml PBS, then centrifuged for 5 min at 300 g, and the supernatant discarded. Sample pellets were then resuspended in 200 µl PBS, including 123count eBeads counting beads if acquiring on the cytometer directly. Where subsequent intracellular/ intranuclear staining was required, see section 2.2.8 below.

2.2.8 Intracellular and intranuclear staining for flow cytometry

When staining with antibodies for intracellular and/or intranuclear markers, the protocol was performed using the FoxP3 Staining kit, beginning with surface staining (Section Surface staining for flow cytometry). After antibody staining for cell surface antigens, the cell pellet was resuspended in 200 µl cell fixative solution (working solution: 1-part Fixation/Permeabilisation Concentrate with 3-parts Fixation / Permeabilisation Diluent), and incubated in the dark at RT for 20 min. 1 ml 1X permeabilisation buffer (PB; 1-part 10X Permeabilisation Buffer to 9-parts deionised

water) was then added and samples centrifuged at 300 g for 5 min. The pellet was resuspended in 50 μ l solution containing PB, with the antibodies for intracellular/intranuclear proteins, as well as Brilliant stain buffer if appropriate. A master mix was prepared when multiple antibodies were used. Samples were incubated in the dark at RT for 20 min before adding 2 ml PBS, centrifuging for 5 min at 300 g, and discarding supernatant. Sample pellets were then resuspended in 200 μ l PBS, including 123count eBeads counting beads, kept at 4°C and acquired on the cytometer within 24 h (Figure 2.3).

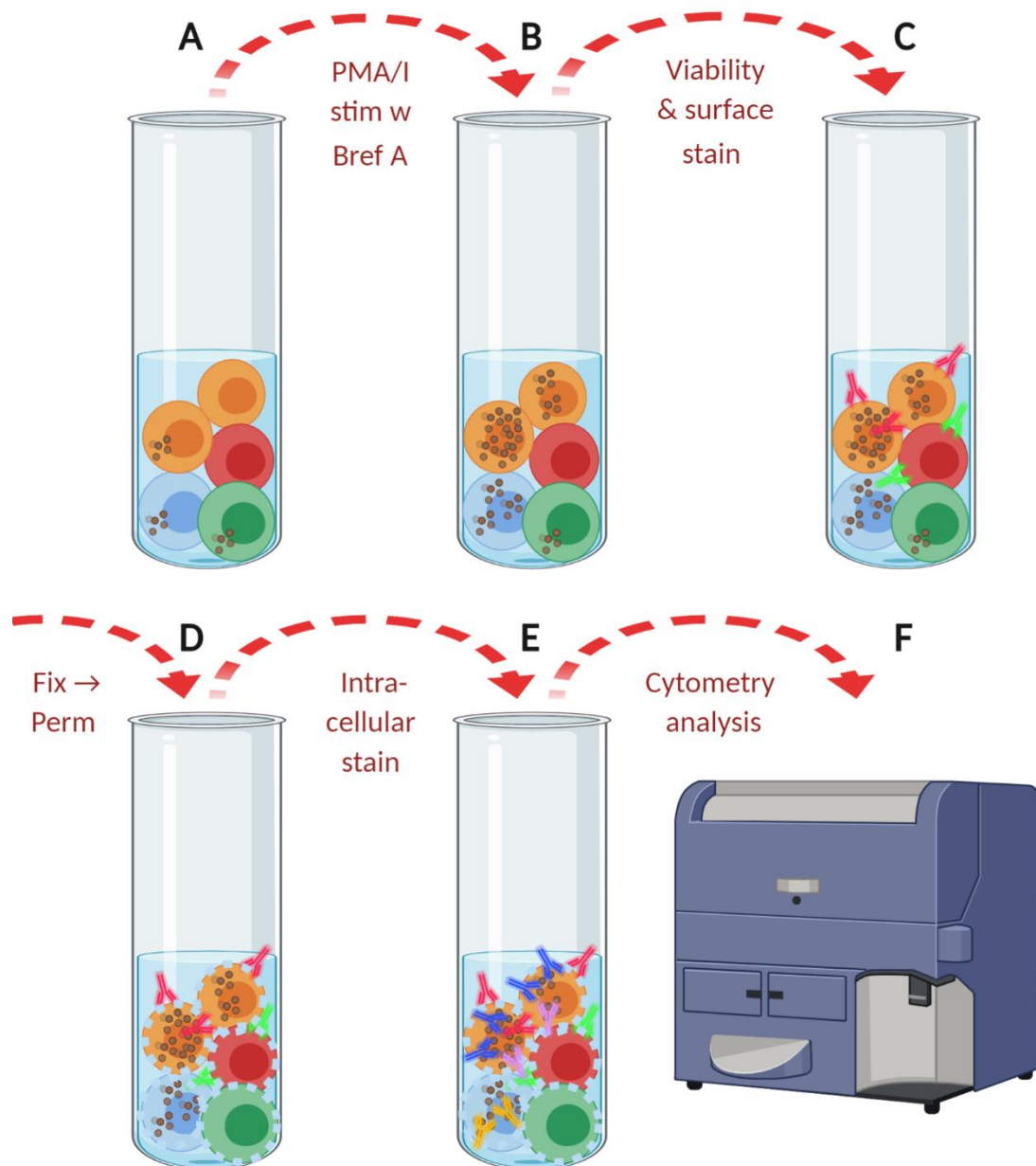


Figure 2.3 Workflow for intracellular cytokine analysis.

Graphic showing the workflow for intracellular cytokine staining, whereby a single cell preparation (A) was treated with PMA/I and Brefeldin A for 16 h in an incubator at 37°C (B), then labelled for viability and surface markers (C). Cells were then preserved (fixed) and their cell membrane permeabilised (D), and then labelled with antibodies targeting intracellular proteins and cytokines, as well as intranuclear proteins (E). Upon washing through centrifugation, flow cytometry was then performed within 24 h on the BD LSRFortessa system (F).

2.2.9 Cytometer set up

The LSRFortessa cytometer (BD Biosciences, San Jose, USA) is configured as a four laser (405 nm, 488 nm, 561 nm and 640 nm), 18 parameter system. Fluorochrome panels were optimally designed to minimise spectral spillover and maximise resolution. Each antibody was titrated to identify the appropriate test concentration. Prior to sample acquisition, voltages were set using single colour controls such that each fluorochrome was detected highest in its primary channel, with maximal signal to noise. These single colour (compensation) controls were treated similar to test samples; e.g. fixed and permeabilised as appropriate, since such treatments may alter the spillover characteristics of the fluorochrome. Brilliant stain buffer was used when staining cells with multiple BD Horizon Brilliant™ polymer conjugates to control for their unwanted interactions. Table 2.1, Table 2.2 and Table 2.3 detail the epitope targets (antibodies) and fluorochromes in each cytometry panel, and their corresponding detectors (configuration).

	Panel 1	
Configuration	Epitope	Fluorochrome
(488) 530/30	CD38	AF488
(488) 695/40	CD16	PerCP-Cy5.5
(633) 670/14	CD20	APC
(633) 730/45	CD45	AF700
(633) 780/60		
(405) 450/50	CD64	BV421
(405) 525/50	FixVia	eF506
(405) 610/20	CD123	BV605
(405) 660/20	CD3	BV650
(405) 710/50	CD19	BV711
(405) 780/60	CD14	BV786
(561) 582/15	HLA-DR	PE
(561) 610/20	CD4	PE-CF594
(561) 670/30	CD161	PE-Cy5
(561) 710/50		
(561) 780/60	CD8	PE-Cy7
	CD16/CD32	Fc Block

Table 2.1 Cytometric fluorochrome panel for immunophenotyping skin samples.

Cells isolated from the skin were stained for the surface markers listed above, and analysed by flow cytometry within 2 h. This panel was applied to samples in Results Chapter 3.

	Panel 2	
Configuration	Epitope	Fluorochrome
(488) 530/30	IL-17	AF488
(488) 695/40	TNF	PerCP-Cy5.5
(633) 670/14		
(633) 730/45	CD45	AF700
(633) 780/60	CD8	APC-eF780
(405) 450/50	CLA	BV421
(405) 525/50	FixVia	eF506
(405) 610/20	IFN- γ	BV605
(405) 660/20	TCR- $\gamma\delta$	BV650
(405) 710/50	CD3	BV711
(405) 780/60	IL-10	BV786
(561) 582/15	GM-CSF	PE
(561) 610/20	IL-2	PE-CF594
(561) 670/30	CD161	PE-Cy5
(561) 710/50		
(561) 780/60	IL-22	PE-Cy7

Table 2.2 Cytometric fluorochrome panel for analysis of PMA/I stimulated T cells in PBMC and skin samples.

PBMC or cells isolated from the skin were treated with PMA/I and Brefeldin A for 16 h, stained for the surface and intracellular markers listed above, and analysed by flow cytometry within 24 h. This panel was applied to samples in Chapter 4.

	Panel 3	
Configuration	Epitope	Fluorochrome
(488) 530/30		
(488) 695/40	CD39	PerCP-eF710
(633) 670/14		
(633) 730/45	CD45	AF700
(633) 780/60	CD127	APC-eF780
(405) 450/50	CLA	BV421
(405) 525/50	FixVia	eF506
(405) 610/20		BV605
(405) 660/20	TCR- $\gamma\delta$	BV650
(405) 710/50	CD3	BV711
(405) 780/60	CTLA-4	BV786
(561) 582/15	FoxP3	PE
(561) 610/20	CD4	PE-CF594
(561) 670/30	CD161	PE-Cy5
(561) 710/50		
(561) 780/60	CD25	PE-Cy7

Table 2.3 Cytometric fluorochrome panel for analysis of unstimulated T cells in PBMC and skin samples.

PBMC or cells isolated from the skin were rested for 16 h, stained for the surface and intracellular markers listed above, and analysed by flow cytometry within 24 h. This panel was applied to samples in Chapter 4.

2.2.10 Cytometric analysis

Cytometry data were acquired on through FACSDiva software v8.0, then analysed offline on FlowJo v10 (FlowJo, Oregon, USA). Polyfunctional cytometric populations were expressed using SPICE freeware (National Institute of Allergy and Infectious Diseases, National Institute of Health, USA). Statistical analysis was generated using Prism 8 software (Graphpad).

2.2.11 Statistical analysis

Statistical analyses were generated using Prism 8 software (Graphpad, San Diego, USA). Non-gaussian distribution was assumed throughout the studies and so non-parametric tests were performed. Differences between two groups were analysed using Mann-Whitney U-test; differences between multiple groups were analysed by Kruskal-Wallis one-way ANOVA test, with Dunn's multiple comparisons post-test.

2.2.12 SPICE analysis

Polyfunctional cytometric populations were expressed using SPICE freeware (Roederer et al., 2011); National Institute of Allergy and Infectious Diseases, National Institute of Health, USA), with sort categories by weighted (alternative order) distribution. The pie charts represent the total distribution for a given population (e.g. CD4 T cells) of particular cytokines (i.e. IL-17, IL-22, TNF, GM-CSF, IFN- γ , IL-2). The segments within the pie chart denote populations producing different combinations of markers (e.g. 6 cytokines, 5 cytokines). The size of the pie segment correlates to the frequency of the population. The arcs indicate the cytokine produced by that proportion of the population.

2.2.13 Illustrations

All illustrations are original and have been generated using illustration software at BioRender.com

2.2.14 Imaging flow cytometry

Following single cell preparation from skin biopsies (Section 2.2.5 Single cell preparation from skin biopsy), 2 ml PBS was added, and cells centrifuged at 300 g for 5 min. The supernatant was discarded, and the cells were then resuspended in 50 μ l PBS containing Fc Block for 15 min at RT. 2 ml PBS was then added, and cells centrifuged at 300 g for 5 min. The supernatant was discarded, and the pelleted cells were resuspended in 50 μ l PBS containing antibodies targeting the surface membrane proteins CD45, CD64 and HLA-DR as well as the nuclear dye Hoechst 33342 (Table 2.4). Samples were incubated in the dark at RT for 15 min, then 2 ml PBS added, and cells centrifuged at 300 g for 5 min. The supernatant was discarded, and the cells were then resuspended in 50 μ l PBS for analysis. Single colour controls and the sample were acquired at low speed and 60X magnification lens within 2 h on the ImageStream X Mark II imaging flow cytometer (Amnis/ Luminex, Seattle, USA).

























Lasers		Configuration	Epitope	Fluorochrome
		435 - 480 (457/45)	Brightfield	Brightfield
		480 - 560 (528/65)		
		560 - 595 (577/35)	HLA-DR	PE
		595 - 642 (610/30)		
		642 - 745 (702/85)	CD64	PerCP-Cy5.5
		745 - 780 (762/35)		
		435 - 480 (457/45)	Nucleus	Hoechst
		480 - 560 (537/65)		
		560 - 595 (582/25)	Brightfield	Brightfield
		595 - 642 (610/30)		
		642 - 745 (702/85)	CD45	BV711
		745 - 780 (762/35)	SSC	SSC

Table 2.4 Fluorochrome panel for imaging flow cytometry.

Cells isolated from the skin were stained for the surface markers listed above, and acquired by imaging flow cytometry within 2 h on the Amnis ImageStream X Mark II imaging flow cytometer.

2.2.15 Histology slide preparation

As per protocol II of the skin preparation protocol (Section 2.2.5.2), approximately one half of the skin sample was detached with a scalpel and added to a vial of 10% formalin and shipped to collaborators at the AbbVie Bioresearch Centre (Worcester, USA). Samples were formalin fixed, paraffin embedded, sectioned at 4 μm width and stained for haematoxylin and eosin (H&E). Stained slides were imaged using a Panoramic 250 Flash III™ (3D Histech, Budapest, Hungary) whole slide imager for digital pathology. Image analysis and interpretation was carried out in TCD using CaseViewer (3D Histech) (Figure 2.4).

2.2.16 scRNA-Seq

Skin dissociation was performed as per protocol II (Section 2.2.5.2) and the dissociated cells for scRNA-Seq were frozen in CryoStor cryopreservation media. These vials were then shipped to collaborators at the AbbVie Bioresearch Centre. There, the cells were thawed with warm RPMI media and thereafter maintained at 4°C. Samples were twice centrifuged at 514 g and the pellet resuspended with PBS/0.5% BSA. Cells were resuspended in 100 μl PBS/0.5% BSA and 2 μl CD45 antibody added. Samples were incubated for 30 min and then 2 ml PBS/0.5% BSA added and centrifuged at 300 g. The supernatant was aspirated, and cells resuspended in 200 μl PBS/0.5% BSA followed by 35 μm filtration. 1 μl of SYTOX™ Blue dead cell stain was added to distinguish dead cells. Live, single CD45⁺ and CD45⁻ cells were sorted using a FACSAria IIu cytometric cell sorter (BD Biosciences) into 500 μl of PBS/0.5% BSA. The sorted cells were then centrifuged, the supernatant aspirated and cells resuspended in PBS/0.5% BSA at a concentration of 1000 cells/ μl based on the number of sorted cells collected.

The 10X Single Cell 3' Reagent Kits v2 Rev C User Guide was followed to generate the Gel Bead-In-Emulsion (GEM) and barcoding, the post GEM-RT clean up and cDNA amplification (10X Genomics, Pleasanton, USA). To prepare the cDNA library, the Chromium Single Cell 3' Library & Gel Bead Kit v2, Chromium Single Cell A Chip Kit and Chromium & Multiplex Kit (10X Genomics) was used following the 10X Single Cell 3' Reagent Kits v2 Rev C User Guide to produce a CD45⁺ and CD45⁻ library for each donor. cDNA libraries were assessed for quality and quantity using D1000 Screen Tapes (Agilent

Technologies, San Francisco, USA). Together in one batch, 22 μ l of each library was sequenced on the Illumina HiSeq RNA sequencing system (Illumina, San Diego, USA) at the AbbVie Genomics Research Center (Worcester, USA). Sequencing revealed sample recoveries within a range of 930-3900 cells per sample (Appendix; Table 6.4 and Table 6.5).

2.2.17 scRNA-Seq data analysis

scRNA-Seq data for the CD45⁺ cell cohort were then analysed at TCD by the author in collaboration with Mr Conor Smith and Dr Karsten Hokamp. The gene expression raw sequencing data for the CD45⁺ cell sort cohort were processed using Cell Ranger v.3.0.2 (10X Genomics), with the 10X human transcriptome GRCh38-3.0.0 serving as a reference. Only genes found in a minimum of 3 cells were considered in downstream analysis. EmptyDrops (DropletUtils Bioconductor), a computational method which distinguishes between droplets containing cells from droplets containing ambient mRNA, was used to remove potential empty droplets (Lun et al., 2019). Cells were clustered using the Seurat processing pipeline (Stuart et al., 2019). Apoptotic/decaying cells were removed using a mitochondrial gene expression threshold of 5%, and doublets excluded using the DoubletFinder prediction package. Data were normalised, scaled and variable features found using SCTransform (Hafemeister et al., 2019).

By default, Seurat employs a global-scaling normalisation strategy which normalises gene expression measurements by total expression of that cell and multiplies this by a factor of 10,000 and log-transforms the result. The subsequent data were linear-transformed in a process known as scaling, ensuring that highly expressed genes did not dominate downstream analysis. PCA (principal component analysis) was then performed on the scaled data, using the previously identified variable genes as input. Seurat clusters cells based on their PCA scores to overcome technical noise associated with any single gene in the scRNA-Seq data. To counteract challenges associated with the integration of patient samples, whereby real biological differences may be interspersed with technical differences, the algorithm Harmony was used (Korsunsky et al., 2019). Clusters were then identified using the FindCluster function in Seurat, which iteratively groups cells together into clusters (Blondel VD, 2008). UMAP plots (Uniform

Manifold Approximation and Projection) were the preferred tool for dimensionality reduction and visualisation of this single cell data (Becht et al., 2018).

SingleR automated clustering was employed as an initial indicator of cluster identification (Aran et al., 2019). As SingleR is not skin specific, most clusters (n=30) were vague at best, and so all clusters were re-annotated manually based on literature and phenotypic detail. For visualisation purposes (i.e. Fig 3.17-3.22), the MAGIC method was used which imputes missing data as a result of dropout events (van Dijk et al., 2018). This enables clearer visualisation of the distribution of a given gene. Differential gene expression was generated through the statistical framework MAST (Finak et al., 2015) and differentially expressed genes in HS v Control were visualised using the EnhancedVolcano R package (Blighe, 2020). Pathway analysis employed the R package PathfindR (Ulgen et al., 2019).

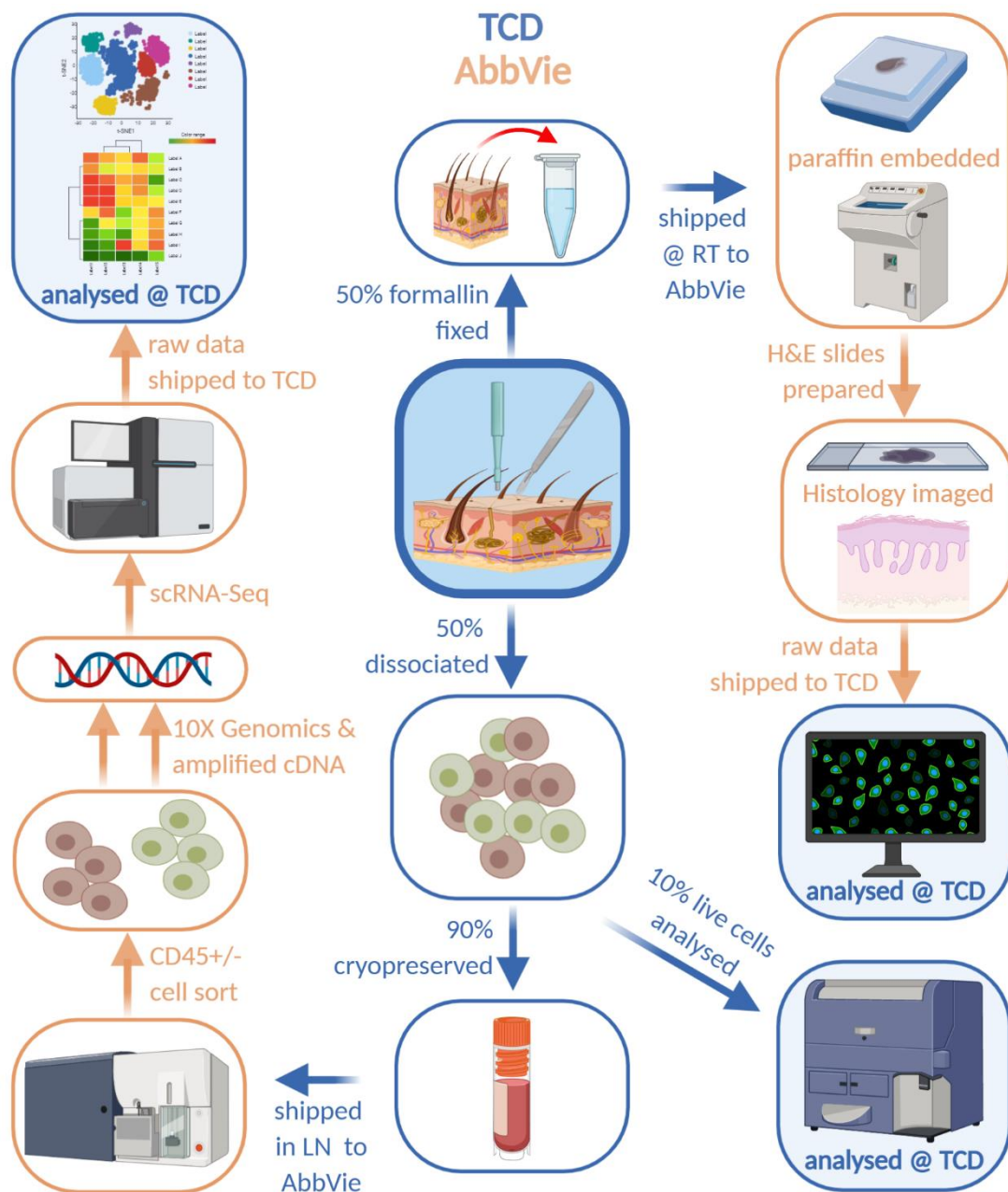


Figure 2.4 Workflow for histology and scRNA-Seq.

Following skin biopsy excision, 50% approx. was added to a solution of 10% formalin and prepared for shipping to AbbVie, USA for paraffin embedding and slide preparation, before histology. Interpretation was then performed in TCD. The remaining 50% of the skin biopsy was enzymatically dissociated, with 10% of this preparation stained for surface markers, and directly analysed by flow cytometry. The remaining 90% of dissociated cells were cryo-preserved and shipped to AbbVie, USA. There, CD45+/- cells were purified and single cell cDNA libraries prepared through 10X Genomics systems. scRNA-Seq was performed on the Illumina HiSeq RNA sequencer. The raw data generated was sent to TCD for all subsequent analysis.

Chapter 3

Phenotypic and transcriptomic characterisation of hidradenitis suppurativa skin

3 Phenotypic and transcriptomic characterisation of hidradenitis suppurativa skin

3.1 Introduction

HS aetiology remains unclear, although the key trigger appears to be hair follicle occlusion, which leads to cyst development. If this cyst subsequently ruptures, this elicits a potent immune response with inflammation. Abscess and sinus tract formation may follow. Given the improved outcomes upon anti-TNF therapy, it is clear that this aberrant immune response drives much of the damage in the disease. Proliferating progenitors in the ORS may lead to the hair follicle occlusion, and the ensuing keratin fibres, PAMPs and DAMPs that are released likely drive both an innate and adaptive immune response. In addition to keratinocytes and fibroblasts, resident and infiltrating immune cells are implicated in the disease pathology. Characterising the cells present in HS lesional skin, as well as their gene expression profile, will bring valuable detail in understanding the disease.

T cells, in particular Th17 cells, have been implicated in HS. Schlapbach et al. originally demonstrated a dramatic increase in IL-17 relative gene expression in HS lesional skin compared with normal skin, with two-colour immunofluorescence mapping IL-17 expression to CD4 T cells (Schlapbach et al., 2011). Kelly et al. reported a marked increase in IL-17 producing CD4 T cells in HS lesional, as well as perilesional (2 cm from lesion) skin (G. Kelly et al., 2015). An increase in IL-17 and IFN- γ producing CD4 T cells, but not IL-22⁺ CD4 T cells, was reported in HS skin, whilst in HS patient blood there was an increase of IL-17⁺ and IL-22⁺ CD4 T cells, but not IFN- γ ⁺ CD4 T cells (Hotz et al., 2016). Hence, the increased levels of Th17 associated cytokines do not appear to be limited locally to the HS skin, and IL-17 was reported to be elevated in HS patient serum (Matusiak et al., 2017). CD4 T cells expressing CD161, the pan-marker for IL-17 producing cells, were shown to be increased in both the lesional skin and anal fistulae of patients afflicted with both CD and HS. Clonotypic analysis of CD4 T cells from the peripheral blood, lesion and fistula of the same patients suggested an expansion of the same clones across the sites (Giudici et al., 2015). Studies connecting T cells to HS appear to be limited to CD4 T cells, with no apparent evidence of a role for CD8 T cells.

Macrophages and DC also appear to play a role in HS. Infiltrating, activated macrophages have been shown, via real-time PCR, immunohistochemistry and immunofluorescence, to express IL-23, and to a lesser degree IL-12, in the HS lesional dermis (Schlapbach et al., 2011). IL-23 is a key driver of IL-17 expression, whilst IL-12 is key for Th1 cell activation and IFN- γ production. These macrophages also expressed high levels of the PRR TLR2 in the HS lesion (Hunger et al., 2008). van der Zee et al. demonstrated a progressive increase in both monocytes and macrophages from normal skin, then early lesional, and on to chronic HS skin (van der Zee et al., 2012). CD11c⁺CD1a⁻CD14⁺ cells, unnamed but presumably dermal macrophages, were reported to be the IL-1 β producers in HS skin, both lesional and non-lesional (G. Kelly et al., 2015). The authors established that biologically active (caspase-1 processed) IL-1 β and IL-18, as well as NLRP3 (part of the NALP3 inflammasome) were increased in HS skin, hence implicating the inflammasome in HS inflammation. pDC were recently shown to co-exist with neutrophil NETs in HS skin, and this paired with an enhanced type I IFN signature in HS lesional skin implicated pDC in HS pathology (Byrd et al., 2019).

A higher level of neutrophils was reported in the peripheral blood of HS patients compared with healthy controls in a large-scale Nordic study, with a higher neutrophil: lymphocyte ratio (I. M. Miller et al., 2016). Neutrophils are also populous in HS lesional skin, their migration likely driven by Th17 cells. Neutrophils themselves have been reported as major IL-17 producers in HS (Lima et al., 2015), but as mentioned previously (Section 1.5.7), this may be neutrophils sequestering soluble IL-17 through their receptors. More recently, it has been demonstrated that neutrophils in HS are primed to produce NETs and are associated with a type I IFN local response (Byrd et al., 2019). Citrullinated DAMPs secreted in these NETs act as autoantigens and were shown to be recognised by autoantibodies in HS patient serum. The authors hypothesised that the elevated plasma cells and IgG observed in HS blood and skin may be a consequence of these autoantigens, thus driving an aberrant immune response.

B cells have been demonstrated to be present in HS lesional skin prior to this study, and even in clinically normal perilesional skin (van der Zee et al., 2012). The authors showed that the infiltrate expanded in chronic v early HS lesions, with markedly increased

frequencies of B cells and CD138⁺ plasma cells. In the dermis, ectopic B-cell 'pseudo' lymphoid follicles were observed, which may be bona fide germinal centres. Two more recent studies have suggested a key role for B cells in HS pathogenesis, one demonstrating anti-inflammatory effects of rituximab in HS explant cultures (Vossen et al., 2019) and the other a case study showing successful treatment of HS using B cell depletion with rituximab (Takahashi et al., 2018).

Much of the studies to characterise immune cells in HS thus far have combined small-scale flow cytometry, immunohistochemistry and mRNA analysis. A coherent study, identifying the principal cells present in HS lesional and uninvolved skin compared with healthy control skin, would add value to the field. Combining this with in-depth scRNA-Seq should further the understanding of the immune cells present and their function, as well as suggesting new therapeutic avenues.

3.2 Aims

The aim of the experiments in this chapter was to characterise the immune cells present in HS lesional skin. First, to identify differences in cell frequencies when compared with healthy control skin, and next to identify any transcriptional or pathway disparities between groups.

Specifically, this chapter sought to:

- Phenotype CD45⁺ cell subsets in HS patient skin
 - Identify the key immune subpopulations present in HS lesional skin, compared with HS uninvolved skin and healthy control skin by flow cytometry.

- Image skin sections to identify immune cell infiltrate in HS patient skin
 - Histology analysis to provide in situ localisation detail of immune cells in HS and healthy control skin.

- Perform transcriptional analysis of healthy control and HS patient skin
 - Using scRNA-Seq to confirm phenotyping results, as well as identify novel immune cell populations and pathways.

3.3 Clinical details

Clinical details for the HS patient group are shown in Table 3.1, the healthy control group in Table 3.2. HS patients were recruited during surgical consultation at St Michael's Hospital, Dublin, and all samples were small (≤ 6 mm) biopsies or surgical excisions. All HS patients donated lesional skin, with 5 patients (2HS-1, 2HS-10, 2HS14, 2HS-15 and 2HS-18) also donating uninvolved skin (apparently healthy skin >10 cm from lesion). Healthy control samples were skin tissue donated by patients undergoing breast reduction surgery at St Vincent's Private Hospital Plastic and Reconstructive Surgery Clinic, Dublin. All samples were processed and analysed on the day of sampling.

The mean age was 45 years (y), \pm SD of 14 ($n=18$), for HS patients, 41 y , \pm SD of 17 ($n=3$) for healthy controls. There were 78% females ($n=14$) in the HS group and 100% females ($n=3$) in the healthy control group. 22% ($n=4$) of HS patients were classified as Hurley stage 2 and 78% as Hurley stage 3; there were no Hurley stage 1 patients in this study. 86% (12/14) of female patients and 50% of males (2/4) were Hurley stage 3. HS patients had a mean body mass index (BMI) of 38.7 kg/m^2 , \pm SD of 8.2; 25.1 kg/m^2 , \pm SD of 0.8 for healthy controls. There were 50% smokers ($n=9$), 33% ex-smokers ($n=6$) and 17% non-smokers ($n=3$) in the HS patient group compared with 100% non-smokers in the healthy control group.

44% ($n=8$) of HS patients were taking type II diabetes therapy (metformin, Victoza™, Liraglutide™), 17% ($n=3$) topical corticosteroids (Elocon™, Eumovate™, Betnovate™). and 22% ($n=4$) on antibiotics (Tetralysal™, Flamazine™, Dapsone™). 17% ($n=3$) were on anti-TNF biological therapy (adalimumab [Humira™]) and 6% ($n=1$) on anti-IL-23 biological therapy (guselkumab [Tremfya™]). 78% ($n=14$) had seton surgical interventions; non-absorbable nylon sutures guided through the lesion and tied externally. Medications in the control group include Serc™ (vertigo/tinnitus therapy; $n=1$) and Cymbalta™ (depression medication; $n=1$).

Patients 2HS-3 and 2HS-11 were excluded from this study as they were duplicate samples (of 2HS-14 and 2HS-6 respectively). Patient 2HS-19 and 2HS-20 were excluded

as they had no history of HS; both presented to surgery with pilonidal sinuses and were incorrectly enrolled in this study.

Patient ID	Age (y)	Sex	Hurley	BMI	Smoker	Treatments	scRNA-Seq
2HS-1	50	F	3	42.1	E-S	setons (Sn)	-
2HS-2	22	F	3	45.2	N-S	Sn, Victoza™, Flamazine™	HS1
2HS-3							
2HS-4	43	F	3	38.7	S	Sn, Humira™	HS2
2HS-5	62	F	3	43.4	E-S	Sn, metformin	HS3
2HS-6	56	F	3	46.3	E-S	Sn	-
2HS-7	33	F	2	28.6	E-S	Sn, metformin	-
2HS-8	49	F	3	34.1	N-S	Sn, Elocon™	-
2HS-9	41	F	2	36.8	S	Sn, Eumovate™	-
2HS-10	56	M	2	34.9	S	Dapsone™, metformin	-
2HS-11							
2HS-12	48	F	3	38.6	S	Sn	-
2HS-13	49	F	3	25.7	S	Sn	-
2HS-14	31	F	3	46.1	S	Sn, guselkumab, metformin	-
2HS-15	77	M	3	24.7	S	Sn, Humira™, metformin, Tetralysal™, Betnovate™, Eumovate™	-
2HS-16	57	M	3	29.0	E-S	Humira™, Tetralysal™,	-
2HS-17	31	M	2	43.6	S	Sn, metformin	HS4
2HS-18	39	F	3	39.2	S	Sn	-
2HS-19							
2HS-20							
2HS-21	51	F	3	56.6	N-S	Sn, Liraglutide™, Victoza™	HS8
2HS-22	23	F	3	42.1	E-S	Sn	HS9
	<i>Mean</i>	<i>78% F,</i>	<i>0% 1</i>	<i>Mean</i>	<i>50% S</i>		
	<i>45</i>	<i>22% M</i>	<i>22% 2</i>	<i>38.7</i>	<i>33% E-S</i>		
	<i>SD 14</i>		<i>78% 3</i>	<i>SD 8.2</i>	<i>17% N-S</i>		

Table 3.1 Clinical details for HS patient group 1.

Study clinical details at time of sampling, including patient ID, age, sex, Hurley stage score, body mass index, smoking status, medical & surgical treatments, and enrolment code for scRNA-Seq analysis.

BMI: body mass index, E-S: ex-smoker, F: female, M: male, nrm: no relevant medications, N-S: non-smoker, S: smoker, Sn: setons.

Patient ID	Age (y)	Sex	Hurley	BMI	Smoker	Medication	RNA-Seq
2Con-1	58	F	-	24.2	N-S	Serc	Con5
2Con-2	41	F	-	25.2	N-S	Cymbalta	Con6
2Con-3	24	F	-	25.7	N-S	nrm	Con7
	<i>Mean</i>			<i>Mean</i>			
	41	100% F		25.05	100% N-S		
	<i>SD</i> 17			<i>SD</i> 0.76			

Table 3.2 Clinical details for healthy control group 1.

Study clinical details at time of sampling, including patient ID, age, sex, Hurley stage score, body mass index, smoking status, medical & surgical treatments, and enrolment code for scRNA-Seq analysis.

BMI: body mass index, F: female, nrm: no relevant medications, N-S: non-smoker.

3.4 Results

3.4.1 Increased frequency of leukocytes and T cells in the lesional skin of HS patients compared with healthy control skin

In order to characterise immune cells in the skin of HS patients and healthy controls, surgical and biopsied skin samples were provided. HS patient lesional (HS L) skin samples were taken from the non-infected region of a lesion and uninvolved skin samples (HS U) from >10 cm from lesion. The healthy control group skin samples (Con) were approximately 8x4 cm of residual skin tissue following breast reduction surgery. Both HS U and Con skin appeared clinically normal.

Once samples were received, they were weighed, then dissociated into a single cell preparation as per methods described in Section 2.2.5.1: Protocol II. Samples were then stained for surface expression of CD45, CD3, CD19, CD20, CD38, CD64, HLA-DR, CD14, and CD16 as per Section 2.2.7 and Table 2.1. Samples remained unfixed and were analysed by flow cytometry on the same day, within 2 h of preparation.

A gating strategy on how leukocytes (CD45⁺ immune cells) were identified is shown in Figure 3.1. All acquired events were initially gated as Forward Scatter Channel (FSC) v the live/dead fixable viability dye eFluor506 (FixVia eF506; LD). Cells were coarsely identified within this plot, as well as 123count eBeads (Counting beads) which were added to the sample during sample preparation (Figure 3.1A). These counting beads were then further defined in the subsequent plot of FSC v Side Scatter Channel (SSC)(Figure 3.1B). The CD45⁺ LD- population were next gated from the Cells population based on CD45 expression v FixVia eF506 (Figure 3.1C), then single cells subsequently identified based on FSC Area (A) v Width (W) intensity (Figure 3.1D).

The frequency of this population of single, viable CD45⁺ immune cells, expressed as the absolute number of cells per gram (g) of skin was observed to be significantly increased ($p < 0.01$) in HS L skin when compared with Con skin (Figure 3.1E). There was no significant difference between HS L and HS U, or between Con and HS U.

Within this population of live immune cells, T cells were next identified based on their expression of CD3 and absence of the B cell marker CD19 (CD3⁺CD19⁻; Figure 3.2A). CD3⁺CD19⁻ T cells were then gated on the characteristic lymphocyte population based on FSC v SSC (Figure 3.2B).

The absolute number of T cells (CD3⁺CD19⁻ lymphocytes) was significantly enhanced in HS L skin compared with Con per gram of skin ($p < 0.01$; Figure 3.2C). There was no significant difference between HS L and HS U, or between Con and HS U. When calculated as a percentage of total immune cells (CD45⁺ cells), there was no significant difference observed (Figure 3.2D).

In summary, there was a sharp rise in leukocytes and T cells in HS lesional skin compared with clinically normal HS U or Con skin. The T cell increase was in line with that in leukocytes, and no difference was observed in percentage of T cells across groups, suggesting that there is a surge in immune cells overall in HS L, not just T cells. Given that T cells are approximately 50% of immune cells detected in the skin samples, and their implication in autoimmunity, T cells warrant further detailed investigation (Chapter 4).

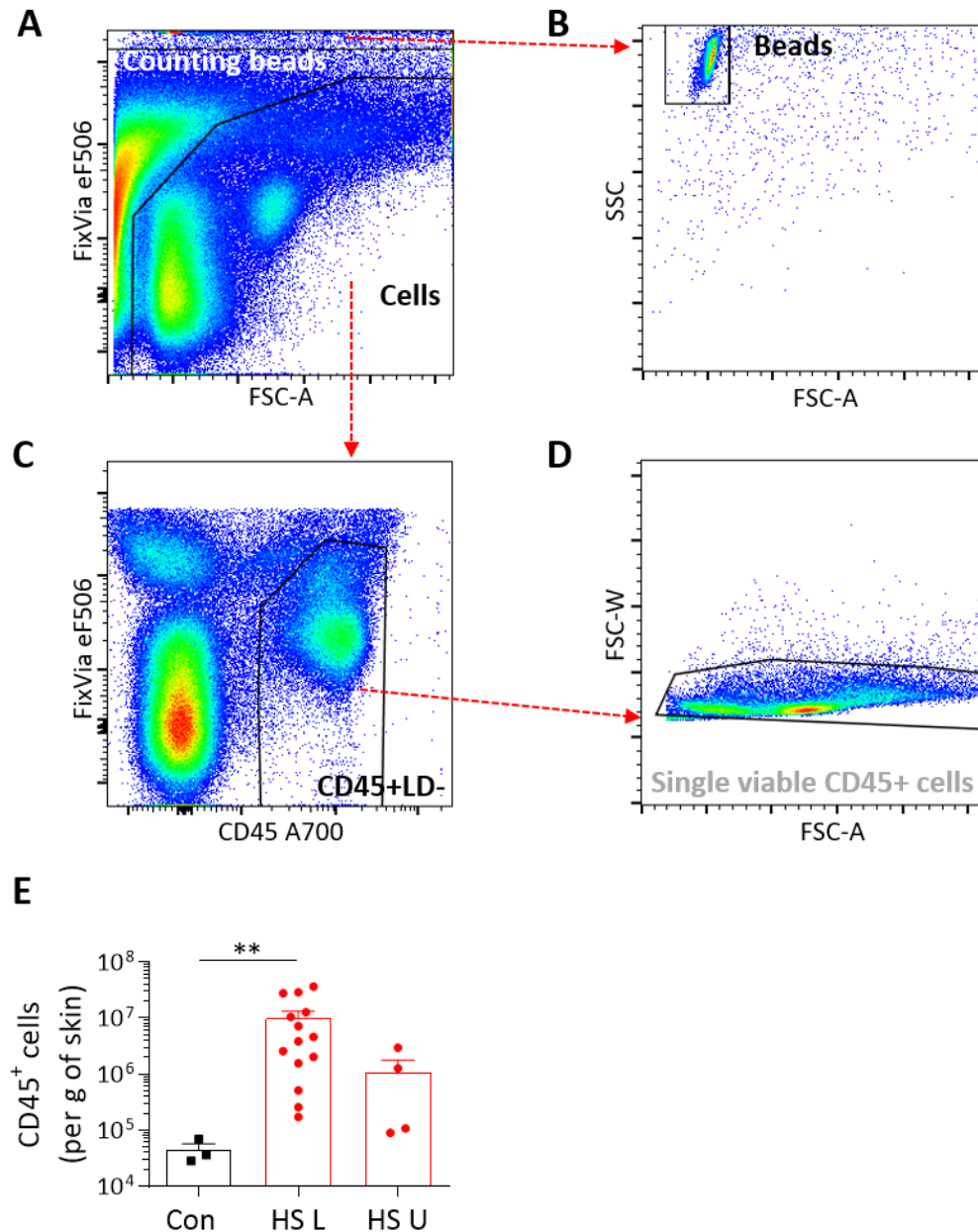


Figure 3.1 CD45⁺ cells were enriched in HS lesions compared with healthy control skin.

Cells isolated from the skin of healthy controls (Con; n=3) or HS patients (HS L: lesional, n=14, U: uninvolved, n=4) were stained for surface markers in the presence of Fc block and analysed by flow cytometry. To identify single, viable CD45⁺ immune cells, sequential gating was performed: Forward Scatter (FSC) v Fixable-Viability-Dye- to identify counting beads and viable cells (A); Forward v Side Scatter (SSC) to gate counting beads and exclude debris (B); CD45⁺, Fixable-Viability-Dye (LD)- to identify viable leukocytes (C); FSC-Area v FSC-Width to exclude doublets (D). Graph shows the number of single, live CD45⁺ immune cells calculated per gram of skin (E). Graph E represents individual samples with mean \pm SEM for each group. Statistical significance was calculated using Kruskal-Wallis one-way ANOVA with Dunn's multiple comparisons test; **p<0.01.

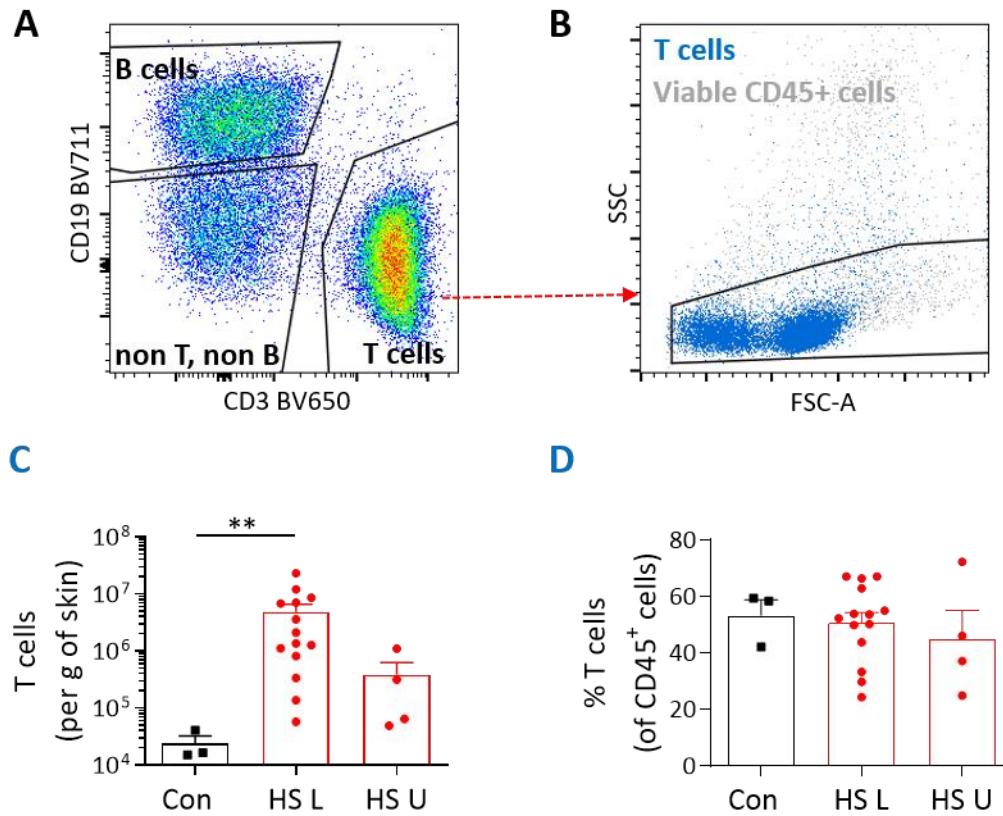


Figure 3.2 T cells were enriched in HS lesional compared with healthy control skin.

Cells isolated from the skin of healthy control (Con; n=3) or HS patients (HS L, n=14, HS U, n=4) were stained for surface markers in the presence of Fc block and analysed by flow cytometry. Single viable immune cells (Figure 3.1D) were then gated on CD3 and CD19 (A); with CD3⁺CD19⁻ T cells (in blue) identified as lymphocytes within the forward v side scatter gate (B). Graphs show the number of single, live CD3⁺ T cells calculated per gram of skin (C) and as a percentage of viable CD45⁺ immune cells (D). Graphs represent individual samples with mean ± SEM for each group. Statistical significance was calculated using Kruskal-Wallis one-way ANOVA with Dunn's multiple comparisons test; **p<0.01.

3.4.2 Increased frequency of B cells in the lesional skin of HS patients compared with healthy control skin

Within the population of live immune cells (Figure 3.1D), B cells were next identified based on their expression of the pan-B cell marker CD19, as well as the lack of expression of the T cell marker CD3 (Figure 3.3A). CD19⁺CD3⁻ B cells were then gated on the characteristic lymphocyte population based on FSC v SSC (Figure 3.3B).

The absolute numbers of B cells (CD19⁺CD3⁻ lymphocytes) were very low in Con skin as expected, and was significantly enhanced in HS L skin compared with Con per gram of skin ($p < 0.01$; Figure 3.3C). The difference was not significant (ns) between HS L and HS U, or between Con and HS U. When calculated as a percentage of total leukocytes (CD45⁺ cells), there was a significant difference observed between HS L and Con ($p < 0.05$; Figure 3.3D).

B cells were further resolved into plasmablasts and plasma cell subsets based on CD20 and CD38 expression (Figure 3.4A). A population enriched for plasmablasts (PB) were identified as CD20⁺CD38⁻, plasma cells (PC) as CD38⁺CD20⁻. In Figure 3.4B, plasmablasts (blue) mapped to the CD38⁻HLA-DR⁺ cluster within the total B cell population (grey), plasma cells (red) to the CD38⁺HLA-DR⁻ cluster. Hence, taken together, plasmablasts were defined as CD19⁺CD20⁺CD38⁻HLA-DR⁺, plasma cells as CD19⁺CD20⁻CD38⁺HLA-DR⁻.

Plasmablasts were significantly increased in HS L skin when compared with Con, both when represented as an absolute number ($p < 0.01$; Figure 3.4C) and as a percentage of CD45⁺ cells ($p < 0.05$; Figure 3.4D). Similarly, plasma cells were significantly enhanced in HS L compared with Con in terms of absolute numbers ($p < 0.05$; Figure 3.4E) and frequency of leukocytes ($p < 0.05$; Figure 3.4F). Although plasmablasts and plasma cells in HS U appeared very low, similar to Con, there was no significant difference observed between HS L and HS U.

To summarise, a significant increase in the number of B cells, plasmablasts and plasma cells was observed in HS L skin compared with HS U and Con.

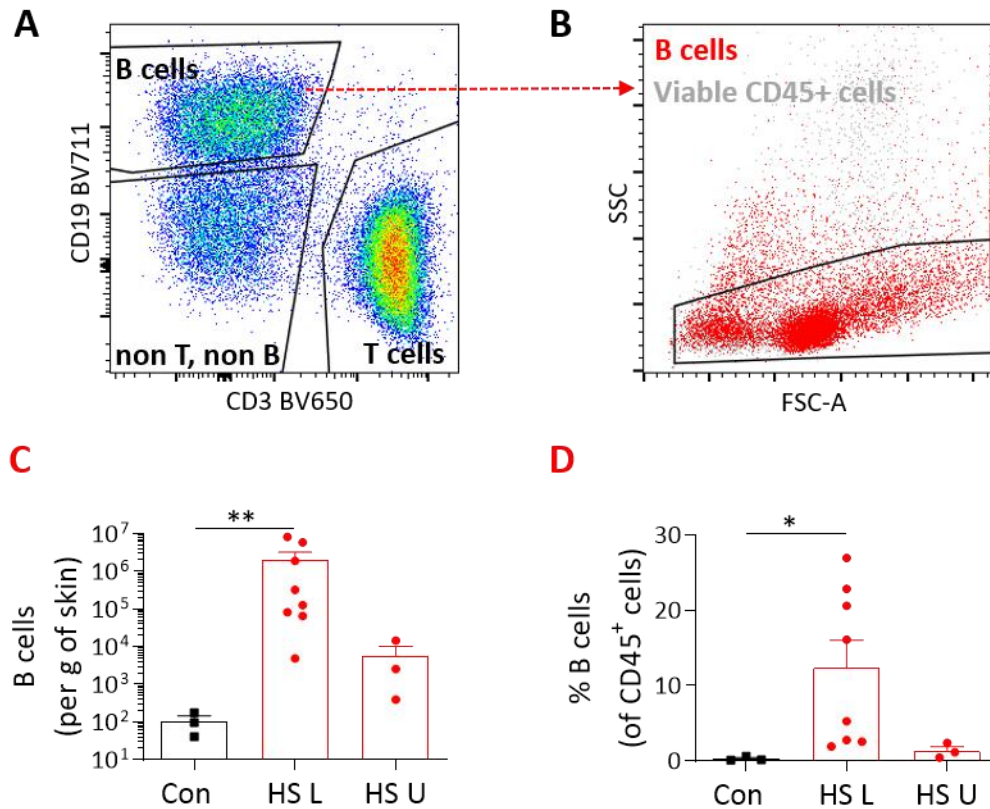


Figure 3.3 B cells were enriched in HS lesional compared with healthy control skin.

Cells isolated from the skin of healthy controls (Con; n=3) or HS patients (HS L, n=8, HS U, n=3) were stained for surface markers in the presence of Fc block and analysed by flow cytometry. Single viable immune cells (Figure 3.1D) were then gated on CD3 and CD19 (A); with CD19⁺CD3⁻ B cells (in red) identified as lymphocytes within the forward v side scatter gate (B). Graphs show the number of single, live CD19⁺ B cells calculated per gram of skin (C) and as a percentage of viable CD45⁺ immune cells (D). Graphs represent individual samples with mean \pm SEM for each group. Statistical significance was calculated using Kruskal-Wallis one-way ANOVA with Dunn's multiple comparisons test; *p<0.05, **p<0.01.

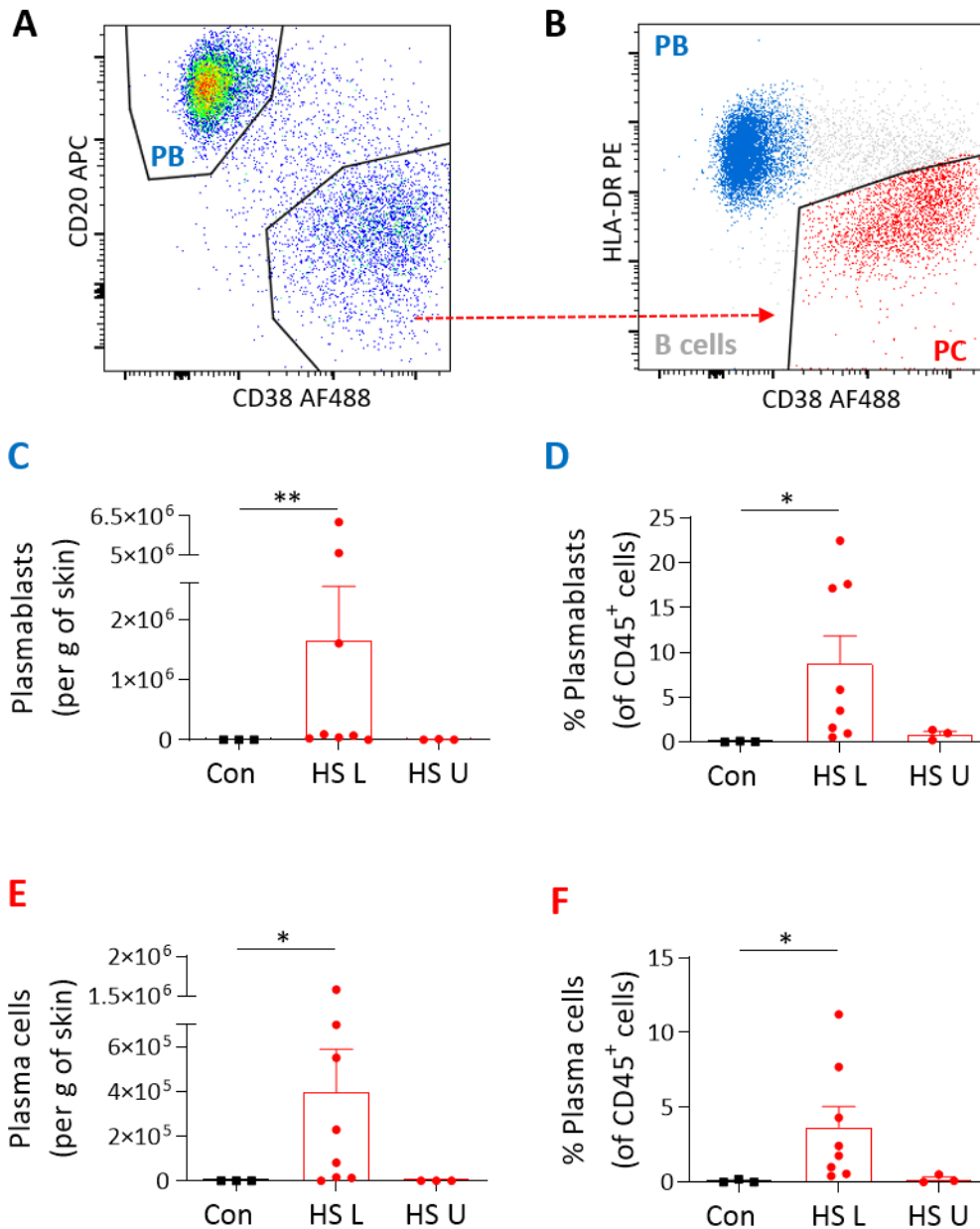


Figure 3.4 Plasmablasts and plasma cells were enriched in HS lesional compared with healthy control skin.

Cells isolated from the skin of healthy controls (Con; n=3) or HS patients (HS L, n=8, HS U, n=3) were stained for surface markers in the presence of Fc block and analysed by flow cytometry. Single viable $CD19^+CD3^-$ B cells (Figure 3.3B) were then gated on CD38 and CD20 to identify $CD20^+CD38^-$ cells as the plasmablast (PB) enriched population (A). The $CD38^+CD20^-$ were then further gated to the $CD38^+HLA-DR^-$ subset to identify the plasma cell (PC) enriched population. Plasmablasts (blue) mapped to the $CD38^+HLA-DR^+$ cluster within the B cell population (grey), plasma cells (red) to the $CD38^+HLA-DR^-$ cluster (B). Graphs show the number of single, live plasmablasts and plasma cells calculated per gram of skin (C and E respectively) and as a percentage of viable $CD45^+$ immune cells (D and F respectively). Graphs represent individual samples with mean \pm SEM for each group. Statistical significance was calculated using Kruskal-Wallis one-way ANOVA with Dunn's multiple comparisons test; * $p < 0.05$, ** $p < 0.01$.

3.4.3 Increased frequency of DC, but not dermal macrophages, in the lesional skin of HS patients compared with healthy control skin

Having investigated the presence of lymphoid cells such as T cells and B cells in HS skin compared with healthy controls, the next step was to identify the differences in innate cells within the skin samples.

Dermal macrophages and DC have been discussed in Section 1.4. These subsets were gated by selecting single, viable leukocytes (Figure 3.1D) and stratifying into “non T, non B” cells based on lack of expression of both CD3 and CD19 (Figure 3.5A). This “non T, non B” population was then gated based on CD64 expression v SSC. CD64 (Fc- γ RI) is constitutively expressed on DC, macrophages and monocytes, and a clear population of CD64^{hi}SSC^{int} was identified and gated (Figure 3.5B). This CD64^{hi}SSC^{int} subset was then divided into CD14⁺ dermal macrophages and CD14⁻ DC based on CD14 v CD64 staining (Figure 3.5C). Both dermal macrophages (in red) and DC (in blue) clustered at the HLA-DR⁺CD16⁻ population (Figure 3.5D).

This study was limited to an 18 parameter cytometer and did not include the DC pan-marker CD11c, the LC marker CD1a, nor CD1c, specific for dermal cDC2. Following the conclusion of this arm of the study, one HS lesional sample was processed and acquired to confirm that the CD64^{hi}SSC^{int} subset incorporated the total DC population. Figure 3.6A and B show the same initial gating as previous; first identifying CD3⁻CD19⁻ cells (non T, non B; Figure 3.6A) and CD64^{hi}SSC^{int} (Figure 3.6B). The CD64^{hi}SSC^{int} subset was shown to be entirely HLA-DR⁺ and CD11c^{lo/+} (Figure 3.6C). The subset could be stratified into the CD14⁺ dermal macrophage population and CD14⁻ DC population based on CD14 v CD1c expression (Figure 3.6D). The DC population was divided into a number of subsets based on CD1a and CD1c staining (Figure 3.6E). Markers for dermal APC subsets are listed in Table 1.2. Hence CD1a⁺⁺CD1c⁺ appeared to identify LC, with a frequency of 18% of total DC in this patient sample. CD1a^{lo}CD1c⁺ were identified as migratory cDC2, at 15% of total DC, and CD1a⁻CD1c⁺ as cDC2 (CD1c⁺ DC) at 24% of total DC). CD1a⁻CD1c⁻ are likely the cDC1 (CD141⁺ DC) at 14% of total DC but this was not confirmed in this sample. Hence, this serves to confirm that CD64^{hi}SSC^{int} cells encompass dermal macrophages and DC.

To visualise this CD64^{hi} population, one HS sample was processed and imaged on an imaging flow cytometer as per Section 2.2.14. Stained cells were acquired at 60X magnification within 2 h of preparation. Figure 3.7A reveals six cell images with a characteristic DC/macrophage morphology (brightfield column), with expression for HLA-DR, CD64 and CD45. Figure 3.7B demonstrates these cells were gated as HLA-DR⁺CD64⁺ cells within the single, viable, in-focus CD45⁺Hoechst⁺ subset, with Figure 3.7C showing the comparable population identified by conventional flow cytometry (i.e. Figure 3.5B).

Having presented the gating strategy for dermal macrophages and DC in this study (Figure 3.5), and confirmed their authenticity (Figure 3.6 and Figure 3.7), the frequency of these cells in HS patient and healthy control samples was analysed. The increase observed in HS L skin compared with HS U or Con was not significant when presented as cell number per g of skin (Figure 3.8A). However, as a percentage of total immune cells, the increase was significant ($p < 0.05$; Figure 3.8B). There was no significant difference for DC between Con and HS U. In the case of dermal macrophages present in HS L, HS U or Con skin, there was no significant difference observed in terms of absolute numbers (Figure 3.8C) or immune cell frequency (Figure 3.8D).

To conclude this section, there is a significant increase in the percentage of DC in HS L skin compared with that of healthy controls.

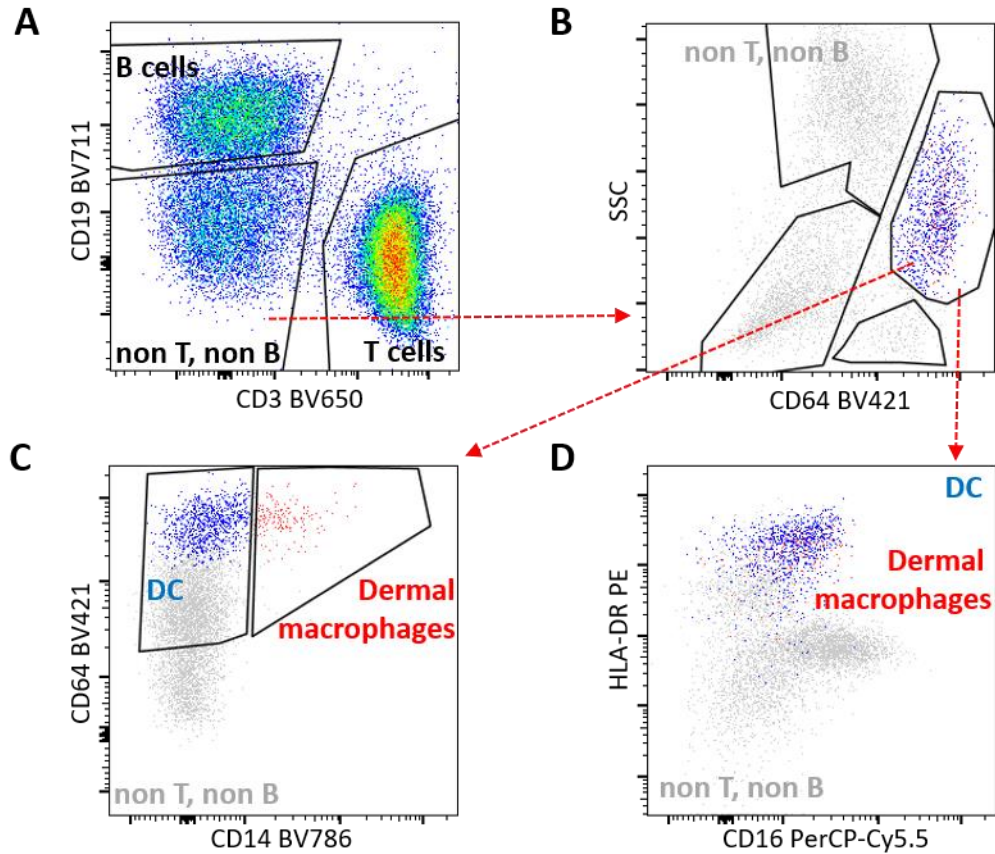


Figure 3.5 Gating strategy for dermal macrophages and DC populations in the skin.

Cells isolated from HS patient lesional skin were stained for surface markers in the presence of Fc block and analysed by flow cytometry. Single viable immune cells (Figure 3.1D), further gated for CD3⁻CD19⁻ cells (non T, non B cells; A), were profiled for CD64 expression v side scatter (B). A cluster of CD64⁺SSC^{int} (blue & red) was gated next, which encompassed a population of CD64⁺CD14⁺ dermal macrophages (red) and CD64⁺CD14⁻ DC (blue; C). Both dermal macrophages (red) and DC (blue) were HLA-DR⁺CD16⁻ (D).

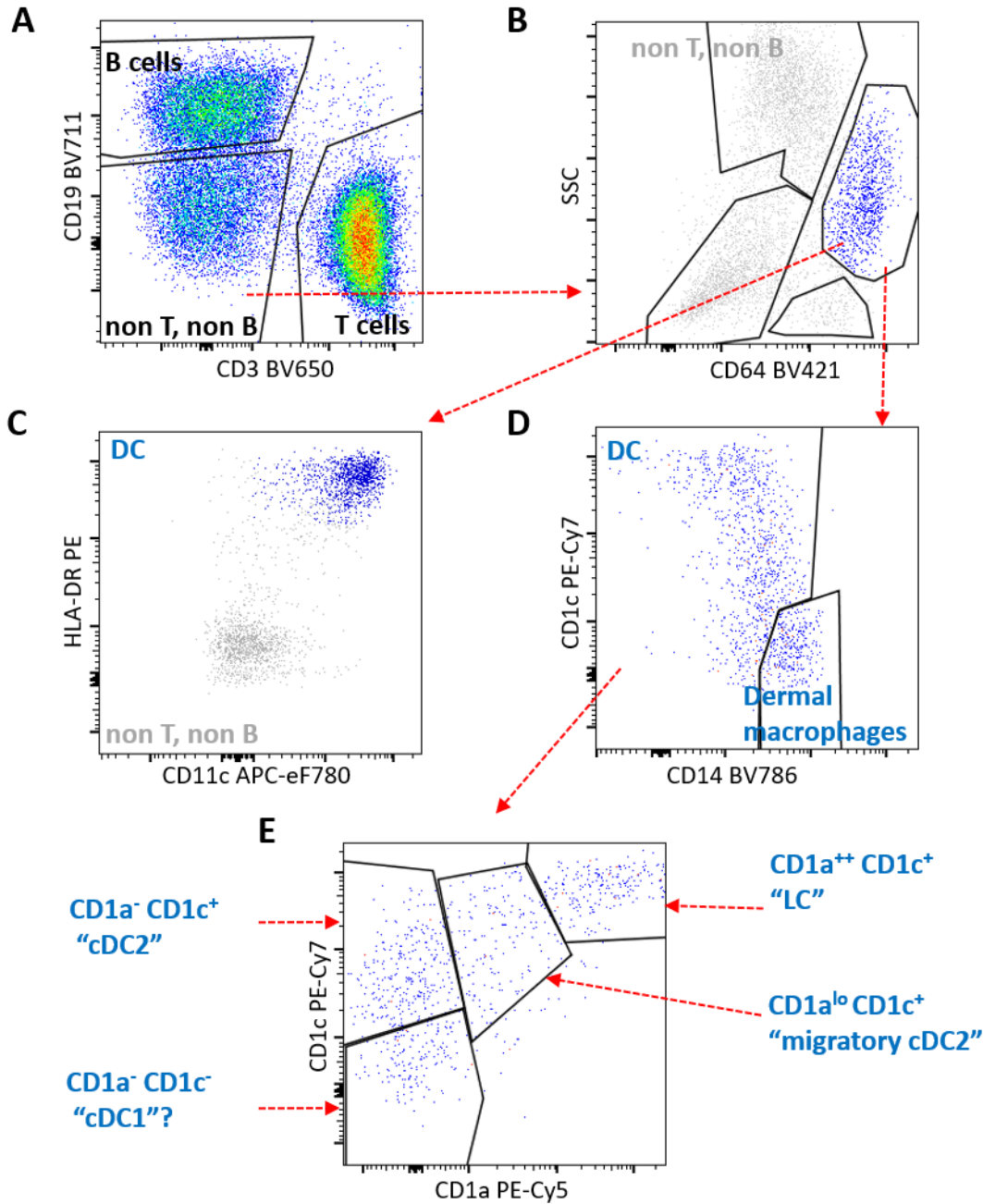


Figure 3.6 CD64⁺SSC^{int} cells in HS lesional skin included multiple DC populations.

To identify DC subsets, cells isolated from the skin of a HS patient (n=1) were stained for surface markers in the presence of Fc block and analysed by flow cytometry. Single viable immune cells (Figure 3.1D), further gated for CD3⁻CD19⁻ cells (non T, non B cells; A), were profiled for CD64 expression v side scatter (B). The CD64⁺SSC^{int} population was identified as entirely CD11c⁺HLA-DR⁺ DC (blue; C). Of this population, CD1c^{lo}CD14⁺ identified a population of CD14⁺ dermal macrophages (26% of total DC)(D), with the remaining DC categorised based on their expression of CD1a and CD1c (E). CD1a⁺⁺CD1c⁺ were identified as Langerhans cells (LC; 18% of total DC), CD1a^{lo}CD1c⁺ as migratory CD1c⁺ DC (15%), CD1a⁻CD1c⁺ as CD1c⁺ DC (24%) and CD1a⁻CD1c⁻ as likely CD141⁺ DC (14%).

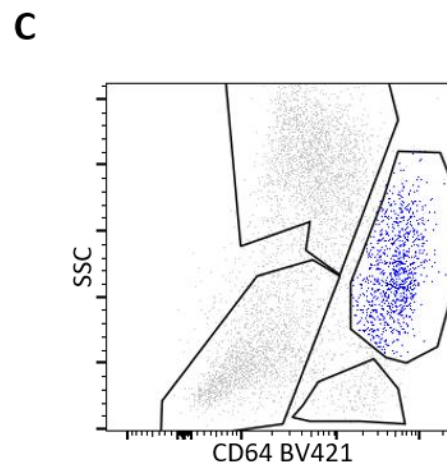
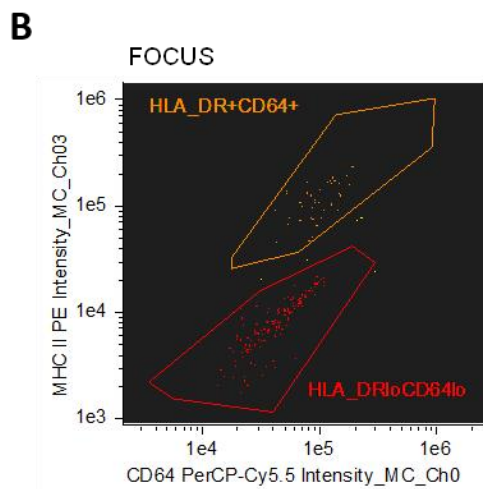
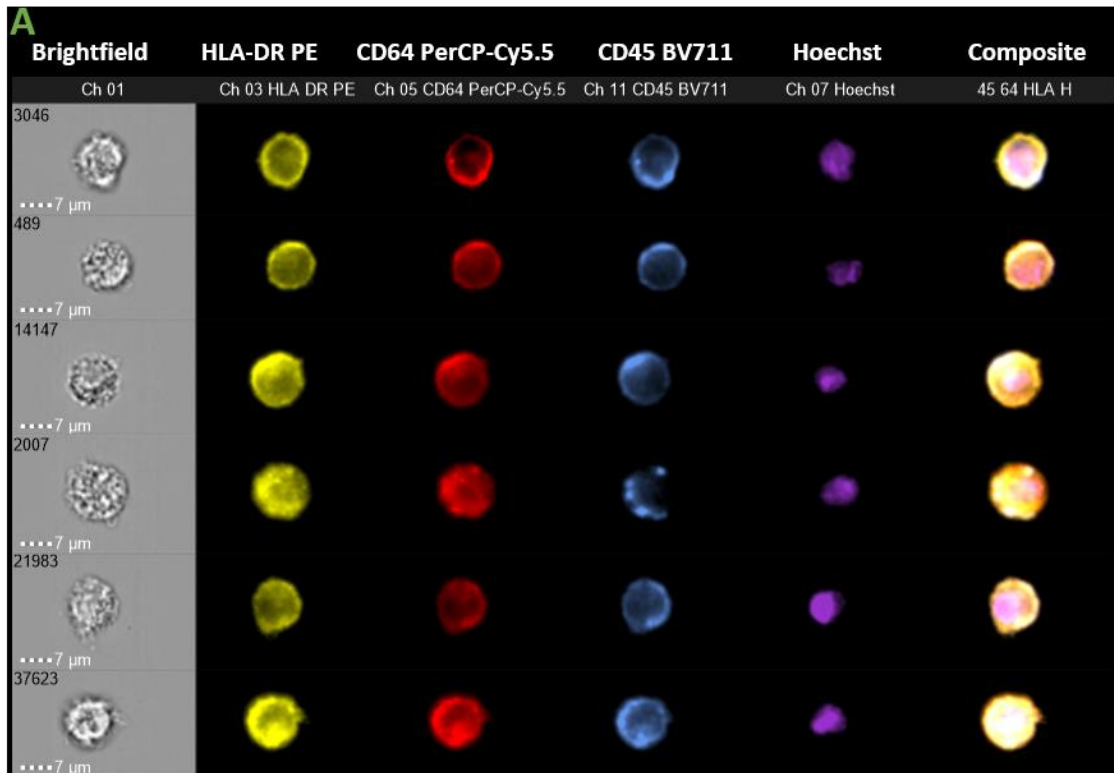


Figure 3.7 Representative images of CD64⁺HLA-DR⁺ cells.

Cells isolated from the skin of a HS patient (n=1) were stained for surface markers in the presence of Fc block and analysed by imaging flow cytometry on the ImageStream X Mark II imaging flow cytometer. Single, viable, in-focus CD45⁺Hoechst⁺ immune cells were then gated based on their CD64 and HLA-DR expression. Six representative cell images are displayed showing the brightfield, individual markers and composite profile for HLA-DR, CD64, CD45 and Hoechst (A). Dot plots demonstrate the gated population (CD64⁺HLA-DR⁺) enriched for DC and dermal macrophages (B), and the comparable population identified by conventional flow cytometry in Figure 3.5B (C).

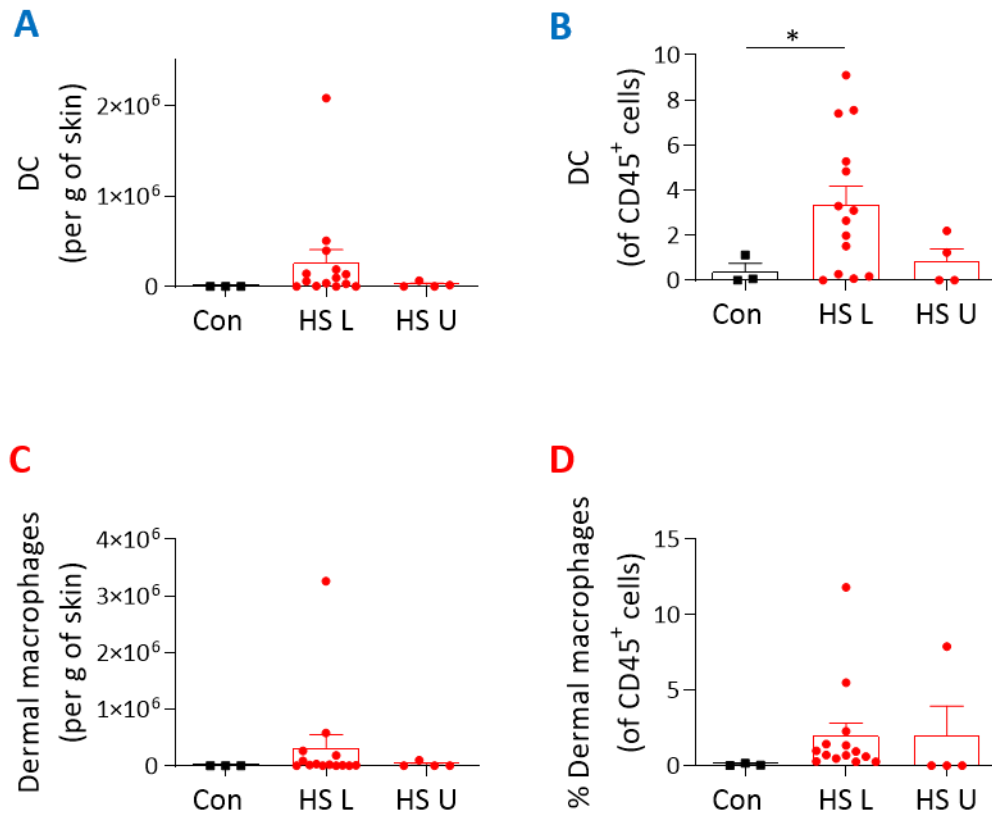


Figure 3.8 Significant enrichment of DC, but not dermal macrophages, in HS skin compared with healthy control skin.

Cells isolated from the skin of healthy controls (Con; n=3) or HS patients (HS L: lesional, n=14, U: uninvolved, n=4) were stained for surface markers in the presence of Fc block and analysed by flow cytometry. DC and dermal macrophages were gated as per Figure 3.5C. Graphs show the number of DC or dermal macrophages calculated per gram of skin (A and C respectively) and as a percentage of viable CD45⁺ immune cells (B and D respectively). Graphs represent individual samples with mean \pm SEM for each group. Statistical significance was calculated using Kruskal-Wallis one-way ANOVA with Dunn's multiple comparisons test; *p<0.05.

3.4.4 Increased frequency of activated and resting neutrophils in the lesional skin of HS patients compared with healthy control skin

Turning now to another innate population in the skin, neutrophils. Although very few neutrophils are expected to be found in healthy tissue, they travel to inflamed sites upon an immune event (Section 1.1.2).

In this study, neutrophils were identified amongst the previously identified CD3⁻CD19⁻ cells (non T, non B cells; Figure 3.5A) within single, viable immune cells (Figure 3.1D). Next, a population of CD64^{lo/int}SSC^{hi} were gated (Figure 3.9A). This population, in blue, was confirmed as HLA-DR⁻CD16⁺ (Figure 3.9B) and CD38⁻CD14⁻ (Figure 3.9C).

To visualise this CD64^{lo/int} population, one HS sample was imaged on an imaging flow cytometer as per Section 2.2.14. Figure 3.10A displays cell images with a characteristic neutrophil morphology (brightfield column), positive for CD45, low or intermediate expression of CD64, with no expression of HLA-DR. Figure 3.10B demonstrates these cells were gated as HLA-DR⁻CD64^{lo/int} cells within the single, viable, in-focus CD45⁺Hoechst⁺ subset, with Figure 3.10C showing the comparable population identified by conventional flow cytometry (Figure 3.5B).

The cells identified as neutrophils (Figure 3.9A) were shown to be markedly enhanced in HS L skin compared with Con ($p < 0.05$; Figure 3.9D). The frequency appeared to be increased (ns) in clinically normal HS U skin also. There was no significant difference in the neutrophil frequencies when taken as a percentage of leukocytes, although the HS U percentage was raised compared with HS L or Con (ns; Figure 3.9E).

Although CD64 is negligible on resting neutrophils, it is upregulated on neutrophils upon activation (Sack, 2017). Hence the neutrophil populations could be stratified into two subsets based on CD64 expression; activated neutrophils were classified as CD64^{int}SSC^{hi}, resting neutrophils as CD64^{lo}SSC^{hi} (in red and blue respectively; Figure 3.11A). Activated neutrophils appeared to be HLA-DR⁻CD16^{hi}, whereas resting neutrophils were HLA-DR⁻CD16^{lo}, (in red and blue respectively; Figure 3.11B).

Activated neutrophils were substantially enhanced in HS skin compared with Con, significantly so for HS L skin ($p < 0.05$) (Figure 3.11C). However, taken as a percentage of leukocytes there were no differences between groups, although HS U appeared to be increased (ns) compared with Con (Figure 3.11D). Similarly, numbers of resting neutrophils in HS L skin were significantly higher in HS L skin compared with Con (Figure 3.11E), but not so when analysed as a percentage of total immune cells (Figure 3.11F).

In conclusion, the numbers of neutrophils and neutrophil subsets detected in the lesional skin of HS patients were significantly enhanced in comparison with healthy control skin.

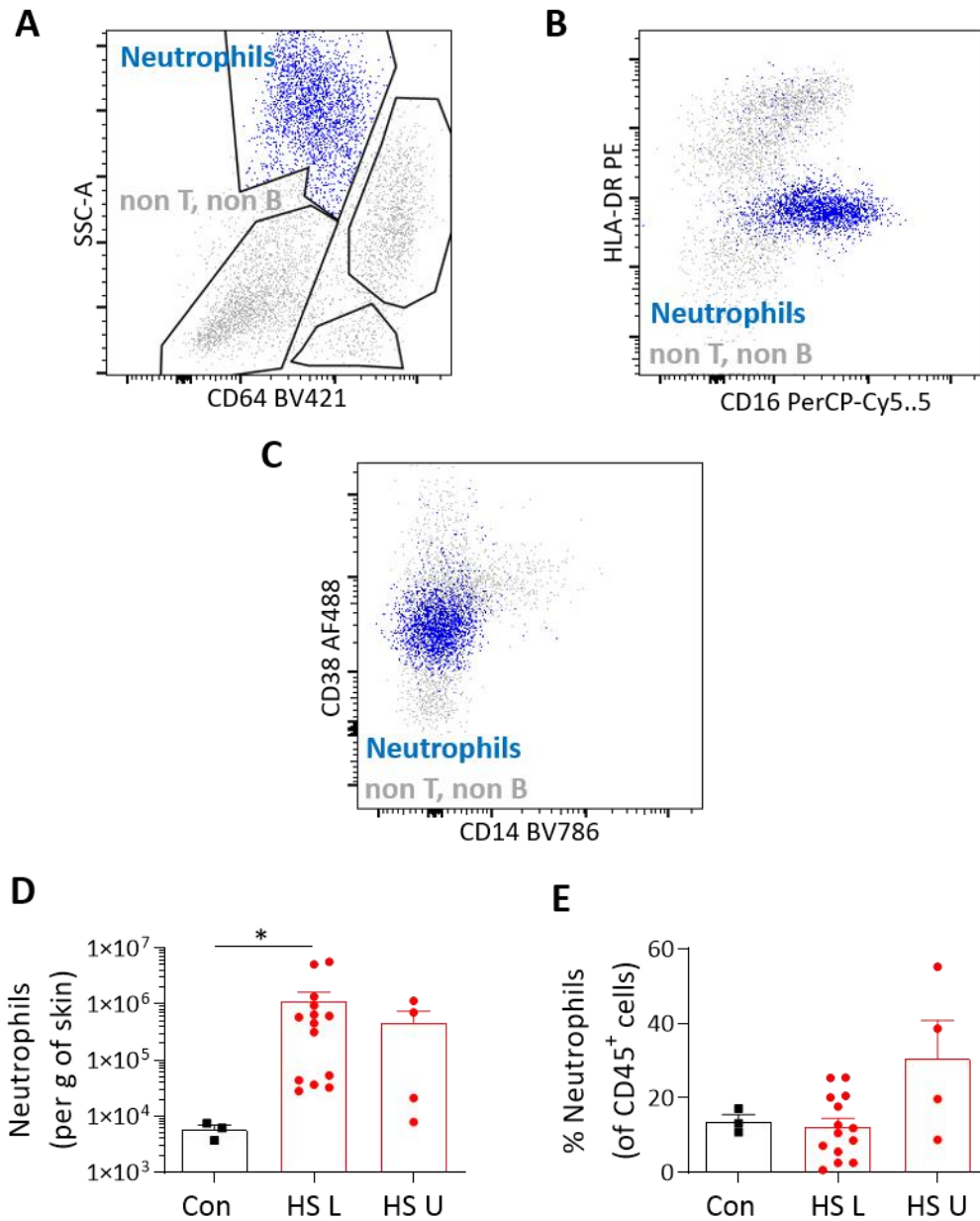


Figure 3.9 Neutrophils were enriched in HS lesional compared with healthy control skin.

Cells isolated from the skin of healthy controls (Con; n=3) or HS patients (HS L: lesional, n=14, U: uninvolved, n=4) were stained for surface markers in the presence of Fc block and analysed by flow cytometry. Single, viable immune cells gated as CD3⁺CD19⁻ cells (non T, non B cells; Figure 3.5A) were further gated based on CD64^{lo}/intSSC^{hi} to identify neutrophils (blue) within the non T, non B cell population (grey; A). These neutrophils were identified as HLA-DR⁻CD16⁺ (B) and CD14⁻CD38⁻ (C). Graphs show the number of single, live neutrophils calculated per gram of skin (D) and as a percentage of viable CD45⁺ immune cells (E). Graphs represent individual samples with mean \pm SEM for each group. Statistical significance was calculated using Kruskal-Wallis one-way ANOVA with Dunn's multiple comparisons test; *p<0.05.

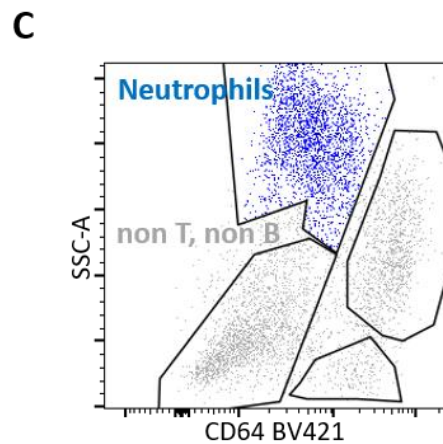
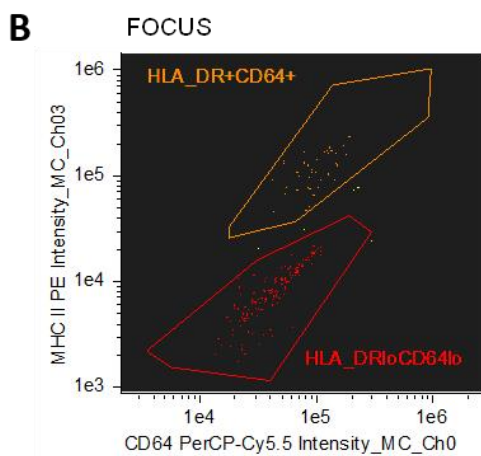
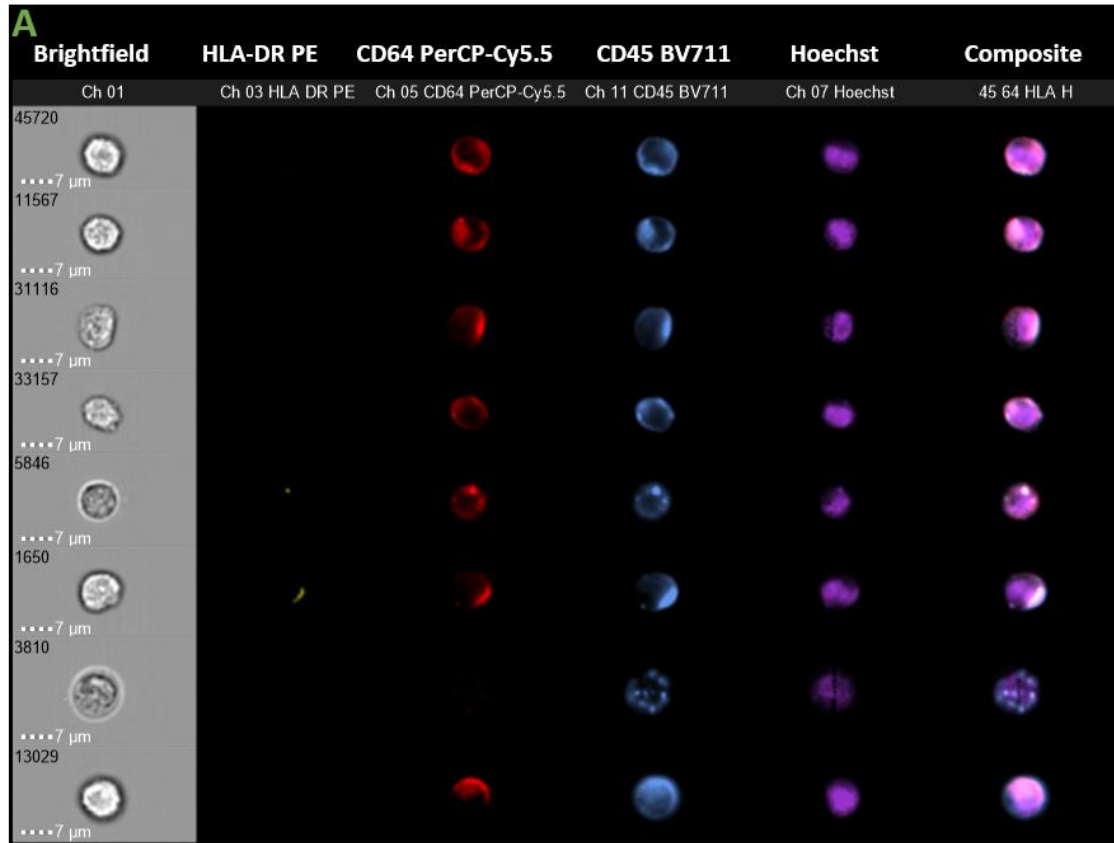


Figure 3.10 Representative images of CD64^{lo}HLA-DR^{lo} neutrophils.

Cells isolated from the skin of a HS patient (n=1) were stained for surface markers in the presence of Fc block and analysed by imaging flow cytometry on the ImageStream X Mark II imaging flow cytometer. Single, viable, in-focus CD45⁺Hoechst⁺ immune cells were then gated based on their CD64 and HLA-DR expression. Eight representative cell images are displayed showing the brightfield, individual markers and composite profile for HLA-DR, CD64, CD45 and Hoechst (A). Dot plots demonstrate the gated population (CD64^{lo}HLA-DR^{lo}; B) and the comparable population identified by conventional flow cytometry in Figure 3.9A (C).

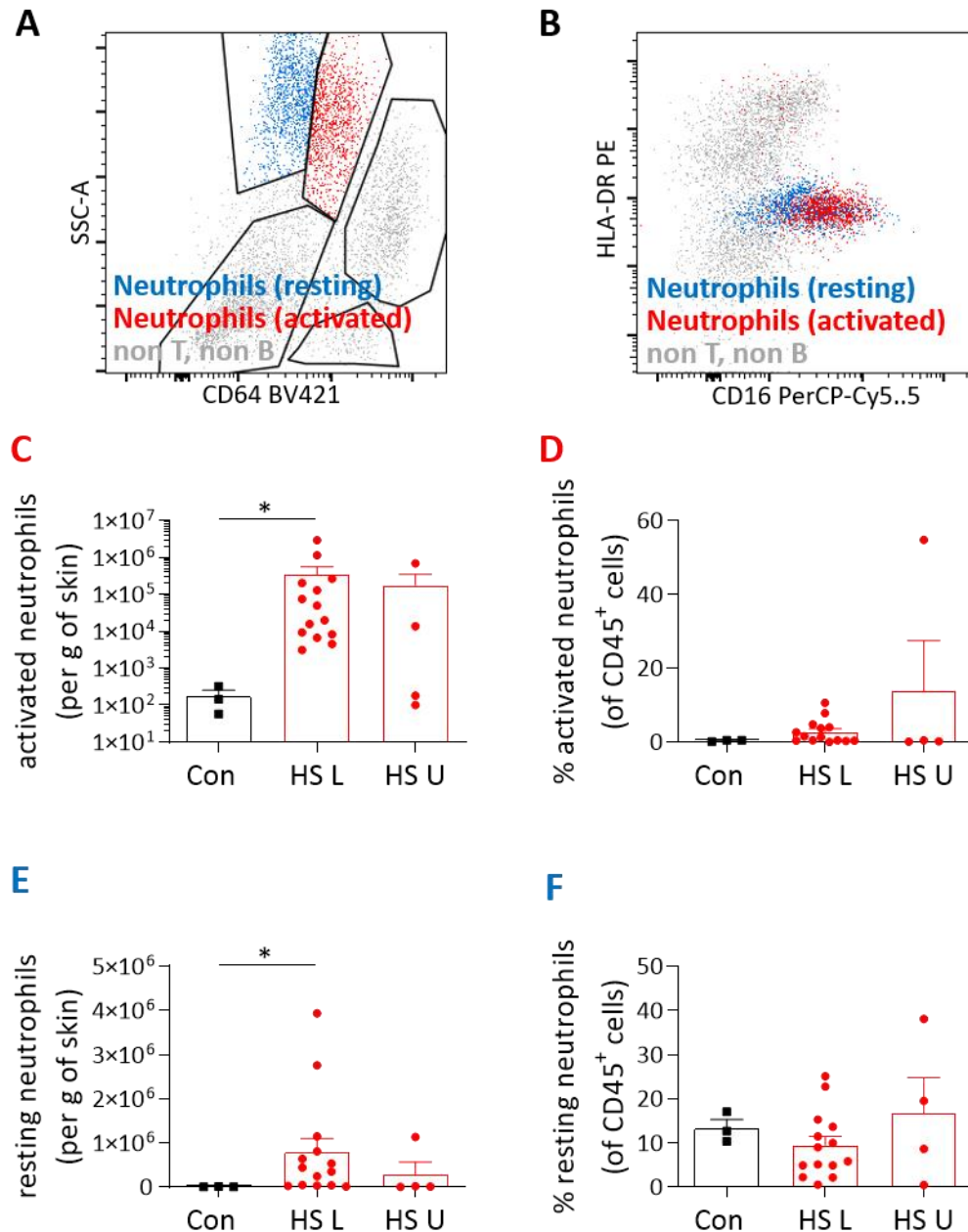


Figure 3.11 Both activated and resting neutrophils were enriched in HS lesional compared with healthy control skin.

Cells isolated from the skin of healthy controls (Con; n=3) or HS patients (HS L: lesional, n=14, U: uninvolved, n=4) were stained for surface markers in the presence of Fc block and analysed by flow cytometry. Single viable neutrophils (Figure 3.9A) were stratified as resting ($CD64^{lo}SSC^{hi}$; blue) or activated ($CD64^{int}SSC^{hi}$; red) neutrophils within the $CD64^{lo}/intSSC^{hi}$ (A) and $HLA-DR^{-}CD16^{+}$ populations (B). Graphs show the number of single, live resting or activated neutrophils calculated per gram of skin (C and E respectively) and as a percentage of viable $CD45^{+}$ immune cells (D and F respectively). Graphs represent individual samples with mean \pm SEM for each group. Statistical significance was calculated using Kruskal-Wallis one-way ANOVA with Dunn's multiple comparisons test; * $p < 0.05$.

3.4.5 Increased frequency of an NK cell-enriched population in the lesional skin of HS patients compared with healthy control skin

In addition to dermal macrophages, DC and neutrophils, other innate immune cell populations were apparent in the CD3⁻CD19⁻ cell gate (Figure 3.5A) when gated for CD64⁻ v SSC (Figure 3.12A). Amongst this “non T, non B” cell population (grey), there is a CD64⁻SSC^{lo} cluster (in blue). Within this subset there is a population of CD38⁺HLA-DR⁻ (Figure 3.12B), which are also CD14⁻CD16⁻ (Figure 3.12C) and group as FSC^{hi}SSC^{int} cells (Figure 3.12D).

CD38 is a marker of cell activation and is expressed on T cells, B cells, plasma cells, monocytes and NK cells (Krejci et al., 2016). Given that T cells, B cells, plasma cells, DC and macrophages have already been identified outside of this CD64^{lo}SSC^{lo} gate, it is likely that the subset identified here (CD3⁻CD19⁻CD64⁻CD14⁻CD16⁻CD38⁺FSC^{hi}SSC^{int}) is enriched for NK cells. CD16 is generally expressed on all CD56^{dim} NK cells so this subpopulation may be enriched for NK cells and yet exclude and CD56^{dim} NK cells. Alternatively, as cytokine activation and target cell stimulation abrogate CD16 expression (Romee et al., 2013), HS lesional skin NK cells may not express CD16.

In terms of absolute numbers, this “NK cell enriched” population was observed to be enhanced in HS L skin relative to HS U (ns), and significantly so compared with Con (p <0.05; Figure 3.12E). There was no significant change between groups in terms of percentage of total immune cells (Figure 3.12F).

In addition to the “NK cell enriched” population, there was another, apparently homogeneous, CD64⁻SSC^{lo} cluster identified (in blue; Figure 3.13A). This subset was CD38⁻HLA-DR⁻ (Figure 3.13B), CD14⁻CD16^{lo} (Figure 3.13C) and clustered as FSC^{lo}SSC^{lo} cells, similar to lymphocyte scatter characteristics (Figure 3.13D). Hence these cells were CD3⁻CD19⁻CD64⁻CD14⁻CD16⁻CD38⁻FSC^{lo}SSC^{lo} and were described here as non TBNK lymphocytes. They may be enriched for ILC but further investigation is required. In any case, this subset appeared to be increased in HS L (p <0.05) and HS U (ns) skin compared with Con (Figure 3.13E). There was no difference observed when presented as a percentage of CD45⁺ immune cells (Figure 3.13F).

In summary, although it will require appropriate cell markers and further investigation to definitively confirm these observed subsets, there appears to be an enhancement of populations enriched for NK cells (Figure 3.12) and ILC (Figure 3.13) in HS L skin compared with Con.

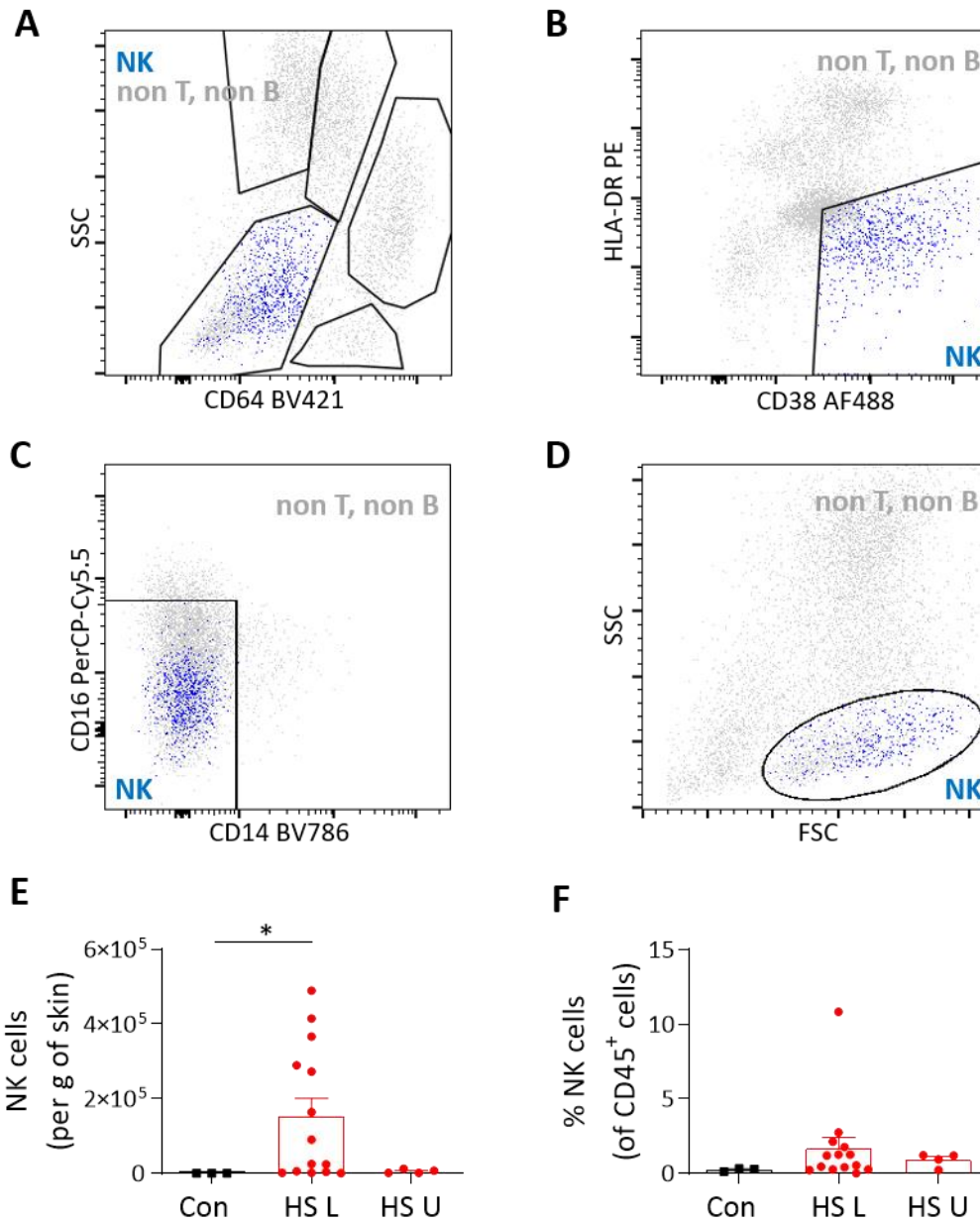


Figure 3.12 NK cells were enriched in HS lesional compared with HS uninvolved skin.

Cells isolated from the skin of healthy controls (Con; n=3) or HS patients (HS L: lesional, n=14, U: uninvolved, n=4) were stained for surface markers in the presence of Fc block and analysed by flow cytometry. Single viable immune cells identified as CD3⁻CD19⁻ cells (non T, non B cells, Figure 3.5A) were then gated as CD64⁺SSC^{lo} (A), CD38⁺HLA-DR⁻ (B), CD14⁻CD16⁺ (C) and FSC^{hi}SSC^{int} (D) to identify an enriched natural killer (NK) cell population. Graphs show the number of single, live NK cells calculated per gram of skin (E) and as a percentage of viable CD45⁺ immune cells (F). Graphs represent individual samples with mean \pm SEM for each group. Statistical significance was calculated using Kruskal-Wallis one-way ANOVA with Dunn's multiple comparisons test; *p<0.05.

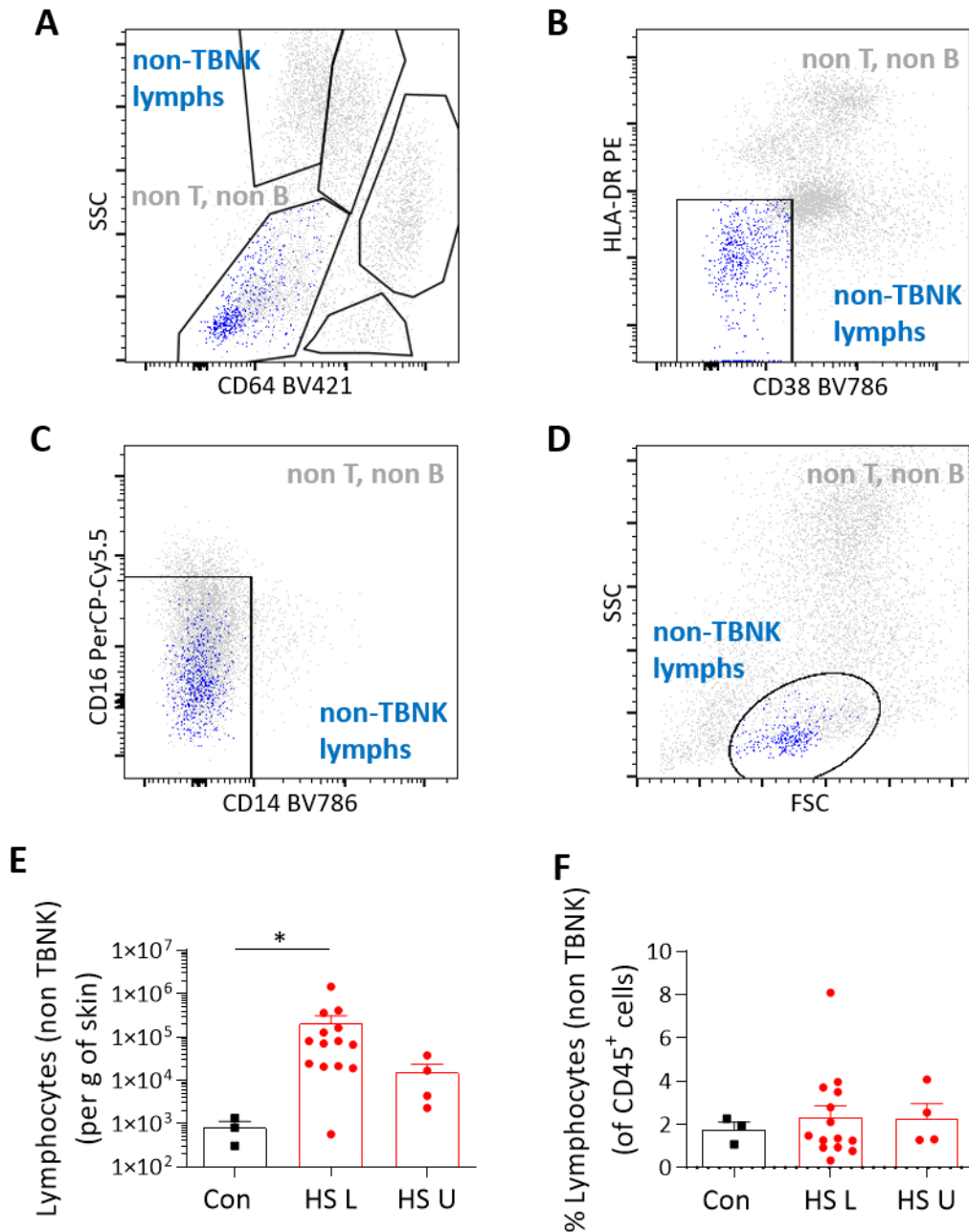


Figure 3.13 Non-TB NK lymphocytes were enriched in HS lesional skin samples compared with healthy control skin.

Cells isolated from the skin of healthy controls (Con; n=3) or HS patients (HS L: lesional, n=14, U: uninvolved, n=4) were stained for surface markers in the presence of Fc block and analysed by flow cytometry. Single viable immune cells identified as CD3⁻CD19⁻ cells (non T, non B cells, Figure 3.5A) were then gated as CD64⁻SSC^{lo} (A), CD38⁻HLA-DR⁻ (B), CD14⁻CD16⁻ (C) and FSC^{lo}SSC^{lo} (D) to identify an enriched non-TB NK lymphocyte population. Graphs show the number of single, live non-TB NK lymphocytes calculated per gram of skin (E) and as a percentage of viable CD45⁺ immune cells (F). Graphs represent individual samples with mean \pm SEM for each group. Statistical significance was calculated using Kruskal-Wallis one-way ANOVA with Dunn's multiple comparisons test; *p<0.05.

3.4.6 Histological analysis of HS skin highlights a heterogeneous inflammatory profile

HS is a highly heterogeneous disease affecting varying areas in different patients. Even within a lesional sample, there are discrete areas with very different phenotypes. For example, a hyperplastic epidermis may be observed. There may be abscesses, cysts or sinus tracts, with or without dermal inflammation (Jemec, 2012). There are areas rich in fibrosis and granulation, which may be all distal to the hair follicle. Hence to interpret phenotypic or transcriptomic data it is helpful to have similar tissue for histological analysis. Therefore, skin samples from tissue adjacent to that used for gene expression analysis, were formalin fixed, paraffin embedded, and H&E stained (Section 2.2.15). The haematoxylin (H) stains nuclei blue, whilst the eosin (E) stains cytoplasm and extracellular matrix pink. Other tissue and cellular structures take on different combinations of these colours.

The pathology was consistent throughout the HS samples imaged (n=6), defined by the heterogeneous inflammatory response in a bed of fibrosis. Figure 3.14 presents representative images (n=6) of a HS patient skin sample (2HS-1). There is some evidence of fibrosis with neovascularisation, indicating chronic inflammation and granulation. There is spongiosis in the keratinocytes surrounding the hair follicle (within blue box; Figure 3.14A [1X], C [10X] & E [60X]). Irregular desmosomes (cell-bridging adhesions) indicate oedema, likely due to inflammation. This weakening of cell junctions contributes to rupture of the hair follicle. Lymphocytes are the primary cell observed at the hair follicle.

The abscess (within green box; Figure 3.14A) is primarily neutrophilic, with a mixed immune infiltrate. It includes neutrophils (lobed nuclei; live and dying), lymphocytes, and plasma cells (large cytoplasm). There is likely bacterial penetration here too. This abscess may be coupled to the hair follicle though a connection that is not visible in this section.

There are epithelial invaginations (tendrils) imaged also (in red box; Figure 3.14A [1X], B [10X] & D [60X]). These are characteristic in HS, extending from the ORS. They can extend into deep dermal tissues and are associated with de novo formation of new cysts

and sinus tracts, irrespective of inflammation intensity. Figure 3.15 is a representative H&E stained slide (n=3) of the skin from the healthy control breast tissue (2Con-3). The hair follicle (within blue box; Figure 3.15A [1X], B [10X] & D [60X]) is smooth, with few surrounding lymphocytes. The normal epidermis and dermis (in red box; Figure 3.15A [1X], B [10X] & D [60X]) are intact, with no neutrophilic infiltration.

To conclude, HS skin imaging displays a heterogeneous, inflammatory site, characterised by lesions, sinus tracts with primarily lymphocytic and neutrophilic infiltration on view.

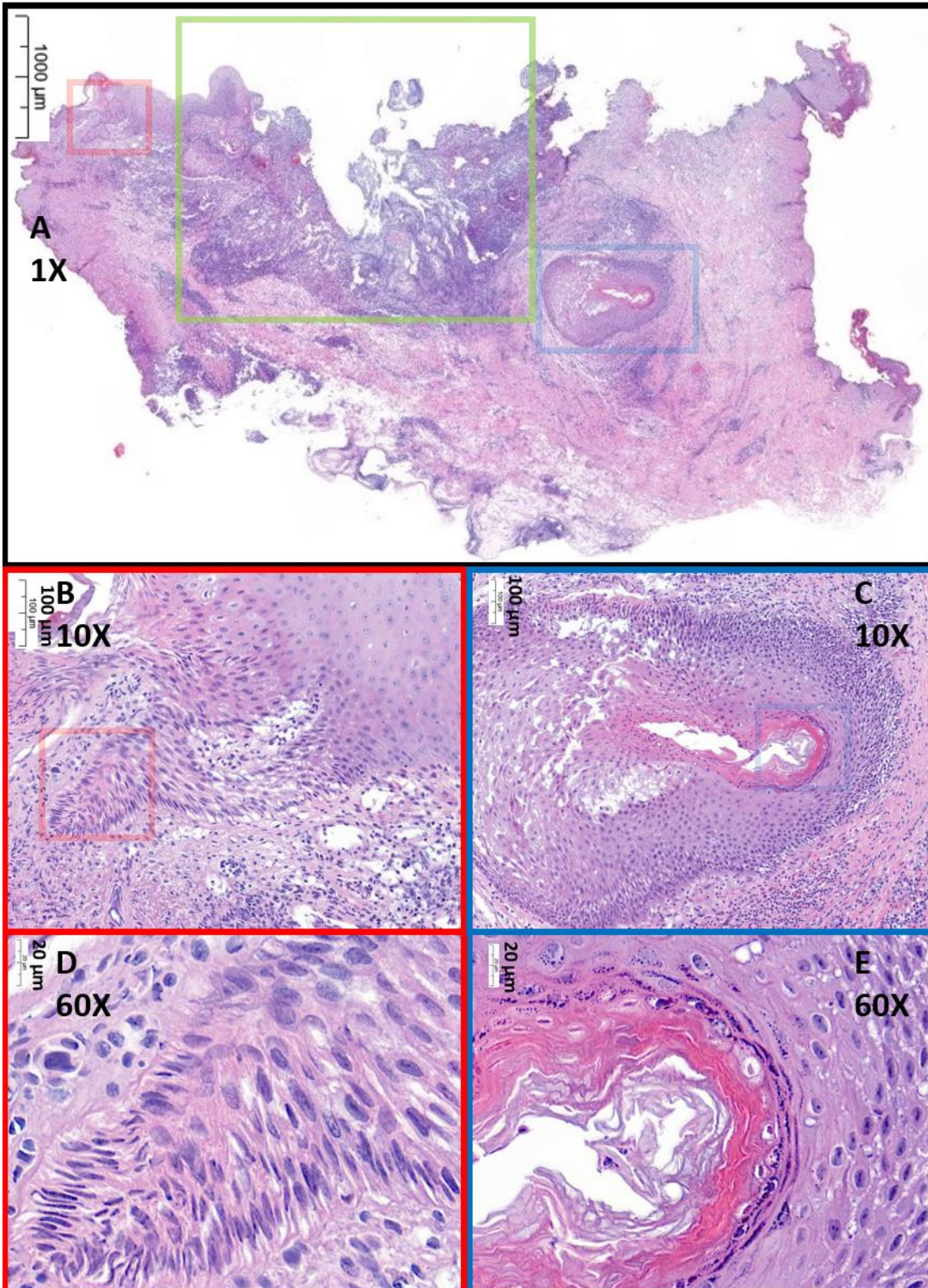


Figure 3.14 Histology illustrates immune cell infiltration in HS lesional skin.

Biopsies from HS lesional skin (n=6) and healthy control skin (n=3) were formalin fixed, paraffin embedded, sectioned at 4 µm and stained with H&E. Representative image of an inflamed HS L skin sample at 1x (A), featuring epithelial invaginations (red box) abscess (green box) and a hair follicle (blue box). The invagination is displayed at 10X (B) and 60X (D); the hair follicle at 10X (C) and 60X (E). Scale bar indicates 1000 µm (A), 100 µm (B & C) and 20 µm (D & E).

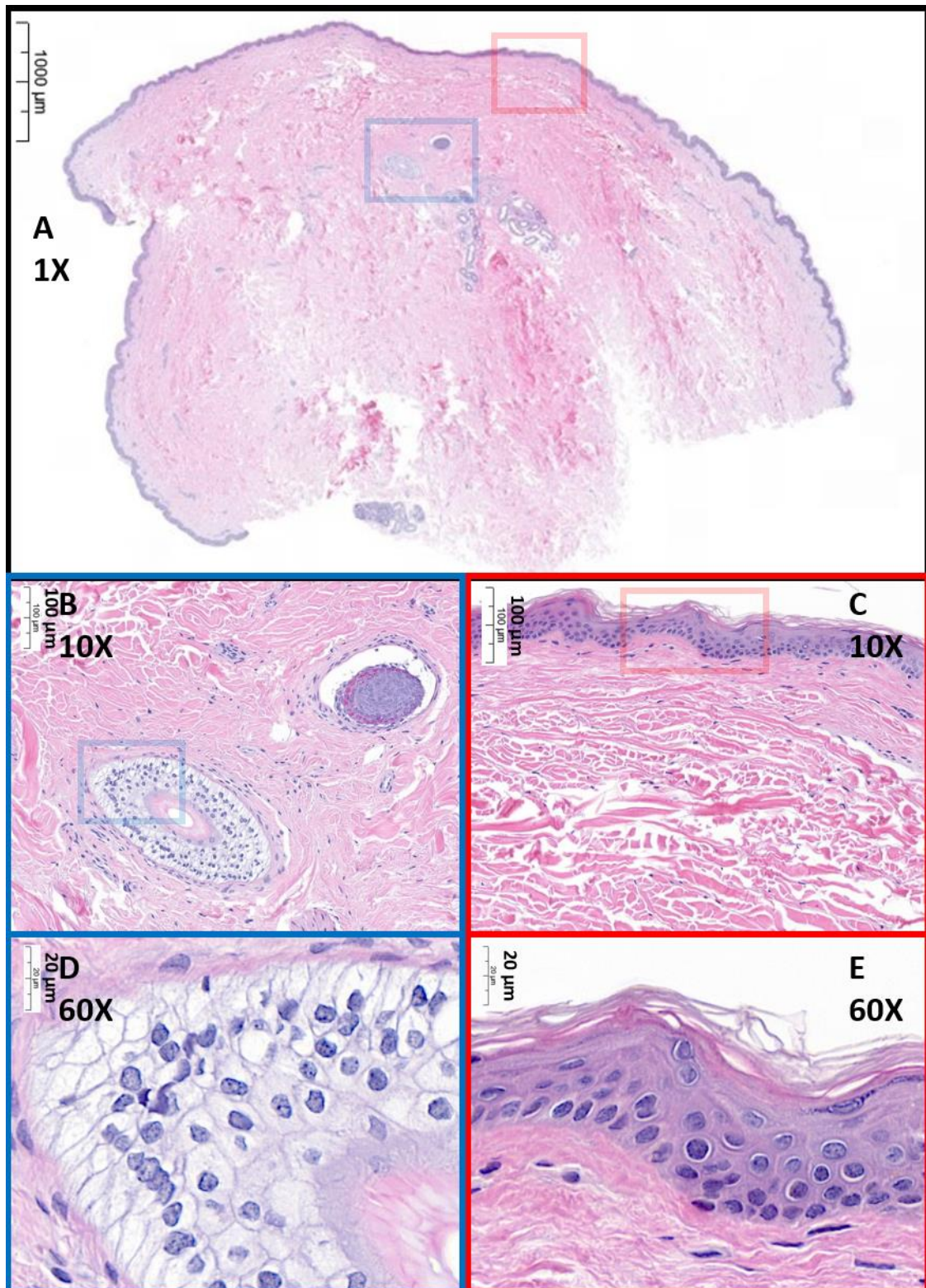


Figure 3.15 Histology illustrates minimal immune cell infiltration in healthy control skin.

Biopsies from HS lesional skin (n=6) and healthy control skin (n=3) were formalin fixed, paraffin embedded, sectioned at 4 µm and stained with H&E. Representative image of a Con skin sample at 1x (A), featuring a hair follicle (blue box) and normal epidermis (red box)). The hair follicle is displayed at 10X (B) and 60X (D); the epidermis at 10X (C) and 60X (E). Scale bar indicates 1000 µm (A), 100 µm (B & C) and 20 µm (D & E).

3.4.7 scRNA-Seq analysis reveals multiple immune cell clusters present in HS skin

To develop upon the phenotypic and histological findings, gene expression detail at the single immune cell level was explored for both Con and HS L skin samples. Live CD45⁺ and CD45⁻ cells were purified from the cryopreserved dissociated tissue, the cells barcoded and scRNA-Seq analysis performed on each cell (Section 2.2.16). Data interpretation was performed on the CD45⁺ cell cohort (Section 2.2.17).

Figure 3.16 shows the UMAP plot displaying the unbiased classification of skin cell subpopulations from the total (HS & Con) dataset (i.e. Con [n=3] and HS [n=6] samples). This figure shows 30 unique cell clusters, each with a distinct transcriptional profile based on differential gene expression (DGE)(Appendix; Figure 6.1). Extensive visual evaluation of marker expression was used to establish cluster identities, bolstered by SingleR and databases such as the Human Cell Atlas (www.humancellatlas.org).

The mean cell number analysed per sample was 3535, \pm SD of 761 (n=6), for HS patients, 3820, \pm SD of 505 (n=3) for healthy controls. As per Table 3.3, the majority of cells are comprised of T cell subsets (clusters 0, 1, 2, 4, 11, 12, 13 and 26; 51.2% for HS v 44.2% for Con), next B cell subsets (clusters 5, 7, 10, 19 and 22; 24.9% for HS v 3.1% for Con) and then myeloid cells (clusters 3, 8, 9, 14, 18, 25, 28 and 29; 15.3% for HS v 24.6% for Con). ILC and NK cell subsets (clusters 15, 16 and 27) make up 3.9% for HS v 6.0% for Con. Although CD45⁻, there was a small keratinocyte population (clusters 17, 20 and 21; 4.0% for HS v 4.3% for Con), likely due to a <100% cell sort. The cluster 6 (0.3% for HS v 14.5% for Con), identified in two healthy control samples but no HS samples, had no identifiable cell subset markers and was removed prior to subsequent analysis. Unsurprisingly given their fragility upon cryopreservation, no neutrophils were identified in the analysis.

To aid in cluster identification as well as elucidating cell function, UMAP heatmaps display the expression profiles (in navy) for genes associated with CD4 T cells (Figure 3.17), Th17 cells (Figure 3.18), ILC, NK cells and CD8 T cells (Figure 3.19), B cells (Figure 3.20), as well as myeloid cell subsets (Figure 3.21 and Figure 3.22). These heatmaps were generated using the MAGIC method for clearer visualisation (Section 2.2.17). In reality,

some clusters likely include various subsets, and indeed clusters are not distinct, with some populations encroaching into neighbouring clusters. Further, expected genes are occasionally absent, most likely on account of the particular gene not being sufficiently transcribed at the exact analysis snapshot. For example, although there are multiple CD4 T cell subsets, *CD4* was very weakly detected, only presenting within the Treg cell cluster, and surprisingly within some myeloid populations. Similarly, the LC pan-marker *CD207* (langerin) was not detected within this dataset. But in any case, cluster generation proves an invaluable tool in approximating and identifying populations.

Clusters were identified based on the presence, absence or levels of expression of multiple (frequently 10-20) genes, and so is challenging to fully disclose here. To give brief examples of the cell cluster characterisation, Tem cells (cluster 0) and Trm cells (cluster 2) were identified based on their gene expression (or absence) of characteristic markers such as *CD3E*, *CD44*, *IL7R* (CD127), *CD40LG* (CD154; not shown), *ITGAE* (CD103), *CD69*, *CD8A* and *SELL* (CD62-L) ; Treg cells (cluster 1) to include *FOXP3* and *IL2RA* (CD25; not shown) . Th17 cell subsets (cluster 12 and 13) were high gene expressors for *KLRB1* (CD161), *IL17A* and *IL17F*. The case was similar for myeloid cells. For example, although *CD207* was not detected, LC could be identified based on *CD1A*, *CD1C* amongst others. Likewise, *THBD* (CD141) was detected in numerous clusters (cDC2, cDC1, and pDC), but cDC2 also expressed *CD1C*, whereas pDC exclusively expressed *NRP1* (CD304/BDCA3) and cDC1 exclusively *CLEC9A* (CD370).

The UMAP at Figure 3.23 displays the cell cluster distribution within the HS patient cohort alone, whilst Figure 3.24 displays the distribution for the healthy control samples. The UMAP at Figure 3.25 overlays the HS cohort (in purple) with the Con group (in green). Taken together, these plots show a greater proportion of lymphoid cells within the HS samples compared with more myeloid cells within the Con samples. There is an almost complete absence of B cells, plasmablasts, plasma cells and Th17 cells within the Con group.

To summarise this section, transcriptomic analysis revealed 30 distinct immune cell clusters within HS and healthy control skin samples, with great variability within HS

lesional samples. On average, over 50% of cells were T cells in HS skin. Whereas the frequency of lymphoid cells was more abundant in HS samples, myeloid subsets appeared to be less populous than in healthy skin. Gene expression analysis identified the cellular source of multiple inflammation-associated markers such as surface receptors, chemokines and cytokines.

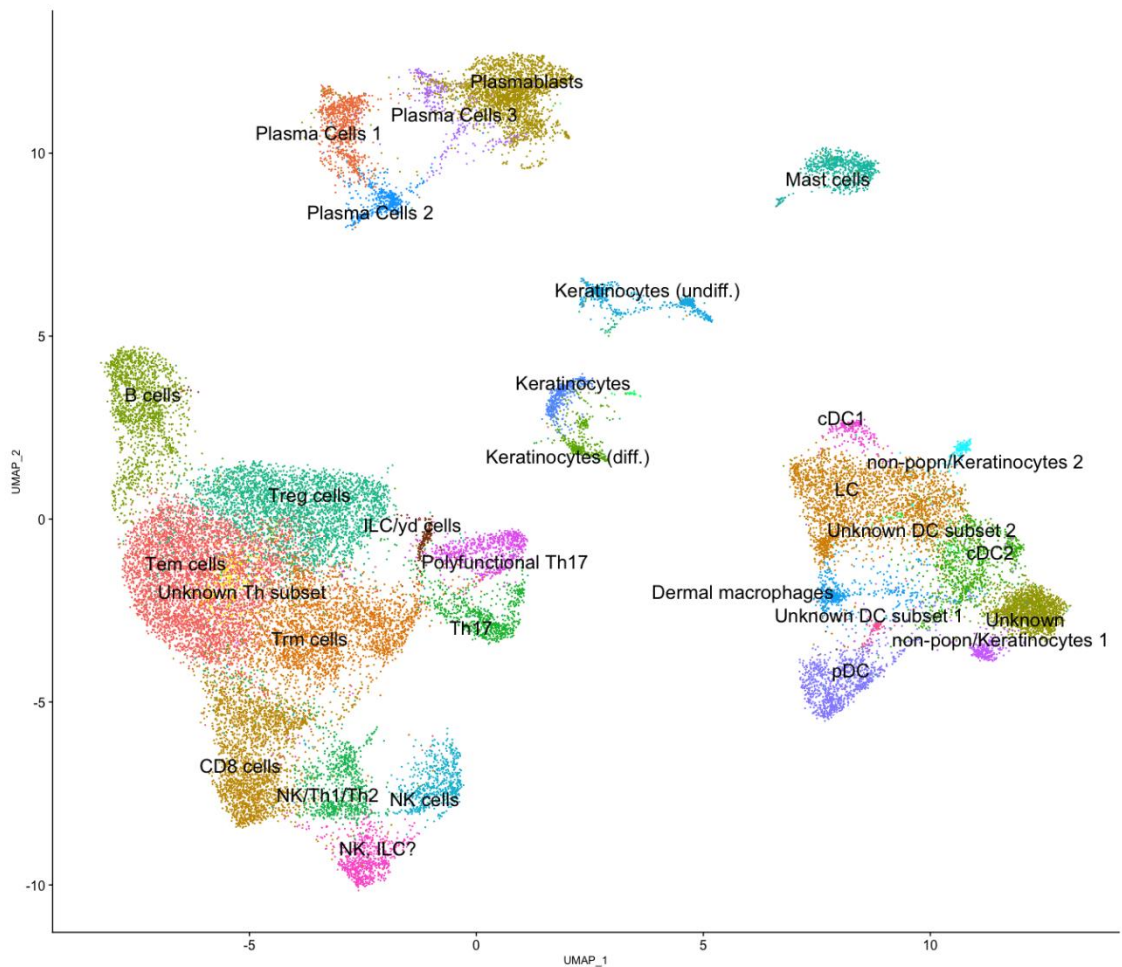


Figure 3.16 UMAP plot identified 30 unique cell clusters within HS patient lesions and healthy control skin.

Cells isolated from the skin of healthy controls (Con; n=3) or HS lesional skin (HS; n=6) were purified based on CD45 expression, barcoded and their gene expression determined by single cell RNA sequencing (scRNA-Seq). UMAP plot displays 30 unique clusters generated by unsupervised classification of the total CD45⁺ dataset.

Cell cluster	Annotation	HS (%)	Con (%)	Significance (p)
0	Tem cells	15.53	13.74	ns
1	Treg cells	11.04	8.31	ns
2	Trm cells	7.30	10.32	ns
3	Langerhans cells (LC)	5.55	12.02	ns
4	CD8 cells	8.36	6.47	ns
5	Plasmablasts	10.58	1.38	ns
6	Unknown	0.31	14.49	*
7	B cells	7.01	1.25	ns
8	pDC	1.86	5.24	*
9	cDC2	2.14	3.70	ns
10	Plasma cells 1	3.95	0.30	ns
11	NK/Th1/Th2	2.27	3.29	ns
12	Polyfunctional Th17	2.61	1.63	ns
13	Th17	3.17	0.44	*
14	Mast cells	2.69	1.20	ns
15	NK, ILC?	1.50	3.30	ns
16	NK cells	1.96	1.92	ns
17	Keratinocytes	1.71	1.66	ns
18	Dermal macrophages	2.01	1.06	ns
19	Plasma cells 2	1.92	0.16	*
20	Keratinocytes	1.13	1.54	ns
21	Keratinocytes	1.14	1.09	ns
22	Plasma cells 3	1.43	0.03	*
23	non pop	0.08	2.26	ns
24	non pop	0.37	1.12	ns
25	cDC1	0.50	0.79	ns
26	Unknown Th subset	0.88	0.00	ns
27	ILC/γδ cells	0.43	0.76	ns
28	Unknown DC subset	0.15	0.54	ns
29	Unknown DC subset	0.43	0.00	*

Table 3.3 Cell cluster frequency.

Frequency of cell clusters, identified through scRNA-Seq, within the HS and Con cohorts. Clusters are listed 0-29 in order of overall frequency. Statistical difference between HS and Con samples was calculated using Mann-Whitney t-test; *p<0.05, ns: non-significant.

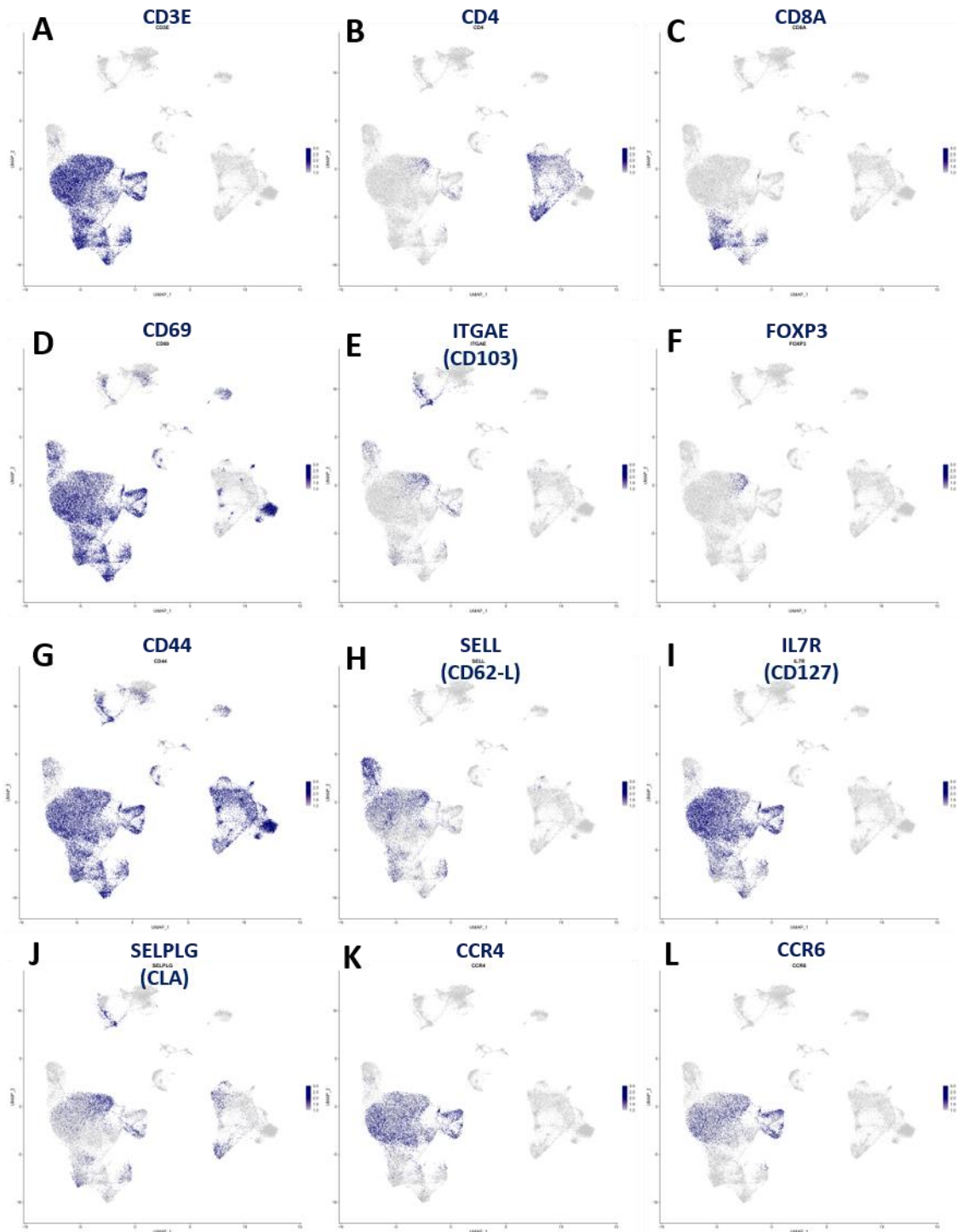


Figure 3.17 scRNA-Seq expression profiles for genes associated with CD4 T cell clusters within HS patient lesions and healthy control skin.

Cells isolated from the skin of healthy controls (Con; n=3) or HS lesional skin (HS; n=6) were purified based on CD45 expression, barcoded and their gene expression determined by scRNA-Seq. UMAP plots display gene expression (navy) for CD3E (A), CD4 (B), CD8A (C), CD69 (D), ITGAE (CD103; E), FOXP3 (F), CD44 (G), SELL (CD62-L; H), IL7R (CD127; I), SELPLG (CD162/ CLA; J), CCR4 (K), CCR6 (L), of clusters generated by unsupervised classification of the dataset for the overall CD45⁺ cohort.

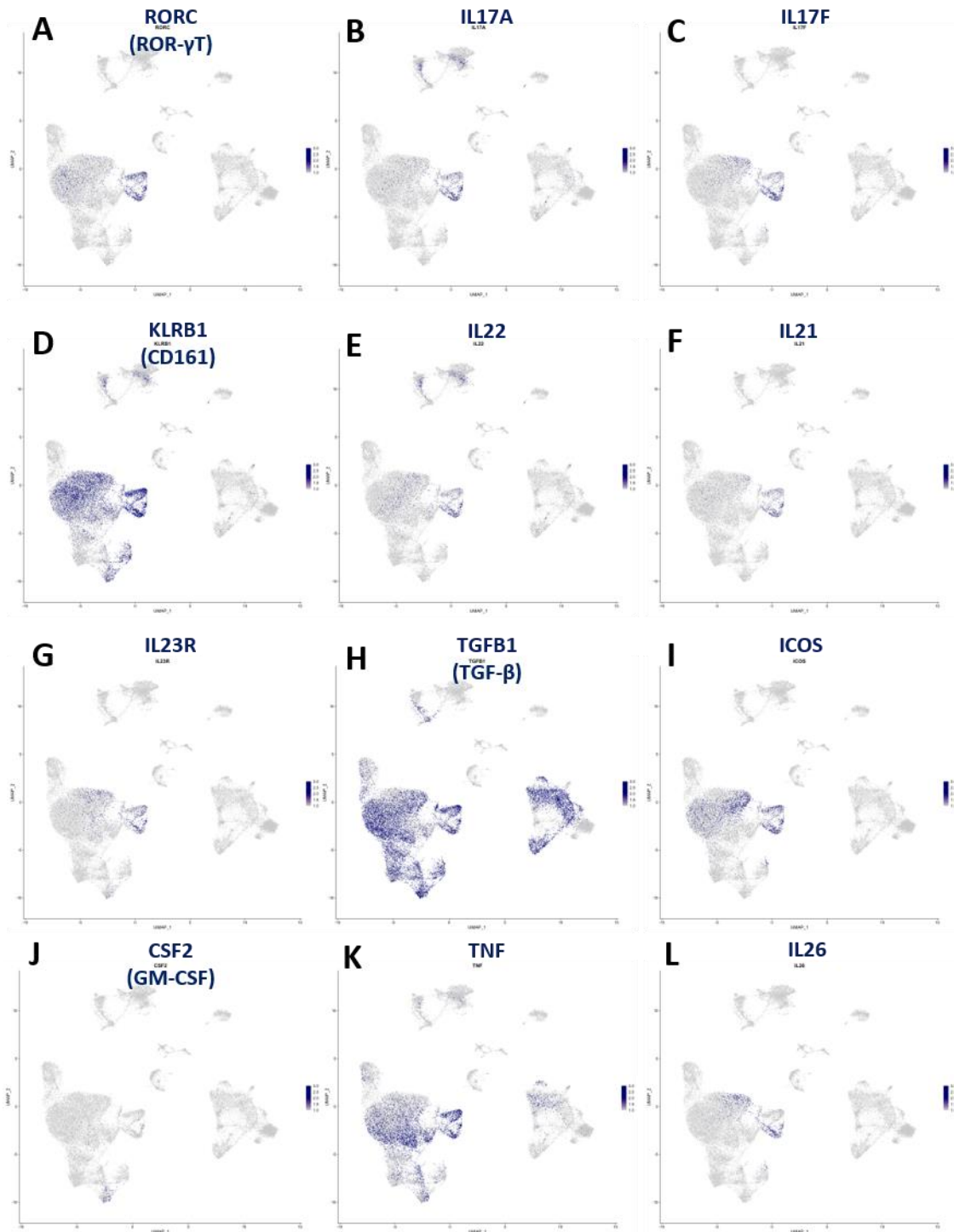


Figure 3.18 scRNA-Seq expression profiles for genes associated with Th17 cell clusters within HS patient lesions and healthy control skin.

Cells isolated from the skin of healthy controls (Con; n=3) or HS lesional skin (HS; n=6) were purified based on CD45 expression, barcoded and their gene expression determined by scRNA-Seq. UMAP plots display gene expression (navy) for RORC (ROR- γ T; A), IL17A (B), IL17F (C), KLRB1 (CD161; D), IL22 (E), IL21 (F), IL23R (G), TGFB1 (TGF- β ; H), ICOS (I), CSF2 (GM-CSF; J), TNF (K), IL26 (L) of clusters generated by unsupervised classification of the dataset for the overall CD45⁺ cohort.

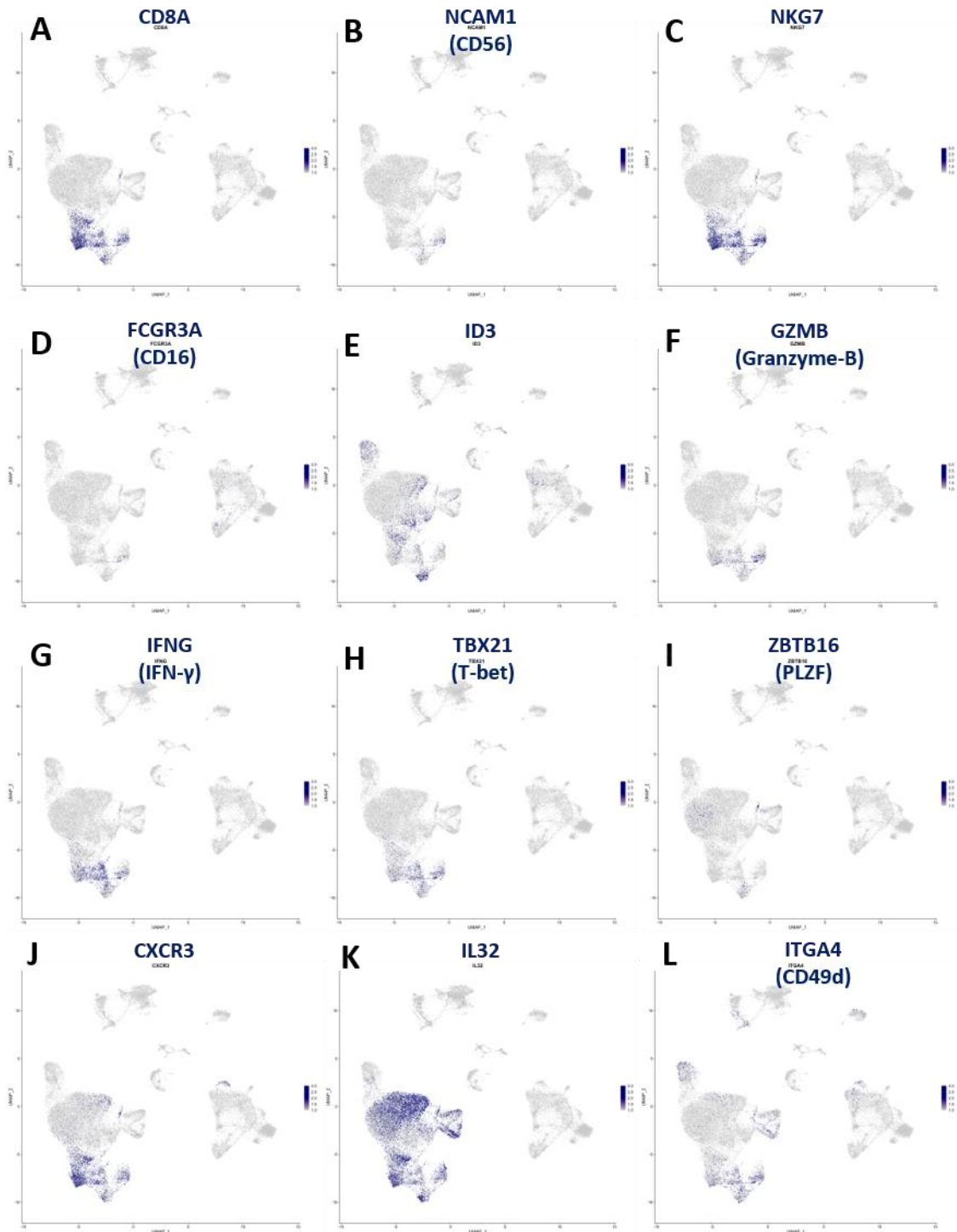


Figure 3.19 scRNA-Seq expression profiles for genes associated with CD8 T cell, NK cell and ILC clusters within HS patient lesions and healthy control skin.

Cells isolated from the skin of healthy controls (Con; n=3) or HS lesional skin (HS; n=6) were purified based on CD45 expression, barcoded and their gene expression determined by scRNA-Seq. UMAP plots display gene expression (navy) for CD8A (A), NCAM1 (CD56; B), NKG7 (C), FCGR3A (CD16; D), ID3 (E), GZMB (Granzyme-B; F), IFNG (IFN- γ ; G), TBX21 (T-bet; H), ZBTB16 (PLZF; I), CXCR3 (J), IL32 (K), ITGA4 (CD49d; L) of clusters generated by unsupervised classification of the dataset for the overall CD45⁺ cohort.

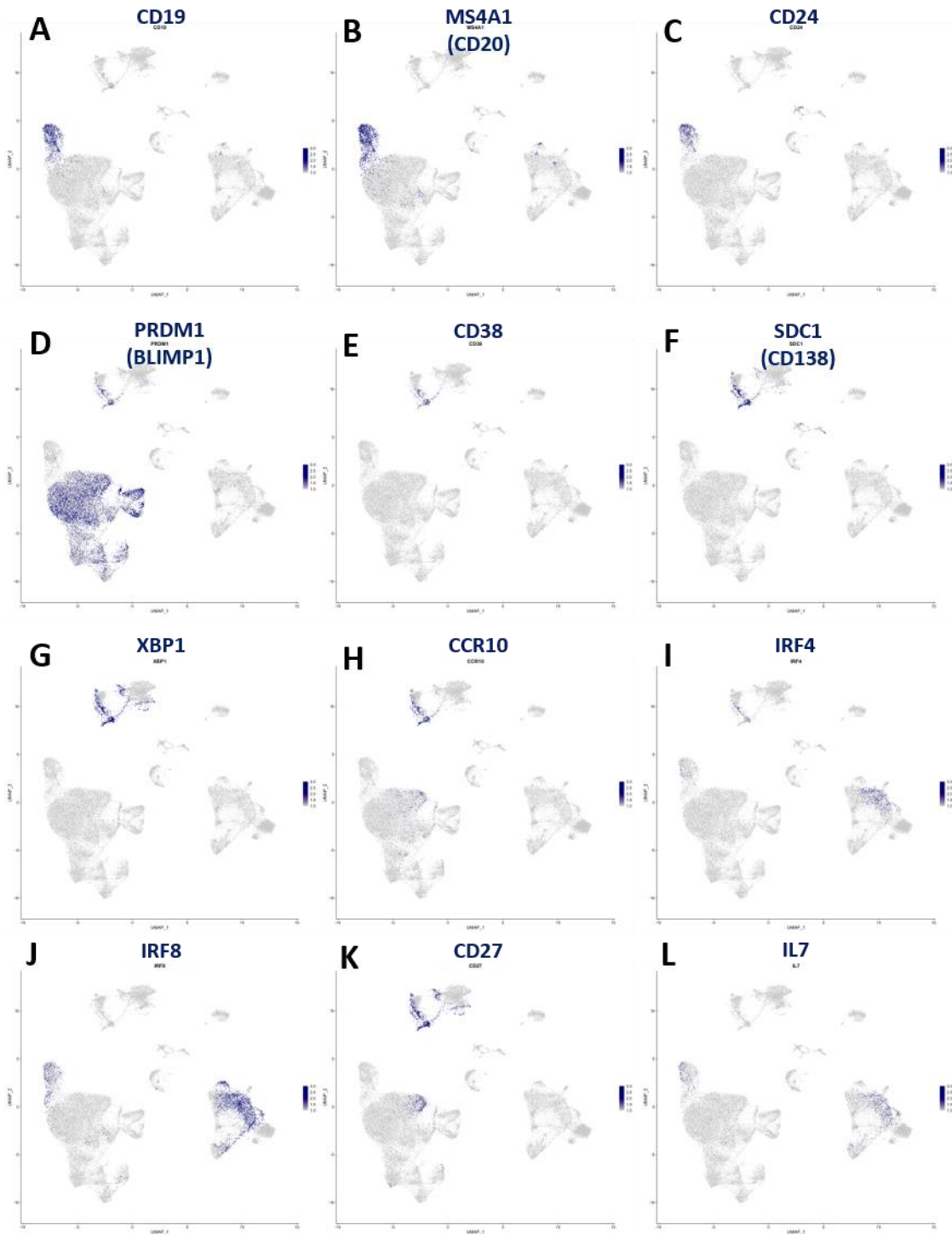


Figure 3.20 scRNA-Seq expression profiles for genes associated with B cell clusters within HS patient lesions and healthy control skin.

Cells isolated from the skin of healthy controls (Con; n=3) or HS lesional skin (HS; n=6) were purified based on CD45 expression, barcoded and their gene expression determined by scRNA-Seq. UMAP plots display gene expression (navy) for CD19 (A), MS4A1 (CD20; B), CD24 (C), PRDM1 (BLIMP1; D), CD38 (E), SDC1 (CD138; F), XBP1 (G), CCR10 (H), IRF4 (I), IRF8 (J), CD27 (K), IL7 (L) of clusters generated by unsupervised classification of the dataset for the overall CD45⁺ cohort.

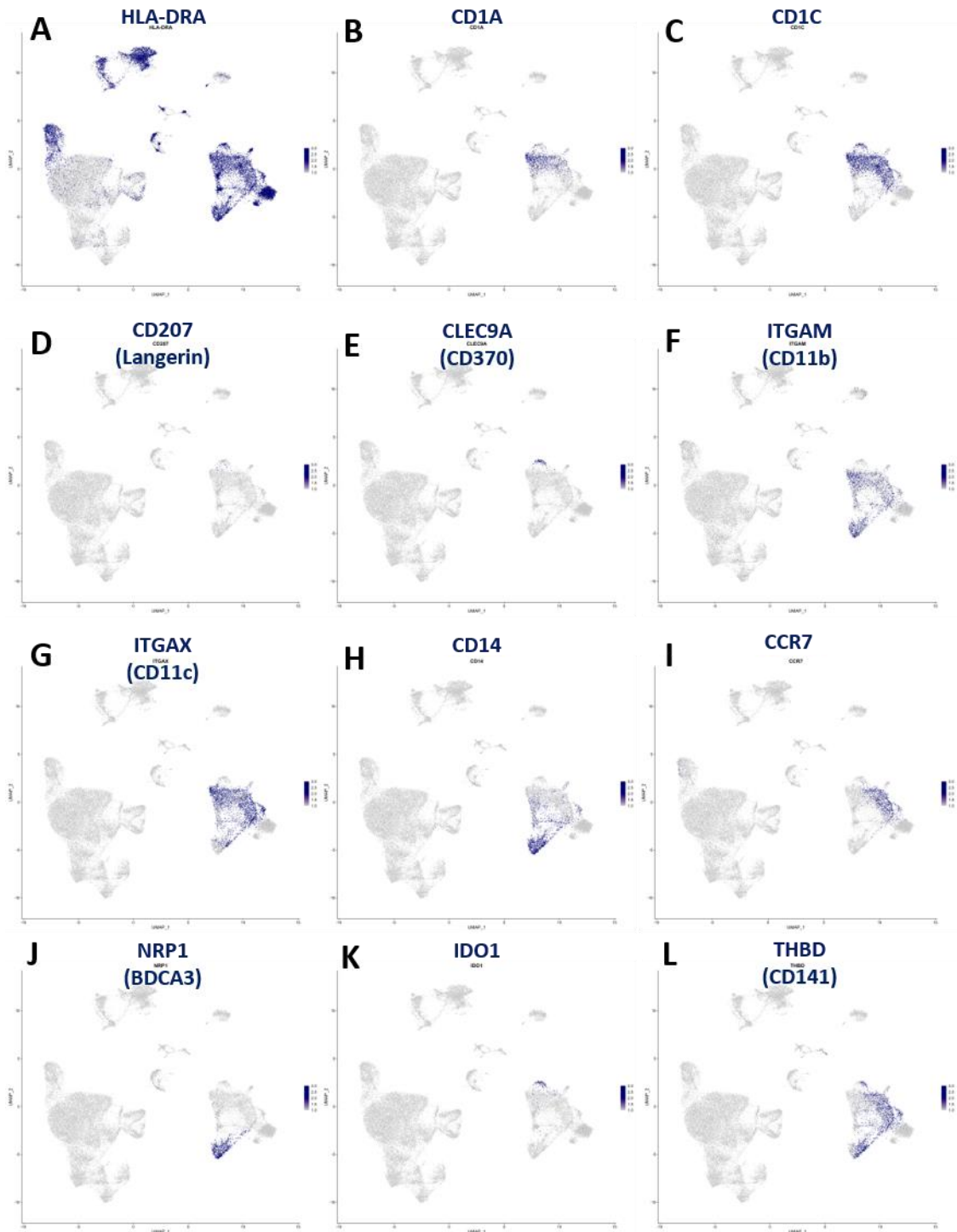


Figure 3.21 scRNA-Seq expression profiles for genes associated with myeloid cell clusters within HS patient lesions and healthy control skin (I).

Cells isolated from the skin of healthy controls (Con; n=3) or HS lesional skin (HS; n=6) were purified based on CD45 expression, barcoded and their gene expression determined by scRNA-Seq. UMAP plots display gene expression (navy) for HLA-DRA (A), CD1A (B), CD1C (C), CD207 (langerin; D), CLEC9A (CD370; E), ITGAM (CD11b; F), ITGAX (CD11c; G), CD14 (H), CCR7 (I), NRP1 (CD304/BDCA3; J), IDO1 (IDO; K), THBD (CD141; L) of clusters generated by unsupervised classification of the dataset for the overall CD45⁺ cohort.

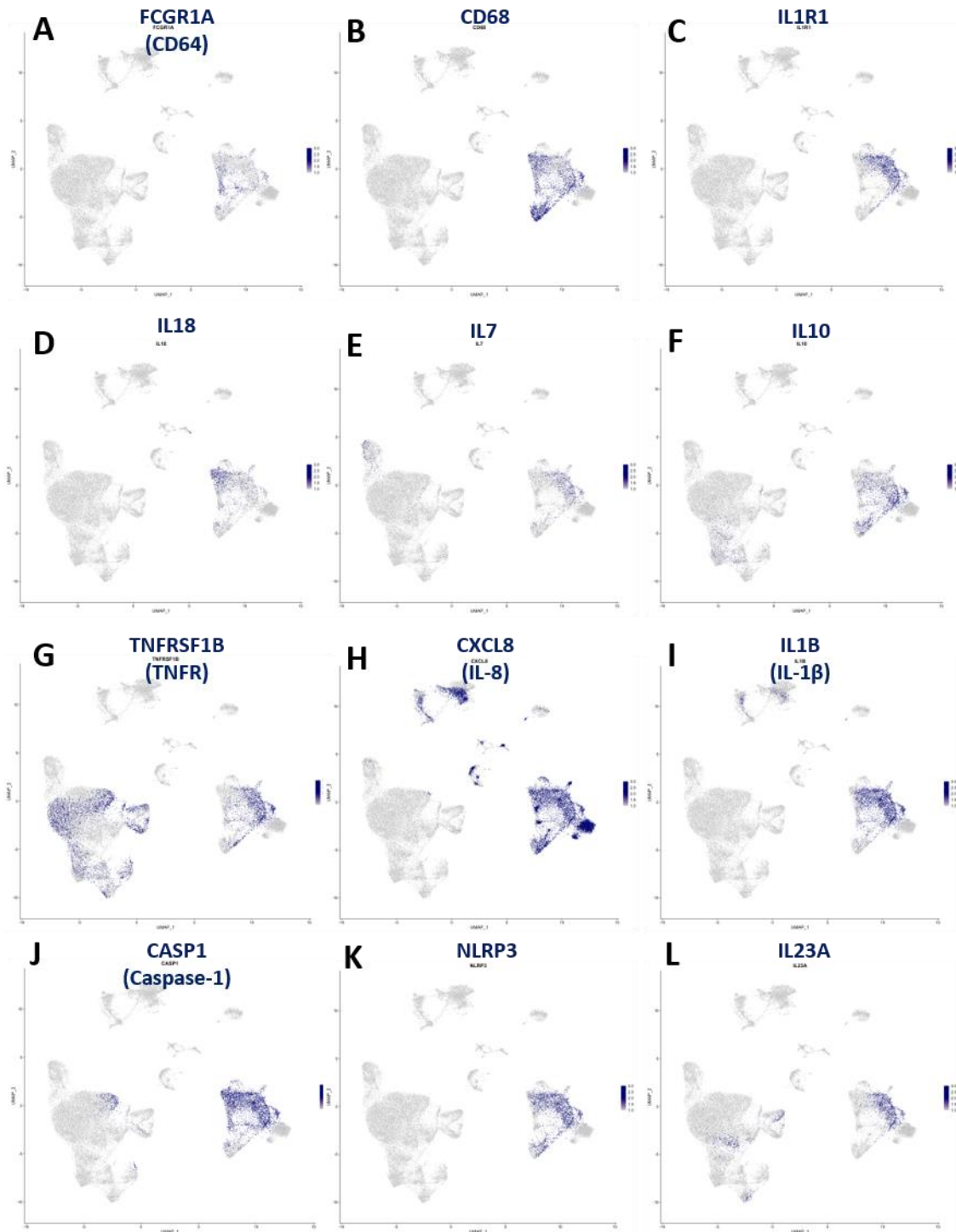


Figure 3.22 scRNA-Seq expression profiles for genes associated with myeloid cell clusters within HS patient lesions and healthy control skin (II).

Cells isolated from the skin of healthy controls (Con; n=3) or HS lesional skin (HS; n=6) were purified based on CD45 expression, barcoded and their gene expression determined by scRNA-Seq. UMAP plots display gene expression (navy) for FCGR1A (CD64; A), CD68 (B), IL1R1 (C), IL18 (D), IL7 (E), IL10 (F), TNFRSF1B (TNFR; G), CXCL8 (IL-8; H), IL1B (IL-1 β ; I), CASP1 (Caspase-1; J), NLRP3 (K), IL23A (L) of clusters generated by unsupervised classification of the dataset for the overall CD45⁺ cohort.

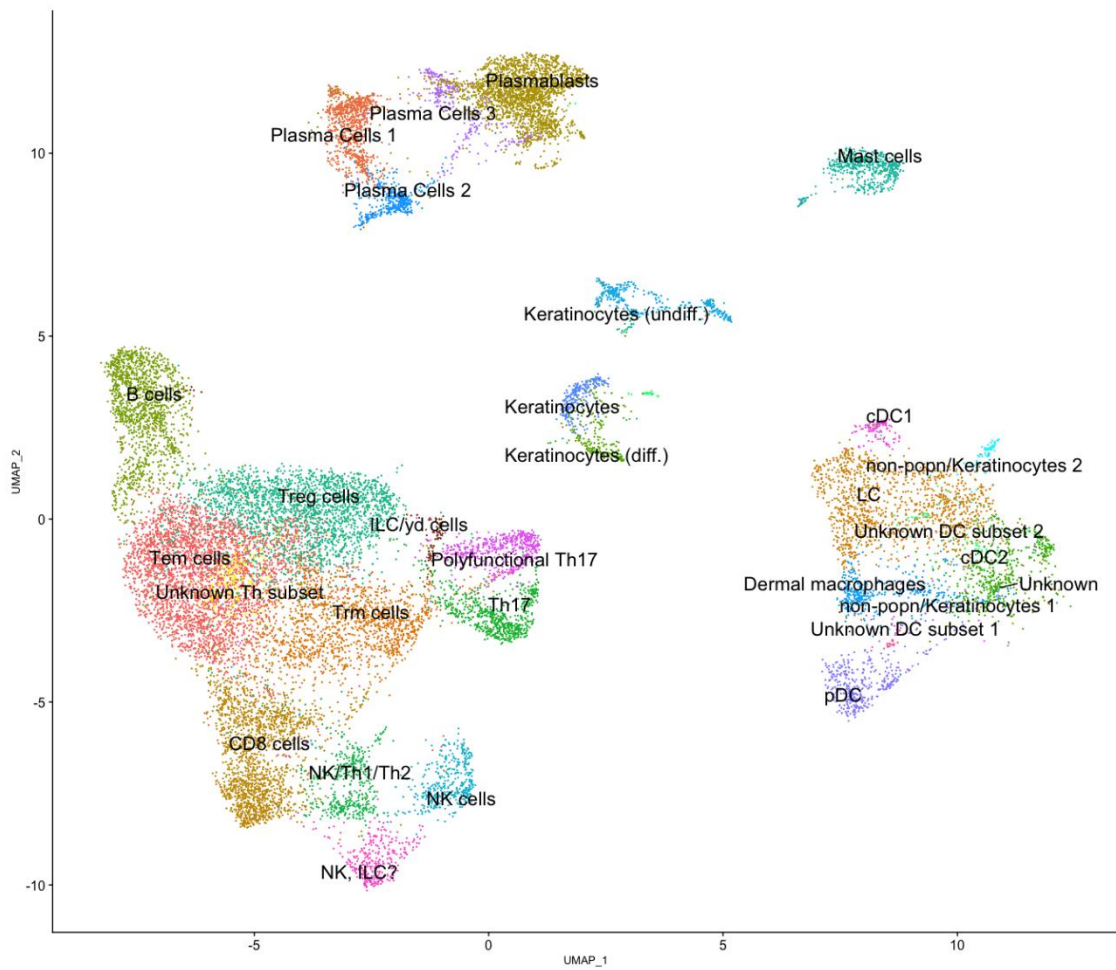


Figure 3.23 UMAP plot visualising cell clusters within HS patient lesional skin.

Cells isolated from HS lesional skin (HS; n=6) were purified based on CD45 expression, barcoded and their gene expression determined by scRNA-Seq. UMAP plot displays unique clusters generated by unsupervised classification of the dataset for the HS patient CD45⁺ cohort.

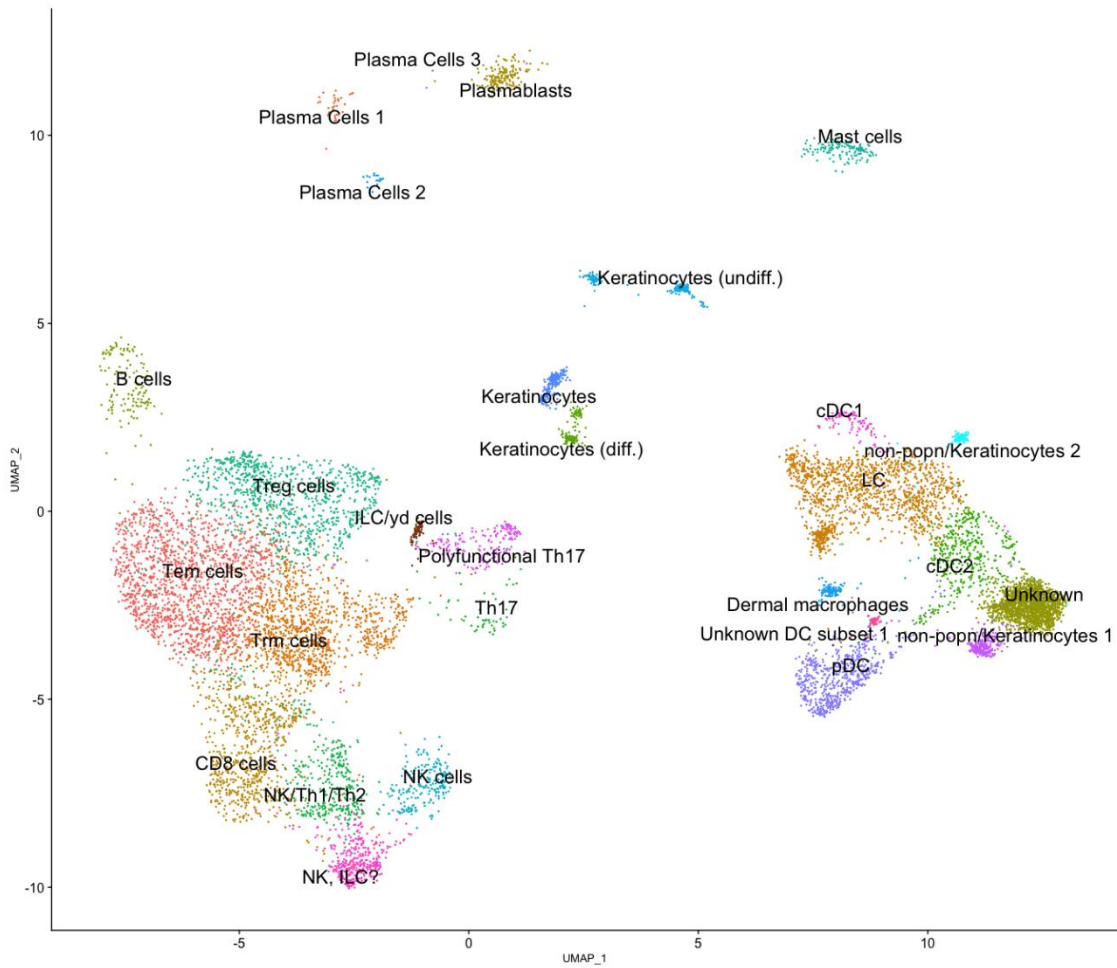


Figure 3.24 UMAP plot visualising cell clusters within healthy control skin.

Cells isolated from the skin of healthy controls (Con; n=3) were purified based on CD45 expression, barcoded and their gene expression determined by scRNA-Seq. UMAP plot displays unique clusters generated by unsupervised classification of the dataset for the healthy control CD45⁺ cohort.

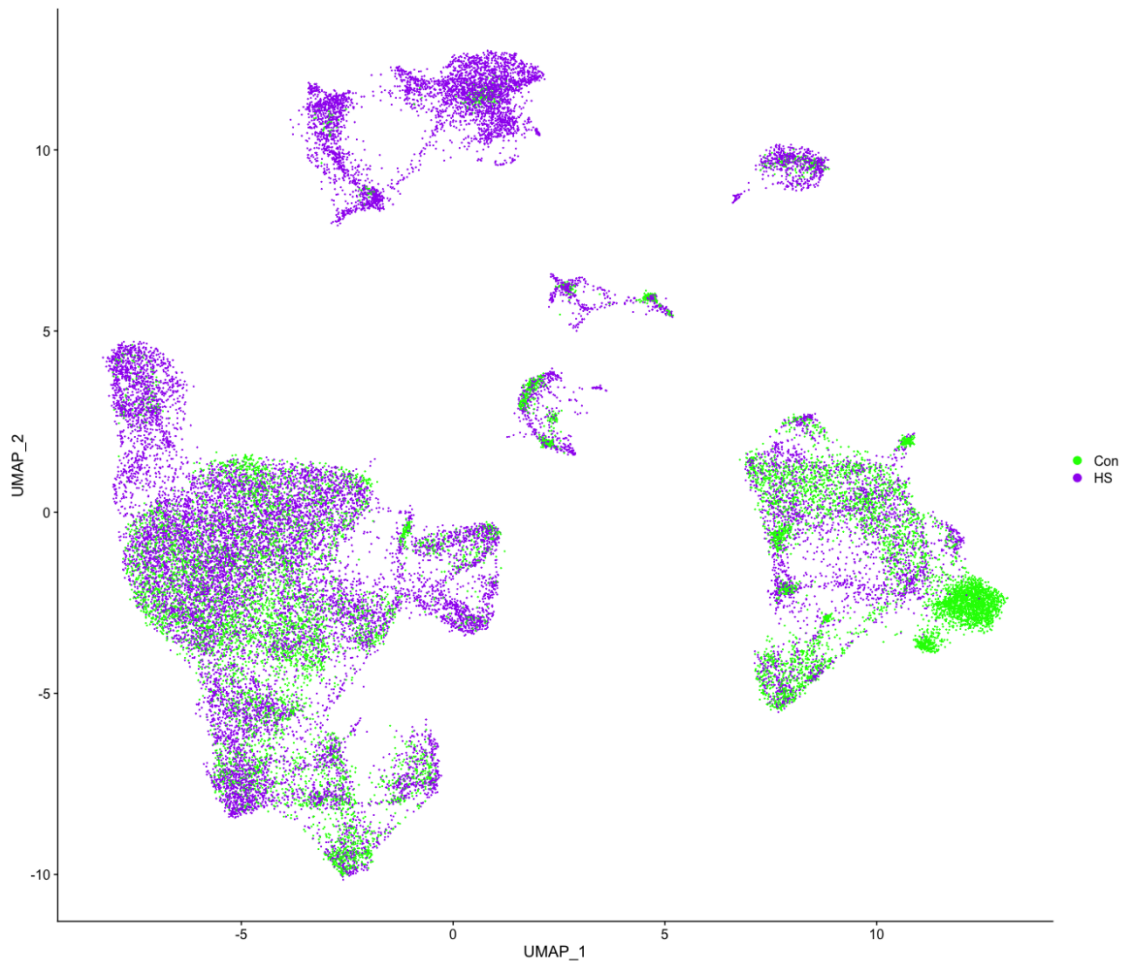


Figure 3.25 UMAP plot overlaying cell populations of HS patient lesional skin with healthy control skin.

Cells isolated from the skin of healthy controls (Con; n=3) or HS lesional skin (HS; n=6) were purified based on CD45 expression, barcoded and their gene expression determined by scRNA-Seq. UMAP plot displays the overlay of cell populations generated by unsupervised classification of the dataset for the HS patient (purple) and healthy control (green) CD45⁺ cohort.

3.4.8 scRNA-Seq analysis showed clear differences in gene expression between HS lesional skin and healthy control skin

The HS and healthy control scRNA-Seq sample data have presented 30 unique cell clusters and illustrated differences in gene expression and cell frequency between the cohorts. This section delves further into the differences between groups and highlights specific differences in terms of genes and pathways.

Figure 3.26 features individual UMAP plots for each HS patient (A-F) and Con sample (G-I). Whereas the Con samples appear quite consistent and homogenous, the variability is apparent within the HS samples. Some samples have few B cells, plasmablasts or plasma cells, whereas 2HS-21 has effectively no myeloid cells. This variability is likely on account of the heterogenous nature of HS lesions, as well as differences in sample size and location (both anatomically and within the lesion).

Principal component analysis (PCA)(Figure 3.27A) reduces the dimensionality within the scRNA-Seq data and shows the three healthy control samples (in blue) clustering together, suggesting a similarity in terms of cells present and their gene expression. However, the six HS lesional samples (in red) are spread throughout the plot signifying a heterogenous population of cells and transcriptome. Although 2HS-22 is very close to the Con cluster, its UMAP plot shows the distinction, with plasmablasts, plasma cells and mast cells that are absent in all Con samples.

Figure 3.27B displays the differential gene expression (DGE) of the healthy control samples (to the left) compared with the HS lesional samples. Each column is colour coded at the top of the plot; the column width is proportional to the number of cells analysed for that sample. The top half of the plot gives an overview of the DGE for the 100 most expressed genes in the HS skin samples compared with healthy control, whilst the bottom half highlights the 100 most expressed genes in the healthy control skin samples compared with HS lesions. The homogenous healthy control cohort as compared with a highly variable HS group evident in the PCA is clear in this DGE. Sample 2HS-17 and 2HS-22, which are most proximal to the Con cluster in the PCA, appear the

most similar to Con samples in terms of DGE, particularly for genes expressed more in the healthy controls.

The volcano plot in Figure 3.28 features the specific genes over or under expressed in HS samples compared with healthy controls. The X-axis is a measure of the fold change (natural log) with the significance along the Y-axis ($-\text{Log}_{10} P$). Genes in red are those with a significant fold change. Those genes displaying the most marked DGE increase include *IGLL5* (Appendix; Figure 6.2A), *JCHAIN* (Figure 6.2B), *MZB1* (Figure 6.2C) and *SSR4* (Figure 6.2D), which all appear to be most abundant in the plasma cell and plasmablast cell clusters. *S100A8* (Figure 6.3A), and *S100A9* (Figure 6.3B) in some myeloid subpopulations and *IL17A* in Th17 cells (Figure 6.4).

Those downregulated in HS compared with healthy controls include *ZFP36L2* principally in T cells (Figure 6.5A), *TOB1* (Figure 6.5B) and *RGCC* (Figure 6.5C) across myeloid and T cells and *CEBPD* (Figure 6.5D) in the myeloid cell cluster. *RNASE1* appears to be downregulated solely in pDC (Figure 6.6).

Beyond individual genes, there were 36 pathways with a fold enrichment greater than 1 identified in HS lesions compared with healthy control skin. (Figure 3.29). Some pathways of note include BCR (pathway 1) and TCR (pathway 2) signalling, Th differentiation (pathways 4 and 8), immune checkpoint pathways (pathway 2), TNF signalling (pathway 11), IL-17 signalling (pathway 18) FcεRI (pathway 13), NOTCH signalling (pathway 19) and oestrogen signalling (pathway 31).

In conclusion, despite variability within HS lesions, there is a clear difference in expression of hundreds of genes in HS lesional skin compared with healthy control skin, with markedly enhanced and downregulated genes clustering to B cells, T cells and myeloid subpopulations. Taken together, these variations implicate numerous signalling pathways in HS pathology.

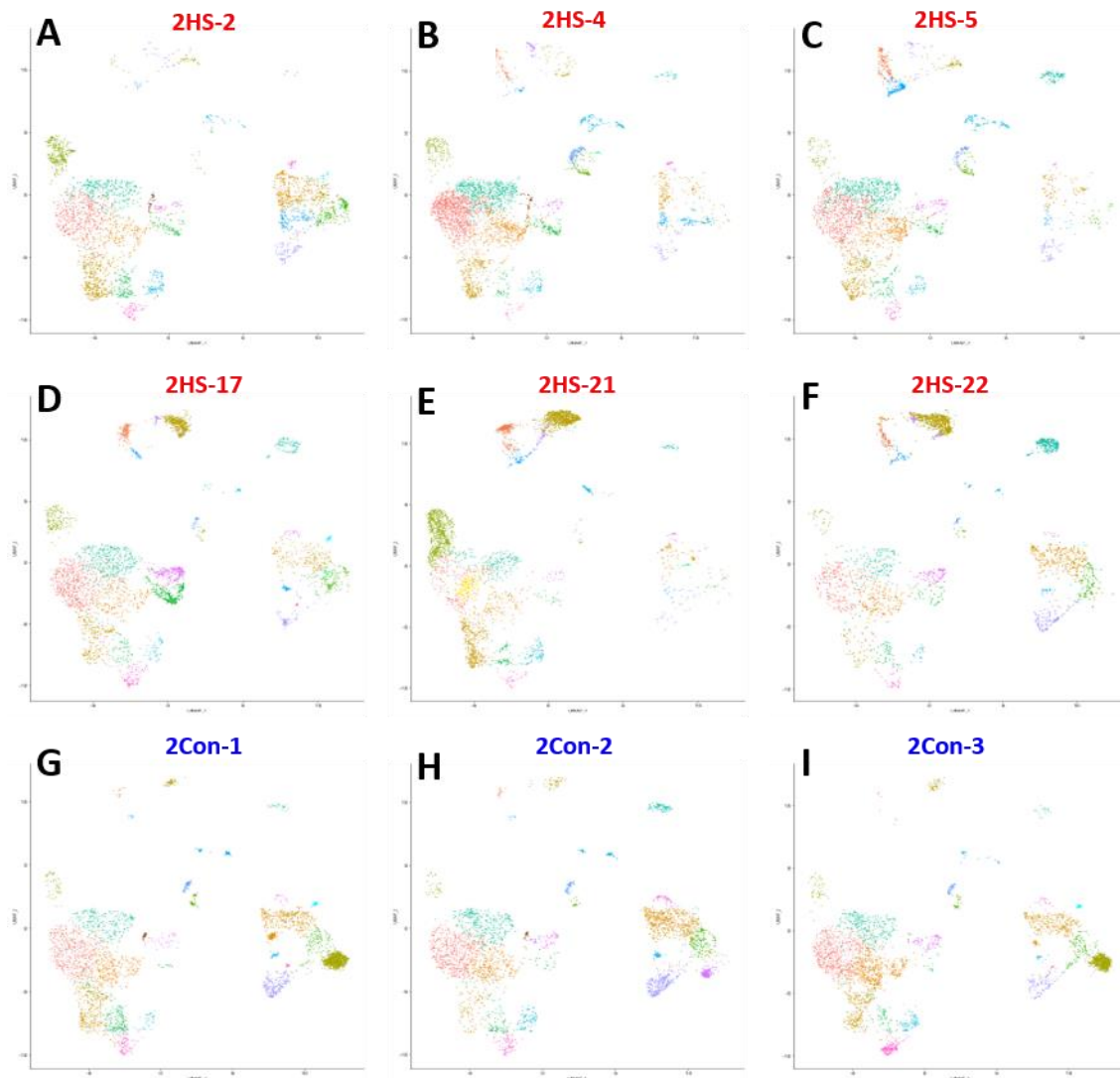


Figure 3.26 UMAP plots for each individual HS patient lesions and healthy control skin sample.

Cells isolated from the skin of healthy controls (Con; n=3) or HS lesional skin (HS; n=6) were purified based on CD45 expression, barcoded and their gene expression determined by scRNA-Seq. UMAP plots for each HS patient skin sample (A to F) and healthy control sample (G to I).

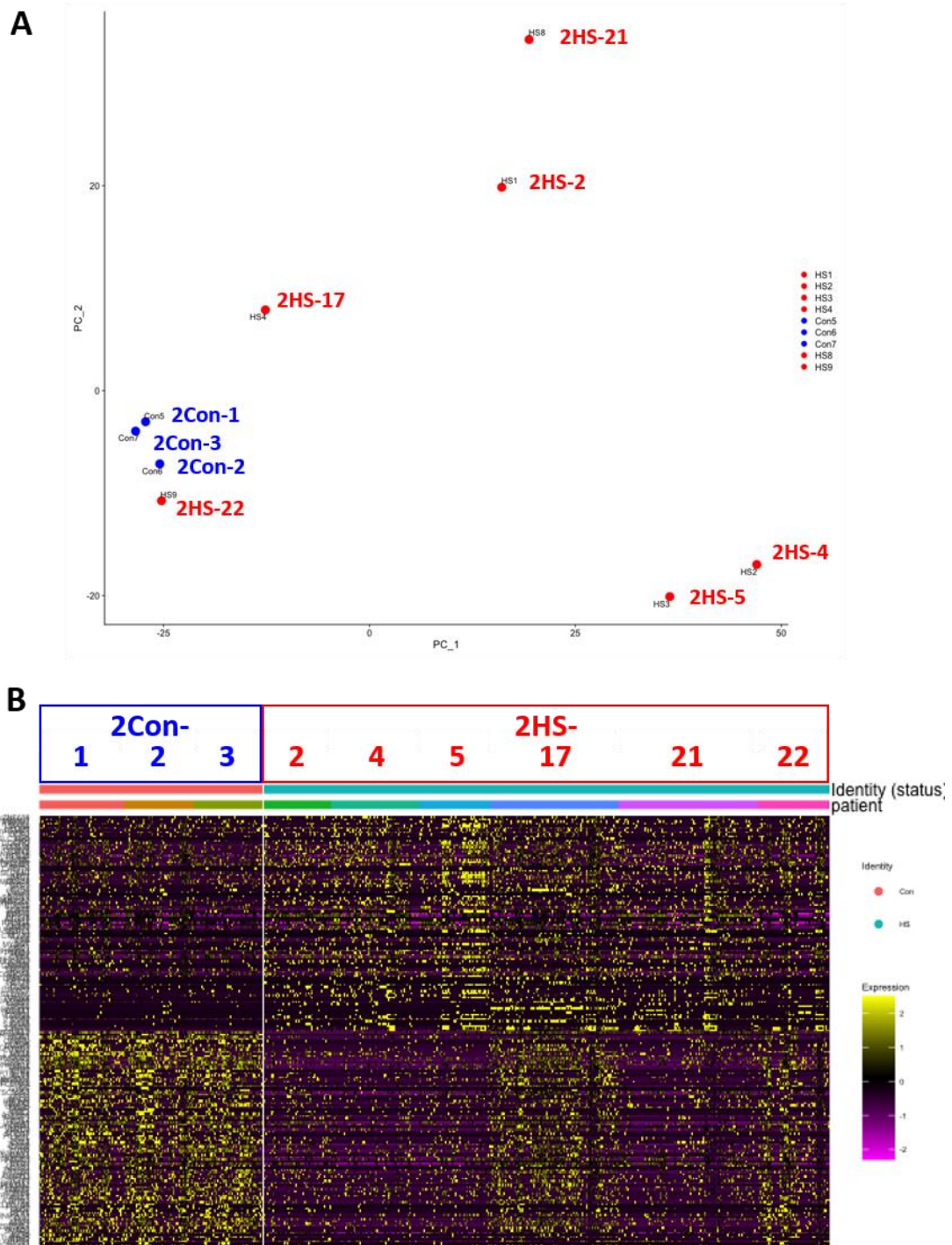


Figure 3.27 Principal component analysis and differential gene expression for HS patient lesions compared with healthy control skin.

Cells isolated from the skin of healthy controls (Con; n=3) or HS lesional skin (HS; n=6) were purified based on CD45 expression, barcoded and their gene expression determined by scRNA-Seq. Principal component analysis illustrates a homogeneous healthy control population but heterogeneity within the HS cohort (A). Differential gene expression analysis of expression differences between of healthy control skin (left column) and HS patient lesions (right column) in relation to the top 100 genes and bottom 100 gene expression differences (B).

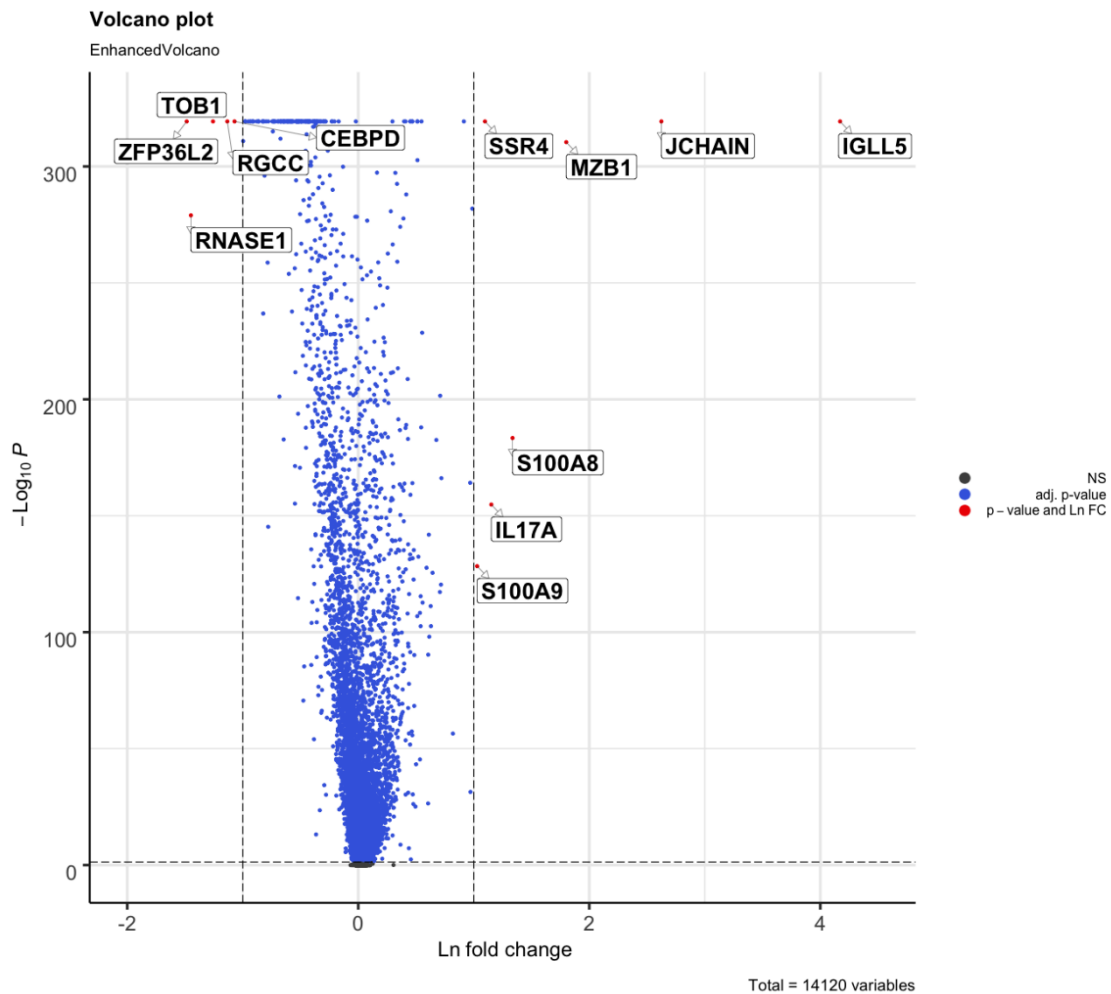


Figure 3.28 Volcano plot highlights gene expression fold change for HS patient lesions compared with healthy control skin.

Cells isolated from the skin of healthy controls (Con; n=3) or HS lesional skin (HS; n=6) were purified based on CD45 expression, barcoded and their gene expression determined by scRNA-Seq). Volcano plot visualises differential gene expression in HS samples compared with healthy controls, labelling genes significantly over (positive along Ln fold change X-axis) or under (negative along Ln fold change X-axis) expressed. The $-\text{Log}_{10} P$ Y-axis is a measure of significance.

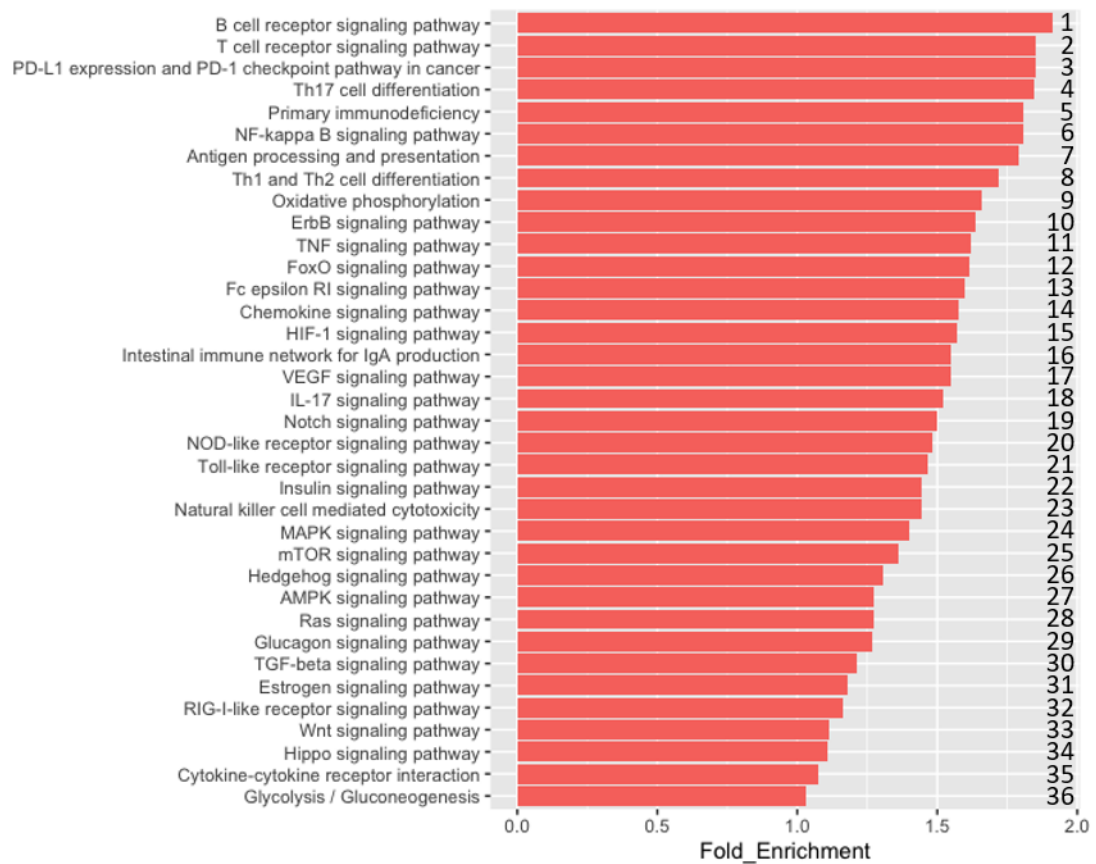


Figure 3.29 scRNA-Seq pathway analysis for HS patient lesions compared with healthy control skin.

Cells isolated from the skin of healthy controls (Con; n=3) or HS lesional skin (HS; n=6) were purified based on CD45 expression, barcoded and their gene expression determined by scRNA-Seq. Analysis through the R package Enrichr highlights 36 pathways displaying a fold enrichment in HS patient samples. Only enriched categories with a p value <0.05 are shown.

3.5 Discussion

This chapter comprises the classification of an extensive range of immune cells in HS skin, availing of state-of-the-art techniques. It illustrates the heterogenous nature of HS lesional skin, contrasting the inflammation and damage in the disease with healthy skin. It convincingly shows the de novo appearance, or significant increase, of a number of immune cell subsets in HS lesional skin compared with healthy control skin. It identifies genes which are substantially up- and downregulated in HS skin, implicates aberrant cellular pathways in HS pathogenesis and ultimately suggests potential therapeutic targets.

3.5.1 Myeloid cells in HS lesional skin

Myeloid cells make up a large proportion of immune cells in both HS L (15.3%) and Con (24.6%) samples. While subsets were not thoroughly phenotyped, overall, DC and dermal macrophages were not significantly enhanced in HS L compared with Con. In fact, scRNA-Seq analysis showed decreased frequency of all myeloid cells in HS, significantly so for pDC. Of course, these data are tempered by the massive increase in immune cells which is not represented by percentages analysed. Many pathways linked with myeloid cells were enriched in HS, including antigen processing and presentation, FcεRI signalling, TGF-β signalling, and TLR and NOD-like receptor signalling.

Neutrophils were absent from scRNA-Seq data, a consequence of the tissue cryopreservation process prior to shipping which kills all neutrophils. Phenotyping the freshly dissociated skin showed neutrophils at approximately 15% of total immune cells in both HS L and Con, but absolute numbers significantly increased in HS L, and enhanced (ns) in HS U skin. This significant enhancement in cell numbers per gram of skin was observed for both resting and activated neutrophils. Although the role of neutrophils in HS has been reported to be via IL-17 production (Lima et al., 2015) or NET secretion (Byrd et al., 2019) neither could be effectively investigated further within this project.

As is the case in normal, healthy skin LC were the predominant myeloid cell in this study, followed by cDC2. Given the expression profiles, it is likely that the cDC2 population infringe into the LC cluster. The most prominent cytokine genes expressed by LC were

IL18 and *CXCL8* (IL-8). Genes in cDC2 appear much more upregulated, with high levels detected for *IL1R1*, *IL10*, *IL1B* (IL-1 β), *IL7*, *CXCL8* (IL-8) and the Th17 cell driving *IL23A*.

Given the high level of gene expression of the LN homing chemokine *CCR7* within these cells, it is suggestive that cDC2 are initiating the adaptive immune response in HS lesions. Whereas the inflammasome has been previously implicated in HS (Kelly et al., 2015; Lima et al., 2015), there has been no conclusive evidence, nor has the cellular source been identified. Here, the inflammasome components *NLRP3* and *CASP1* (caspase-1) were highly expressed within this cDC2 population. IL-1 β , together with IL-18 and IL-23, has been shown to be a potent inducer of Th17 cells (Lalor et al., 2011; Sutton et al., 2009). It has recently been shown that in early stage autoimmunity IL-17 may play a priming role, recruiting IL-1 β producing myeloid cells (McGinley et al., 2020), further implicating these cDC2 in pathogenesis and damage in a feedback loop with Th17 cells. Tissue cDC2 have previously been shown to be distinct from peripheral blood, induce T cell responses and play a pathogenic role in the autoimmune disease inflammatory arthritis (Canavan et al., 2018).

Although CD68⁺ macrophages have been reported to be by far the most abundant myeloid cell in HS (Hunger et al., 2008), our transcriptome and phenotyping data suggested a frequency for dermal macrophages of only 2% in HS. *CD14* gene expression was only detected in pDC and the dermal macrophage population (cluster 18). However, interestingly, there was a marked fold change in gene expression of *S100A8* (MRP8) and *S100A9* (MRP14), both primarily mapping to the dermal macrophages as well as a keratinocyte cluster. *S100A8* and *S100A9* are DAMPs secreted principally by neutrophils and monocytes and can activate the inflammasome (Tan et al., 2017). Despite the absence of neutrophils and keratinocytes within the HS scRNA-Seq samples, the data suggests that these particular alarmins may well play a prominent role in HS, given their large fold change in the HS samples.

Surprisingly, pDC were significantly less abundant in HS, despite their reported interplay with NETs in HS (Byrd et al., 2019). They have been shown to be involved in psoriasis, where endogenous DNA complexes with the anti-microbial peptide LL-37 to activate

pDC, enabling autoantigen presentation to T cells (Lande et al., 2014). The RNA-degrading gene *RNASE1* was markedly downregulated in HS in this study; its expression limited to pDC in both Con and HS. It seems unlikely that its absence plays a pathogenic role, but rather may be primarily due to the almost entire absence of pDC in the HS samples. The gene *CEBPD* (*C/EBPδ*), expressed on almost all myeloid clusters, is also virtually absent in HS. *C/EBPδ* is an immunomodulator, playing apparently contrasting roles in promoting cell differentiation, inhibiting proliferation as well as proinflammatory signalling (Balamurugan & Sterneck, 2013). Its absence in HS likely aligns with other downregulated genes such as *TOB1* and *RGCC* in enabling immune cell activation and accumulation (Section 3.5.4).

cDC1 were infrequent in both HS and Con samples at <1%, with the only apparent upregulated cytokine being IL-8. Given its exclusive, high expression of the gene *IDO1* which transcribes to IDO (indoleamine 2, 3-Dioxygenase), cDC1 may play a suppressive role in HS. IDO acts to suppress activated T cells as well as inducing Treg cell proliferation (Mbongue et al., 2015).

The frequency of mast cells was increased (ns) from 1.2% to 2.7% in HS samples. However, they appeared to be relatively inert, with no genes of note up- or downregulated. Although mast cells have been reported to produce IL-17 and IL-22 in diseases such as atopic dermatitis and psoriasis (Section 1.5.6), no IL-17 (A-F), IL-22 or indeed IL-17 receptor (IL-17RA-E) gene expression was detected.

3.5.2 ILC and NK cells in HS lesional skin

ILC and NK cells probably make up a small but significant proportion of the overall immune cells, though their identification is not definitive in this study. A population of “likely” NK cells were phenotyped as CD3⁻CD19⁻CD64⁻CD14⁻CD16⁻CD38⁺FSC^{hi}SSC^{int}, and made up 2% of immune cells in HS lesions, 1% in HS uninvolved skin and undetected in healthy skin. Similarly, “non-TBNK lymphocytes” were characterised as CD3⁻CD19⁻CD64⁻CD14⁻CD16⁻CD38^{lo}SSC^{lo} and were significantly increased in HS L. The clusters incorporating ILC and NK cells include cluster 11 (“NK/Th1/Th2”), 15 (“NK, ILC”) 16 (“NK cells”) and 27 (“ILC/γδ cells”). Cluster 16 frequency is equivalent in both HS L and Con,

whereas it is lower in HS for both cluster 11, 15 and 27. All four populations have high expression for *CD69*, *CD44* with little if any *SELL* (CD62-L).

Given the variable expression patterns of numerous genes amongst these clusters, it is likely there are multiple populations present, including ILC subsets, NK cells, iNKT cells, $\gamma\delta$ T cells and MAIT cells. Of note, although there was no evident *IL17A* or *IL17F* expression amongst this cohort, there was *KLRB1* (CD161) expression within the “NK cells” and “NK, ILC?” clusters. While CD161 is expressed on the majority of NK cells, it is a marker for their pro-inflammatory function, suggesting a potential inflammatory role for these cells in the disease (Kurioka et al., 2018). *CD3E* overlays to these cells suggesting an iNKT cell group, and perhaps also MAIT cells. However, the MAIT cell marker MR1 was not overly expressed in any of these clusters (data not shown) and *ZBTB16* (PLZF; expressed in iNKT cell subsets) was at barely detectable levels except for cluster 27, further confounding the detail. Although there are few reports implicating NK cells or ILC in HS pathology, they have been reported in HS lesions, and NK cell mediated toxicity is an enhanced pathway within the HS cohort in this study. They have been shown to express the proinflammatory IL-32 in HS, which correlated with IL-17 and IFN- γ expression (Thomi et al., 2017). Here, *IL32* principally mapped to the “CD8 T cells” and “Treg cell clusters” and to a subset within the “NK, ILC?”.

3.5.3 B cells in HS lesional skin

B cells were shown to be almost completely absent in healthy controls as well as HS uninvolved skin, with a large, significant influx in HS lesional skin. With collaborators, an increase in plasmablasts and plasma cells has been shown in PBMC as well as skin (Musilova et al., 2020). The total B cell populations (i.e. B cells, plasmablast and plasma cells) made up a large component of the immune cells in HS lesional skin; up to 25% by phenotyping and transcriptomics. Plasmablasts were the most frequent subpopulation (approximately 10%), with marked expression of *CD44*, *CD69*, *CD83* (not shown) and *HLA-DRA*. Plasma cells are less populous in HS lesional skin at approximately 5%, expressing high levels of SELPLG (CLA), CD69, ITGAE (CD103), and CD44.

The BCR signalling pathway is the most enriched in HS lesions, with genes associated with plasmablasts and plasma cells (*IGLL5*, *JCHAIN*, *MZB1* and *SSR4*) featuring the largest fold change. This may reflect the lack of almost all B cell subsets in healthy skin rather than playing a central role in HS pathology. However, they do express many potent proinflammatory genes in this study; both plasmablasts and plasma cells expressed *KLRB1* (CD161), *IL22* and *TGFB1* (TGF- β), albeit not at the level of Th17 cells. Both subsets also express proinflammatory *IL1B* (IL-1 β) and *CXCL8* (IL-8), suggesting a potent inflammatory role in HS lesions. Given that NETs and their autoantibodies have been identified in HS lesions (Byrd et al., 2019), it is conceivable that NETs play a major role in activating the B cells and generating plasmablasts and plasma cells.

3.5.4 T cells in HS lesional skin

T cells constitute approximately 50% of total immune cells in HS L, as observed via both flow cytometry and scRNA-Seq. This was in line with Con, although the absolute T cell numbers are increased in the order of hundreds in HS L. This suggests that T cells are a major contributor to HS lesional pathology, be it via infiltration or proliferation of resident cells. Transcriptional analysis showed multiple T cell associated pathways with a fold enrichment in HS, including TCR signalling, immune checkpoint signalling and Th1 and Th2 cell differentiation. Th17 differentiation and IL-17 signalling were particularly prominent.

There was high gene expression of the memory T cell marker *CD44* and the Trm cell marker *CD69* in almost all T cell clusters cohorts, whilst the gene *SELL* (CD62-L; expressed on naïve T cells) was identified on few T cell clusters. This suggests the T cells are primarily resident, reactivated T cells in HS lesions. The CD8 cluster (cluster 4) is 8.4% of the total immune cells in HS L, compared with 6.5% in Con. They are high expressors of *CD69* and *CD44*, and to a lesser degree *IL7R* (CD127), *TGFB1* (TGF- β) and *TNF*. A subset expressed high levels of *IFNG* (IFN- γ), with none detectable amongst the Th cell subsets. They appear to be the highest expressor of *CXCR3*, a chemokine receptor associated with activated T cell trafficking.

There appeared to be a number of Th cell populations present, with a general Tem cell subset being the most populous cluster (i.e. Cluster 0) and a Trm cell cohort as Cluster 2. Although no specific Th cell subset marker genes were noted, these cells expressed T cell activation genes such as *IL7R* (CD127) and *CD40LG* (CD154; not shown). They may well be primed towards a specific Th cell subset, though not yet transcribing detectable quantities of the relevant genes. In particular, the Tem cell cluster expressed high levels of *KLRB1* (CD161) and *CCR6*, identifiers for Th17 and ex-Th17 cells (Basdeo et al., 2017)), although *CXCR3*, expressed in ex-Th17 cells, was not observed in this subset. This population is of note given the apparent autoimmune pathogenesis in HS, and that Th17 cells have been previously implicated (Kelly et al., 2015; Schlapbach et al., 2011). The Th17 cell transcription factor ROR- γ T (*RORC* gene) was expressed to a small degree in the Tem cells cluster, but primarily in the Th17 cell clusters 12 and 13. These clusters 12 and 13 expressed high levels of Th17 cell associated genes *IL17A*, *IL17F*, *KLRB1* (CD161) and *TNF*. The population entitled Th17 cells (cluster 13) appears to express lower levels of *TNF* and *TGFB1* (TGF- β) genes, but higher levels of *IL17A*, *IL17F*, *IL22*, *IL21*, *IL26*, the receptor *IL23R* and the skin-homing molecule CLA (gene *SELPLG*) than the polyfunctional Th17 cell cluster (cluster 12). Hence this cluster 13 could potentially be skin-homing Th17 cells whereas cluster 12 may be skin-resident Th17 cells. Interestingly, clusters 12 and 13 appear to be the only T cell clusters with frequencies substantially enhanced in HS L compared with Con, significantly so for the Th17 cell cluster, whilst *IL17A* was one of the genes with the highest fold change in HS L.

TOB1 expression was substantially downregulated in HS compared with Con. Although Th17 cells reportedly express higher amounts of *TOB1* than other T cells (Santarlaschi et al., 2014), *TOB1* in fact inhibits T cell proliferation and its downregulation is required for T cell activation and expansion (Baranzini, 2014). Hence, its decreased expression is in line with the T cell accumulation and activation in HS lesions. Indeed, its expression is observed in Th17 cells but few other clusters in HS skin, whilst being expressed at high levels in most T cell clusters in Con samples. Similarly, the anti-proliferative genes *ZFP36L2* (Suk et al., 2018) and *RGCC* (Badea, Niculescu, Soane, Shin, & Rus, 1998) are markedly downregulated in HS in almost all T cell clusters except the Th17 cell populations.

IL26 expression was detected in the Th17 cells (cluster 13), and to a lesser degree in a Treg cell subset (cluster 1). IL-26 is a potent antimicrobial mediator, and its increased gene expression in HS has recently been reported (Scala et al., 2019). However, although overexpressed in HS samples in this project, it is proposed to be defective in HS and unable to mount a sufficient antimicrobial defence, thus allowing bacterial colonisation.

Th1 cells were not readily identified here by transcriptomics, but may be among the Trm cell cluster, with many cells there being *CCR4⁺CCR6⁻KLRB1⁻TNF⁺*, although these cells appear to have no expression of the Th1 cell associated *IFNG* or the transcription factor *TBX21* (T-bet). They are all *CCR4⁺*, a chemokine receptor reported to be key in T cell trafficking to the skin; to both dermis and epidermis (Tubo, McLachlan, & Campbell, 2011). Similarly, Th2 cell genes are not apparent in this study and do not group to the same cluster; e.g. *IL13* (not shown) homes to cluster 26 and 13, IL-4 to cluster 11 (“NK/Th1/Th2” cluster) and *GATA3* (not shown) appears to be expressed throughout the T cell clusters.

Amongst the principal populations are Treg cells (cluster 1); their frequency marginally increased in HS L compared with Con, at 11.03% v 8.31%. This may be somewhat surprising given their suppressive role. A subset within this cluster appear to express lower expression levels of *CD69* but higher *FOXP3*, *ITGAE* (CD103), *SELPLG* (CLA), *ENTPD1* (CD39; not shown), *CTLA4* (not shown) as well as the T cell activation marker *ICOS*. Although they exhibit high expression of *SELL* (CD62-L), these cells may be infiltrating Treg cells, actively attempting to suppress the inflammation in HS skin.

Overall, this chapter has added substantially to the understanding of the immune cell interplay in HS. Important findings include identifying cDC2 as a potent producer of inflammatory mediators as well as being the cellular source of IL-1 β and the inflammasome in HS. Also, the substantial increase of B cell subsets in HS lesions. But perhaps most notably, T cells have been identified as the predominant cell type in HS, with a Th17 skewed profile. As such, the next chapter will focus on T cells in HS patient blood and skin, comparing them with healthy controls. It will also investigate the effects of anti-TNF therapy on T cell subsets in HS patient skin.

Chapter 4

Hidradenitis suppurativa is
characterised by T cell dysregulation

4 Hidradenitis suppurativa is characterised by T cell dysregulation

4.1 Introduction

The previous chapter illustrated a considerably increased number of immune cells in HS lesional skin, with a predominance of T cells among them. Transcriptomic analysis suggested that many of the lesional T cells may be skewed towards a Th17 cell phenotype, with multiple proinflammatory cytokines upregulated in these cells. Surprisingly given the inflammatory profile, Treg cells were amongst the most frequent T cell subset in the lesions. Therefore, in order to further understand the roles of proinflammatory and suppressive T cells in HS, numerous functional markers and cytokines of interest were analysed in HS blood and skin samples and compared with healthy controls.

IL-17A (IL-17) is the signature cytokine expressed by Th17 cells and has been implicated in autoimmunity, particularly in psoriasis where IL-17 blockade has effectively transformed disease management (Papp et al., 2012). While the presence of IL-17⁺ CD4 T cells in HS skin has been demonstrated previously (G. Kelly et al., 2015; Schlapbach et al., 2011), this was not in conjunction with co-expression of other cytokines. IL-22, produced by both Th22 and Th17 cells, has been shown to be upregulated in psoriasis (Nogralles et al., 2008). There have been few studies linking IL-22 to HS and those yielded somewhat conflicting results, reporting both an IL-22 deficiency in HS lesional skin (Wolk et al., 2011) as well as an increased level of IL-22 in HS patient blood but no change in IL-22 production in CD4 T cells in HS patient skin (Hotz et al., 2016).

TNF has been shown to act synergistically with IL-17 to enhance inflammatory effects on keratinocytes and epithelial cells in psoriasis (Chiricozzi et al., 2011). TNF blockade therapies are extremely effective in autoimmune diseases such as psoriasis, RA, AS and CD, and they are the only biologic intervention currently licenced for treating HS (Kimball et al., 2016). Levels of TNF have been shown in multiple studies to be raised in HS serum and skin, without identifying the cellular source (G. Kelly et al., 2015; Matusiak et al., 2009; van der Zee et al., 2011).

GM-CSF secretion is associated with Th17 cells, and like IL-17 its expression is driven by IL-23 and the transcription factor ROR- γ T. It is thought to play a dominant role in autoimmunity, recruiting neutrophils, monocytes and lymphocytes to the site of infection (Shi et al., 2006). Th cells lacking GM-CSF failed to induce experimental autoimmune encephalomyelitis (EAE) (Codarri et al., 2011), and antibodies targeting GM-CSF (mavrimumab) have shown encouraging results in RA (Cook et al., 2018). Although there are no previous studies of GM-CSF association with HS, there is one surprising case report which cites excellent results in treating a HS patient with injections of GM-CSF (Sharon-Guidetti et al., 2006).

IFN- γ is a primary driver of the immune response and is produced by Th1 cells, ex-Th17 and transitioning ex-Th17 cells (Section 1.2.5.8). Elevated levels of IFN- γ have been shown in HS lesional skin at similar levels to that in psoriasis (Wolk et al., 2011), whilst CD4 T cells expressing both IFN- γ and IL-17 were identified in HS lesional skin (Hotz et al., 2016).

IL-2 potently induces T cell expansion and proliferation, stimulating naïve CD4 T cells to differentiate into Th1 and Th2 cells, while inhibiting Th17 and Tfh cells (Ross et al., 2018). Treg cells have abundant expression of the IL-2 receptor (CD25) and are reliant on IL-2 production from activated T cells. Despite its central role in orchestrating T cell response, there does not appear to be any current data showing levels of IL-2 in HS.

Treg cells are associated with autoimmunity and inflammation. (Dominguez-Villar et al., 2018). They have been implicated in CD, where the balance of Th17 and Treg cells is tipped in favour of Th17 cells (Brand, 2009). However, there is limited detail of Treg cells in HS. A recent study has reported that increased levels of Treg cells are associated with bacterial biofilm in uninvolved HS skin (Kjaersgaard Andersen et al., 2019). Similarly, γ -secretase complex mutations, implicated in familial HS, are associated with destabilised Treg cell function (Melnik & Plewig, 2013; Wang et al., 2010).

Following on from the phenotypic and transcriptomic evidence, CD4 and CD8 T cells were analysed in blood, lesional skin as well as clinically normal skin for their production

of these Th17 cell associated cytokines. Treg cells were quantified and markers of their suppressive function analysed. Finally, given the efficacy of anti-TNF therapy on moderate to severe HS, the effect of this treatment on these cells was studied.

4.2 Aims

The aim of the experiments in this chapter was to examine the role of T cell dysregulation in HS pathogenesis. In particular, to characterise T cell subsets in the peripheral blood and skin of healthy controls and HS patients.

Specifically, this chapter sought to:

- Examine the phenotype and function of T cells in HS patient peripheral blood
 - Define the proinflammatory and suppressive profile of T cells in healthy control and HS patient peripheral blood.

- Examine the phenotype and function of T cells in HS patient skin
 - Define the proinflammatory or suppressive profile of T cells in healthy control and HS patient normal and lesional skin.

- Examine the effect of TNF blockade therapy on T cells in HS patient skin
 - Identify any difference in the T cell profile in HS patient skin upon anti-TNF treatment.

4.3 Clinical details

Clinical details for the HS patient group 2 are shown in Table 4.1, the healthy control group 2 in Table 4.2, and the anti-TNF therapy HS patient group in Table 4.3. All HS patients were recruited at a dermatology consultation at St Vincent's Hospital, Dublin, and all samples were 4 or 6 mm biopsies. Healthy control samples were three x 6mm skin biopsies from the hip donated by healthy volunteers from St Vincent's Hospital and Trinity Biomedical Sciences Institute, Dublin. All samples were processed on the day of sampling.

The mean age of the HS patient group 2 was 34.5 years (y), \pm SD of 9.4 (n=11), for HS patients, 32.5 y, \pm SD of 8.6 (n=13) for healthy controls (Table 4.1 and Table 4.2). There were 91% females (n=10) in the HS group and 85% females (n=11) in the healthy control group. 18% (n=2) of the HS patient group were classified as Hurley stage 1, 55% (n=6) as Hurley stage 2 and 27% as Hurley stage 3. HS patients had a mean BMI of 31.1 kg/m², \pm SD of 6.2. There were 64% smokers (n=7), 18% ex-smokers (n=2) and 18% non-smokers (n=2) in the HS patient group compared with 8% ex-smokers (n=1) and 92% non-smokers (n=12) in the healthy control group. 18% (n=2) of HS patients were taking Type II Diabetes therapy (metformin), 9% (n=1) taking hypothyroidism treatment (Eltroxin™), 9% (n=1) taking anaemia therapy (Galfer™), and 18% (n=2) on antibiotics (clindamycin, rifampicin and Tetralysal™). No patients in this group were undergoing any biological therapy, including anti-TNF treatment. There were no relevant medicines in the healthy control group.

Clinical details for the group of patients undergoing anti-TNF therapy (α -TNF+ HS patients) are shown in Table 4.3, with a mean patient age of 33.5 y, \pm SD of 8.4 (n=7). There were 83% females (n=6), with 66% of patients classified as Hurley stage 2 (n=4) and 33% as Hurley stage 3 (n=2). The mean BMI value was 30.0 kg/m², \pm SD of 7.5. 66% were current smokers (n=4), 17% ex-smoker (n=1) and 17% non-smoker (n=1). 14% (n=1) of patients were on antibiotics (doxycycline). All patients (n=7) were being treated with the anti-TNF therapy adalimumab (Humira™), with an average of 63% improvement reported in the Hidradenitis Suppurativa Clinical Response score (HiSCR).

Patient ID	Age (y)	Sex	Hurley	BMI	Smoker	Medication	Anti-TNF therapy
1HS-1	45	F	2	39.7	E-S	Eltroxin™	No
1HS-2	39	F	2	26.8	S	nrm	No
1HS-3	24	F	2	23.1	N-S	nrm	No
1HS-4	41	F	2	32.3	S	nrm	No
1HS-5	23	F	1	32.6	E-S	nrm	No
1HS-6	35	F	2	35	S	Galfer™	No
1HS-7	30	F	2	23.1	S	metformin	No
1HS-8	41	F	3	36.6	S	clindamycin & rifampicin	No
1HS-9	35	F	3	39.6	S	metformin	No
1HS-10	47	F	3	27.3	S	nrm	No
1HS-11	19	M	1	26.2	N-S	Tetralysal™	No
	Mean 34.5 SD 9.4	91% F, 9% M	18% 1 55% 2 27% 3	Mean 31.1 SD 6.2	64% S 18% E-S 18% N-S		

Table 4.1 Clinical details for HS patient group 2.

Study clinical details at time of sampling, including patient ID, age, sex, Hurley stage score, body mass index, smoking status, medication and if undergoing anti-TNF therapy.

BMI: body mass index, E-S: ex-smoker, F: female, M: male, nrm: no relevant medications, N-S: non-smoker, S: smoker.

Patient ID	Age (y)	Sex	Hurley	BMI	Smoker	Medication
Con-1	49	F	-	-	N-S	nrm
Con-2	39	M	-	-	E-S	nrm
Con-3	31	F	-	-	N-S	nrm
Con-4	27	F	-	-	N-S	nrm
Con-5	25	F	-	-	N-S	nrm
Con-6	25	F	-	-	N-S	nrm
Con-7	30	M	-	-	N-S	nrm
Con-8	50	F	-	-	N-S	nrm
Con-9	26	F	-	-	N-S	nrm
Con-10	30	F	-	-	N-S	nrm
Con-11	31	F	-	-	N-S	nrm
Con-12	25	F	-	-	N-S	nrm
Con-13	34	F	-	-	N-S	nrm
	<i>Mean</i>	85%				
	32.5	F,			8% E-S	
	<i>SD</i> 8.6	15%			92% N-S	
		M				

Table 4.2 Details for healthy control group.

Study clinical details at time of sampling, including patient ID, age, sex, Hurley stage score, body mass index, smoking status, medication and if undergoing anti-TNF therapy.

BMI: body mass index, E-S: ex-smoker, F: female, M: male, nrm: no relevant medications, N-S: non-smoker.

Patient ID	Age (y)	Sex	Hurley	BMI	Smoker	Medication	HiSCR
1HS-aT1	34	M	2	26	S	Humira™	60%
1HS-aT2	47	F	3	20.5	N-S	Humira™, doxycycline	60%
1HS-aT3	32	F	2	27	S	Humira™	60%
1HS-aT4	38	F	3	28.5	S	Humira™, doxycycline	60%
1HS-aT5	*	*	*	*	*	*	*
1HS-aT6	24	F	2	40	S	Humira™	70%
1HS-aT7	26	F	2	38	E-S	Humira™	70%
	Mean 33.5 SD 8.4	83% F, 17% M	0% 1 66% 2 33% 3	Mean 30.0 SD 7.5	66% S 17% E-S 17% N-S		63%

Table 4.3 Clinical details for anti-TNF therapy HS patient group.

Study clinical details at time of sampling, including patient ID, age, sex, Hurley stage score, body mass index, smoking status, medical treatments and Hidradenitis Suppurativa Clinical Response score.

*BMI: body mass index, E-S: ex-smoker, F: female, HiSCR: Hidradenitis Suppurativa Clinical Response score, M: male, N-S: non-smoker, S: smoker, *: awaiting details.*

4.4 Results

4.4.1 Similar frequency of T cells in the peripheral blood of HS patients and healthy controls

In order to characterise T cells in the blood of HS patients (HS patient group 2; Table 4.1) and healthy controls Table 4.2), whole blood was refined to PBMC and stimulated with PMA/I in the presence of Brefeldin A for 16 h at 37°C (Section 2.2.6). Samples were then stained for surface expression of CD45, CD3, TCR- $\gamma\delta$, CD8, CLA and CD161, along with a viability stain, then fixed, permeabilised and stained for the intracellular cytokines IL-2, IL-17, IL-22, GM-CSF, IFN- γ and TNF. Samples were analysed by flow cytometry within 24 h.

A gating strategy for identifying CD4 and CD8 T cells is shown in Figure 4.1. Briefly, the ungated sample was plotted for CD45 v Fixable Viability dye eFluor506 (FixVia eF506), with the CD45⁺FixVia-eF506⁻ population gated as live leukocytes (Figure 4.1A). Next, lymphocytes were gated based on their characteristic Forward Scatter Channel (FSC) v Side Scatter Channel (SSC) profile (Figure 4.1B). Single cells were then identified by FSC-area (FSC-A) v FSC-width (FSC-W) profile (Figure 4.1C); then TCR- $\alpha\beta$ T cells classified as CD3⁺TCR- $\gamma\delta$ ⁻ cells (Figure 4.1D). Analysis of $\gamma\delta$ T (CD3⁺TCR- $\gamma\delta$ ⁺) cells was not compatible with these incubation or stimulation conditions, with 4-6 hour of PMA/I more suitable. Hence TCR- $\gamma\delta$ was primarily used as an exclusion marker, and $\gamma\delta$ T cells were not investigated further in this study. From CD3⁺TCR- $\gamma\delta$ ⁻ cells CD8 T cells were characterised as CD3⁺CD8⁺ cells (Figure 4.1E). As CD4 surface expression has been shown to be internalised on PMA/I stimulated cells (Hoxie et al., 1986), an antibody targeting CD4 was not used in this cytometry panel and CD4 T cells were characterised as CD3⁺TCR- $\gamma\delta$ ⁻ CD8⁻ cells.

Further validation of this CD4 T cell gating strategy is shown in Figure 4.2, whereby in a sample not treated with PMA/I (Figure 4.2A), the vast majority (94.4%) of CD3⁺CD8⁻ cells were shown to be CD4 T cells, and CD4⁺ cells mapped directly to the CD3⁺CD8⁻ population (Figure 4.2B). The small cohort in the CD4⁺CD8⁺ quadrant (0.8%; Figure 4.2A) are most likely doublets and dead cell artefacts rather than true viable double positive cells (such as double positive thymocytes).

Having established a PBMC gating strategy, the frequency of CD3 T cells was observed as approximately 80% of lymphocytes, with no difference between PBMC from healthy controls (Con) and HS patients (Figure 4.3A). Likewise, frequencies for both CD8 (Figure 4.3B) and CD4 (Figure 4.3C) T cells within the T cell population were unchanged between groups (approximately 25% and 70% respectively).

CLA enables the recruitment of T cells into the skin, facilitating rolling of T cells over endothelial cells through E-selectin interactions. CLA is expressed on memory T cells, and the vast majority of T cells in normal skin have been reported to be CLA positive (R. A. Clark, Chong, Mirchandani, Yamanaka, et al., 2006). Hence expression of CLA on T cells in HS is likely to be of interest. Representative plots show CLA expression on CD8 (Figure 4.4A) and CD4 (Figure 4.4C) T cells. CLA expression was significantly increased, on both CD8 ($p < 0.05$; Figure 4.4B) and CD4 ($p < 0.01$; Figure 4.4D) T cells in PBMC from HS patients relative to healthy controls.

In summary, no difference in the frequency of CD3, CD8 or CD4 T cells was observed in PBMC from HS patients compared with healthy controls. However, relative to healthy controls there was a marked increase in CLA expression in both CD8 and CD4 T cells within PBMC from HS patients.

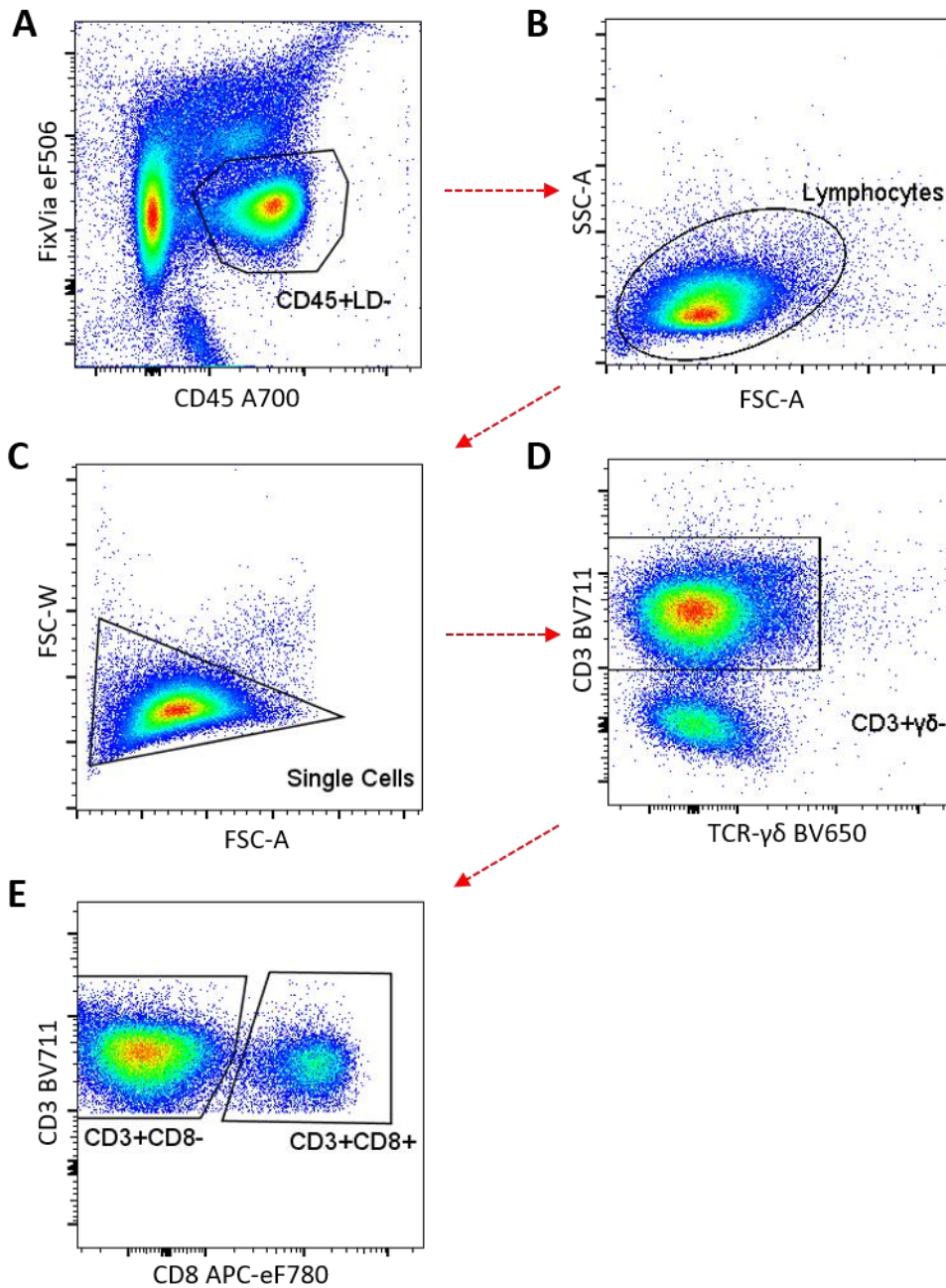


Figure 4.1 Plots representing the gating strategy to identify CD4 and CD8 T cells in peripheral blood.

PBMC were treated with PMA/I and Brefeldin A for 16 h, stained for surface and intracellular markers, and analysed by flow cytometry. To identify CD8 and the vast majority of CD4 T cells in stimulated samples, sequential gating was performed: CD45⁺, Fixable-Viability-Dye- to identify viable leukocytes (A); Forward (FSC) v Side (SSC) Scatter to exclude debris and non-lymphocytes (B); FSC-Area v FSC-Width to exclude doublets (C); CD3⁺TCR- $\gamma\delta$ ⁻ to exclude $\gamma\delta$ T cells and non-T cells (D); CD3⁺CD8⁺ to identify CD8 T cells, and CD3⁺CD8⁻ to identify CD4 T cells (E).

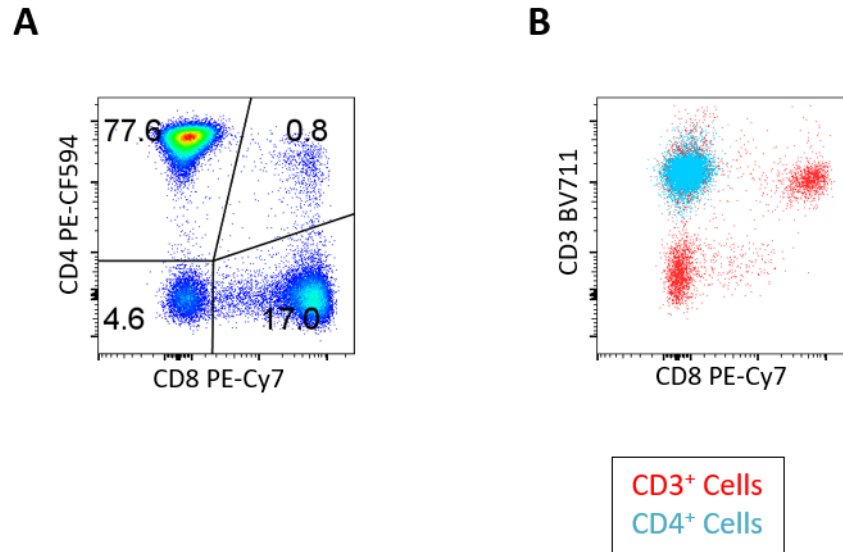


Figure 4.2 Representative plots validating the gating strategy to identify CD4 T cells in peripheral blood.

PBMC were rested for 16 h, stained for surface and intracellular markers, and analysed by flow cytometry. CD4 T cells represent 94.4% (77.6% v. 4.6%) of CD3⁺CD8⁻TCR- $\gamma\delta$ ⁻ cells in an unstimulated PBMC sample (A), and CD4⁺ stained cells map directly to the CD3⁺CD8⁻ population (B). This serves to validate identifying CD4 T cells as CD3⁺CD8⁻TCR- $\gamma\delta$ ⁻ cells in PMA/I treated samples.

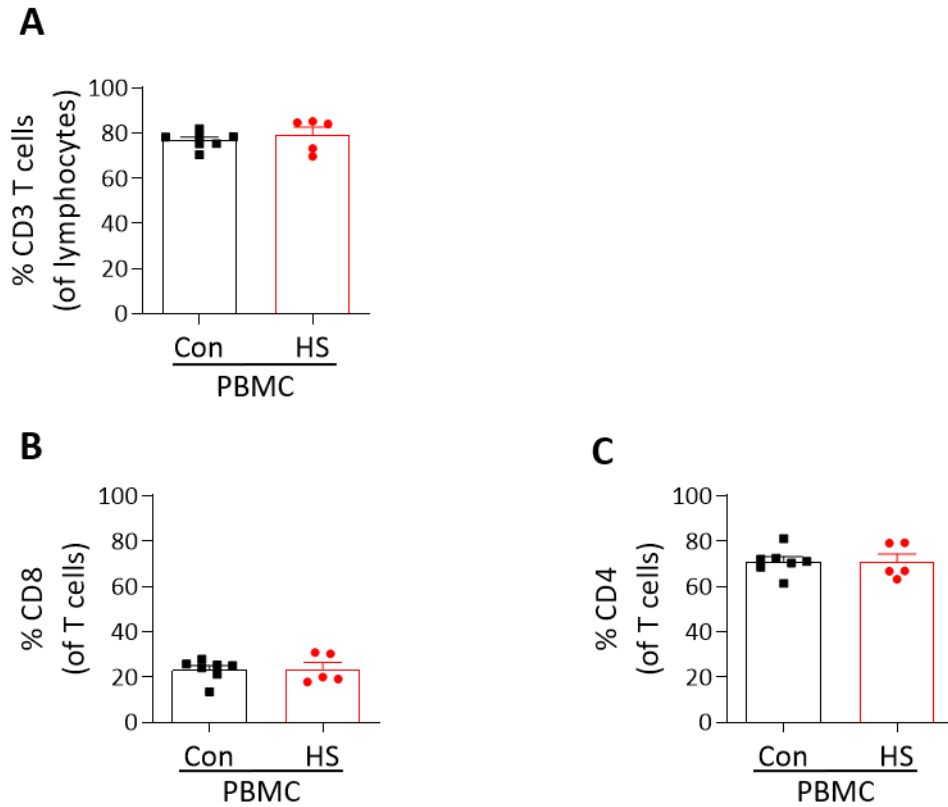


Figure 4.3 Similar frequency of CD3, CD8 and CD4 T cells in healthy control and HS patient peripheral blood.

PBMC from healthy controls (Con; n=7) or HS patients (n=5) were treated with PMA/I and Brefeldin A for 16 h, stained for surface and intracellular markers, and analysed by flow cytometry. Plots show the frequency of CD3 (A) within the lymphocyte gate, and CD8 (B) and CD4 (C) T cells within the T cell population. Graphs represent individual samples with mean \pm SEM for each group. Statistical significance was calculated using Mann Whitney U test.

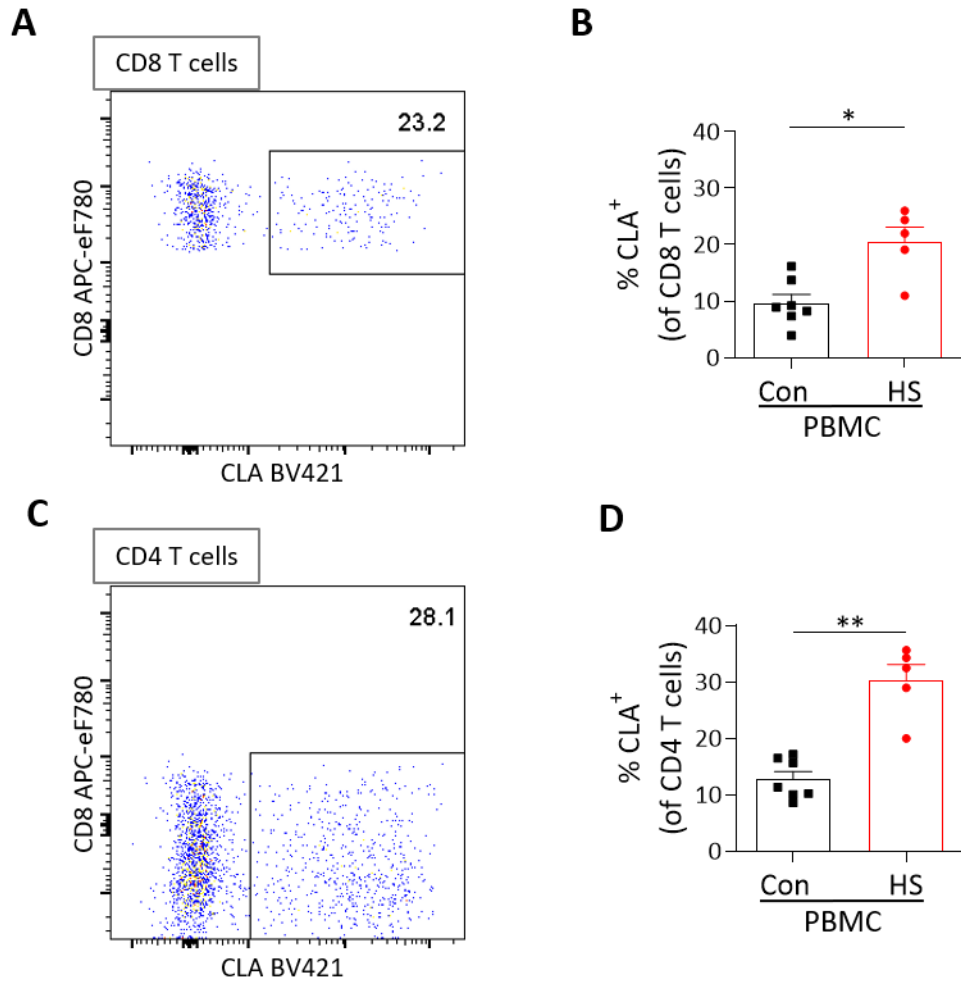


Figure 4.4 Increased frequency of CLA expressing CD8 and CD4 T cells in peripheral blood from HS patients v healthy controls.

PBMC from healthy controls (Con; n=7) or HS patients (n=5) were treated with PMA/I and Brefeldin A for 16 h, stained for surface and intracellular markers, and analysed by flow cytometry. Representative dot plots display CLA expression plotted against CD8, gated on CD8 (CD3⁺CD8⁺; A) and CD4 (CD3⁺CD8⁻; C) T cells from a PMA/I treated HS patient PBMC sample. Graphs show the frequency of CLA expressing CD8 (B) and CD4 (D) T cells. Graphs represent individual samples with mean \pm SEM for each group. Statistical significance was calculated using Mann-Whitney U test; *p < 0.05., **p < 0.01.

4.4.2 A minor increase in the proinflammatory T cell profile characterises HS patient peripheral blood

Having established that there were no global alterations within T cells between HS patients and healthy controls, CD8 and CD4 T cells isolated from the peripheral blood of HS patients and healthy controls were analysed for their inflammation-associated markers and cytokines in the context of skin autoimmunity. Six candidate cytokines implicated in immune dysregulation were nominated for investigation; IL-17, IL-22, TNF, GM-CSF, IFN- γ and IL-2.

Figure 4.5A shows representative dot plots for IL-17 v IL-22 expression on CD8 T cells, from a HS patient PBMC sample treated with PMA/I. The number at the top left of the representative plot is the total expression of the cytokine on the y-axis (as a percentage of CD8 T cells), bottom right is total expression of x-axis cytokine. Plots show slightly increased, albeit not significant (ns), frequencies of IL-17 (Figure 4.5B) and IL-22 (Figure 4.5C) production in CD8 T cells in HS patient PBMC compared with that of healthy controls. Likewise, representative plots are shown for CD8 T cell expression of TNF v GM-CSF (Figure 4.5D) and IFN- γ v IL-2 (Figure 4.5G). TNF expression was significantly raised in HS patient PBMC ($p < 0.01$; Figure 4.5E), with GM-CSF and IFN- γ non-significantly so (Figure 4.5F & H). No change was observed for CD8 T cells expressing IL-2 (Figure 4.5I). The case of T cells expressing multiple cytokines simultaneously is discussed later in the chapter (Section 4.4.10).

Cytokine expression from PBMC CD4 T cells is shown in Figure 4.6, with representative plots for IL-17 v IL-22, TNF v GM-CSF and IFN- γ v IL-2 (Figure 4.6A, D & G respectively). PBMC derived CD4 T cells from HS patients exhibited a moderate increase (ns) in IL-17 (Figure 4.6B), IL-22 (Figure 4.6C), TNF (Figure 4.6E) and IFN- γ (Figure 4.6H) relative to healthy controls. GM-CSF actually showed a slightly reduced frequency in CD4 T cells from HS patients (ns; Figure 4.6F), whilst IL-2 expression was markedly decreased ($p < 0.05$; Figure 4.6I).

CD161 is expressed on a subset of T cells and is of interest as it is considered a pan-marker on the cell surface of Th17 cells, and all Th17 cells appear to originate from

CD161⁺CD4 T cells (Cosmi et al., 2008). Representative plots are displayed for CD161 expression on CD8 and CD4 T cells (Figure 4.7A & C respectively), with no difference in the frequency of CD161 expression observed in CD8 (Figure 4.7B) or CD4 (Figure 4.7D) T cells in PBMC from HS patients compared with healthy controls.

CD4 T cells are functionally plastic and ex-Th17 cells and transitioning ex-Th17 cells are subsets that develop from the Th17 cell cohort (Section 1.2.5.8). To investigate these Th subsets in this study, CD4 T cells expressing CD161 were gated, and those cells positive for IL-17 expression but negative for IFN- γ were identified as Th17 cells; those positive for IFN- γ , negative for IL-17 as ex-Th17 cells; and those positive for both IL-17 and IFN- γ as transitioning ex-Th17 cells (Figure 4.8A). CD4 T cells not expressing CD161 but positive for IFN- γ , negative for IL-17 were branded as Th1 cells (Figure 4.8A). There appeared to be a small population of CD161⁻IL-17⁺IFN- γ ⁻; (0.8% of CD161⁻ gated cells); these are likely Th17 cells that have not been adequately gated as CD161⁺ due to weak CD161 staining or perhaps downregulation upon cell stimulation.

Levels of Th17 cells were approximately 0.2% of CD4 T cells in HS patient PBMC with no difference in frequency compared with healthy controls (Figure 4.8B). Although levels of Th1 cells in PBMC appeared higher, no significant difference was noted (Figure 4.8C). ex-Th17 cells (Figure 4.8D) and transitioning ex-Th17 cells (Figure 4.8E) both displayed low levels, with no significant difference between HS patients and healthy control PBMC.

Overall, these data suggest a very subtle increase in inflammatory T cell markers in the peripheral blood of HS patients compared with healthy controls.

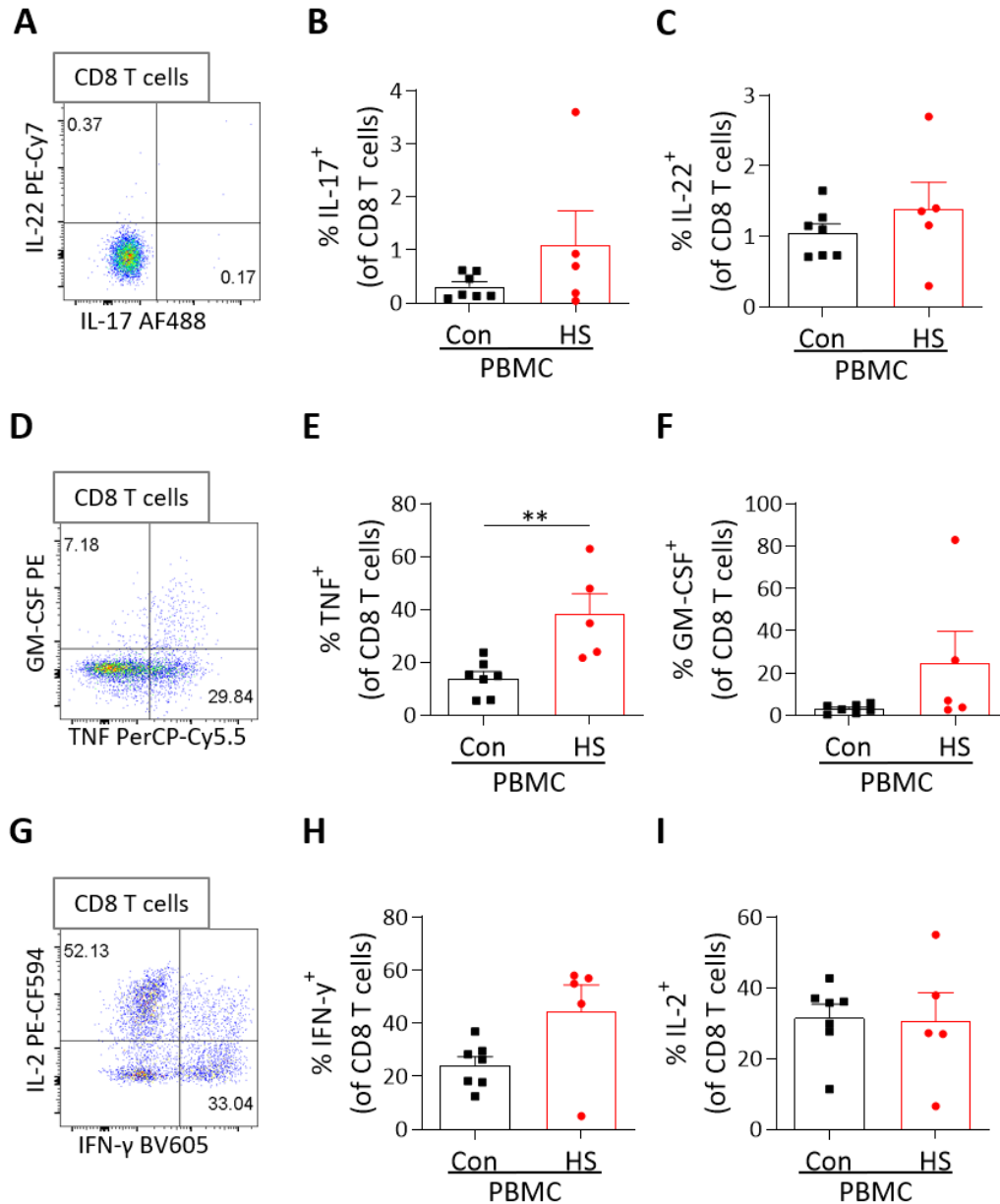


Figure 4.5 Cytokine profile of CD8 T cells in HS patient and healthy control peripheral blood.

PBMC from healthy controls (Con; n=7) or HS patients (n=5) were treated with PMA/I and Brefeldin A for 16 h, stained for surface and intracellular markers, and analysed by flow cytometry. Representative dot plots display expression of cytokines IL-17 v IL-22 (A), TNF v GM-CSF (D) and IFN-γ v IL-2 (G), gated on CD8 T cells from a PMA/I treated HS patient PBMC sample. Top left number represents total expression of y-axis cytokine, bottom right is total expression of x-axis cytokine. Graphs show the frequency of CD8 T cells expressing IL-17 (B), IL-22 (C), TNF (E), GM-CSF (F), IFN-γ (H) and IL-2 (I). Graphs represent individual samples with mean ± SEM for each group. Statistical significance was calculated using Mann-Whitney U test; **p<0.01.

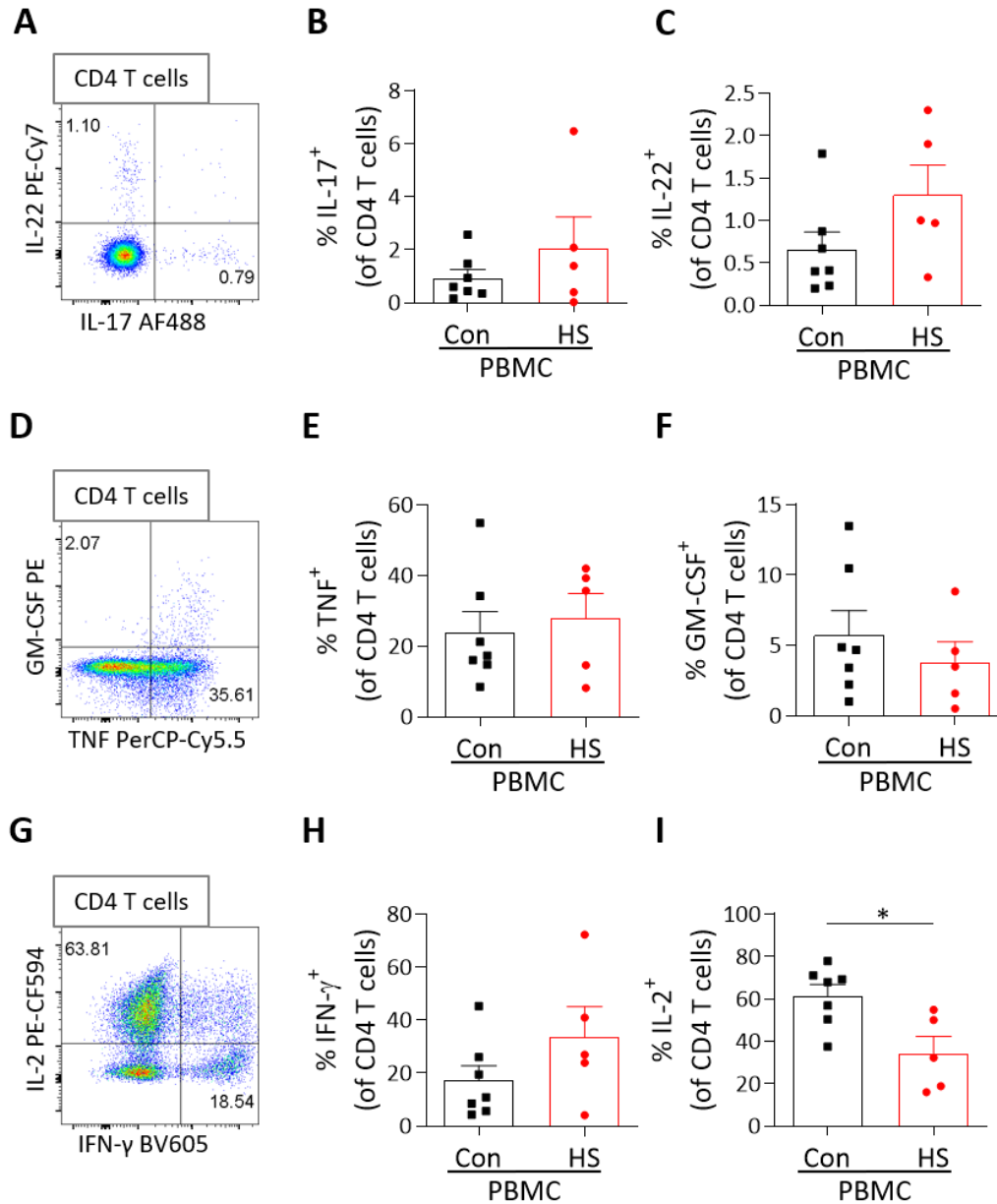


Figure 4.6 Cytokine profile of CD4 T cells in HS patient and healthy control peripheral blood.

PBMC from healthy controls (Con; n=7) or HS patients (n=5) were treated with PMA/I and Brefeldin A for 16 h, stained for surface and intracellular markers, and analysed by flow cytometry. Representative dot plots display expression of cytokines IL-17 v IL-22 (A), TNF v GM-CSF (D) and IFN-γ v IL-2 (G), gated on CD4 T cells from a PMA/I treated HS patient PBMC sample. Top left number represents total expression of y-axis cytokine, bottom right is total expression of x-axis cytokine. Graphs show the frequency of CD4 T cells expressing IL-17 (B), IL-22 (C), TNF (E), GM-CSF (F), IFN-γ (H) and IL-2 (I). Graphs represent individual samples with mean ± SEM for each group. Statistical significance was calculated using Mann-Whitney U test; *p<0.05.

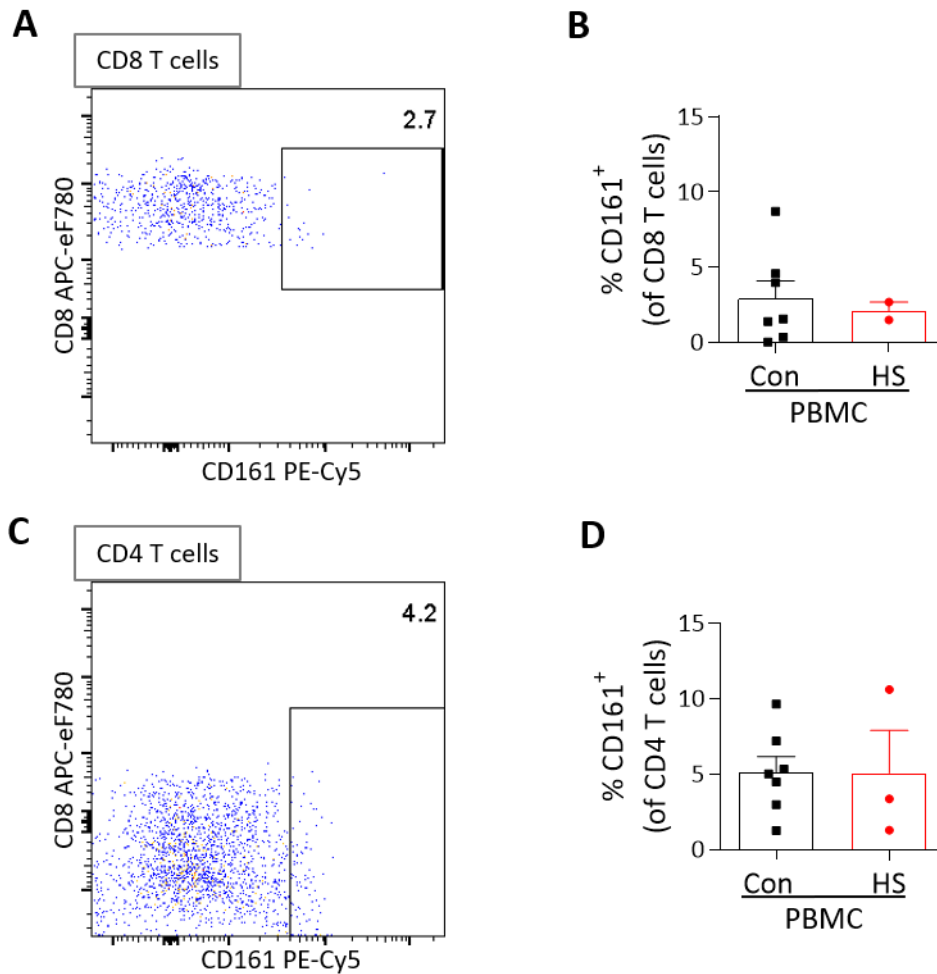


Figure 4.7 Similar frequency of CD161 expression on CD8 and CD4 T cells in HS patient versus healthy control peripheral blood.

PBMC from healthy controls (Con; n=7) or HS patients (n=3) were treated with PMA/I and Brefeldin A for 16 h, stained for surface and intracellular markers, and analysed by flow cytometry. Representative dot plots display CD161 expression plotted against CD8, gated on CD8 (A) and CD4 (CD3⁺CD8⁻) T cells (C) from a PMA/I treated HS patient PBMC sample. Graphs show the frequency of CD161 expressing CD8 (B) and CD4 (D) T cells. Graphs represent individual samples with mean \pm SEM for each group. Statistical significance was calculated using Mann-Whitney U test.

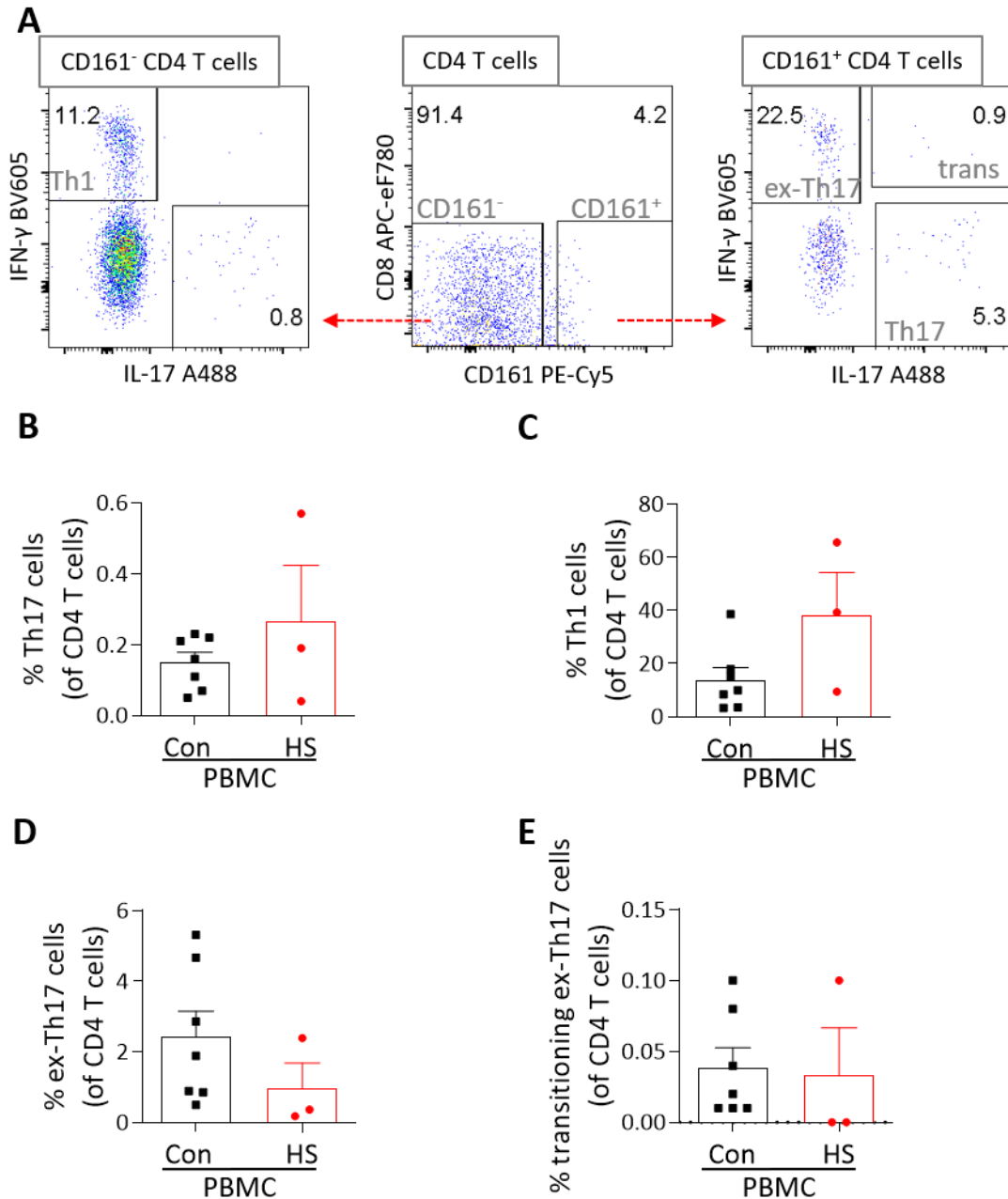


Figure 4.8 Frequency of Th subsets Th17, Th1, ex-Th17 and transitioning ex-Th17 unchanged in HS patient compared with healthy control peripheral blood.

PBMC from healthy controls (Con; n=7) or HS patients (n=3) were treated with PMA/I and Brefeldin A for 16 h, stained for surface and intracellular markers, and analysed by flow cytometry. Representative dot plots display gating strategy to identify T helper subsets Th1 (CD4⁺CD161⁻IL-17⁻IFN- γ ⁺), Th17 (CD4⁺CD161⁺IL-17⁺IFN- γ ⁻), ex-Th17 (CD4⁺CD161⁺IL-17⁻IFN- γ ⁺) and transitioning ex-Th17 cells (CD4⁺CD161⁺IL-17⁺IFN- γ ⁺), from a PMA/I treated HS patient PBMC sample (A). Graphs show the frequency of Th17 cells (B), Th1 cells (C), ex-Th17 cells (D), and transitioning ex-Th17 cells (E). Graphs represent individual samples with mean \pm SEM for each group. Statistical significance was calculated using Mann-Whitney U test.

4.4.3 Reduced frequency of Treg cells in HS patient peripheral blood

Having compared the subsets of proinflammatory T cells in peripheral blood between HS patients and healthy controls, it was important to investigate possible differences in the regulatory arm of T cells. Treg cells function to suppress inflammation and inhibit aberrant immune responses and are implicated in autoimmunity.

In this study, Treg cells were classified based on their phenotype $CD4^+FoxP3^+CD127^{lo}$. As FoxP3 expression may be induced upon stimulation, these samples were not treated with PMA/I and Brefeldin A; but rather they were rested for 16 h at 37°C. Live leukocytes were first gated as $CD45^+FixVia\ eF506^-$ (Figure 4.9A), then lymphocytes based on their characteristic FSC and SSC (Figure 4.9B). Singlets were characterised based on FSC-A v FSC-W (Figure 4.9C), and T cells then gated as $CD3^+TCR-\gamma\delta^-$ (Figure 4.9D). As samples were not treated with PMA/I, an antibody targeting CD4 was included along with CD8 to identify CD8 and CD4 T cells (Figure 4.9E). Treg cells were identified within the CD4 T cell subset as $FoxP3^+CD127^{lo}$ (Figure 4.9F).

Along with $FoxP3^+CD127^{lo}$ (Figure 4.10A), in some cases expression of the IL-2 receptor CD25 was used to identify Treg cells, although staining for CD25 was inconsistent on occasion. When CD25 was included in the gating strategy (Figure 4.10B), effectively all $FoxP3^+$ CD4 T cells were observed to also express CD25 and map to the $CD127^{lo}$ population (Figure 4.10C), further validating the Treg cell gating strategy.

The number of Treg cells as a percentage of CD4 T cells in peripheral blood was found to be approximately 6% in healthy control PBMC, but significantly deficient in HS patients ($p < 0.05$; Figure 4.11A). Given this deficit, along with the modest increase observed in Th17 cells in HS patients (Figure 4.8B), the ratio of Th17 cells to Treg cells was found to be significantly increased in favour of Th17 cells in HS patient peripheral blood ($p < 0.05$; Figure 4.11B).

Given that surface expression of CLA enables the recruitment of T cells into the skin, their expression on Treg cells was explored. Representative plots from HS patient PBMC

show CLA present on approximately 45% of Treg cells (Figure 4.12A), with no significant difference in frequency between HS patients and healthy controls (Figure 4.12B).

Although CD161 is a pan-marker for Th17 cells, it has also been reported on Treg cells in inflammatory conditions (Afzali et al., 2013); these Treg cells are then capable of IL-17 production. In this study CD161 expression on Treg cells in PBMC was noted to be 2-4% (Figure 4.12C), with no difference in frequency between healthy control and HS patients (Figure 4.12D).

Treg cells can suppress via a variety of mechanisms including those involving CD39 and CTLA-4. CD39 is an ectonucleotidase which hydrolyses ATP and is expressed on a subset of human Treg cells. CD39⁺ Treg cells have been reported as the principle suppressors of Th17 cells (Fletcher et al., 2009). CTLA-4 acts as an immune checkpoint to downregulate immune responses. It is expressed on activated T cells and most Treg cells, particularly those which constrain autoimmunity (Jain et al., 2010), and targets the co-stimulatory ligands CD80 and CD86 (Murphy et al., 2016). It may well exercise its suppressive role through competition with CD28 for these ligands rather than directly activating an inhibitory signalling pathway.

Representative plots show expression of CD39 on Treg cells (Figure 4.13A), with no difference in frequency between HS patients and healthy controls (Figure 4.13B). CTLA-4 was expressed on the majority of Treg cells in peripheral blood (Figure 4.13C), but similarly there was no significant difference observed between the two cohorts (Figure 4.13D).

In summary, the frequency of Treg cells in PBMC from HS patients was reduced relative to healthy controls, but expression of functional markers such as CLA, CD39, CTLA-4 and CD161 were unchanged. Taken together with the Th17 data, the Th17: Treg cell axis was found to be unbalanced in favour of Th17 cells in PBMC from HS patients compared with healthy controls and may be suggestive of systemic immune dysregulation in HS.

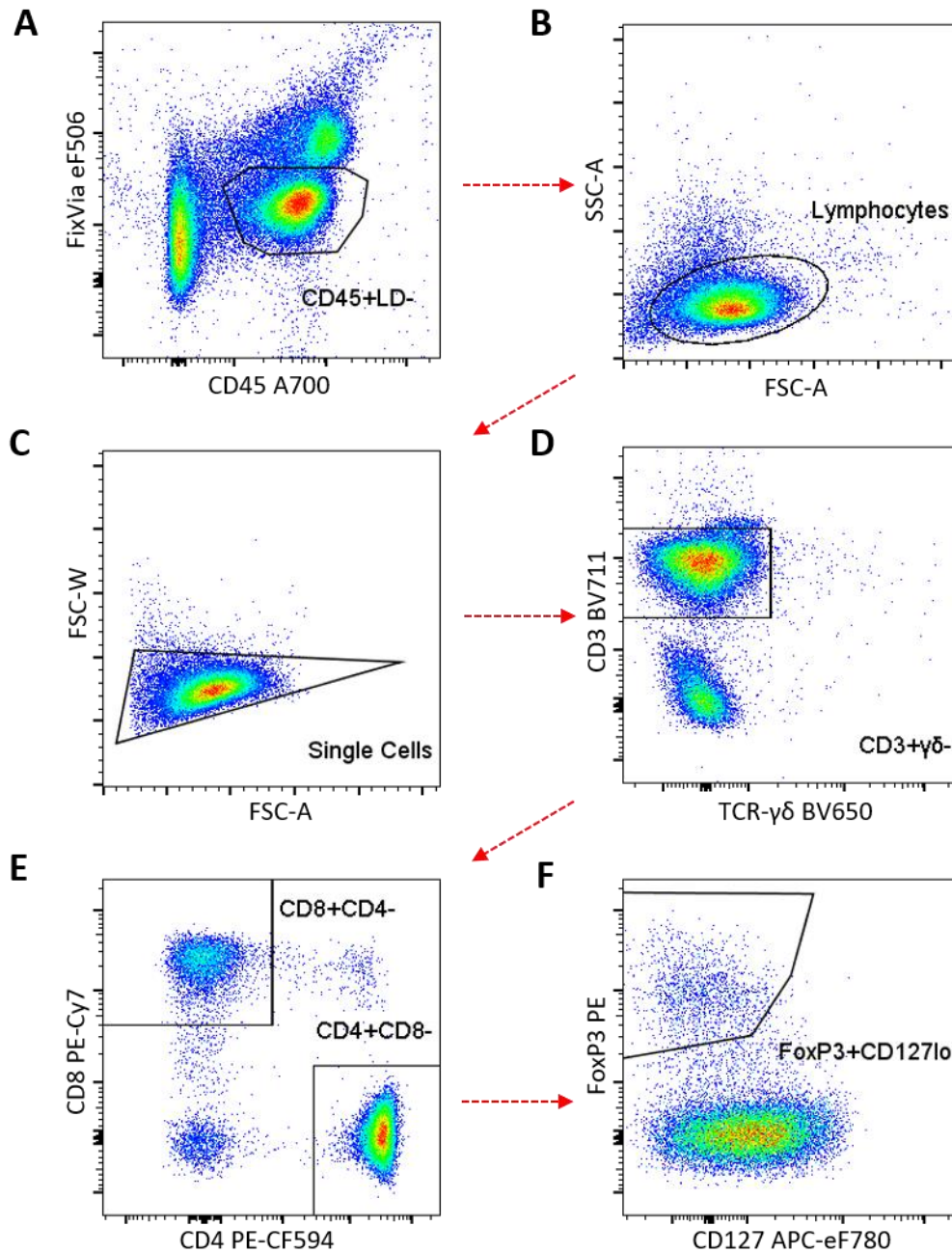


Figure 4.9 Plots representing the gating strategy to identify Treg cells in peripheral blood.

PBMC were rested for 16 h, stained for surface and intracellular markers, and analysed by flow cytometry. To identify CD4, CD8 and Treg cells, sequential gating was performed: CD45⁺, Fixable-Viability-Dye- to identify viable leukocytes (A); Forward v Side Scatter to exclude debris and non-lymphocytes (B); FSC-Area v FSC-Width to exclude doublets (C); CD3⁺TCR- $\gamma\delta$ ⁻ to identify CD3 T cells (D); CD4 v CD8 to identify CD4 and CD8 T cells (E); and FoxP3⁺CD127^{lo} to identify (CD4⁺) Treg cells (F).

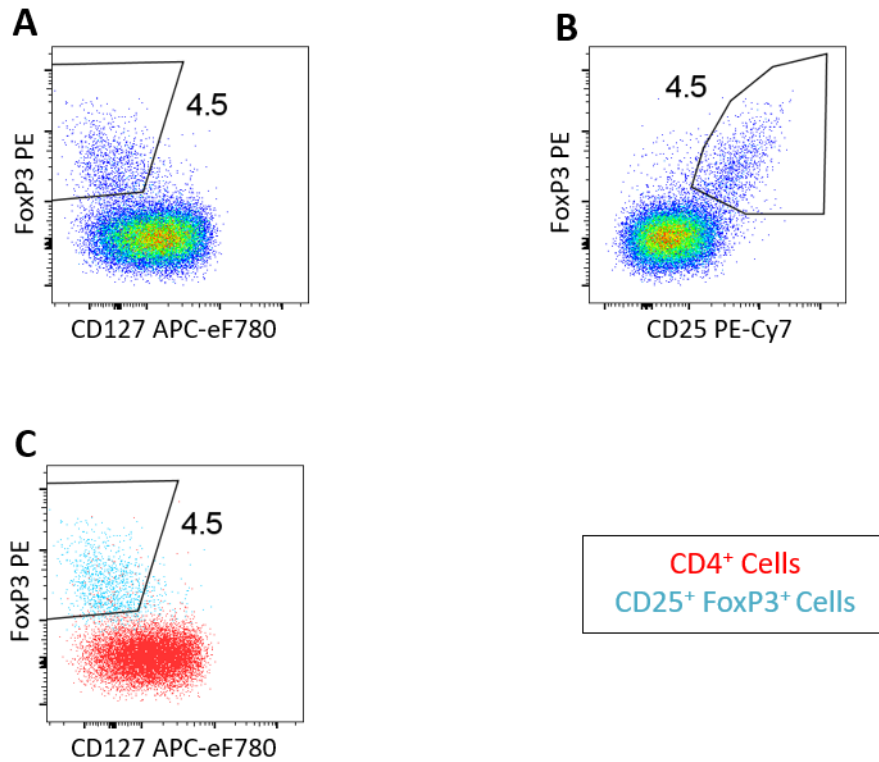


Figure 4.10 Representative dot plots validating the gating strategy to identify Treg cells.

PBMC were rested for 16 h, stained for surface and intracellular markers, and analysed by flow cytometry. To identify Treg cells, plots were gated for the FoxP3⁺CD127^{lo} population of CD4⁺ stained cells as per Figure 4.9 (A). Virtually all the FoxP3⁺CD127^{lo} population co-expressed CD25 (B), and the vast majority of CD25⁺FoxP3⁺ cells map to the FoxP3⁺CD127^{lo} population (C).

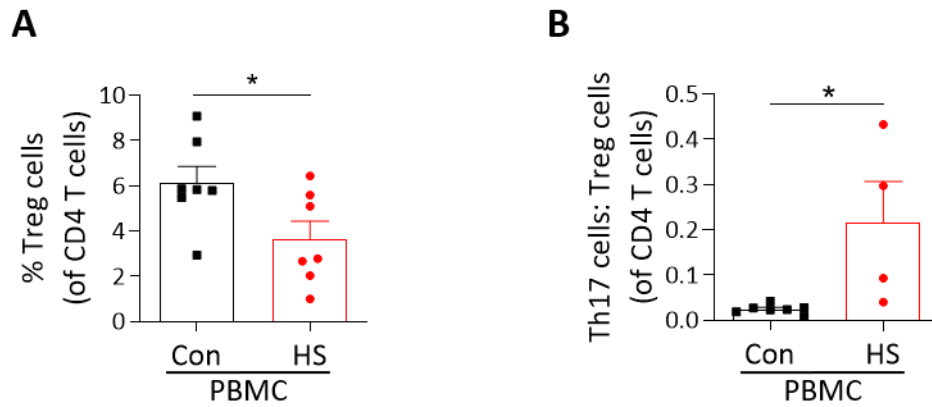


Figure 4.11 Decreased frequency of Treg cells, and an increased ratio of Th17 cells to Treg cells, in HS patient compared with healthy control peripheral blood.

PBMC from healthy controls (Con; n=7) or HS patients (n=7 (A); n=4 (B)) were rested (Treg cells) or treated with PMA/I and Brefeldin A (Th17 cells) for 16 h, stained for surface and intracellular markers, and analysed by flow cytometry. Graphs show the frequency of Treg cells (A) and the ratio of Th17 cells to Treg cells (B). Graphs represent individual samples with mean \pm SEM for each group. Statistical significance was calculated using Mann-Whitney U test; *p<0.05.

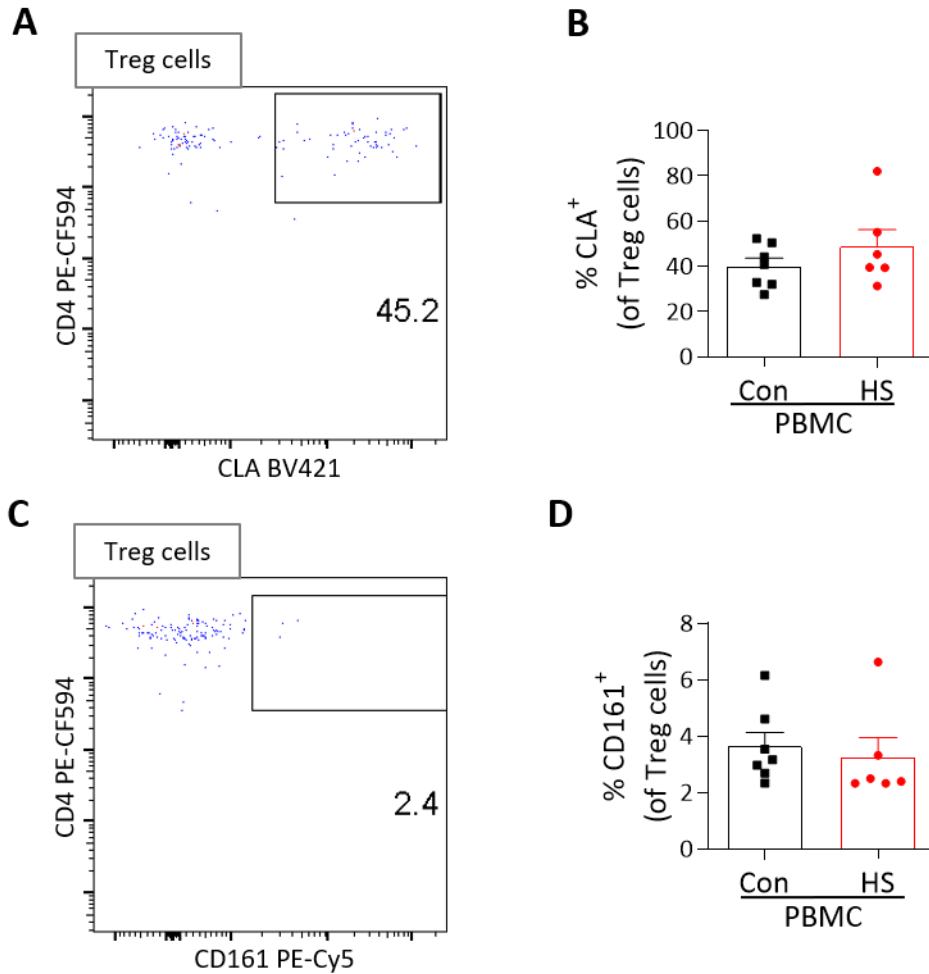


Figure 4.12 Frequency of CLA and CD161 expression on Treg cells unchanged in HS patient versus healthy control peripheral blood.

PBMC from healthy controls (Con; n=7) or HS patients (n=6) were rested for 16 h, stained for surface and intracellular markers, and analysed by flow cytometry. Representative dot plots, gated on Treg cells, display CLA (**A**) and CD161 (**C**) expression, plotted against CD4, from a rested HS patient PBMC sample. Graphs show the frequency of CLA (**B**) and CD161 (**D**) expression on Treg cells. Graphs represent individual samples with mean \pm SEM for each group. Statistical significance was calculated using Mann-Whitney U test.

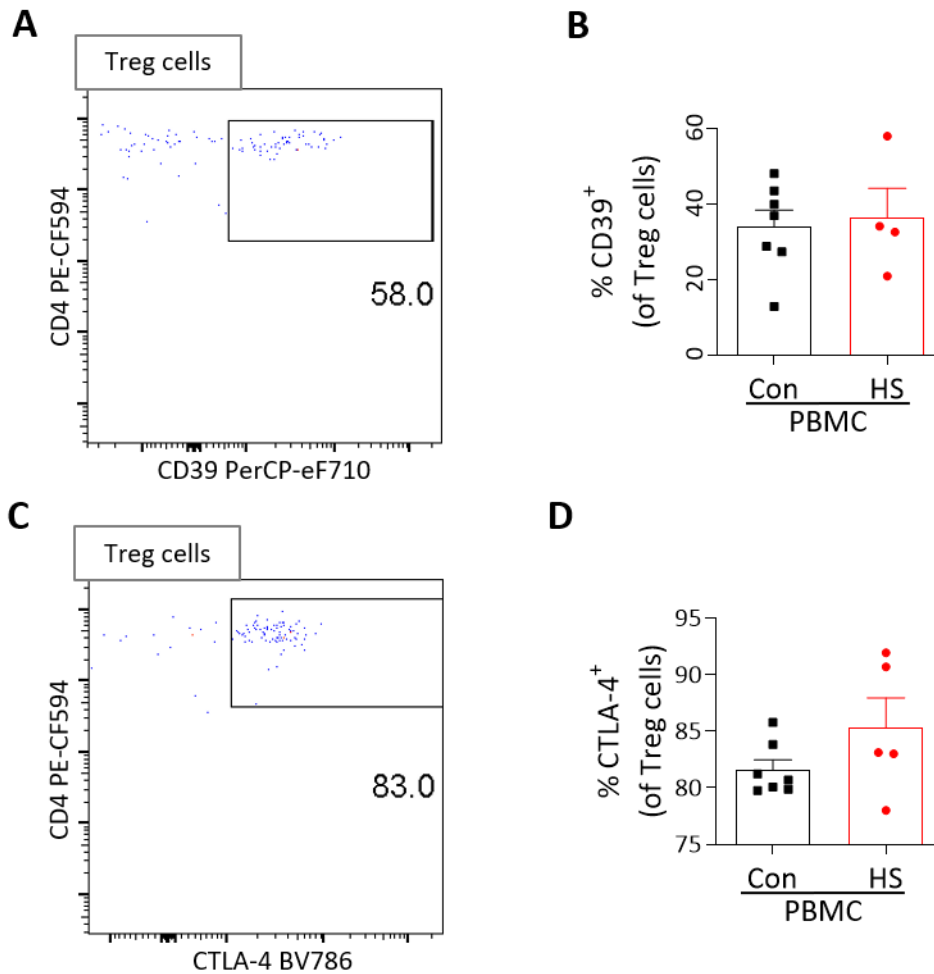


Figure 4.13 Frequencies of CD39 and CTLA-4 expression on Treg cells unchanged in HS patient versus healthy control peripheral blood.

PBMC from healthy controls (Con; n=7) or HS patients (n=4 (B); n=5 (D)) were rested for 16 h, stained for surface and intracellular markers, and analysed by flow cytometry. Representative dot plots, gated on Treg cells, display CD39 (A) and CTLA-4 (C) expression, plotted against CD4, from rested HS patient PBMC sample. Graphs show the frequency of CD39 (B) and CTLA-4 (D) expression on Treg cells. Graphs represent individual samples with mean \pm SEM for each group. Statistical significance was calculated using Mann-Whitney U test.

4.4.4 Substantial increase in the number of T cells in HS lesional skin

Having compared the phenotype and function of T cells in PBMC, the next step was to analyse T cells in the skin of HS patients and healthy controls.

HS lesions primarily occur in areas of skin-skin contact such as the groin, buttocks, underarm, and under the breast. In this study, skin biopsies were taken from HS patients from the non-infected region of a lesion, the perilesion (2 cm from lesion), and the uninvolved area (10 cm from lesion). Both perilesional and uninvolved skin appeared clinically normal. Once biopsies were dissociated into a single cell suspension using an in-house collagenase solution (Section 2.2.5.2), they were treated in a similar manner to PBMC; cells were treated with PMA/I and Brefeldin A for 16 h at 37°C, then stained for viability and CD45, CD3, TCR- $\gamma\delta$, CD8, CLA and CD161. Samples were then fixed, permeabilised and stained for the intracellular cytokines IL-17, IL-22, TNF, GM-CSF, IFN- γ and IL-2. Samples were analysed by flow cytometry within 24 h.

To identify CD3, CD8 and CD4 T cells in the skin, cells were first gated as CD45⁺FixVia eF506⁻ (CD45⁺LD⁻ live leukocytes; Figure 4.14A); then lymphocytes based on their FSC-A v SSC-A profile (Figure 4.14B) and single cells (FSC-A v FSC-W; Figure 4.14C). Next, TCR- $\alpha\beta$ T cells were gated as CD3⁺TCR- $\gamma\delta$ ⁻ cells (Figure 4.14D), and of these CD8 T cells as CD3⁺CD8⁺, and CD4 T cells as CD3⁺CD8⁻ (Figure 4.14E). As was the case for PBMC, this gating strategy for CD4 T cells was validated whereby in a sample not treated with PMA/I (Figure 4.15A), the vast majority (97%) of CD3⁺CD8⁻ cells were shown to be CD4 T cells (Figure 4.14B).

Absolute counts of CD45⁺ and CD3⁺ cells per mm skin were calculated by dividing the total number of acquired cells by the size of the biopsy. Lesional skin exhibited a substantial immune cell (CD45⁺FixVia eF506⁻) infiltrate, in orders of magnitude higher, when compared with the perilesional (ns) and uninvolved (p <0.01) HS skin, as well as healthy control skin (p <0.05; Figure 4.16A). There was no significant difference in CD45⁺ cell counts between the apparently clinically normal HS perilesional, HS uninvolved and healthy control skin.

T cells showed a similar profile, being significantly increased in HS lesional skin compared with HS perilesional ($p < 0.05$), HS uninvolved ($p < 0.0001$), and healthy control skin ($p < 0.0001$; Figure 4.16B), with no differences between the other groups.

Overall, HS perilesional skin trended to more CD45⁺ cells and T cells than HS uninvolved skin (ns), with HS uninvolved slightly more so than healthy control skin (ns). It was noted that the majority of dissociated CD45⁺ cells were T cells in all skin biopsies in this study, suggesting that this method of skin dissociation may preferentially enrich for T cells.

Despite the extensive increase in CD45⁺ immune cells and CD3⁺ T cells overall in HS lesional skin, no difference in the frequency of the CD8 (Figure 4.17A) and CD4 (Figure 4.17B) T cell subsets within the T cell population was observed, with CD8 T cells at 30% approx. and CD4 T cells at 65% approx. of total T cells.

As previously discussed, CLA enables recruitment of T cells into the skin; and its expression is shown in representative plots as CLA v CD8 for CD8 (CD8⁺CLA⁺; Figure 4.18A) and CD4 (CD8⁻CLA⁺; Figure 4.18C) T cells. Surprisingly, although immune cells were dramatically increased in HS lesional skin, the frequency of CLA expression on CD8 T cells was actually significantly reduced when compared with HS perilesional ($p < 0.01$), HS uninvolved ($p < 0.05$) and healthy control skin ($p < 0.05$; Figure 4.18B). No difference was observed in CLA⁺ CD8 T cell frequency between healthy control and HS perilesional and HS uninvolved skin. A similar, albeit non-significant, trend was observed in CD4 T cells, with a deficit (ns) in CD4 T cells expressing CLA in the HS lesion when compared with clinically normal HS perilesional and HS uninvolved skin, as well as healthy control skin (Figure 4.18D). As with CD8 T cells, frequencies of CLA expression, on CD4 T cells were unchanged between HS perilesional, HS uninvolved and healthy control skin.

Taken together, these results show a substantial increase in immune cells in HS lesional skin compared with clinically normal HS skin and healthy control skin, with the ratio of CD8 to CD4 T cells remaining unchanged. Reduced CLA expression on CD8 and CD4 T cells in HS lesional skin may suggest an expansion of CLA⁻ T cells, or downregulation of CLA expression, in the HS lesion.

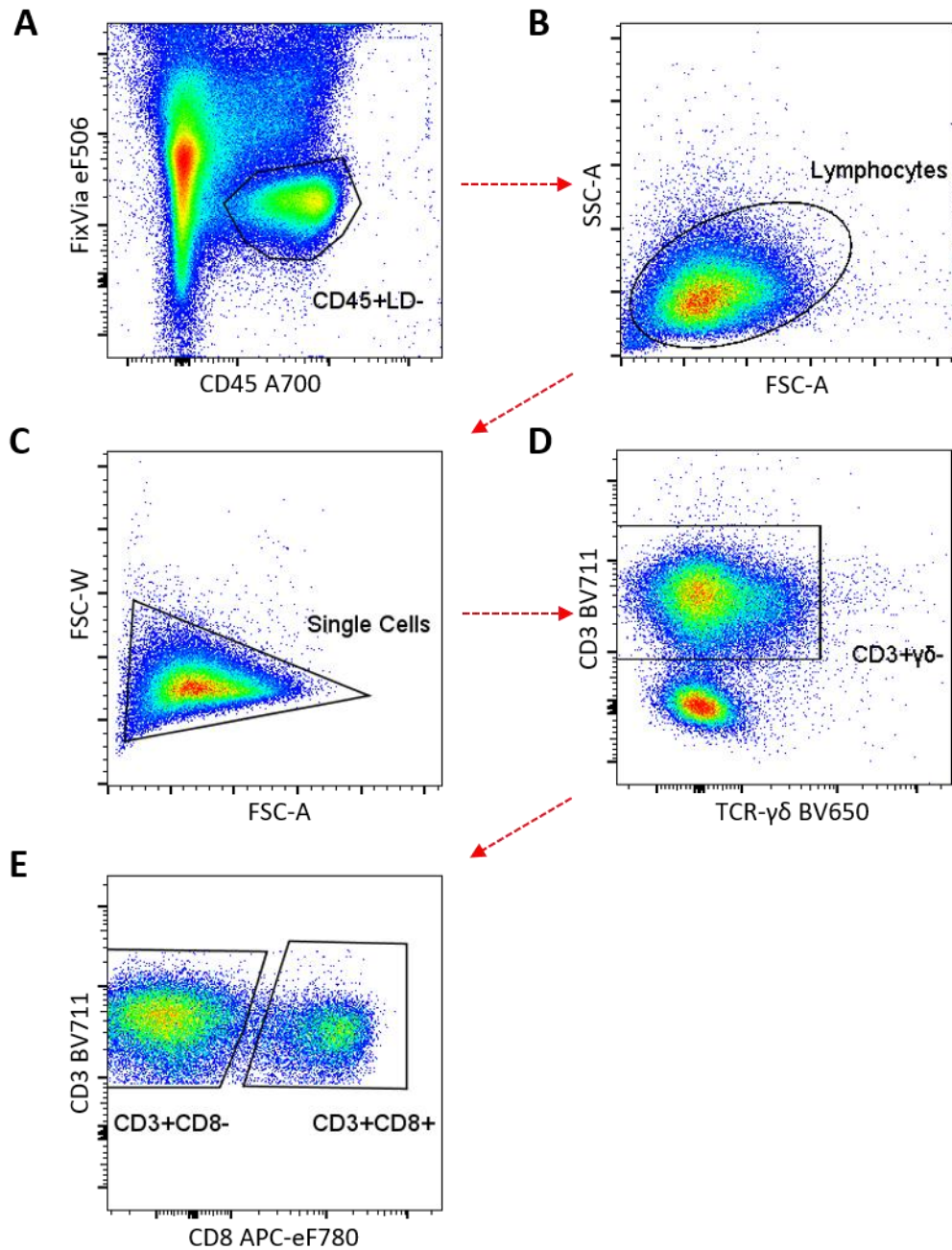


Figure 4.14 Plots representing the gating strategy to identify CD4 and CD8 T cells in skin samples.

Cells isolated from the skin were treated with PMA/I and Brefeldin A for 16 h, stained for surface and intracellular markers, and analysed by flow cytometry. To identify CD8 and the vast majority of CD4 T cells in stimulated samples, sequential gating was performed: CD45⁺, Fixable-Viability-Dye⁻ to identify viable leukocytes (A); Forward v Side Scatter to exclude debris and non-lymphocytes (B); FSC-Area v FSC-Width to exclude doublets (C); CD3⁺TCR- $\gamma\delta$ ⁻ to exclude TCR- $\gamma\delta$ T cells and non-T cells (D); CD3⁺CD8⁺ to identify CD8 T cells, and CD3⁺CD8⁻ to identify CD4 T cells (E).

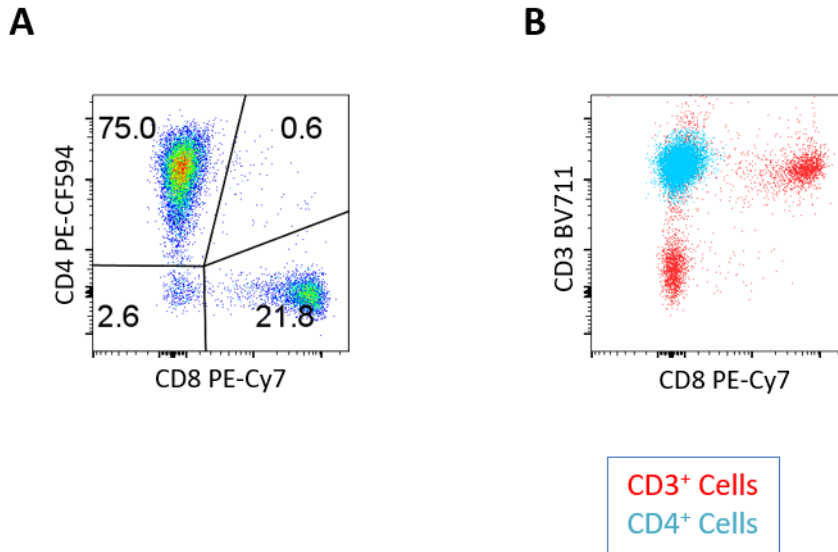


Figure 4.15 Representative plots validating the gating strategy to identify CD4 T cells. Cells isolated from the skin were rested for 16 h, stained for surface and intracellular markers, and analysed by flow cytometry. CD4 T cells represent 97% (75% v. 2.6%) of CD3⁺CD8⁻TCR- $\gamma\delta$ ⁻ cells in an un-stimulated skin sample (A), and CD4⁺ stained cells map directly to the CD3⁺CD8⁻ population (B). This serves to validate identifying CD4 T cells as CD3⁺CD8⁻TCR- $\gamma\delta$ ⁻ cells in PMA/I treated samples.

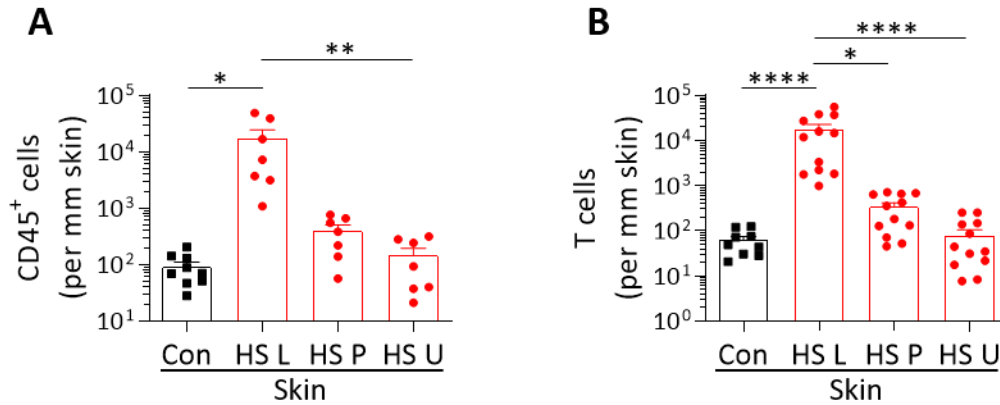


Figure 4.16 Increased number of CD45⁺ cells and CD3 T cells in HS lesional compared with healthy control skin.

Cells isolated from the skin of healthy controls (Con; n=9) or HS patients (HS L: lesional, P: perilesional, U: uninvolved skin; n=7 (A); n=12 (B)) were treated with PMA/I and Brefeldin A for 16 h, stained for surface and intracellular markers, and analysed by flow cytometry. Graphs show the absolute numbers for CD45⁺ leukocytes (A) or CD3⁺ T cells (B) per mm of skin. Graphs represent individual samples with mean \pm SEM for each group. Statistical significance was calculated using Kruskal-Wallis one-way ANOVA with Dunn's multiple comparisons test; *p<0.05, **p<0.01, ****p<0.0001.

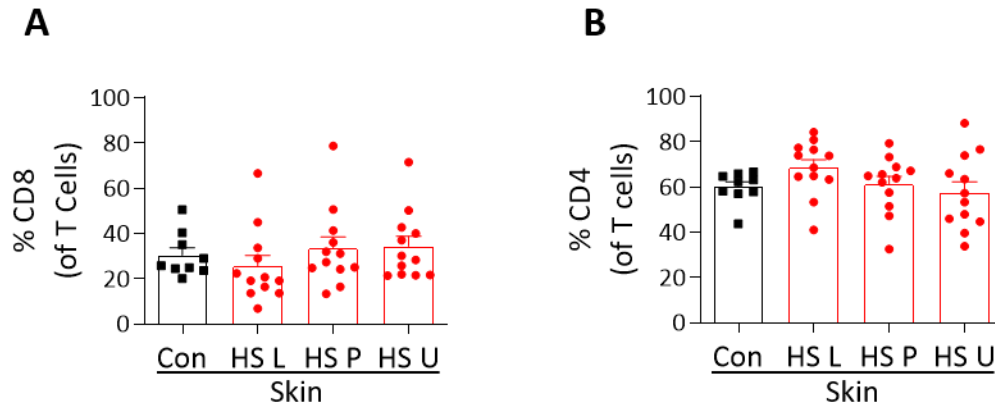


Figure 4.17 Similar frequency of CD8 and CD4 T cells in HS patient compared with healthy control skin.

Cells isolated from the skin of healthy controls (Con; n=9) or HS patients (HS L: lesional, P: perilesional, U: uninvolved skin; n=12) were treated with PMA/I and Brefeldin A for 16 h, stained for surface and intracellular markers, and analysed by flow cytometry. Graphs show the frequency of CD8 (A) and CD4 (B) T cells within the total T cell population (CD3⁺TCR $\gamma\delta$ ⁻ lymphocytes). Graphs represent individual samples with mean \pm SEM for each group. Statistical significance was calculated using Kruskal-Wallis one-way ANOVA with Dunn's multiple comparisons test.

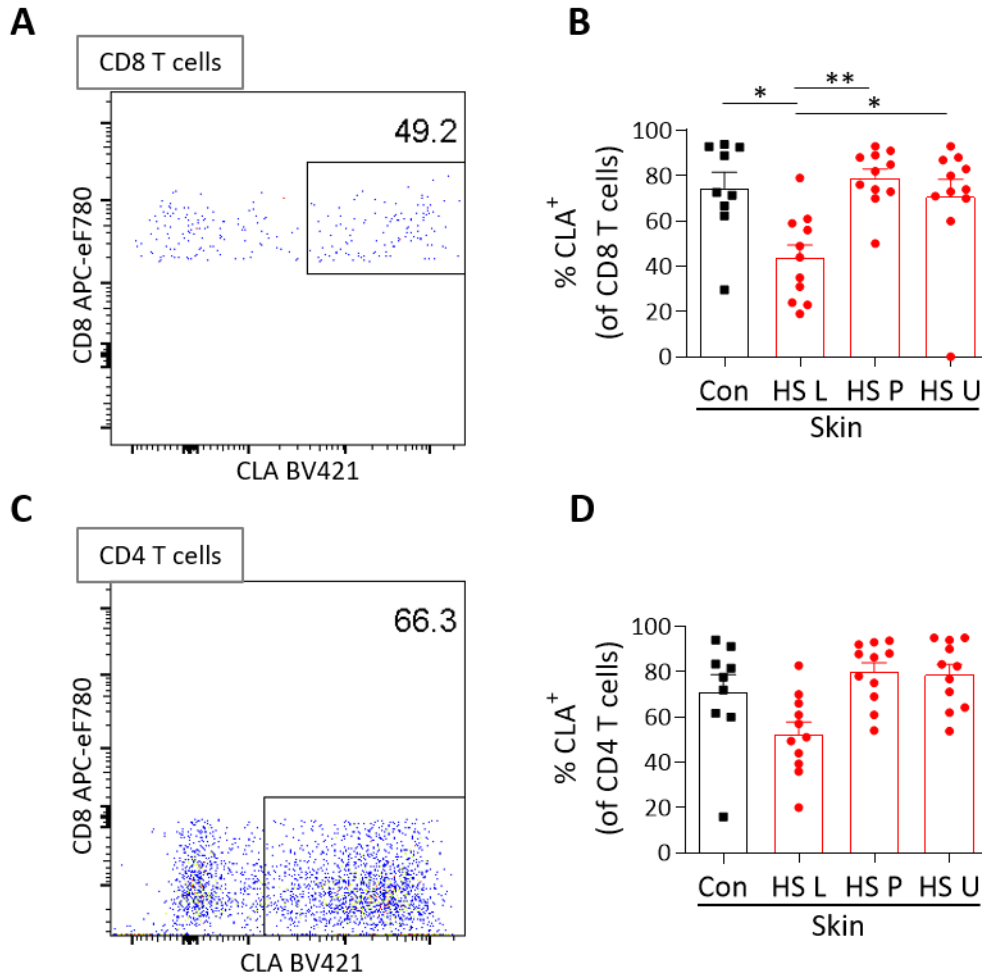


Figure 4.18 Reduced frequency of CLA expression on CD8 and CD4 T cells in the lesional skin of HS patients compared with healthy control skin.

Cells isolated from the skin of healthy controls (Con; n=9) or HS patients (HS L: lesional, P: perilesional, U: uninvolved skin; n=11) were treated with PMA/I and Brefeldin A for 16 h, stained for surface and intracellular markers, and analysed by flow cytometry. Representative dot plots display CLA expression plotted against CD8, gated on CD8 (CD3⁺CD8⁺; A) and CD4 (CD3⁺CD8⁻; C) T cells from a PMA/I treated HS patient skin sample. Graphs show the frequency of CLA expressing CD8 (B) and CD4 (D) T cells. Graphs represent individual samples with mean \pm SEM for each group. Statistical significance was calculated using Kruskal-Wallis one-way ANOVA with Dunn's multiple comparisons test; *p<0.05, **p<0.01.

4.4.5 T cells in HS patient skin display a marked proinflammatory profile, characterised by Th17 associated cytokines

Having demonstrated an extensive increase in T cells in HS patient lesional skin, the next step was to characterise the inflammatory cytokine signature of the T cells. Intracellular cytokine analysis revealed a marked inflammatory profile in HS skin, even in clinically normal perilesional and uninvolved skin. Representative plots reveal the expression profile of the cytokines IL-17 v IL-22 (Figure 4.19A), TNF v GM-CSF (Figure 4.19B) and IFN- γ v IL-2 (Figure 4.19C) on CD8 T cells in healthy control, HS lesional, perilesional and uninvolved skin.

IL-17 expression in CD8 T cells was increased in HS skin overall, although the increase was significant only between HS perilesional skin and healthy control skin ($p < 0.01$; Figure 4.20A). Likewise, IL-22 production by CD8 T cells in HS skin was increased relative to healthy control skin, significantly so only in HS uninvolved skin ($p < 0.05$; Figure 4.20B). Relative to healthy control skin, the frequency of TNF⁺ CD8 T cells appeared increased in lesional (ns), perilesional ($p < 0.001$) and uninvolved (ns) skin (Figure 4.20C). GM-CSF levels in CD8 T cells increased from negligible amounts in healthy skin to $>50\%$ expression in HS patient skin, significantly so in perilesional and uninvolved HS skin ($p < 0.05$; Figure 4.20D). IFN- γ expression on CD8 T cells approached mean levels of 80% on CD8 T cells in HS skin relative to healthy control skin (HS lesional $p < 0.0001$, perilesional $p < 0.01$; uninvolved ns; Figure 4.20E). Increases in frequency of CD8 T cells expressing IL-2 in HS skin compared with healthy control skin reached significance for HS perilesional ($p < 0.01$) and HS uninvolved skin ($p < 0.05$; Figure 4.20F).

The proinflammatory cytokine profile for CD4 T cells derived from HS skin was even more pronounced than that observed for CD8 T cells, particularly so in HS lesional skin. Representative plots show the expression profile of cytokines IL-17 v IL-22 (Figure 4.21A), TNF v GM-CSF (Figure 4.21B) and IFN- γ v IL-2 (Figure 4.21C) on CD4 T cells in healthy control, HS lesional, perilesional and uninvolved skin.

There was a striking increase in IL-17 production in CD4 T cells in HS lesional and perilesional skin, from less than 2% in healthy control skin to a mean of 40% in HS

lesional ($p < 0.001$) and perilesional ($p < 0.0001$) skin (Figure 4.22A). The frequency of IL-17 on CD4 T cells was also increased in HS uninvolved (ns) but not to the same degree, and in fact it was significantly reduced compared with HS perilesional skin ($p < 0.01$). IL-22 production by CD4 T cells increased from $< 1\%$ in healthy control skin to almost 20% in HS lesional ($p < 0.05$) and perilesional ($p < 0.001$) skin; less so for HS uninvolved skin (ns; Figure 4.22B). The mean frequency for CD4 T cells expressing TNF in HS skin more than doubled relative to healthy control skin, to levels above 50%; significantly so for HS perilesional ($p < 0.001$) and uninvolved ($p < 0.01$) skin (Figure 4.22C). Increases in GM-CSF production by CD4 T cells in HS skin were less striking, though significant for perilesional ($p < 0.05$) and uninvolved skin ($p < 0.01$) relative to healthy control skin (Figure 4.22D). IFN- γ levels on CD4 T cells enhanced 1.5-fold, significantly so for HS perilesional ($p < 0.05$) and uninvolved ($p < 0.05$) skin compared with healthy control skin (Figure 4.22E). IL-2 expression on CD4 T cells increased in HS perilesional ($p < 0.01$) and uninvolved ($p < 0.05$) tissue relative to healthy control skin (Figure 4.22F).

Given the dramatic differences in the frequency of CD4 T cells in HS skin, it was next investigated if these trends could be related to patient weight, which is a substantial risk factor in HS. Hence the same data for CD4 expression for the three cytokines that exhibited the largest shift (IL-17, IL-22 and TNF) were stratified by patient BMI index; above 30 (obese; left column) and lower than 28 (right column; Figure 4.23). However, no significant differences between HS lesional, perilesional and uninvolved skin were observed for CD4 T cell production of IL-17 (Figure 4.23A&B), IL-22 (Figure 4.23C&D) and TNF (Figure 4.23E&F). Although this suggests no deviation based on BMI, the sample size may be too small in this case. There was no correlation noted when stratified by Hurley score or smoker status either (data not shown).

Given the striking increase in IL-17 producing T cells observed in HS skin, CD161, which is the Th17 lineage-marker, was analysed next in order to identify T cell subsets with greater specificity. CD161 was expressed on a proportion of CD8 T cells (Figure 4.24A), and more so on CD4 T cells (Figure 4.24C). The frequency of CD161 expression on CD8 T cells was increased in HS lesional (ns), perilesional ($p < 0.05$) and uninvolved (ns) skin compared with healthy control skin (Figure 4.24B). The percentage of CD161 expressing

CD4 T cells increased two-fold in HS lesional ($p < 0.05$) and perilesional ($p < 0.001$) relative to healthy control skin, though less so in uninvolved skin (ns; Figure 4.24D).

Within CD4 T cells in the skin, Th17 cells were gated as CD161⁺IL-17⁺IFN- γ ⁻, ex-Th17 as CD161⁺IL-17⁻IFN- γ ⁺ and transitioning ex-Th17 cells as CD161⁺IL-17⁺IFN- γ ⁺ (Figure 4.25A). Th1 cells were defined as CD161⁻IL-17⁻IFN- γ ⁺. The high proportion of CD161⁻IL-17⁺IFN- γ ⁻ in these representative plots may be due to CD161 epitope damage (Figure 2.2). More likely, it was noticed that CD161 expression appeared downregulated upon PMA/I stimulation when compared with rested samples. In either case, this would suggest that the frequency of Th17 cells is in fact much higher than presented here and cannot be accurately characterised without detecting CD161 in its entirety.

Nonetheless, the frequency of Th17 cells as a percentage of CD4 T cells was markedly increased in HS lesional ($p < 0.01$) and perilesional ($p < 0.01$) skin compared with healthy control skin; while it was also much reduced in HS uninvolved skin relative to HS lesional ($p < 0.05$) and perilesional ($p < 0.05$) skin (Figure 4.25B). Both Th1 (Figure 4.25C) and ex-Th17 (Figure 4.25D) cells displayed no significant difference between HS lesional, perilesional, uninvolved and healthy control skin. However, there was a marked increase in the frequency of transitioning ex-Th17 cells in HS lesional ($p < 0.01$) and perilesional ($p < 0.001$) skin compared with healthy control skin (Figure 4.25E).

In summary, HS lesional skin was characterised by a large increase in T cells, with no change in the ratio of CD4 and CD8 T cells. Further, HS lesional and perilesional skin exhibited a dramatic Th17 skewed profile, with an increased frequency of IL-17 and associated cytokines in both CD8 and CD4 T cells.

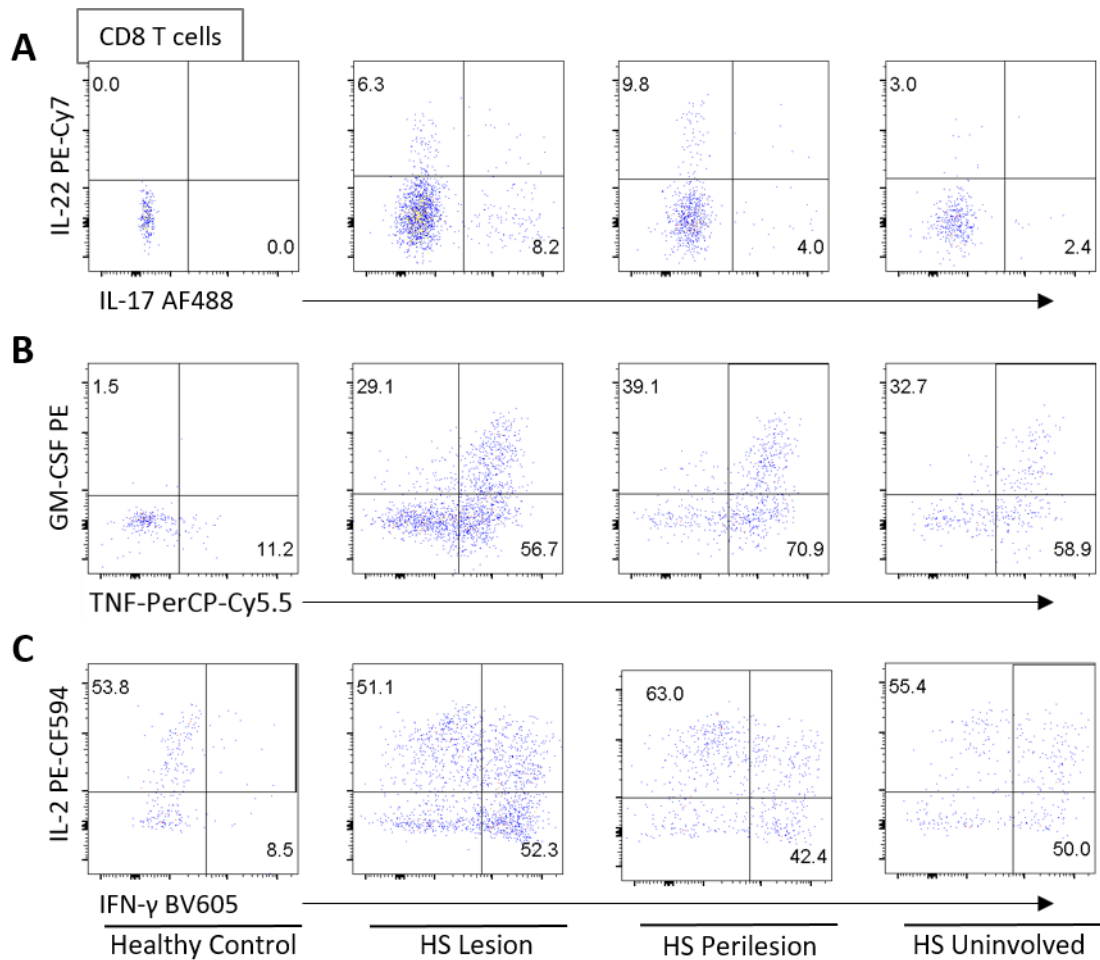


Figure 4.19 Representative dot plots for CD8 T cell cytokine expression in healthy control and HS patient skin.

Cells isolated from the skin of healthy controls or HS patients (HS Lesion, Perilesion, and Uninvolved skin) were treated with PMA/I and Brefeldin A for 16 h, stained for surface and intracellular markers, and analysed by flow cytometry. Representative dot plots for expression of IL-17 v IL-22 (A), TNF v GM-CSF (B), and IFN- γ v IL-2 (C) on CD8 T cells. Top left number represents total expression of y-axis cytokine, bottom right is total expression of x-axis cytokine. All plots were gated on single, live, CD45⁺TCR- $\gamma\delta$ CD3⁺CD8⁺ lymphocytes.

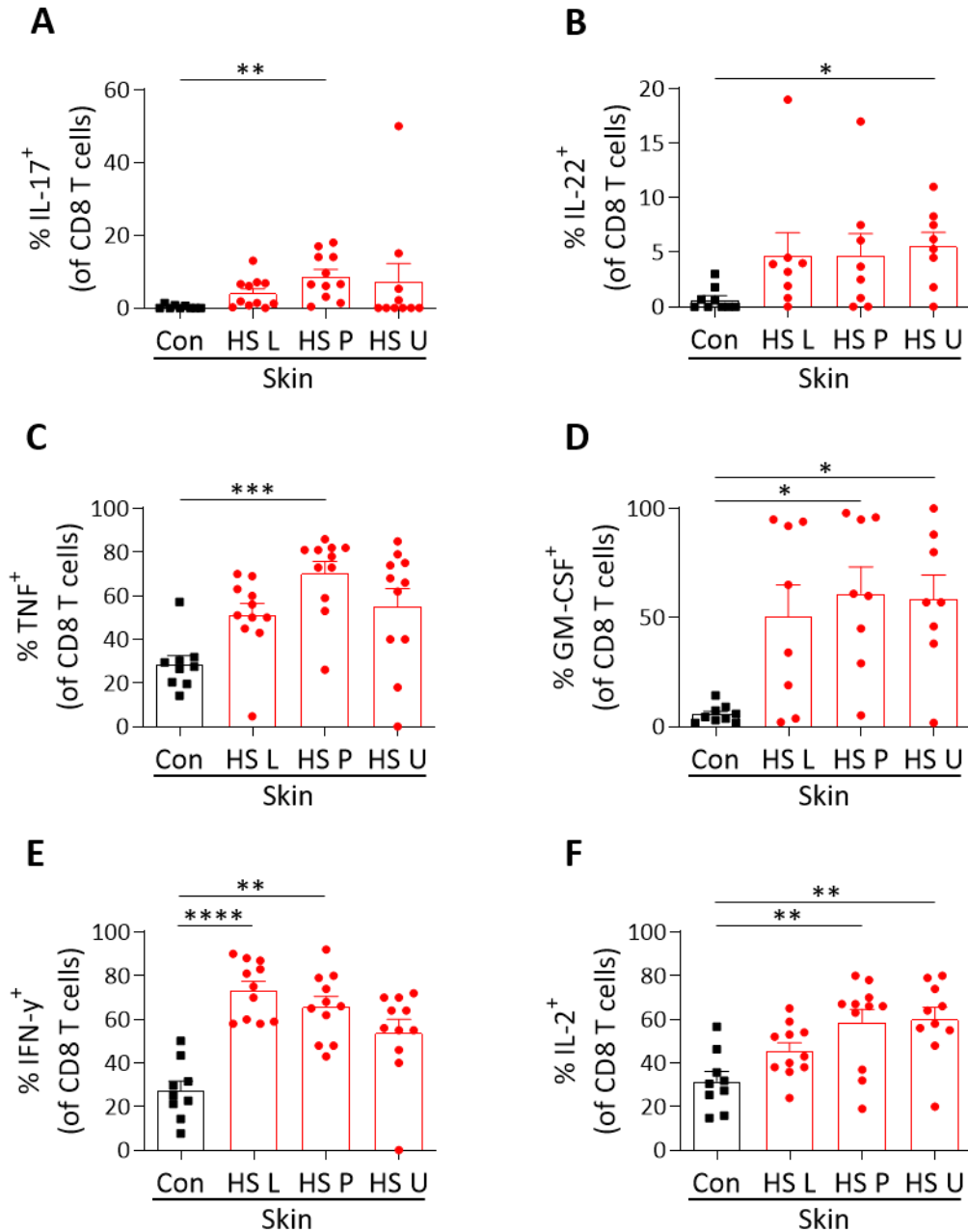


Figure 4.20 CD8 T cells in HS patient skin secrete multiple proinflammatory cytokines.

Cells isolated from the skin of healthy controls (Con; n=9) or HS patients (HS L: lesional, P: perilesional, U: uninvolved skin; n=9 (A-B); n=11 (C, E, F) n=8 (D)) were treated with PMA/I and Brefeldin A for 16 h, stained for surface and intracellular markers, and analysed by flow cytometry. Graphs show the frequency of CD8 T cells expressing cytokines IL-17 (A), IL-22 (B), TNF (C), GM-CSF (D), IFN-γ (E), and IL-2 (F). Graphs represent individual samples with mean ± SEM for each group. Statistical significance was calculated using Kruskal-Wallis one-way ANOVA with Dunn's multiple comparisons test; *p<0.05, **p<0.01, ***p<0.001, ****p<0.0001.

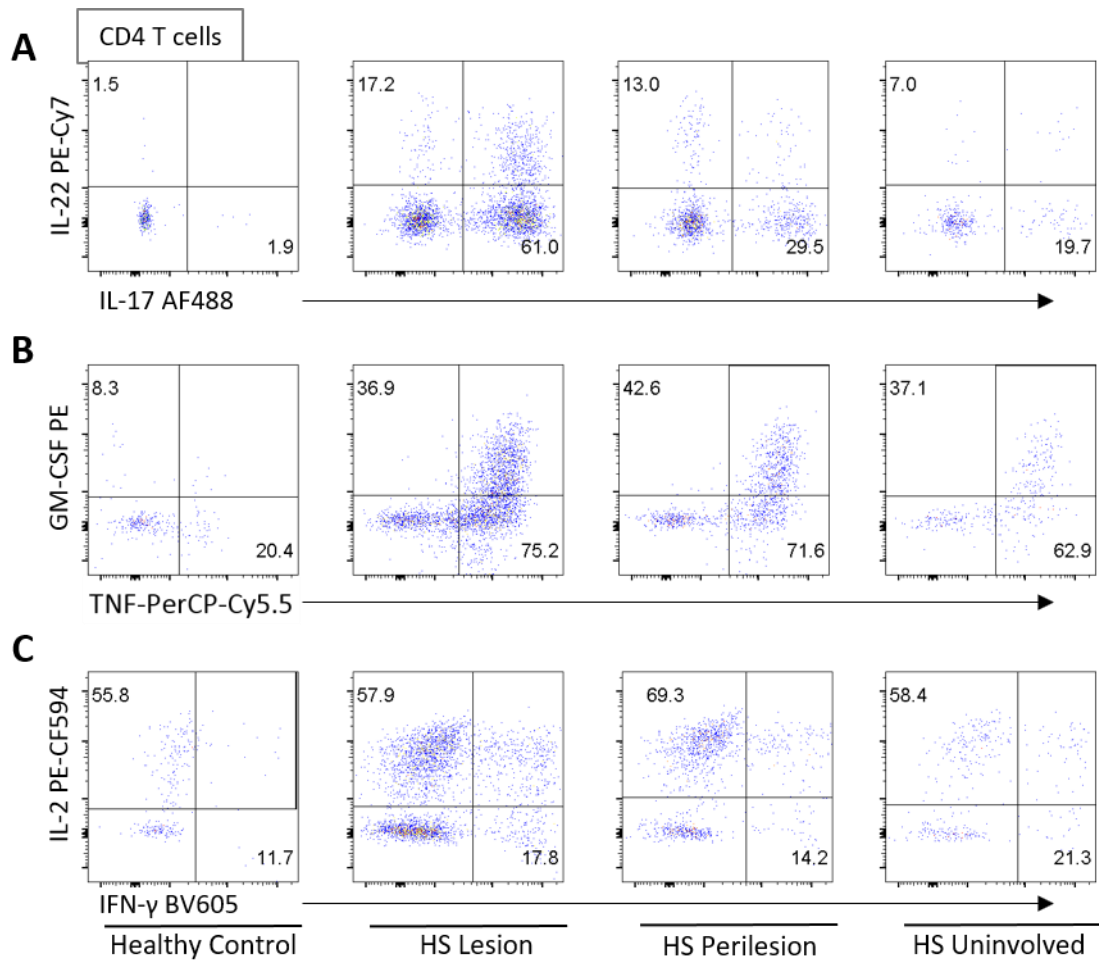


Figure 4.21 Representative dot plots for CD4 T cell cytokine expression in healthy control and HS patient skin.

Cells isolated from the skin of healthy controls or HS patients (HS Lesion, Perilesion, and Uninvolved skin) were treated with PMA/I and Brefeldin A for 16 h, stained for surface and intracellular markers, and analysed by flow cytometry. Representative dot plots for expression of IL-17 v IL-22 (A), TNF v GM-CSF (B), and IFN- γ v IL-2 (C) on CD4 T cells. Top left number represents total expression of y-axis cytokine, bottom right is total expression of x-axis cytokine. All plots were gated on single, live, CD45⁺TCR- $\gamma\delta$ ⁺CD3⁺CD8⁺ lymphocytes.

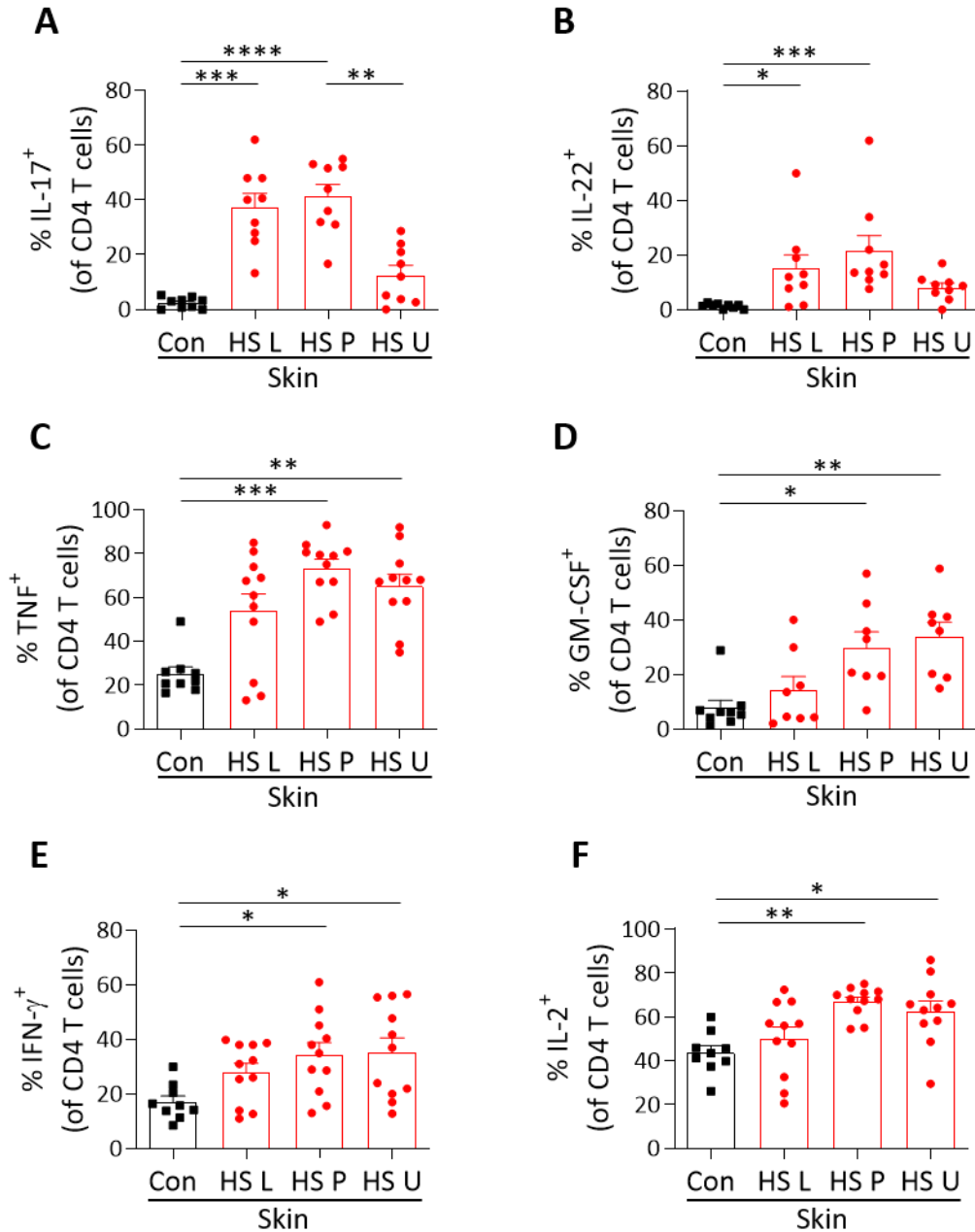


Figure 4.22 CD4 T cells in HS patient skin secrete multiple proinflammatory cytokines.

Cells isolated from the skin of healthy controls (Con; n=9) or HS patients (HS L: lesional, P: perilesional, U: uninvolved skin; n=9 (A-B); n=11 (C, E, F) n=8 (D)) were treated with PMA/I and Brefeldin A for 16 h, stained for surface and intracellular markers, and analysed by flow cytometry. Graphs show the frequency of CD4 T cells expressing cytokines IL-17 (A), IL-22 (B), TNF (C), GM-CSF (D), IFN- γ (E), and IL-2 (F). Graphs represent individual samples with mean \pm SEM for each group. Statistical significance was calculated using Kruskal-Wallis one-way ANOVA with Dunn's multiple comparisons test; *p<0.05, **p<0.01, ***p<0.001, ****p<0.0001.

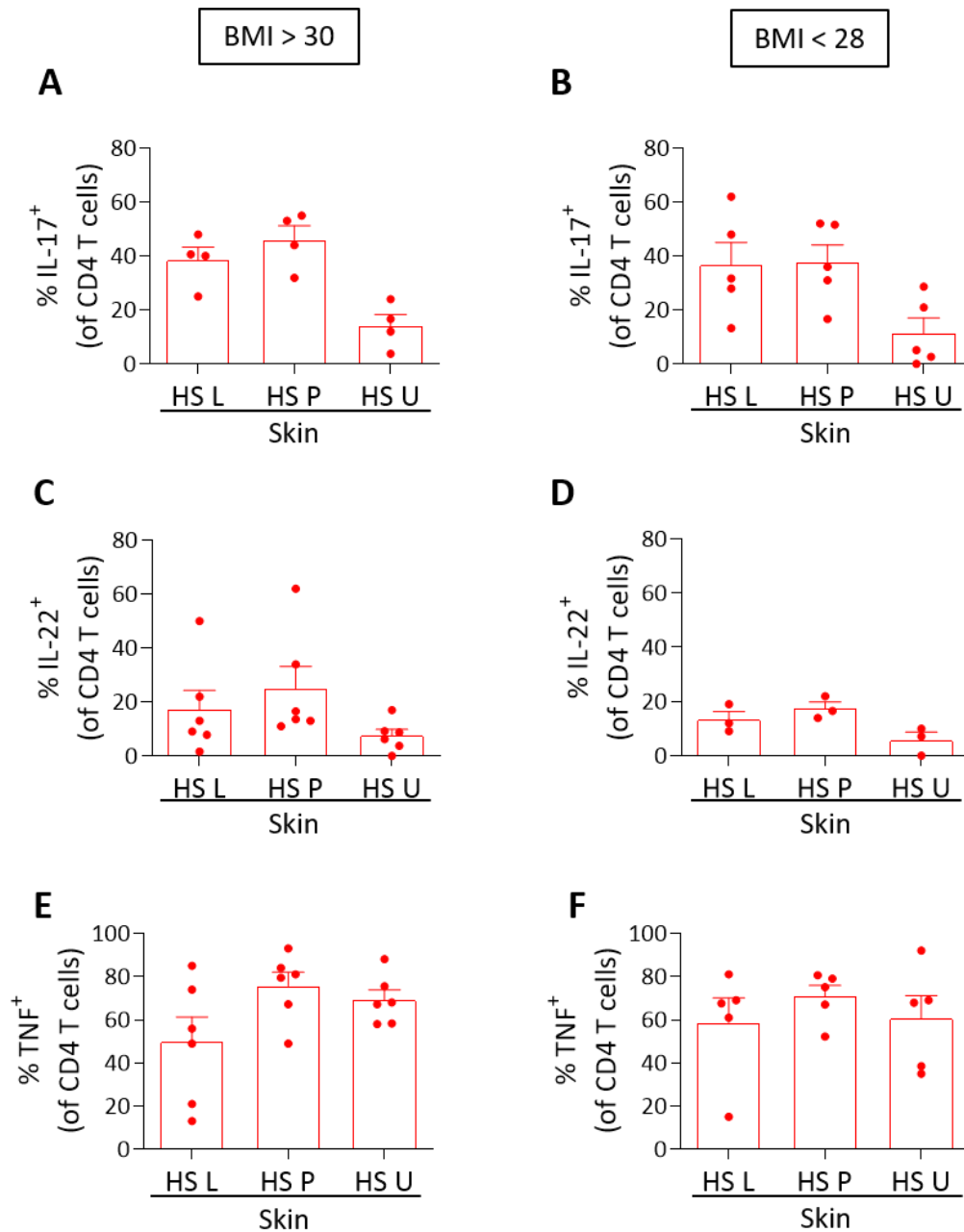


Figure 4.23 No association between CD4 T cell cytokine expression in HS patient skin and body mass index.

Cells isolated from the skin of HS patients (HS L: lesional, P: perilesional, U: uninvolved skin; n=4 (A), n=5 (B); n=6 (C); n=3 (D); n=6 (E); n=5 (F)) were treated with PMA/I and Brefeldin A for 16 h, stained for surface and intracellular markers, and analysed by flow cytometry. Graphs show the frequency of CD4 T cells expressing cytokines IL-17 (A), IL-22 (B) and TNF (C) for HS patients with a higher (>30; left column) or lower (<28; right column) body mass index (BMI). Plots represent individual samples with mean \pm SEM for each group. Statistical significance was calculated using Kruskal-Wallis one-way ANOVA with Dunn's multiple comparisons test; * p <0.05, ** p <0.01, *** p <0.001.

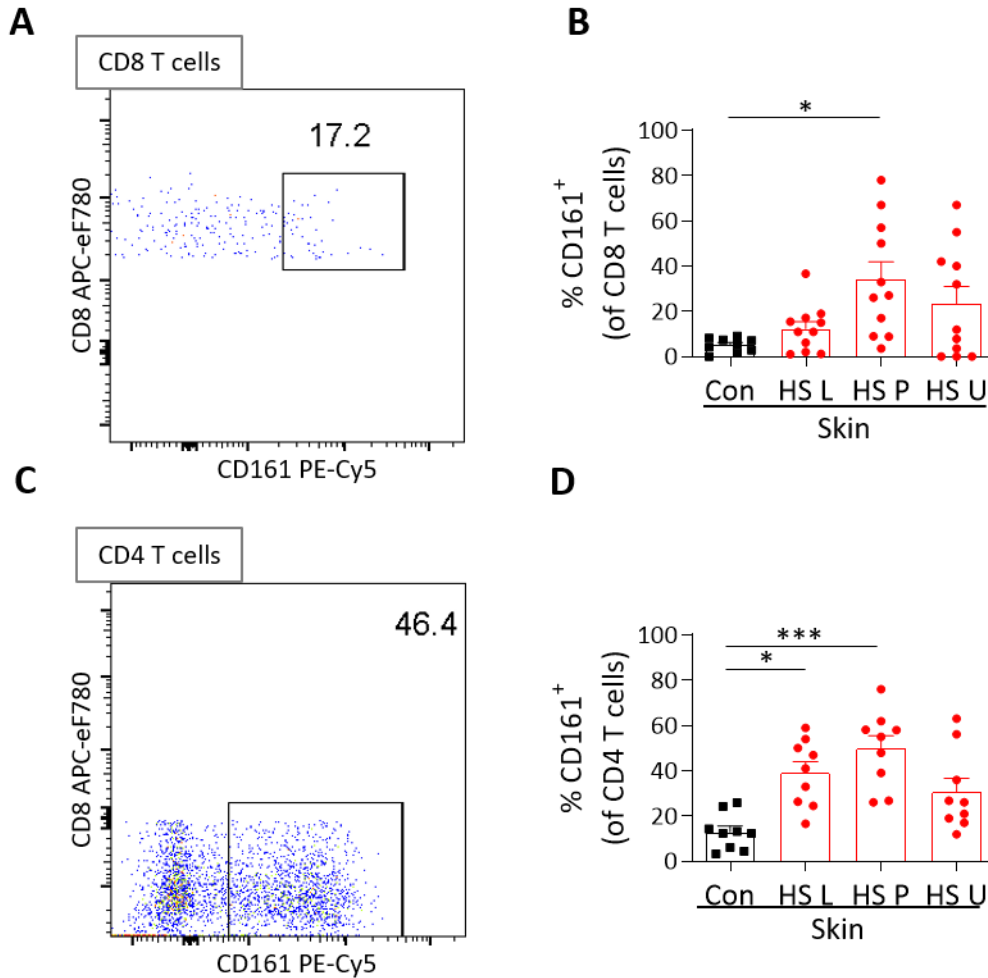


Figure 4.24 Increased frequency of CD161⁺ T cells in HS patient skin.

Cells isolated from the skin of healthy controls (Con; n=9) or HS patients (HS L: lesional, P: perilesional, U: uninvolved skin; n=11 (B); n=9 (D))) were treated with PMA/I and Brefeldin A for 16 h, stained for surface and intracellular markers, and analysed by flow cytometry. Representative dot plots display CD161 expression plotted against CD8, gated on CD8 (CD3⁺CD8⁺; A) and CD4 (CD3⁺CD8⁻; C) T cells from a PMA/I treated HS patient skin sample. Graphs show the frequency of CD161 expressing CD8 (B) and CD4 (D) T cells. Graphs represent individual samples with mean \pm SEM for each group. Statistical significance was calculated using Kruskal-Wallis one-way ANOVA with Dunn's multiple comparisons test; *p<0.05, ***p<0.001.

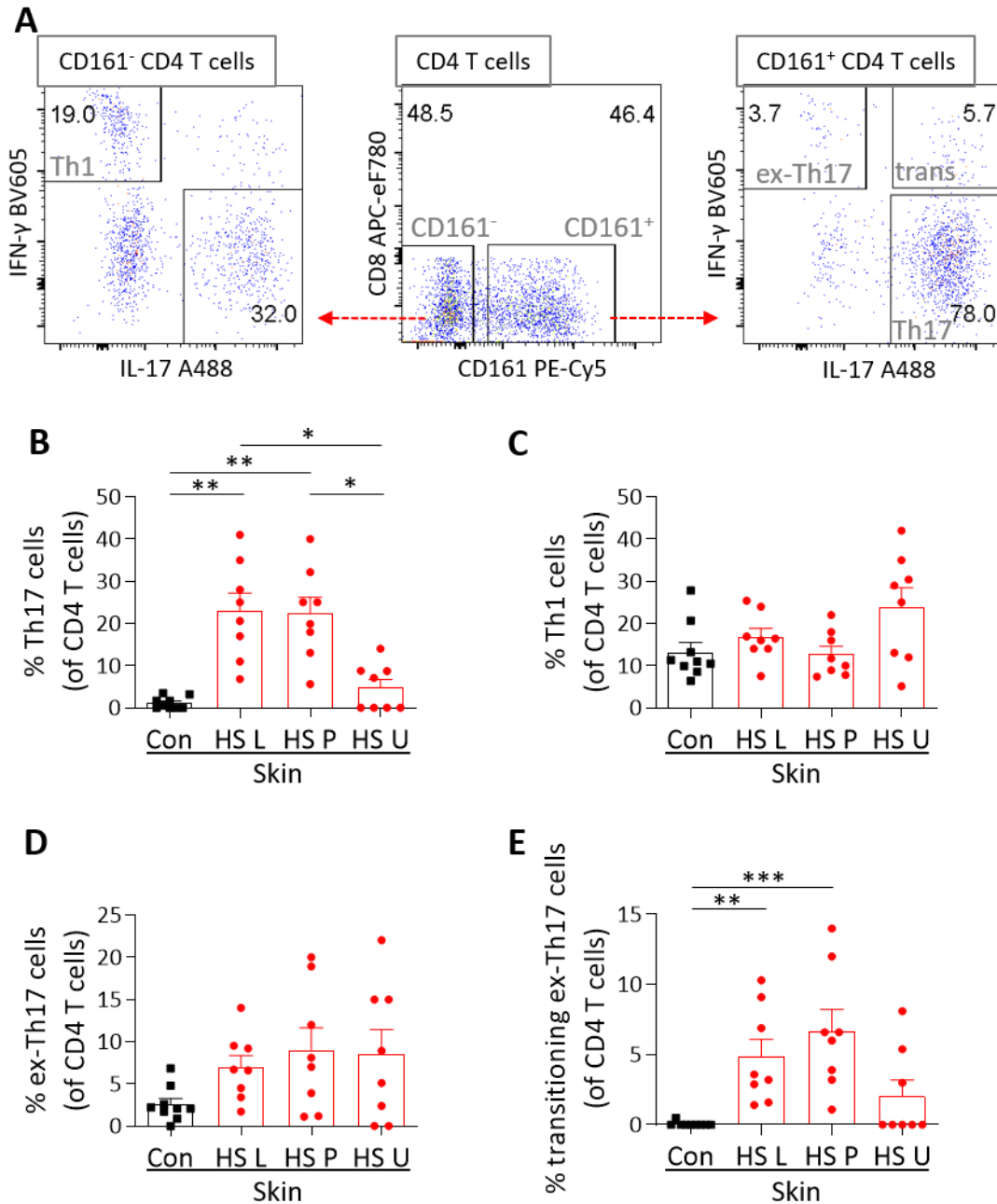


Figure 4.25 Frequency of T helper subsets in HS patient and healthy control skin.

Cells isolated from the skin of healthy controls (Con; n=9) or HS patients (HS L: lesional, P: perilesional, U: uninvolved skin; n=8) were treated with PMA/I and Brefeldin A for 16 h, stained for surface and intracellular markers, and analysed by flow cytometry. Representative dot plots display gating strategy to identify T helper subsets Th1 (CD4⁺CD161⁻IL-17⁺IFN- γ ⁺), Th17 (CD4⁺CD161⁺IL-17⁺IFN- γ ⁻), ex-Th17 (CD4⁺CD161⁺IL-17⁻IFN- γ ⁺) and transitioning ex-Th17 cells (CD4⁺CD161⁺IL-17⁺IFN- γ ⁺), from a PMA/I treated HS patient skin sample (A). Graphs show the frequency of Th17 cells (B), Th1 cells (C), ex-Th17 cells (D), and transitioning ex-Th17 cells (E). Graphs represent individual samples with mean \pm SEM for each group. Statistical significance was calculated using Kruskal-Wallis one-way ANOVA with Dunn's multiple comparisons test; *p<0.05, **p<0.01, ***p<0.001.

4.4.6 HS patient lesional skin exhibited a significant increase in Treg cells

To further investigate the role of T cells in HS skin, analysis was performed to identify and analyse Treg cells and their function. Given the very low number of T cells present after dissociating HS perilesional or uninvolved skin, Treg cell staining was only performed on HS lesional skin. As per PBMC, dissociated cells from skin biopsies were rested for 16 h, then surface stained for CD45, CD3, CD4, CD8, CD127, CD25, fixed and permeabilised, then intra-nuclear staining to identify FoxP3 and CTLA-4. Samples were acquired by flow cytometry within 24 h.

Treg cells in the skin were identified in the same manner as PBMC; sequentially gating viable leukocytes (CD45⁺live/dead⁻; Figure 4.26A), then lymphocytes (FSC-A v SSC-A; Figure 4.26B), single cells (FSC-A v FSC-W; Figure 4.26C), T cells (CD3⁺TCR- $\gamma\delta$ ⁻; Figure 4.26D), CD4⁺ T cells (CD4⁺CD8⁻; Figure 4.26E), and finally Treg cells (FoxP3⁺CD127^{lo}; Figure 4.26F). As was the case for PBMC (Figure 4.10), the vast majority of FoxP3⁺CD127^{lo} were also CD25⁺.

Treg cells constituted approximately 5% of CD4 T cells in healthy control skin, but in a shift contrary to that in PBMC, there was a two-fold increase in Treg cell frequency in HS lesional skin ($p < 0.01$; Figure 4.27A). Despite the increase in Treg cells in HS lesional skin, the ratio between Th17 cells and Treg cells was still markedly skewed towards Th17 cells in HS lesional skin, from a mean of 0.3 in healthy controls to 3 in HS lesional skin ($p < 0.001$; Figure 4.27B).

The skin-homing molecule CLA was expressed on approximately 50% of Treg cells in the skin (Figure 4.28A), but there was no difference observed between healthy control skin and HS lesional skin (Figure 4.28B). The Th17 cell associated marker CD161 was expressed on a proportion of Treg cells (Figure 4.28C), with a marked increase in HS lesional skin when compared with healthy control skin ($p < 0.001$; Figure 4.28D).

CD39, linked with suppression of Th17 cells, was expressed on a large proportion of Treg cells (Figure 4.29A), and although a trend to increased frequency of CD39 expression on Treg cells in HS lesional skin was noted, it was not significant (Figure 4.29B). Similarly,

CTLA-4 expression, implicated in autoimmunity, was observed in almost all Treg cells in HS lesional skin (Figure 4.29C), but the increase compared with healthy control skin was not significant (Figure 4.29D).

In summary, the data show that HS lesions have an enrichment of Treg cells, but these were still significantly outnumbered by Th17 lineage cells. Although there was no difference in expression of CLA, CD39 or CTLA-4, the frequency of CD161 was increased on Treg cells between HS lesional skin and healthy control skin.

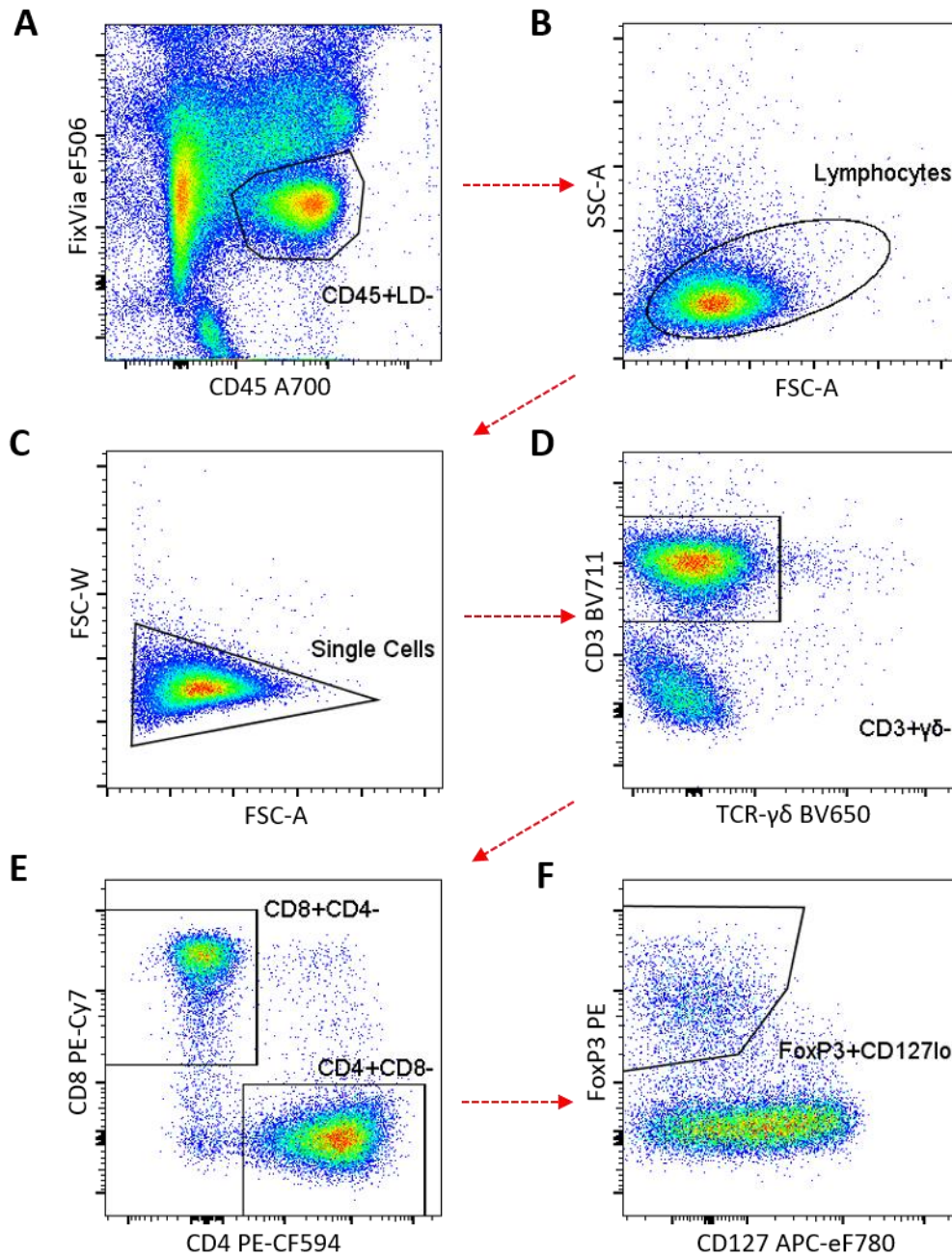


Figure 4.26 Plots representing the gating strategy to identify Treg cells in skin samples.

Cells isolated from the skin were rested for 16 h, stained for surface and intracellular markers, and analysed by flow cytometry. To identify CD4, CD8 and Treg cells, sequential gating was performed: CD45⁺, Fixable-Viability-Dye- to identify viable leukocytes (A); Forward v Side Scatter to exclude debris and non-lymphocytes (B); FSC-Area v FSC-Width to exclude doublets (C); CD3⁺TCR- $\gamma\delta$ ⁻ to identify CD3 T cells (D); CD4 v CD8 to identify CD4 and CD8 T cells (E); and FoxP3⁺CD127^{lo} to identify (CD4⁺) Treg cells (F).

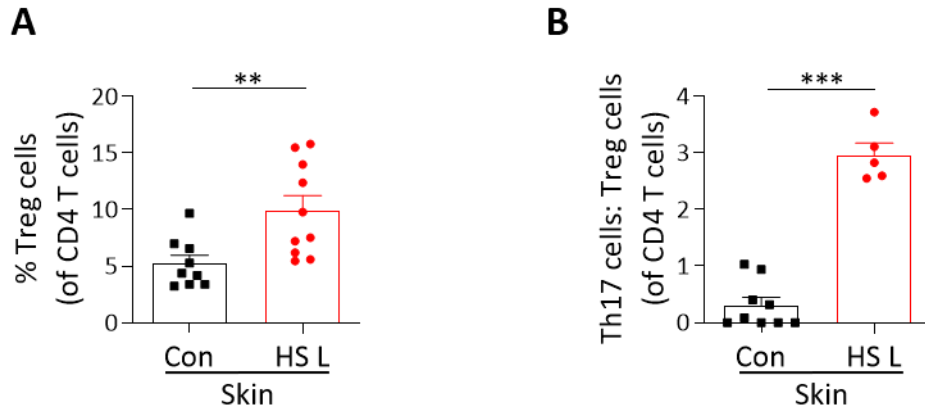


Figure 4.27 Increased frequency of Treg cells, and an unbalanced ratio of Th17 cells to Treg cells, in HS patient lesional skin compared with healthy control skin.

Cells isolated from the skin of healthy controls (Con; n=9) or HS patients (HS L: lesional n=10 (A); n=5 (B)) were rested (Treg cells) or treated with PMA/I and Brefeldin A (Th17 cells) for 16 h, stained for surface and intracellular markers, and analysed by flow cytometry. Graphs show the frequency of Treg cells (A) and the ratio of Th17 cells to Treg cells (B). Graphs represent individual samples with mean \pm SEM for each group. Statistical significance was calculated using Mann-Whitney U test; **p<0.01, ***p<0.001.

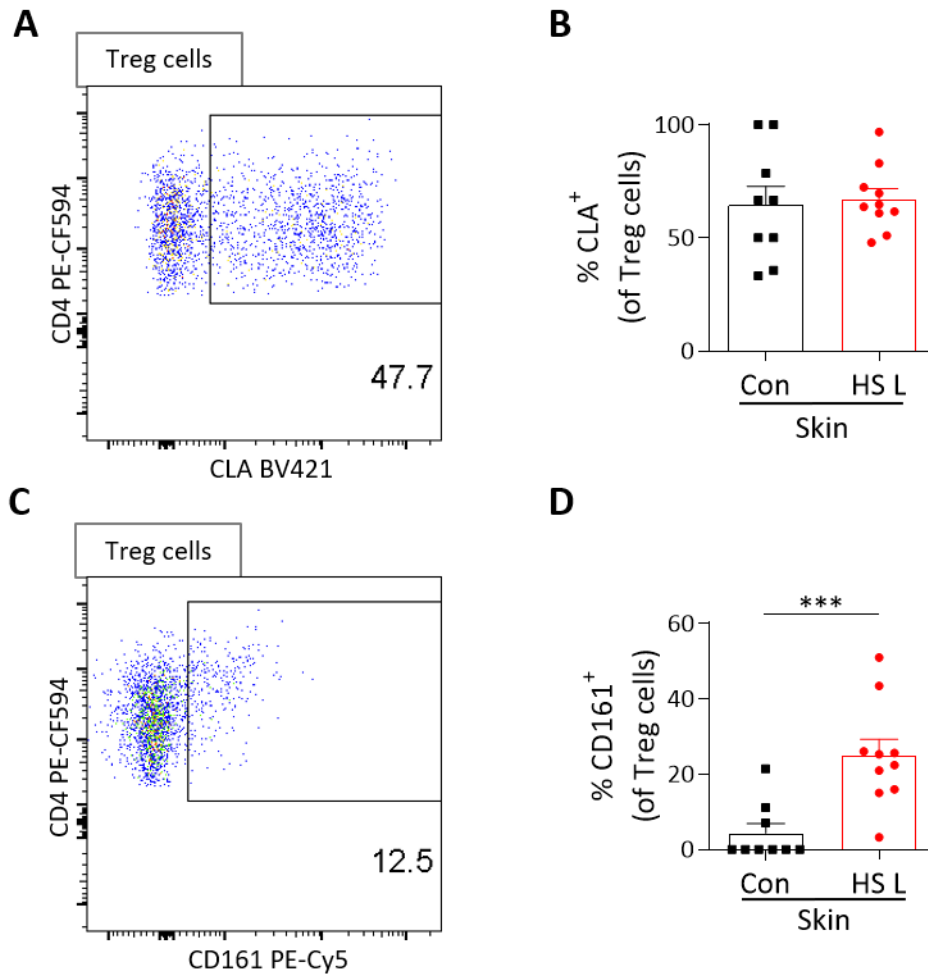


Figure 4.28 Frequency of CLA expression unchanged, but significant increase in CD161 expression, in Treg cells in HS patient lesional skin compared with healthy control skin.

Cells isolated from the skin of healthy controls (Con; n=9) or HS patients (HS L: lesional skin; n=10) were rested for 16 h, stained for surface and intracellular markers, and analysed by flow cytometry. Representative dot plots, gated on Treg cells, display CLA (A) and CD161 (C) expression, plotted against CD4, from a rested HS patient skin sample. Graphs show the frequency of CLA (B) and CD161 (D) expression on Treg cells. Graphs represent individual samples with mean \pm SEM for each group. Statistical significance was calculated using Mann-Whitney U test; *** $p < 0.001$.

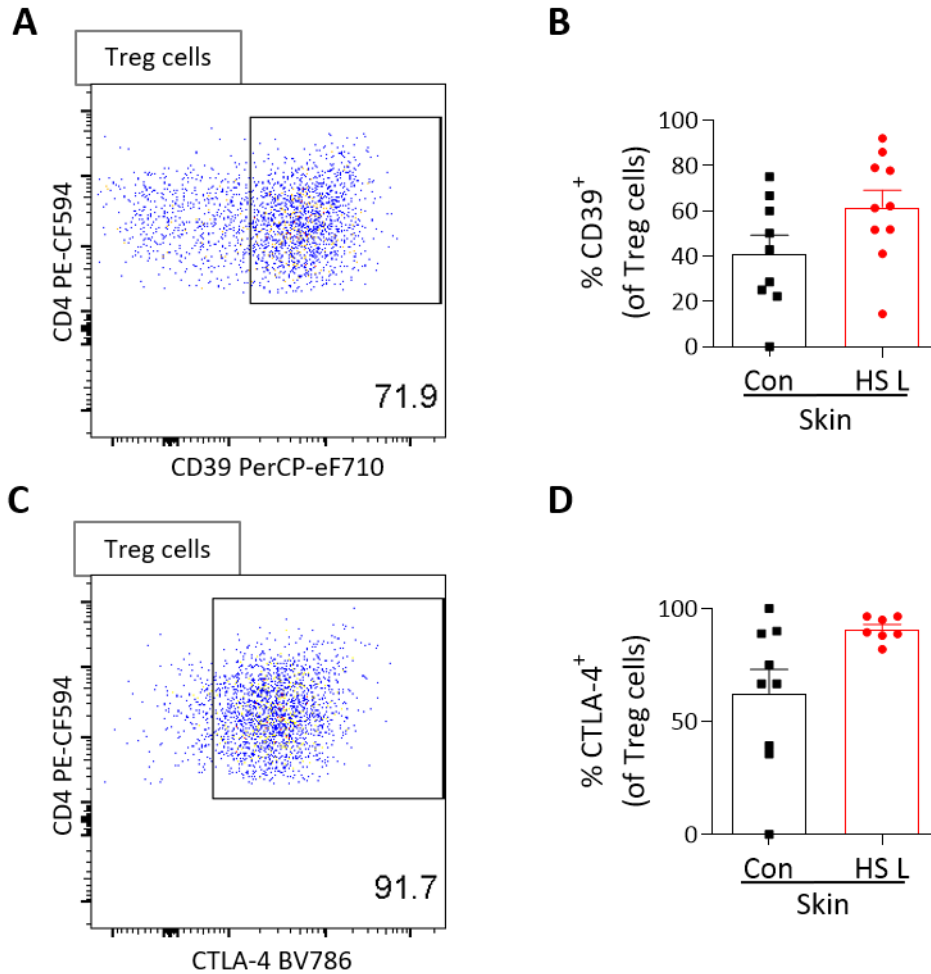


Figure 4.29 Frequencies of CD39 and CTLA-4 expression unchanged in Treg cells in HS patient lesional skin compared with healthy control skin.

Cells isolated from the skin of healthy controls (Con; n=9) or HS patients (HS L: lesional skin; n=10 (B); n=7 (D)) were rested for 16 h, stained for surface and intracellular markers, and analysed by flow cytometry. Representative dot plots, gated on Treg cells, display CD39 (A) and CTLA-4 (C) expression, plotted against CD4, from a rested HS patient skin sample. Graphs show the frequency of CD39 (B) and CTLA-4 (D) expression on Treg cells. Graphs represent individual samples with mean \pm SEM for each group. Statistical significance was calculated using Mann-Whitney U test.

4.4.7 Frequency of T cells in the skin remained unchanged in HS patients treated with anti-TNF therapy.

Having demonstrated an increase in Th17 cells and associated cytokines in HS skin, along with a skewed ratio of Th17 cells to Treg cells, it was pertinent to next address whether therapeutic interventions corrected this phenomenon. Anti-TNF therapy (α -TNF; e.g. adalimumab [Humira™] and infliximab [Remicade™]) has been a recognised treatment for moderate to severe HS as far back as 2009 (Blanco et al., 2009), but its effects on T cell cytokines have yet to be investigated. Hence, the T cell profile in the skin of HS patients undergoing α -TNF treatment was examined and compared with unmatched treatment naïve HS patients.

Clinical details for the group of patients undergoing α -TNF therapy (α -TNF+ HS patients) are shown in Table 4.3. This cohort appears to be well matched to the anti-TNF treatment naïve (α -TNF-) HS patient group 2 (Table 4.1). For example, the α -TNF- HS patient group 2 had a mean age of 34.5 y, 91% female, and mean BMI of 31.1, compared with a mean age of 33.5 y, 83% female, and mean BMI of 30.0 in this α -TNF+ set.

Although all α -TNF+ HS patients in this trial showed marked clinical improvement some lesions nevertheless persisted, albeit much less abundant or severe. Hence, as per treatment naïve HS patients, α -TNF+ HS patients donated 6 mm punch biopsies from lesional, perilesional and uninvolved skin. Tissue dissociation, analysis and gating was as previously described (Figure 4.14).

When compared with skin biopsies from α -TNF- HS patients, α -TNF+ HS patient skin showed little difference in the number of immune (CD45⁺) cells (Figure 4.30A) or T cells (Figure 4.30B) calculated per mm skin, with HS lesional, perilesional and uninvolved displaying no significant difference in frequency between treatment groups. Likewise, the frequency of CD8 (Figure 4.31A) and CD4 (Figure 4.31B) T cells as a percentage of total T cells showed no difference in HS lesional, perilesional and uninvolved skin between α -TNF- and α -TNF+ HS patients. In addition, there was no significant difference in the expression of the skin homing surface marker CLA on both CD8 (Figure 4.32A) and

CD4 (Figure 4.32B) T cells in the skin of α -TNF- HS patients compared with α -TNF+ HS patients.

These results suggest that anti-TNF therapy has no effect on the frequency of T cell subsets or overall T cell numbers in the skin of HS patients.

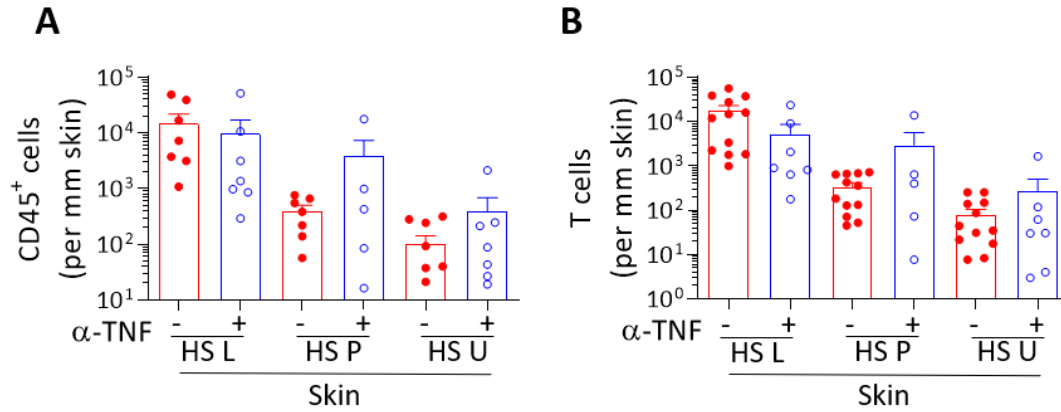


Figure 4.30 Similar number of CD45⁺ cells and CD3 T cells in the skin of treatment naïve HS patients compared with those treated with anti-TNF.

Cells isolated from the skin of treatment naïve (α -TNF⁻; n=7 (A); n=12 (B)) or anti-TNF treated (α -TNF⁺; n=7 (HS-L, HS-U); n=5 (HS-P)) HS patients (HS L: lesional, P: perilesional, U: uninvolved skin) were treated with PMA/I and Brefeldin A for 16 h, stained for surface and intracellular markers, and analysed by flow cytometry. Graphs show the absolute numbers for CD45⁺ leukocytes (A) or CD3⁺ T cells (B) per mm of skin. Graphs represent individual samples with mean \pm SEM for each group. Statistical significance was calculated using Kruskal-Wallis one-way ANOVA with Dunn's multiple comparisons test.

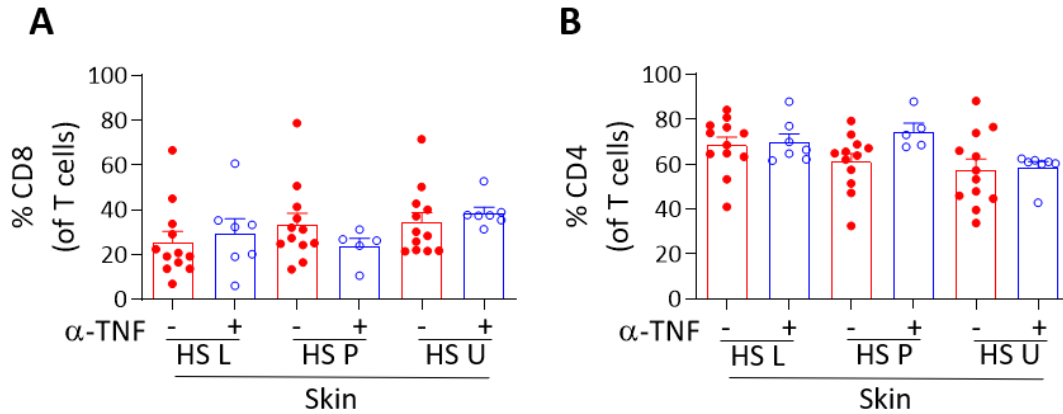


Figure 4.31 Similar frequency of CD8 and CD4 T cells in the skin of treatment naïve HS patients compared with those treated with anti-TNF.

Cells isolated from the skin of treatment naïve (α -TNF $^-$; $n=12$) or anti-TNF treated (α -TNF $^+$; $n=7$) (HS-L, HS-U); $n=5$ (HS-P)) HS patients (HS L: lesional, P: perilesional, U: uninvolved skin) were treated with PMA/I and Brefeldin A for 16 h, stained for surface and intracellular markers, and analysed by flow cytometry. Graphs show the frequency of CD8 (A) and CD4 (B) T cells within the total T cell population ($CD3^+TCR-\gamma\delta^-$ lymphocytes). Graphs represent individual samples with mean \pm SEM for each group. Statistical significance was calculated using Kruskal-Wallis one-way ANOVA with Dunn's multiple comparisons test.

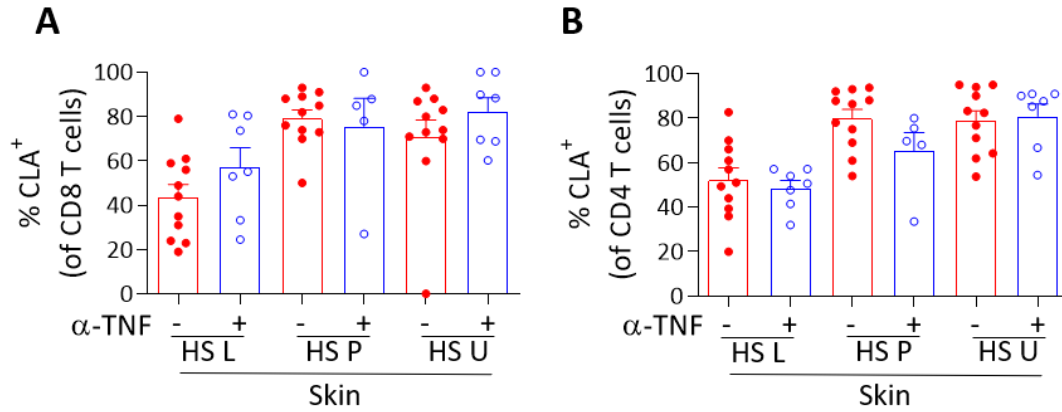


Figure 4.32 Similar frequency of CLA expression on CD8 and CD4 T cells in the skin of treatment naïve HS patients compared with those treated with anti-TNF.

Cells isolated from the skin of treatment naïve (α -TNF-; n=12) or anti-TNF treated (α -TNF+; n=7 (HS-L, HS-U); n=5 (HS-P)) HS patients (HS L: lesional, P: perilesional, U: uninvolved skin) were treated with PMA/I and Brefeldin A for 16 h, stained for surface and intracellular markers, and analysed by flow cytometry. Graphs show the frequency of CLA expressing CD8 (A) and CD4 (B) T cells. Graphs represent individual samples with mean \pm SEM for each group. Statistical significance was calculated using Kruskal-Wallis one-way ANOVA with Dunn's multiple comparisons test. Significance is shown only between +/- α -TNF treatment samples.

4.4.8 The proinflammatory profile of T cells in the skin was reduced in HS patients undergoing anti-TNF therapy

Despite no significant difference in T cell frequency or absolute numbers in α -TNF+ HS patients, there may be changes in the inflammatory markers and cytokine profile, therefore this was explored next.

IL-17 expression in CD8 T cells was unchanged in HS skin between α -TNF- and α -TNF+ HS patients (Figure 4.33A). IL-22 trended to reduced expression in CD8 T cells in the lesional (ns) and perilesional (ns) skin of α -TNF+ HS patients, with no apparent change in HS uninvolved skin (Figure 4.33B). The decreased mean frequency of TNF expression in CD8 T cells observed in HS lesional, perilesional and uninvolved skin of α -TNF+ HS patients was not statistically significant (Figure 4.33C). GM-CSF production in CD8 T cells went from a mean level of 50% in α -TNF- HS patient lesional, perilesional and uninvolved skin to approximately 10% in α -TNF+ HS patients; this reduction being significant in uninvolved skin only ($p < 0.05$; Figure 4.33D). The frequency of CD8 T cells producing IFN- γ was observed to be decreased in α -TNF+ HS patient skin, significantly so only in lesional skin ($p < 0.01$; Figure 4.33E). No significant reduction in IL-2 expression in CD8 T cells was observed in α -TNF+ compared with α -TNF- HS patient skin (Figure 4.33F).

CD4 T cells exhibited reduced IL-17 production in α -TNF+ HS patient lesional ($p < 0.05$) and perilesional (ns) skin compared with α -TNF- HS patient skin, with no difference in uninvolved skin (Figure 4.34A). In α -TNF+ HS patient skin CD4 T cells there was a trend (ns) towards decreased production of IL-22 (Figure 4.34B), TNF $^+$ (Figure 4.34C) and GM-CSF $^+$ (Figure 4.34D), relative to α -TNF- patient skin. The decreased IFN- γ production in CD4 T cells in α -TNF+ HS patient was only significant in HS uninvolved skin ($p < 0.01$; Figure 4.34E). Similarly, the frequency of CD4 T cells expressing IL-2 was decreased in α -TNF+ HS patient lesional (ns), perilesional ($p < 0.05$) and uninvolved (ns) skin (Figure 4.34F).

Expression of the Th17 associated lineage-marker CD161 appeared reduced on CD8 T cells in lesional, perilesional, and uninvolved skin in α -TNF+ compared with α -TNF- HS patients, although the reduction was not significant in any instance (Figure 4.35A). The

decline in CD161 expression on CD4 T cells in α -TNF+ HS patient lesional and perilesional was not significant, with no change observed in uninvolved skin (Figure 4.35B).

Within the CD4 T cell population, Th17 cells were reduced in the lesional ($p < 0.05$) and perilesional (ns) skin of α -TNF+ compared with α -TNF- HS patients, with no apparent change in uninvolved skin (Figure 4.36A). The frequency of Th1 cells showed no apparent difference in lesional and perilesional skin, but was significantly reduced in the uninvolved skin of α -TNF+ HS patients ($p < 0.05$; Figure 4.36B). The apparent reduction in ex-Th17 cells in lesional, perilesional and uninvolved skin of α -TNF+ compared with α -TNF- HS patients was not significant (Figure 4.36C). Finally, the mean level of transitioning ex-Th17 cells was less in α -TNF+ HS patients' lesional and perilesional skin, but not significantly so, and was in fact slightly increased (ns) in uninvolved skin relative to α -TNF- HS patients (Figure 4.36D).

In summary, α -TNF therapy seems to drive a general reduction in the expression of proinflammatory markers in HS patient skin, with a significant reduction in pathogenic IL-17 expressing CD4 T cells and Th17 cells in HS lesional skin.

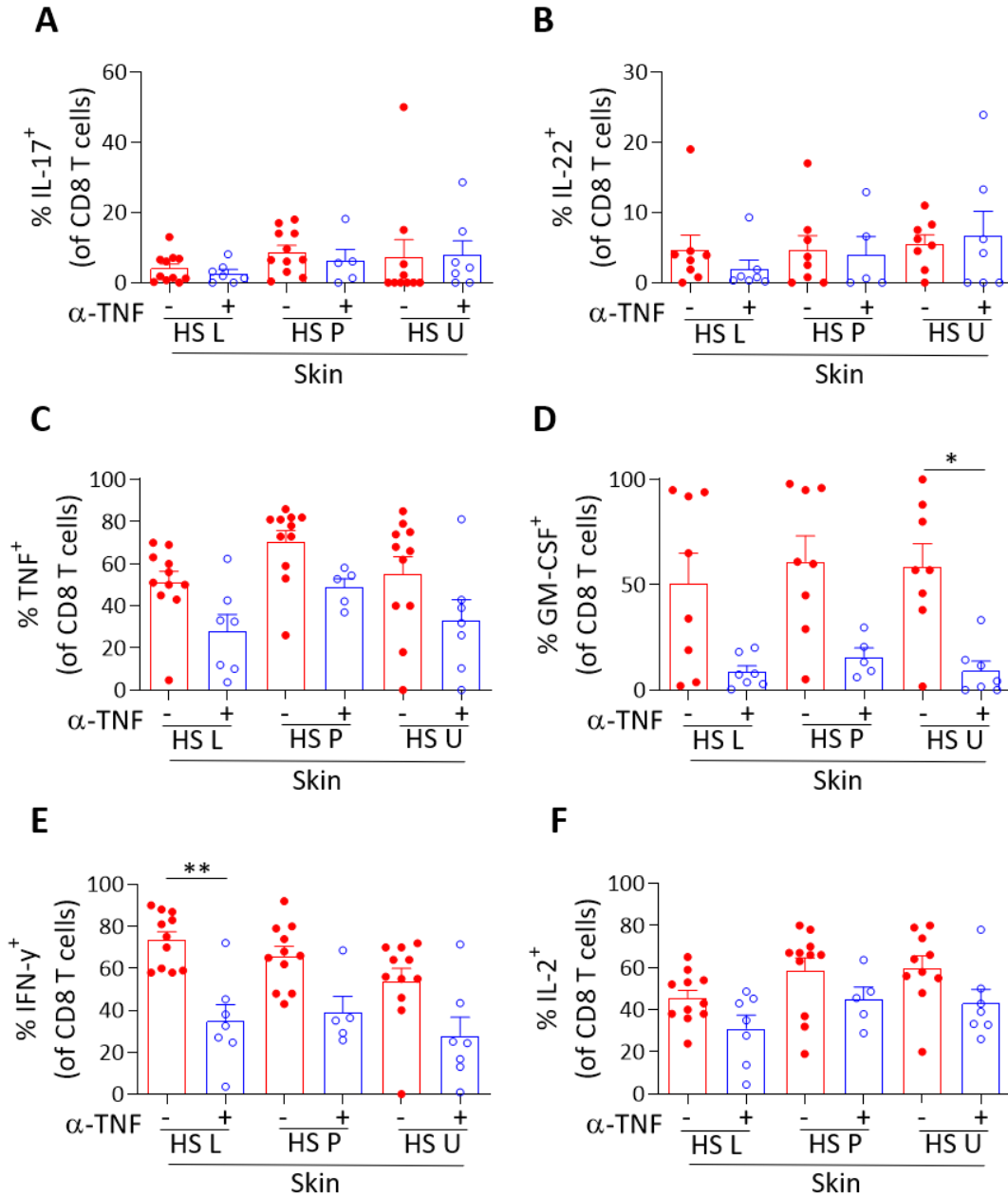


Figure 4.33 CD8 T cell cytokine expression in the skin of treatment naïve HS patients compared with those treated with anti-TNF.

Cells isolated from the skin of treatment naïve (α -TNF⁻; n=10 (A); n=8-(B&D); n=11 (C, E, F) or anti-TNF treated (α -TNF⁺; n=7 (HS-L, HS-U); n=5 (HS-P)) HS patients (HS L: lesional, P: perilesional, U: uninvolved skin) were treated with PMA/I and Brefeldin A for 16 h, stained for surface and intracellular markers, and analysed by flow cytometry. Graphs show the frequency of CD8 T cells expressing cytokines IL-17 (A), IL-22 (B), TNF (C), GM-CSF (D), IFN- γ (E), and IL-2 (F). Graphs represent individual samples with mean \pm SEM for each group. Statistical significance was calculated using Kruskal-Wallis one-way ANOVA with Dunn's multiple comparisons test. Significance is shown only between +/- α -TNF treatment samples; *p<0.05, **p<0.01.

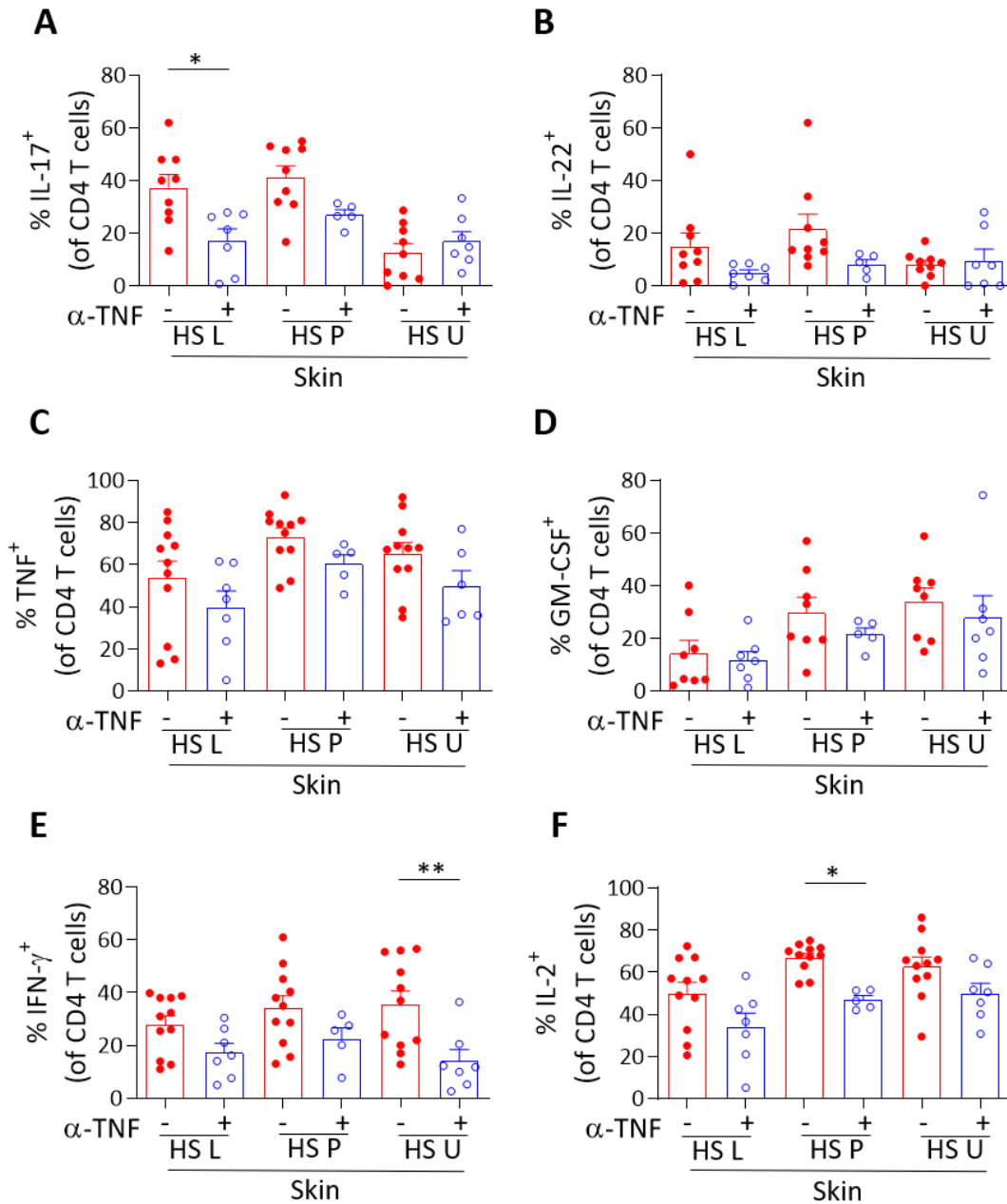


Figure 4.34 CD4 T cell cytokine expression in the skin of treatment naïve HS patients compared with those treated with anti-TNF.

Cells isolated from the skin of treatment naïve (α -TNF⁻; n=9 (A&B); n=11 (C, E, F); n=8 (B&D)) or anti-TNF treated (α -TNF⁺; n=7 (HS-L, HS-U); n=5 (HS-P)) HS patients (HS L: lesional, P: perilesional, U: uninvolved skin) were treated with PMA/I and Brefeldin A for 16 h, stained for surface and intracellular markers, and analysed by flow cytometry. Graphs show the frequency of CD4 T cells expressing cytokines IL-17 (A), IL-22 (B), TNF (C), GM-CSF (D), IFN- γ (E), and IL-2 (F). Graphs represent individual samples with mean \pm SEM for each group. Statistical significance was calculated using Kruskal-Wallis one-way ANOVA with Dunn's multiple comparisons test. Significance is shown only between +/- α -TNF treatment samples; * p <0.05, ** p <0.01.

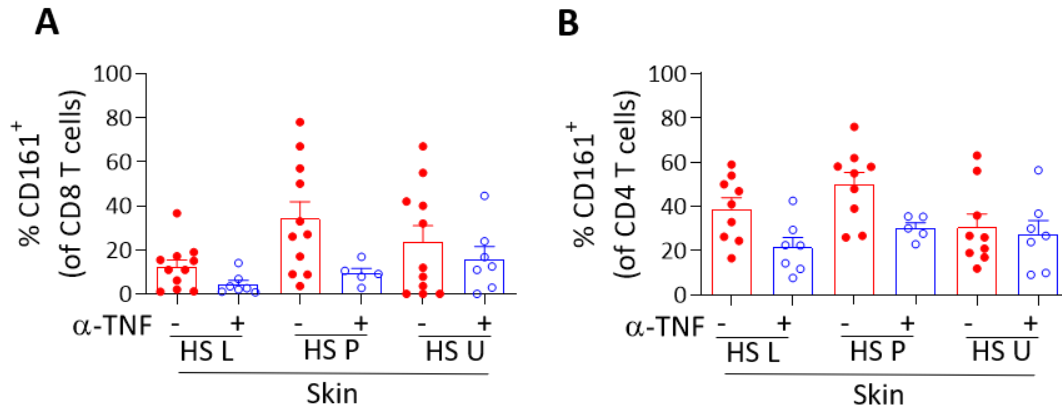


Figure 4.35 Frequency of CD161 expression on CD8 and CD4 T cells in the skin of treatment naïve HS patients compared with those treated with anti-TNF.

Cells isolated from the skin of treatment naïve (α -TNF $^-$; n=11 (A); n=8 (B)) or anti-TNF treated (α -TNF $^+$; n=7 (HS-L, HS-U); n=5 (HS-P)) HS patients (HS L: lesional, P: perilesional, U: uninvolved skin) were treated with PMA/I and Brefeldin A for 16 h, stained for surface and intracellular markers, and analysed by flow cytometry. Graphs show the frequency of CD161 expressing CD8 (A) and CD4 (B) T cells. Graphs represent individual samples with mean \pm SEM for each group. Statistical significance was calculated using Kruskal-Wallis one-way ANOVA with Dunn's multiple comparisons test. Significance is shown only between +/- α -TNF treatment samples; *p<0.05.

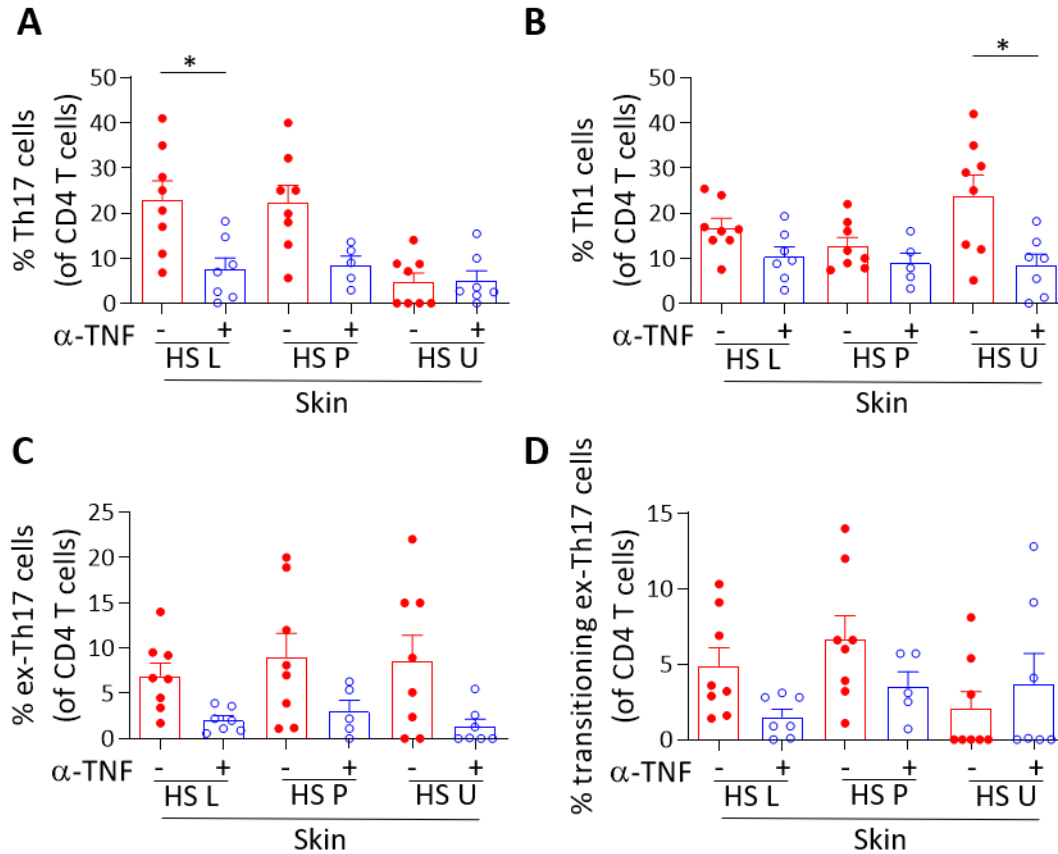


Figure 4.36 Frequency of Th subsets in the skin of treatment naïve HS patients compared with those treated with anti-TNF.

Cells isolated from the skin of treatment naïve (α -TNF $^-$; n=8) or anti-TNF treated (α -TNF $^+$; n=7 (HS-L, HS-U); n=5 (HS-P)) HS patients (HS L: lesional, P: perilesional, U: uninvolved skin) were treated with PMA/I and Brefeldin A for 16 h, stained for surface and intracellular markers, and analysed by flow cytometry. Graphs show the frequency of Th17 cells (CD4 $^+$ CD161 $^-$ IL-17 $^+$ IFN- γ $^-$; A), Th1 cells (CD4 $^+$ CD161 $^-$ IL-17 $^-$ IFN- γ $^+$; B), ex-Th17 cells (CD4 $^+$ CD161 $^+$ IL-17 $^-$ IFN- γ $^+$; C) and transitioning ex-Th17 cells (CD4 $^+$ CD161 $^+$ IL-17 $^+$ IFN- γ $^+$; D). Graphs represent individual samples with mean \pm SEM for each group. Statistical significance was calculated using Kruskal-Wallis one-way ANOVA with Dunn's multiple comparisons test. Significance is shown only between +/- α -TNF treatment samples; *p<0.05.

4.4.9 Similar frequency of Treg cells in the skin of HS patients undergoing anti-TNF therapy compared with treatment naïve patients

Having demonstrated an overall reduction in inflammatory cytokines in the skin of α -TNF+ HS patients, the frequency of Treg cells was examined next. As was the case for α -TNF- HS patient skin samples, Treg cell staining was only performed on lesional skin as cell counts were inevitably too low in perilesional and uninvolved skin samples.

No significant difference in the frequency of Treg cells between α -TNF+ and α -TNF- HS patient lesional skin was observed (Figure 4.37A). However, given the significant reduction in Th17 cells in α -TNF+ HS patient lesional skin (Figure 4.36A), the ratio of Th17 cells to Treg cells was significantly reduced in α -TNF+ HS patient lesional skin when compared with the α -TNF- group ($p < 0.01$; Figure 4.37B). With a mean ratio of < 1 , this level approached that of healthy control skin (ratio of 0.3; Figure 4.27B).

Within the Treg cell population, there was no significant difference in the frequency of cells expressing CLA (Figure 4.38A), CD161 (Figure 4.38B), or CD39 (Figure 4.38C) in α -TNF v α -TNF- HS lesional skin. However, the percentage of Treg cells expressing CTLA-4 in lesional skin was reduced from a mean of 90% in α -TNF- HS patients to 60% in α -TNF+ HS patients ($p < 0.01$; Figure 4.38D).

In summary, this section shows that although the frequency of Treg cells was similar in HS patients that were untreated or treated with anti-TNF, the ratio of Th17 cells to Treg cells was corrected upon α -TNF treatment in HS patients.

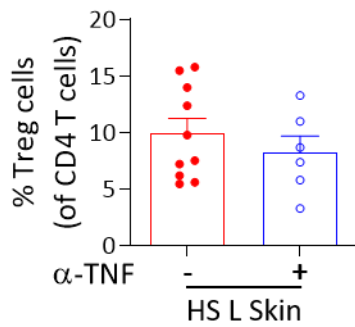
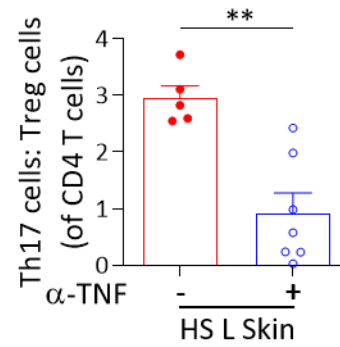
A**B**

Figure 4.37 Frequency of Treg cells, and ratio of Th17 cells to Treg cells, in the skin of treatment naïve HS patients, or those treated with anti-TNF.

Cells isolated from the lesional skin (HS L Skin) of unmatched treatment naïve (α -TNF-; n=10 (A); n=5 (B)) or anti-TNF treated (α -TNF+; n=6 (A); n=7 (B)) HS patients were rested (Treg cells) or treated with PMA/I and Brefeldin A (Th17 cells) for 16 h, stained for surface and intracellular markers, and analysed by flow cytometry. Graphs show the frequency of Treg cells (A) and the ratio of Th17 cells to Treg cells (B). Statistical significance was calculated using Mann-Whitney U test; **p<0.01.

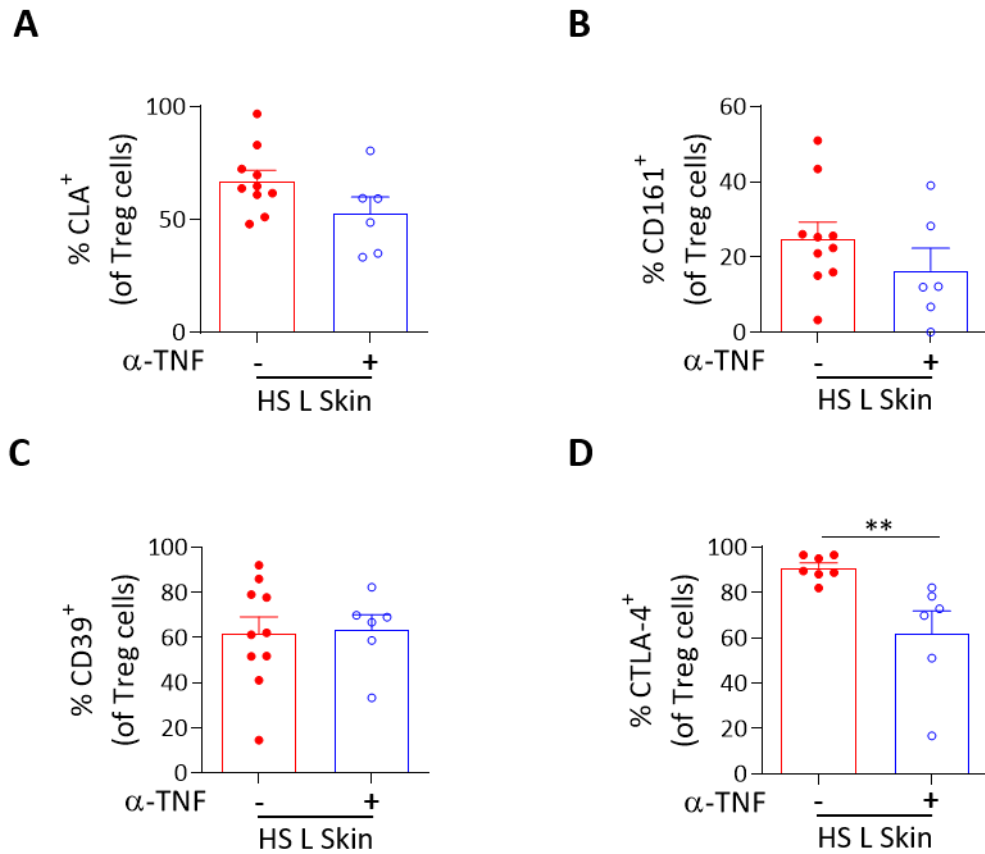


Figure 4.38 Frequency of CLA, CD161, CD39, and CTLA-4 expression on Treg cells in the skin of treatment naïve HS patients, or those treated with anti-TNF.

Cells isolated from the lesional skin (HS L Skin) of unmatched treatment naïve (α -TNF⁻; n=10 (A-C); n=7 (D)) or anti-TNF treated (α -TNF⁺; n=6) HS patients were rested for 16 h, stained for surface and intracellular markers, and analysed by flow cytometry. Graphs show the frequency of CLA (A), CD161 (B), CD39 (C) and CTLA-4 (D) expression on Treg cells. Plots represent individual samples with mean \pm SEM for each group. Statistical significance was calculated using Mann-Whitney U test; **p<0.01.

4.4.10 Reduction in T cell polyfunctionality in HS patients undergoing anti-TNF therapy

This study has shown that CD8 and CD4 T cells express proinflammatory cytokines in HS patient skin, and that this is reduced following anti-TNF therapy. However, it is important to determine whether the T cells express individual cytokines exclusively, or multiple cytokines together. Such so-called polyfunctional T cells have been shown to be more pathogenic in autoimmune conditions such as RA (Basdeo et al., 2015).

Hence T cell polyfunctionality was investigated next, in healthy control skin, treatment naïve HS patients and those undergoing anti-TNF therapy. T cells expressing multiple cytokines (IL-2, IFN- γ , IL-22, GM-CSF, TNF and IL-17) were presented graphically using SPICE software (Roederer et al., 2011); with multiple samples represented within one chart. The segments within SPICE pie charts denote populations producing increasing numbers of cytokines and is heat-map coded; from the segment in black being the proportion producing zero cytokines, to a deep red segment producing all six cytokines. The outer arcs are colour-coded and represent the specific cytokine(s) being expressed by cells within that segment.

At a glance, CD8 T cells in α -TNF+ HS patient skin (right column) appeared to be less polyfunctional than α -TNF- HS patient skin (left column; Figure 4.39). Only one-third approximately of the overall proportion of CD8 T cells in α -TNF+ HS patient lesional skin expressed 2 or more cytokines, compared with two-thirds in α -TNF- HS lesional skin, with a significant increase in the proportion of CD8 T cells producing no cytokine ($p < 0.01$), and a decrease in simultaneous production of two cytokines ($p < 0.01$), in α -TNF+ compared with α -TNF- HS lesional skin (Figure 4.39A).

The trend was even more apparent in HS perilesional skin, with proportionally more polyfunctional CD8 T cells than in lesional skin for both α -TNF- and α -TNF+ HS patient skin. Here also α -TNF- perilesional CD8 T cells appeared more polyfunctional than in α -TNF+ HS patients, with a significant increase in the proportion of CD8 T cells producing no cytokines in α -TNF+ HS patients ($p < 0.01$; Figure 4.39B).

Similarly, CD8 T cells in α -TNF+ HS uninvolved skin displayed reduced polyfunctionality relative to α -TNF- HS uninvolved skin, with a significantly less proportion of CD8 T cells producing two cytokines ($p < 0.01$; Figure 4.39C). CD8 T cells in healthy control skin showed minimal polyfunctionality, with the vast majority expressing two cytokines or less (primarily cytokines IL-2, TNF or IFN- γ), and over one-half expressing no cytokines (Figure 4.39D).

Overall, CD4 T cells appeared more polyfunctional than CD8 T cells (Figure 4.40). Almost half of the CD4 T cell population in α -TNF- HS patient lesional skin produced three or more cytokines, compared with one-third in α -TNF+ HS patients; with the proportion expressing four cytokines being significantly reduced in α -TNF+ HS patients (Figure 4.40A).

Perilesional CD4 T cells seemed more polyfunctional than their lesional counterparts, and α -TNF+ HS patient perilesional skin had a lesser share of polyfunctional CD4 T cells than α -TNF- HS patients (Figure 4.40B). Indeed, the proportion producing no cytokine was significantly increased in α -TNF+ HS patient perilesional skin ($p < 0.05$).

The uninvolved skin of α -TNF+ HS patients also had less polyfunctional CD4 T cells than that of α -TNF- HS patients, significantly reduced in the proportion expressing four cytokines ($p < 0.05$; Figure 4.40C). As was the case with CD8 T cells, almost one-half of CD4 T cells in healthy control skin produced no cytokine, and most of the remainder expressing only one to two cytokines (Figure 4.40D).

To summarise, polyfunctional CD8 and CD4 T cells were reduced in the skin of HS patients undergoing anti-TNF therapy, with HS perilesional and uninvolved T cells appearing proportionately more polyfunctional than those in lesional skin.

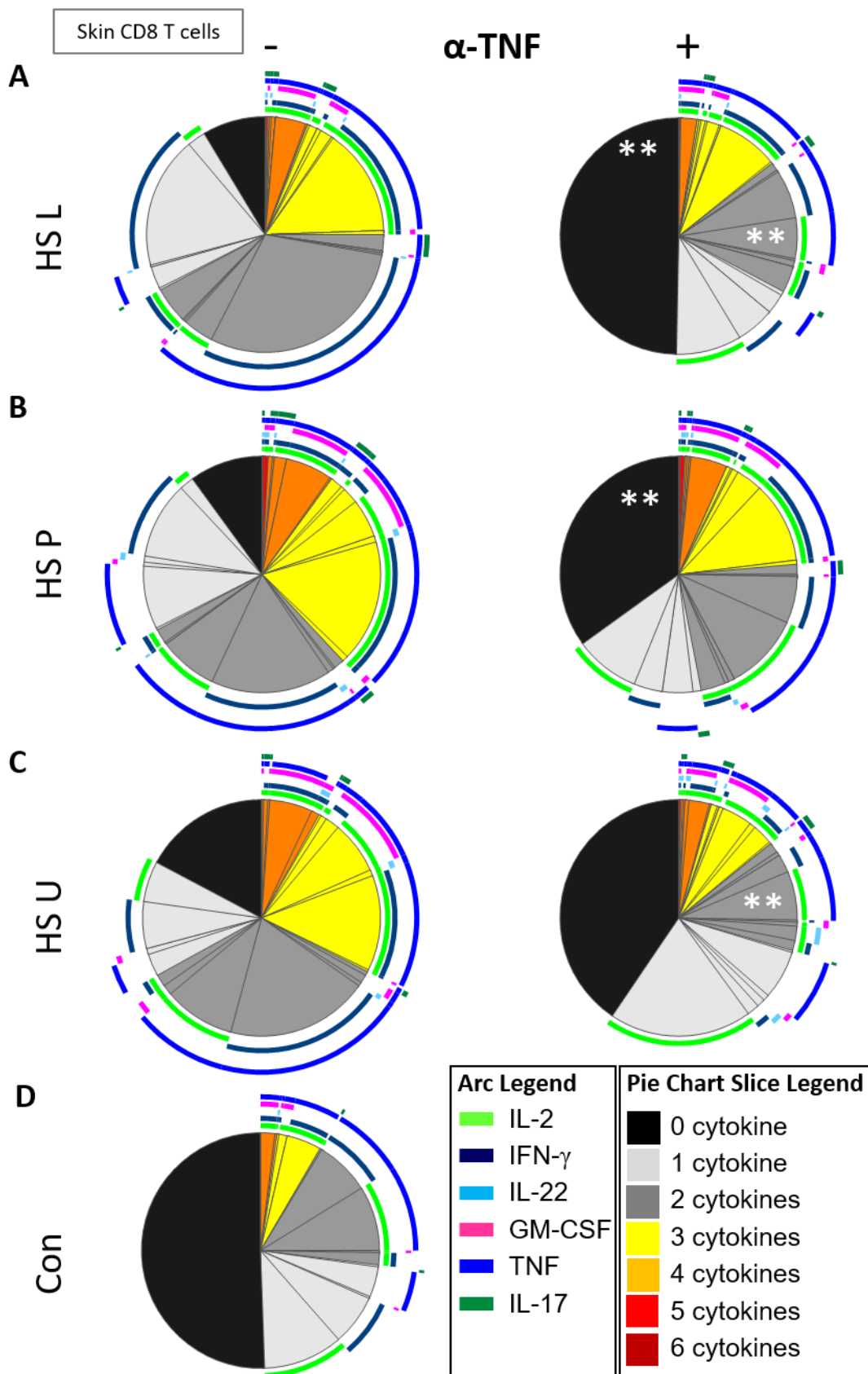


Figure 4.39 Increased cytokine polyfunctionality of CD8 T cells in the skin of treatment naïve HS patients compared with those treated with anti-TNF.

Cells were isolated from the skin of healthy controls (n=9), treatment naïve (α -TNF⁻; n=7) or anti-TNF treated (α -TNF⁺; n=6) HS patients, treated with PMA/I and Brefeldin A for 16 h, stained for surface and intracellular markers, and analysed by flow cytometry. Cytokine expression of CD8 T cells was analysed using SPICE software; with pie charts representing the average frequencies for HS lesional (HS L; A), perilesional (HS P; B), uninvolved (HS U; C) and healthy control (Con; D) skin. α -TNF⁻ are on the left column, α -TNF⁺ on the right. Charts represent CD8 T cells producing every combination of six cytokines (IL-2, IFN- γ , IL-22, GM-CSF, TNF & IL-17). The segments within the pie chart are heat-map coded to indicate increasing number of cytokines produced. The size of the pie segment correlates to the frequency of the population, and the arcs indicate the cytokine produced by that proportion. Statistical significance for number of cytokines being expressed was calculated for +/- anti-TNF treatment using Mann-Whitney U test; **p<0.01.

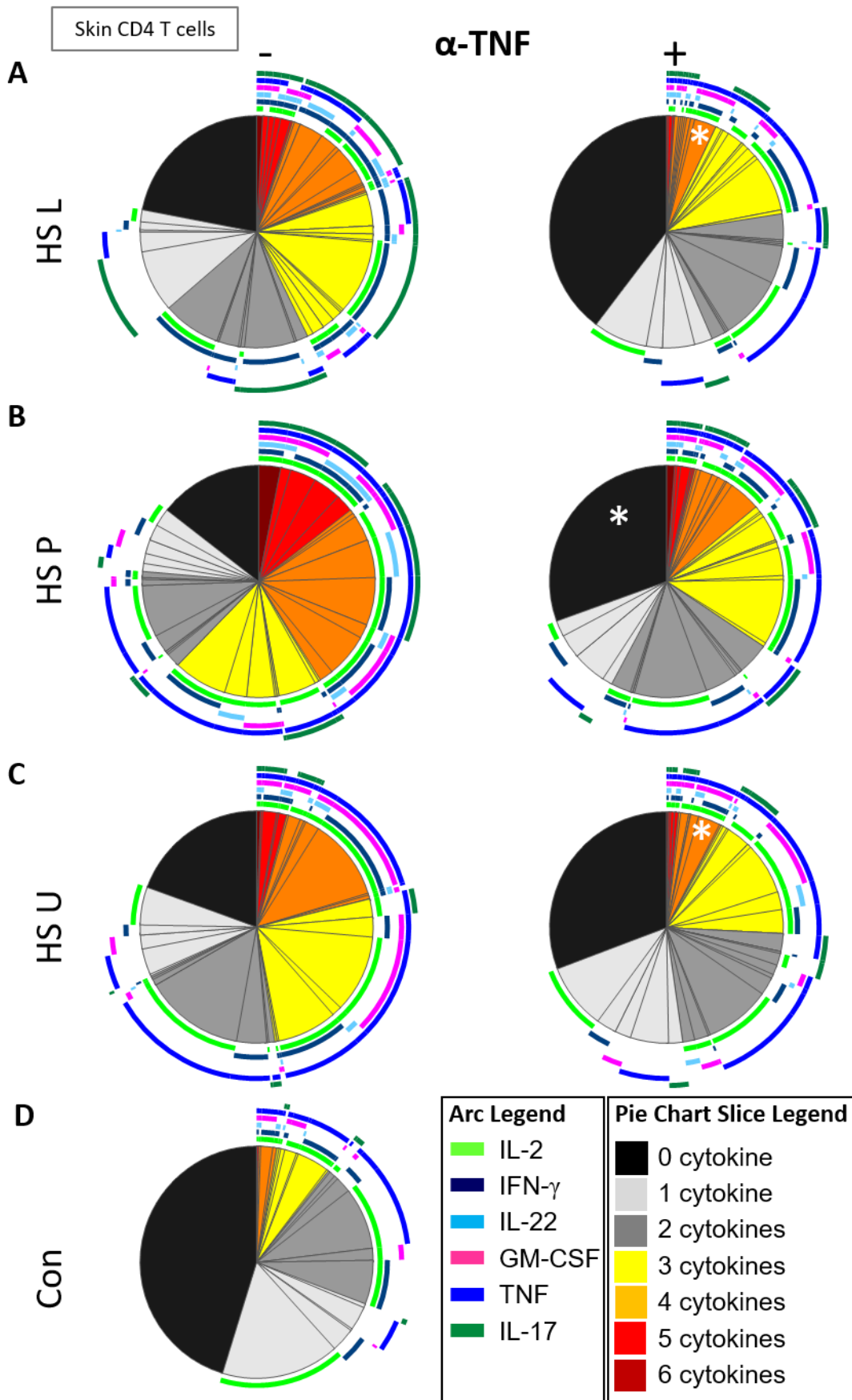


Figure 4.40 Increased cytokine polyfunctionality of CD4 T cells in the skin of treatment naïve HS patients compared with those treated with anti-TNF.

Cells were isolated from the skin of healthy controls (n=9), treatment naïve (α -TNF⁻; n=7) or anti-TNF treated (α -TNF⁺; n=6) HS patients, treated with PMA/I and Brefeldin A for 16 h, stained for surface and intracellular markers, and analysed by flow cytometry. Cytokine expression of CD4 T cells was analysed using SPICE software; with pie charts representing the average frequencies for HS lesional (HS L; A), perilesional (HS P; B), uninvolved (HS U; C) and healthy control (Con; D) skin. α -TNF⁻ are on the left column, α -TNF⁺ on the right. Charts represent CD4 T cells producing every combination of six cytokines (IL-2, IFN- γ , IL-22, GM-CSF, TNF & IL-17). The segments within the pie chart are heat-map coded to indicate increasing number of cytokines produced. The size of the pie segment correlates to the frequency of the population, and the arcs indicate the cytokine produced by that proportion. Statistical significance for number of cytokines being expressed was calculated for +/- anti-TNF treatment using Mann-Whitney U test; *p<0.05.

4.5 Discussion

The study described within this chapter sought to elucidate the role of T cells in HS, from peripheral blood to lesional and clinically normal skin. It made use of complex multicolour flow cytometry panels to maximise the amount of information gleaned from the limited number of cells available. It has uncovered differences in both the proinflammatory and suppressive arm of T cells in PBMC between HS patients and healthy controls, which may be instructive in terms of diagnosis and prognosis. Further, it has revealed a substantial increase in T cells in the lesional skin of HS patients and shown convincingly that many of these cells are polyfunctional and associated with a Th17 cell profile, known to be particularly pathogenic in autoimmunity. In fact, many of the T cells in apparently normal perilesional and uninvolved HS skin have a similar polyfunctional profile to those from lesional skin, although numerically equivalent to healthy control skin. Moreover, the findings show for the first time that this proinflammatory output in T cells in HS skin is corrected through anti-TNF therapy. Although the higher levels of T cells observed in HS lesional skin coincided with an increase in the frequency of Treg cells in the HS lesion; there was nonetheless an imbalance in the ratio between the Th17 cells and Treg cells. The PBMC of HS patients showed a decrease in Treg cell frequency, but with a similar skewed ratio of Th17 to Treg cells to that in HS lesional skin. This imbalance in the Th17: Treg cell axis for PBMC and lesional skin in HS patients was resolved through anti-TNF intervention (Moran et al., 2017).

The enrichment of Th17 cells in HS lesions reported here is highly significant, since it far exceeds that observed at inflamed sites of other diseases where Th17 cells are known to play an important role in pathogenesis, and where IL-17 has been targeted therapeutically. For example in psoriasis, IL-17⁺ CD4 T cells have been reported to be enriched to approximately twice the frequency observed in atopic dermatitis (8 v 4% approx.) (Nogales et al., 2009) and twice the normal frequency in the gut of CD patients (Annunziato et al., 2007). The results in this chapter have demonstrated that the frequency of IL-17⁺ CD4 T cells in the lesions of some HS patients were at least 40-fold increased (~40%) compared with normal skin and peripheral blood (~1%). The observed increase in IL-17⁺ CD4 T cells in HS lesional and perilesional skin is in agreement with

recent findings by Hotz et al, although that study showed much less IL-17 expression, and no increase in IL-22 expression (Hotz et al., 2016). This may be in part due to different stimulation conditions in the Hotz study, with a shorter stimulation (5 h) and twice the concentration of PMA, ionomycin, and Brefeldin A as was used in this study. A more likely reason however may be that cells in our study were treated in cIMDM, which has a more suitable Ca^{++} concentration for maximising cytokine output than the more routinely used cRPMI (Figure 2.1) (Zimmermann et al., 2015).

The findings from this study also indicated that the majority of IL-17 was produced by CD4 T cells, and then to a much lesser degree CD8 T cells (5-10% IL-17 expression for CD8 T cells in HS skin). $\gamma\delta$ T cells are rare in healthy human skin. Although IL-17⁺ $\gamma\delta$ T cells have been reported as associated with elements of skin disease, there are very few human studies, and none regarding HS (Section 1.5.5). In any case, conditions in this study did not suit investigating whether there was any IL-17 production by $\gamma\delta$ T cells; in this project cells were treated with PMA/I for 16 hours whereas a much shorter time (3-6 h) would be appropriate for $\gamma\delta$ T cells. Further, the pan-marker used (clone B1) yielded very poor positive staining, perhaps due to poor reagent quality control, or perhaps epitope damage upon skin processing. Similarly, no MAIT cells were detected given the stimulation conditions and lack of markers. As MAIT cells are $\text{CD3}^+\text{CD161}^{\text{hi}}\text{CD4}^-\text{CD8}^{\pm}$ it is possible that some were within the CD8 or CD4 ($\text{CD3}^+\text{CD4}^-$) cells but further, appropriate studies would be required. There was no obvious CD161⁺ population in the skin but this may well be due to epitope damage rather than absence of the cells.

Albeit controversial, neutrophils have also been reported as major IL-17 producing cells in human skin (Lin et al., 2011), and have been noted as a major source of IL-17 in HS lesional skin (Lima et al., 2015) (Section 1.5.7). However, this was not explored here given that the vast majority of CD45⁺ cells in this study were observed to be CD3⁺ cells. This is most likely a consequence of the dissociation method utilised (Section 2.2.5.2), as well as culture conditions and absence of relevant antibodies.

Another novel finding from this study was the decreased frequency of Treg cells in the PBMC of HS patients, along with an increase in HS lesional skin. One may surmise that

the reduction of Treg cells in PBMC is due to the Treg cells leaving the peripheral system to migrate to the sites of cutaneous inflammation in order to dampen the inflammatory response. The concurrent increase in Treg cells in HS lesional skin supports this. Despite the increased Treg cell frequency, HS lesional skin nonetheless exhibited a profound dysregulation of the Th17: Treg cell axis. An imbalance in the ratio of Th17 cells to Treg cells has been demonstrated previously in PG, suggesting that there may be similar immune dysregulation underlying both HS and PG (Caproni et al., 2015). The dysregulation of the Th17: Treg cell axis observed here in HS lesional skin reinforces how substantial the increase in Th17 cells is, given the parallel Treg cell increase detected in the HS lesion.

The phenotypic profile observed within the Treg cell population cannot necessarily be extrapolated towards Treg cell function, and indeed there was no significant difference in the expression of the markers CD39, CTLA-4 and CD161 on Treg cells in skin v PBMC. However, although there was no change in CD39 or CTLA-4 in HS lesional skin, CD161 expression was markedly increased compared with PBMC. CD161⁺ Treg cells have previously been shown to be enriched in inflammatory environments, and although they behave like classical Treg cells in many ways, they can also express the cytokines IL-17 or IFN- γ upon expansion (Pesenacker et al., 2013). It has previously been shown that Treg cell function is impaired in the blood of MS patients (Fletcher et al., 2009), as well as the blood and skin of psoriasis patients, (Soler et al., 2013; Sugiyama et al., 2005), whilst CD161⁺ Treg cells are present in juvenile idiopathic arthritis (Pesenacker et al., 2013). Hence it would be of interest to determine whether these CD161⁺ Treg cells in HS skin express proinflammatory cytokines, or indeed if their suppressive capacity is diminished. However, more thorough investigation into Treg cell function was not possible in this study given the very small cell numbers available per sample. In fact, only HS lesional skin and healthy control skin Treg cells were evaluated, whilst HS perilesional and uninvolved skin samples were prioritised for inflammatory cytokine analysis.

The polyfunctionality demonstrated here in HS skin T cells, particularly CD4 T cells, is striking. It illustrates that T cells in HS skin may express multiple inflammatory cytokines simultaneously, and that T cells in clinically normal perilesional and uninvolved HS skin

are in fact even more polyfunctional than in HS lesional skin. In actuality, CD4 and CD8 T cells rarely expressed IL-17 in isolation, but co-expressed other cytokines, in particular TNF and GM-CSF. Many of the CD4 T cells in HS skin expressed five or six of the screened cytokines simultaneously. T cells co-expressing multiple cytokines are associated with enhanced pathogenesis, and polyfunctional CD161⁺ CD4 T cells have been shown to be highly proinflammatory and resistant to Treg cell mediated suppression in RA (Basdeo et al., 2015). Thus, it is possible that the polyfunctional CD161⁺ CD4 T cells in HS skin may also be resistant to suppression by Treg cells. Further, the authors have recently implicated polyfunctional CD4 and CD8 T cells in paradoxical psoriasis, where patients undergoing TNF blockade develop psoriasis-like symptoms (Moran et al., 2020). Despite the increase in Treg cells in HS lesional skin, it is apparent that the proinflammatory environment, likely potently driven by these polyfunctional T cells, is not being adequately suppressed.

IL-22, GM-CSF, IFN- γ , IL-2 and TNF were also all upregulated in HS lesions as well as in clinically normal HS P and HS U skin in parallel with the enhanced IL-17 production, with most IL-17⁺ CD4 T cells co-producing some or all of these cytokines. However, in CD8 T cells where IL-17 production was limited to a small population (5-10%), GM-CSF, IFN- γ , IL-2 and TNF were produced by >50% of CD8 T cells in HS L, P and U skin. These levels were considerably reduced upon anti-TNF treatment, significantly so for GM-CSF in HS U and IFN- γ in HS L, suggesting a proinflammatory role for these cells. CD8 T cells in PBMC appeared to be much more proinflammatory than CD4 T cells, with most cytokines showing a two-fold increase, albeit significantly so only for TNF. Taken in conjunction with a significant decrease in Treg cells in PBMC, this suggests low level systemic inflammation.

Given the significantly increased frequencies of TNF-producing T cells in HS skin, and even in CD8 T cells in HS PBMC, TNF is a valid therapeutic target. Adalimumab treatment in this study appeared to exert its therapeutic effects in HS in part by reducing the extremely high expression of IL-17 in the skin, a finding previously unreported. Following anti-TNF treatment, the polyfunctional profile of both CD8 and CD4 T cells is much reduced, approaching that of healthy control skin. Similar effects on IL-17 in the skin

have been observed in psoriasis patients treated with anti-TNF, though not in relation to polyfunctional cells (Piaserico et al., 2014).

The mechanism by which TNF inhibition reduces IL-17 expression in T cells is unclear and is likely via an intermediate cell rather than direct. For example, in a mouse model mimicking severe asthma, TNF produced by DC plays a central role in IL-17 production from CD4 T cells, and a lack of TNF reduced IL-17 expression and reduced neutrophilia (Fei et al., 2011). In RA patients, TNF in the synovium has been demonstrated to promote Th17 cells through high levels of IL-1 β and IL-6 produced by monocytes in a TNF receptor (TNFRI and TNFRII) dependent manner, with TNF blockade reducing levels of IL-1 β , IL-6 and IL-17 (Zheng et al., 2014). Given the high levels of gene expression of IL-1 β , IL-8, IL-23A as well as TNFR in cDC2 this may well be the primary target for TNF inhibition in HS and warrants further investigation.

The frequency of CD4 and CD8 T cells within the T cell subset was shown to be similar between healthy controls and HS patients in both PBMC and skin. However, both CD4 and CD8 T cells in the PBMC of HS patients exhibited a modest increase in cytokine production, suggestive of low-level systemic inflammation. This may be in line with activated T cells trafficking from the periphery to distant sites on the skin (e.g. uninvolved) where new lesions may emerge. Alternatively, or additionally, perhaps these circulating inflammatory T cells may settle in other tissue, leading to related conditions such as CD, or vice versa.

In addition, this chapter showed that the skin homing marker CLA was upregulated two-fold within the CD4 and CD8 T cell populations in HS patient PBMC when compared with healthy controls, suggesting that the circulating T cells may be primed to traffic to the skin in HS. However, the frequency of CLA expression was in fact reduced on T cells in HS lesional skin compared with perilesional and uninvolved skin, as well as healthy control skin, which is perhaps contrary to expectation. This finding is tempered by the fact that there is an exponentially expanded T cell cohort present in HS lesional skin, hence there are still far more CLA⁺ T cells in the HS lesion than other skin sites. Further, although expression of skin-homing molecules is required for T cells to enter normal

skin, active inflammation, as seen in HS lesional skin, makes T cell entry more permissive (Ho & Kupper, 2019). Nevertheless, it may suggest that the majority of HS lesional T cells are proliferating from resident T cells rather than having trafficked de novo from the periphery. Interestingly, the scRNA-Seq studies in Chapter 3 showed *SELPLG* (CLA) upregulation primarily limited to Treg cells and Th17 cells (Figure 3.17), perhaps suggesting the infiltrating cells in HS lesions are largely limited to these two subsets. However, this is unlikely to explain why most T cells in the perilesional and uninvolved HS skin are positive for CLA expression. Perhaps in perilesional and uninvolved HS skin, these CLA⁺ T cells are those cells that have egressed from HS lesional skin and travelled to distal skin sites, driving further inflammation. CLA⁺ Trm cells have recently been shown to be capable of down-regulating CD69, exiting the skin and re-entering the circulation (Klicznik et al., 2019).

It would be of interest to further characterise these peripheral and skin CLA⁺ T cells, and whether they express a particular memory phenotype. Tcm cells (CCR7⁺CD62L⁺) are considered to circulate between the blood and LN whilst Tem cells express tissue-homing receptors allowing them to access peripheral tissues. However, CCR7⁺CD62L⁺ T cells that also express CLA and CCR4 have recently been identified, suggesting that a Tcm subset can enter peripheral tissues, and these cells can give rise to Trm cells (Gehad et al., 2018). The skin of a healthy adult is reported to contain nearly 20 billion memory T cells (R. A. Clark, Chong, Mirchandani, Brinster, et al., 2006), almost twice that of the circulation, and four distinct populations of memory T cells have recently been identified in human skin (Watanabe et al., 2015). These include two populations of Trm cells (CD69⁺CD103⁻ and CD69⁺CD103⁺), CCR7⁺CD62L⁺ Tcm cells, and a population of CCR7⁺CD62L⁻ cells, termed migratory memory T (Tmm) cells. These subsets have distinct functional activities; identifying their presence and role in lesional, perilesional and uninvolved HS skin was beyond the scope of this study but is the subject of further investigation.

Overall, these findings heavily implicate polyfunctional T cells, and IL-17 in particular, in the pathogenesis of HS. Hence it would be of interest to determine the benefit of therapeutic targeting of IL-17 in HS. The anti-IL-17 therapy secukinumab has shown

promising results in HS intervention (Prussick et al., 2019; Thorlacius et al., 2018). However, there have been discouraging results in trials for secukinumab treatment in CD (Hueber et al., 2012), as well as an apparent emergence of inflammatory bowel disease as a side-effect in a psoriasis and an ankylosing spondylitis patient undergoing secukinumab treatment (Fobelo Lozano et al., 2018). Of further concern, there is a recent report of paradoxical secukinumab-induced HS in a psoriasis patient (Marasca et al., 2019). Hence identifying potential upstream targets along the IL-17 pathway such as the inflammasome or IL-23p19, or downstream targets such as the IL-17 receptor, may be more effective.

Taken together, the findings reported in this chapter have substantially added to the understanding of the role of T cells in HS pathogenesis. In identifying polyfunctional T cells with a potent Th17 cell phenotype, it proposes new therapeutic targets. The data aligns with that of the previous chapter, where T cells are the major immune cell population in HS lesional skin, and suggests an interplay between the immune cell subsets. With this new information, it allows new hypotheses in the underlying mechanisms in skin inflammation.

Chapter 5

General discussion

5 General discussion

5.1 Introduction

HS is a gravely understudied disease that causes severe distress and pain to patients. It can persist for decades with little relief. It is underreported and underdiagnosed, and disproportionately affects those in lower socioeconomic conditions. Treatments have been varied, of limited benefit and in general unsatisfactory. Hence, studies elucidating the underlying pathogenesis are necessary and may lead to new drug targets and improved therapeutics. Further, research findings here may contribute to a deeper understanding of autoimmunity, autoinflammation and other IL-17- associated pathologies.

With the overarching hypothesis of an aberrant immune response driving the pathology in HS, this study sought to analyse the immune cell phenotype and function in greater detail than previously undertaken. It highlighted, for the first time, multiple B cell, T cell and myeloid cell subsets present in HS lesional skin that were absent, or present at very low levels, in healthy skin. It illustrated the inflammatory gene expression profile of the lesional immune cells and identified cDC2 as the cellular source of an activated NLRP3 inflammasome in HS lesional skin (Figure 5.1).

Having presented an immune profile dramatically skewed towards a Th17 cell profile, the project then investigated the role of IL-17⁺ T cell subpopulations in the disease, showing an unprecedented level of IL-17 production from polyfunctional T cells. Given the pathological role of a Th17 cell: Treg cell imbalance in autoimmunity, it also examined Treg cells in HS skin and PBMC, identifying a dramatically skewed ratio between the two subsets in favour of Th17 cells. Finally, it demonstrated a significant reduction in this polyfunctional T cell inflammation, with correction of the Th17 cell: Treg cell imbalance, upon TNF blockade suggesting a mode of action for this intervention.

Like most chronic inflammatory diseases, HS is initiated through multiple genetic, lifestyle and environmental factors. Together with mechanical friction, these factors

likely combine in HS to lead to an accumulation of endogenous DAMPs which activate resident immune cells (Sabat et al., 2020). The phenotyping and cluster analysis presented herein convincingly showed LC and cDC2 as the most frequent innate cells in the HS lesions, whilst the inflammatory gene expression profile of these subsets leads to a strong argument that LC, and in particular cDC2, were the dominant innate cell drivers of the subsequent immune cell infiltration. Key genes of the NLRP3 inflammasome complex, *NLRP3*, *CASP1* and *IL1B* were detected almost exclusively in cDC2 and to a lesser degree LC. The NLRP3 inflammasome has been implicated in HS, but the cell source never previously identified (Kelly et al., 2015; Witte-Handel et al., 2018). High expression of *IL23* in addition to IL-1 β within the cDC2 suggested a strong bias towards Th17 cell activation. The markedly high levels of the alarmins *S100A8* and *S100A9*, found to be expressed in dermal macrophages, suggest they may play a role in priming these DC.

When comparing these data showing unprecedented high levels of IL-17 producing T cells in HS lesions to their virtual absence in healthy control skin, the majority of expanded T cells appear to be Th17 lineage cells. Interestingly, although the polyfunctional cytometry data did not include memory markers, the gene expression studies showed that cells expressing high levels of *KLRB1* (CD161), *IL17A* or *IL17F* were also high for memory (*CD44*) and Trm cell markers (*CD69*) and were low for the naïve marker *SELL* (CD62-L). This suggests that these Th17 lineage cells may be expanded from a resident population rather than infiltrating IL-17⁺ T cells. However surprisingly, CLA expression (both via scRNA-Seq and cytometry) was reduced on these cells in HS lesional skin. Further, since CD69 is an activation marker as well as Trm cell marker, these data may be considered inconclusive, and requires further investigation. In any case, the specificity of Th17 cells within HS skin is as yet unknown, although it may be speculated that they are specific for commensal bacteria or perhaps citrullinated antigens.

These polyfunctional T cells were also found in clinically normal HS skin, with cytokine expression levels similar to the lesional skin T cells, albeit overall T cell numbers were much lower, similar to that in healthy skin. That TNF blockade reduces the inflammatory

profile in all sites (HS L, P and U) suggests this treatment likely suppresses new lesion outbreaks as well as dampening inflammation in existing lesions.

The IL-17⁺ T cells likely play a role in activating keratinocytes and fibroblasts in HS which leads to follicular occlusion, then dilatation and build-up of bacteria and cell debris within the follicle. Upon follicular rupture, the cycle escalates, further activating innate cells, driving Th17 lineage cell influx and the observed massive influx of neutrophils. An inflamed, aberrant keratinocyte response leads to acanthosis, tissue destruction and fistula formation, with neutrophils contributing to pus formation. This tissue damage manifests in the bloody, odorous discharge.

The observed increased number of Treg cells, as well as high levels of the anti-inflammatory IL-10 gene expression in cDC2, is somewhat anomalous to the overall inflammation observed. Rather than defective regulatory immune responses, this may well reflect that the regulatory response is overwhelmed by the inflammatory cell influx.

It is not clear if the consequence of the demonstrated enhancement of B cells, plasma cells and plasmablasts is facilitating the T cell activation or if B cells are playing a separate, pathogenic role through antibody production. A suppressive role is unlikely given that there is no detectable IL-10, the hallmark cytokine of regulatory B cells, within any B cell clusters in this study. Coupling these data with that of collaborators showing a significant increase of plasmablasts and plasma cells in PBMC (Musilova et al., 2020), along with reports of B cell depletion being beneficial in HS (Takahashi et al., 2018; Vossen et al., 2019), there may well be a direct pathogenic role for B cells in the disease. Antibodies may be contributing to HS pathology through complement or innate cell activation or immune complex formation. Although beyond the scope of this study, increased levels of autoantibodies have been found in HS lesions and along with NET generation may contribute to B cell activation and plasmablast and plasma cell generation (Byrd et al., 2019). Citrullinated proteins can serve as autoantigens in RA, and in the same study (Byrd et al., 2019) ACPA were shown to be increased in HS skin.

This may illuminate the contribution of smoking, since it can lead to protein citrullination (Schellekens et al., 1998). Smoking may also contribute to bacterial burden, given that nicotine in cigarette smoke can inhibit bacterial clearance through suppression of antimicrobial peptides (Radek et al., 2010) and increase biofilm formation (Wu et al., 2018). Microbiome dysbiosis is a consistent feature of CD, which also has a smoking association. However, conclusive evidence that the microbiome plays a role in HS pathogenesis remains elusive.

A role for T cells in HS systemic inflammation may also be inferred through these findings. There was a modest increase demonstrated in expression of inflammatory cytokines in HS patient blood. Likewise, T cells in perilesional and uninvolved HS skin were shown to have a consistently increased inflammatory profile. Some of this may be correlated with obesity where subclinical inflammation and metabolic disorders are common. Hence an in-depth comparison of blood and skin from HS patients with appropriately matched obese individuals would be helpful here.

Conducting this study at the specific pathological location is invaluable, evidenced by the different profiles observed between HS skin and blood. This highlights limitations in other inflammatory diseases where studying the primary site is impractical or impossible (e.g. MS or Alzheimer's disease). Despite the limited tissue obtained, the research data yield was maximised by applying high-parameter cytometry, histology and scRNA-Seq analysis on the small number of cells.

There are no suitable mice models for HS being extensively used, although *PSEN1*-, *PSEN1*-/ *PSEN2*-, *NCSTN* +/- have been reported to recapitulate many anatomical and histological features (T. Li et al., 2007; Pan et al., 2004). However, <5% of all HS cases have identified genetic variants in these genes (T. Nomura, 2020) and it remains to be seen if these mice have similar immune cell profiles to that seen in patients.

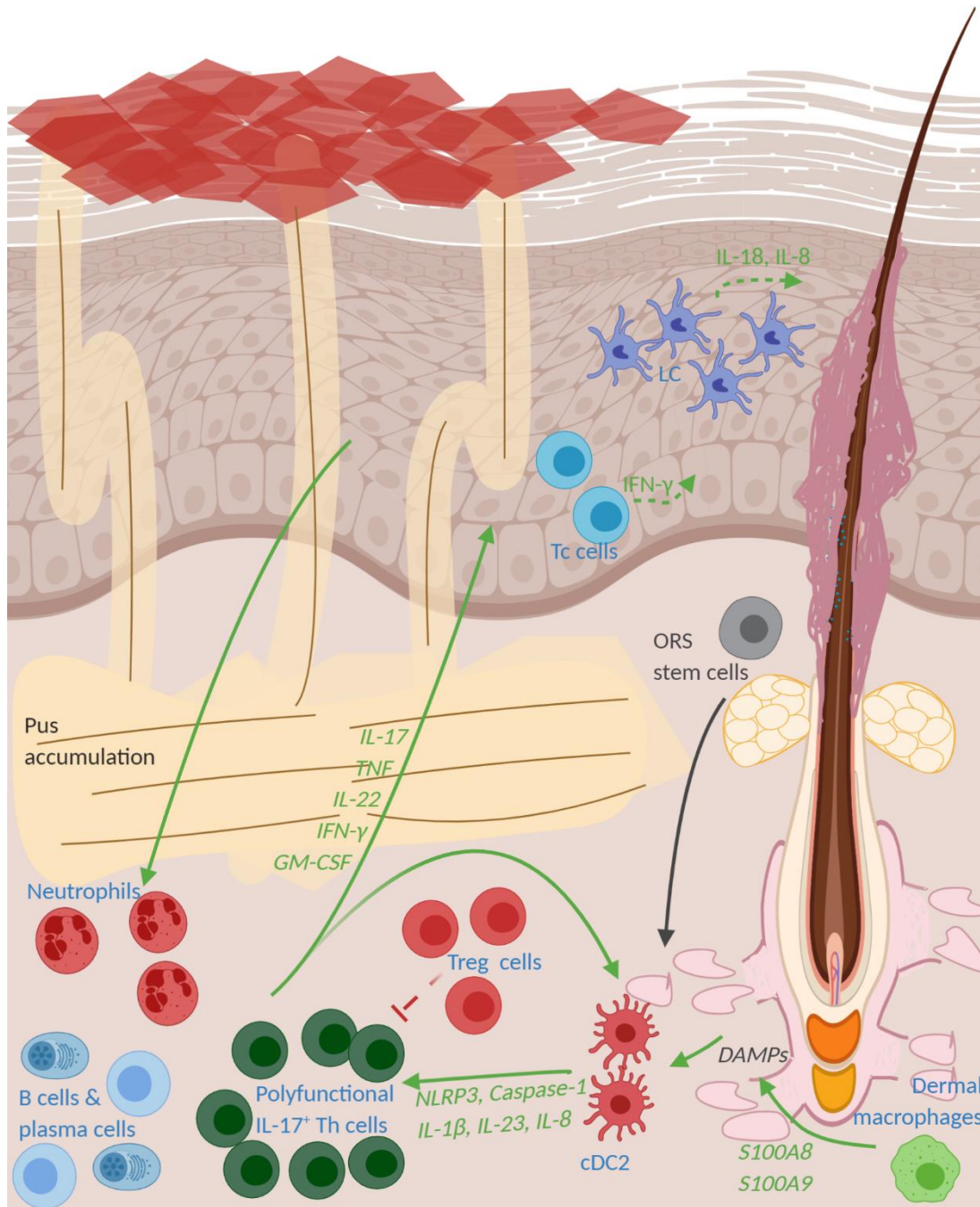


Figure 5.1 Proposed mechanism of immune dysfunction in HS.

Hyperkeratosis and follicular dilation cause release of ORS DAMPs, driving cDC2-derived NLRP3 inflammasome activation with IL-1 β and IL-23 driving an influx of polyfunctional IL-17 producing T cells. This drives neutrophil inflammation via keratinocyte activation, with an influx of B cells and other inflammatory cells. This leads to sinus tract formation with inflammatory lesions.

5.2 Implications for HS therapy

The findings within this thesis reinforce the rationale for targeting cytokines and receptors of the IL-17 pathway with therapeutic inhibition, and suggest this may be a more direct strategy than TNF blockade (Figure 5.2). The levels of IL-17⁺ T cells detected in HS lesional skin in this study were far in excess of other conditions such as psoriasis and ankylosing spondylitis where anti-IL-17 therapy is effective.

The IL-17A targeting treatments secukinumab and ixekizumab have essentially revolutionised the treatment of severe psoriasis. Early reports on directly inhibiting IL-17 secretion from T cells with secukinumab (anti-IL17A) and bimekizumab (anti-IL17A/F) are yielding promising early results in HS. However, there is a note of caution since despite IL-17 also being secreted at high levels in IBD (Fujino et al., 2003), secukinumab trials in CD patients were disappointing, with worse outcomes in patients treated with anti-IL-17 than with placebo (Hueber et al., 2012). Targeting the IL-17 receptor is also a potential strategy. However, similar to the poor outcome in the secukinumab trial, a trial in CD patients for brodalumab which targets IL-17R was terminated early due to worsening disease in the brodalumab-treated cohort (Moschen et al., 2019). Given the association between HS and CD, this is a concerning consideration for the direct targeting of IL-17/IL-17R in HS.

Having demonstrated high levels of *IL23* gene expression in cDC2 in HS lesional skin, blocking IL-23 is a rational therapeutic intervention. Ustekinumab and briakinumab are two such IL-23 inhibitors; ustekinumab is now a licensed treatment for CD but the primary endpoint was not met in briakinumab trials (Panaccione et al., 2015). The two treatments block the IL-12p40 subunit, common to both IL-23 and IL-12, hence interfering with Th1 cells as well as Th17 cells. Several antibodies recognise the IL-23p19 subunit, and hence IL-23 specifically. These include guselkumab, risankizumab, brazikumab and mirikizumab. Guselkumab has been shown to be effective in severe psoriasis (Nogueira et al., 2019) with promising results for treating CD and psoriatic arthritis. Hence these p19 inhibitors may well prove to be more effective in HS, with less adverse effects.

Depleting B cells has shown potential in one case study as well as *ex vivo* HS explants (Takahashi et al., 2018; Vossen et al., 2019) but more specific targets may yield less collateral damage and adverse effects. Given the upregulation of *IL1B*, *IL18* and *NLRP3* in cDC2, inhibition of IL-1 β (e.g. canakinumab) or pharmacological blocking of the inflammasome may warrant further investigation. Additionally, candidates targeting IL-23R, JAK and ROR- γ T, thereby directly inhibiting the Th17 cell, may prove effective (Moschen et al., 2019).

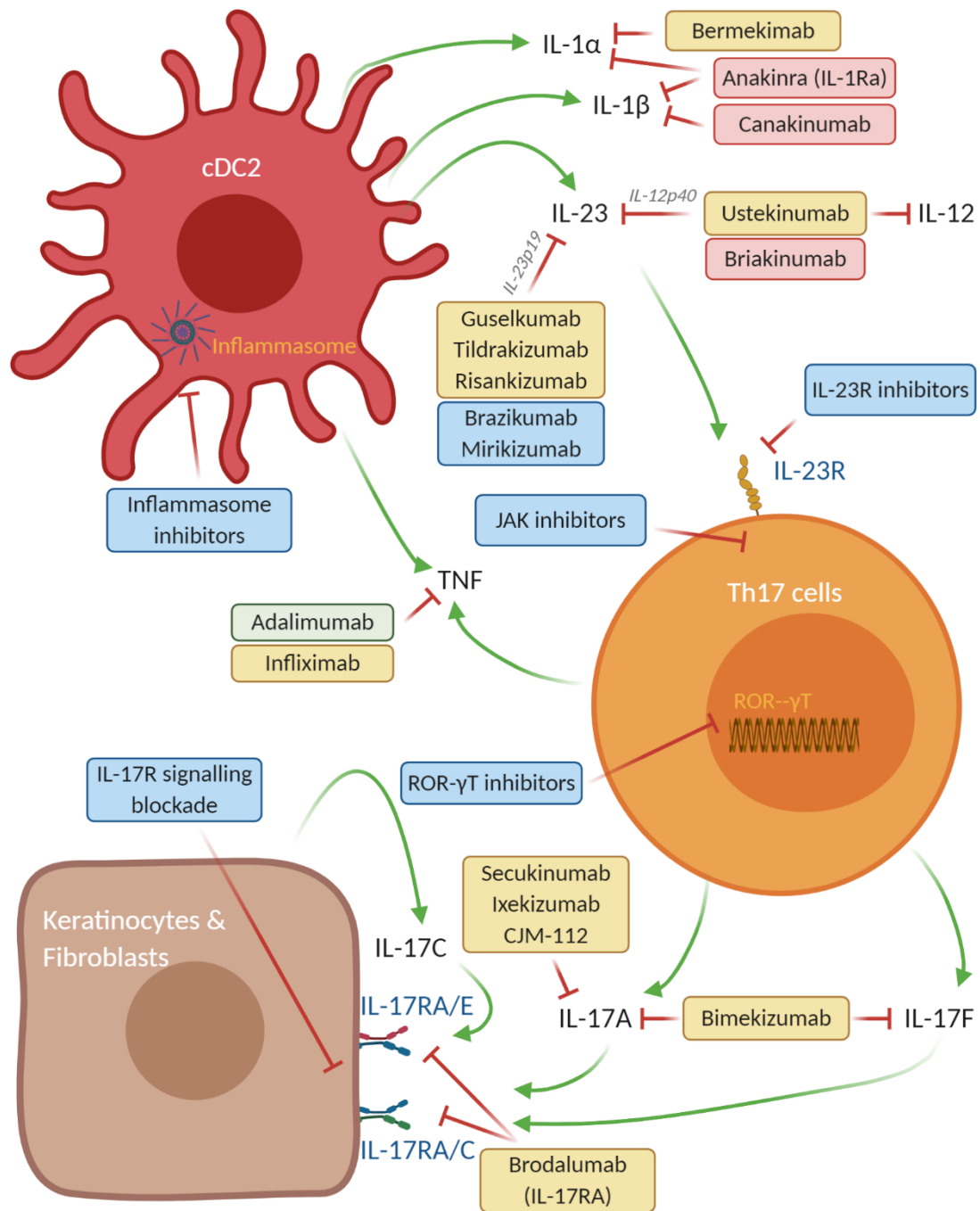


Figure 5.2 Therapies targeting the IL-17 pathway in HS.

The data presented in this thesis suggests multiple targets within the IL-17 pathway for potential treatments in HS. Upstream of IL-17, the cytokines that drive Th17 cells include IL-23 and IL-1 β shown here to be secreted by cDC2 in HS skin. IL-1 cytokines IL-1 α and IL-1 β can be targeted with specific monoclonal antibodies or receptor antagonists and release of mature IL-1 β can be inhibited using small molecule inhibitors of the inflammasome. Monoclonal antibodies specific for IL-23p19 or the p40 subunit shared with IL-12 are available which inhibit the development of Th17 cells or Th17/Th1 cells respectively. Blocking the IL-23R, its signalling via the JAK/STAT pathway or ROR- γ T could also inhibit Th17 cells. Given the key role for Th17 cells presented here, direct inhibition of IL-17A or IL-17A plus IL-17F may be an effective option. Alternatively blockade of IL-17RA would inhibit signalling induced by not only IL-17A and IL-17F but also IL-17C produced by keratinocytes and fibroblasts. Small molecule drugs targeting IL-17R signalling may be another possibility. Red boxes indicate disappointing results in HS, blue are potential therapeutics, yellow are under investigation in HS and green are licensed HS treatments.

5.3 Limitations

There were inevitably some limitations to this project, primarily regarding sample availability, experimental restrictions and overall scope. The study was relatively small with a maximum of thirteen samples in any one group, and significantly less in others. Collaborating with leading clinicians and surgeons proved an excellent, fruitful partnership and having access to the primary lesional tissue, as well as patient's healthy skin and blood, was vital to effectively study the HS immune pathology. However, accruing sufficient numbers of samples within the Irish patient cohort is challenging and so a larger study would require international collaborative projects. Even more so than for HS patient samples, the ability to examine skin samples from healthy donors was exceptionally fortunate and proved an essential resource. Recruitment of patients donating skin samples from reduction mammoplasty occurred midway through the project and so final numbers were very low. Biopsies taken from healthy volunteers yielded only small numbers of immune cells.

Optimally matched healthy controls with HS patients were ultimately impossible within this study. HS is strongly associated with smoking and obesity, but all healthy controls were non- or ex-smokers. Likewise, although the BMI data were absent for most healthy controls, anecdotally very few of these volunteers had a BMI >30. Similarly, the sampling site locations varied anatomically between HS patients and healthy controls. The majority of HS patient lesional samples were from the axilla and groin, whereas it was excess skin from the breast in the reduction mammoplasty patient cohort, and hip skin biopsies in the other healthy donors. In any case, the PBMC and skin immune profile and histology were within expected normal, healthy limits.

The studies of the effects of anti-TNF treatment on T cells in HS patients would ideally have been performed using pre- and post-treatment samples from the same patient and would be optimal to do so in future projects. But given the reduction in the inflammatory profile of T cells upon TNF inhibition, and the fact that this therapy is licensed only for patients with moderate to severe disease, it is likely that if anything the results would have been more pronounced.

Given the lack of suitable test tissue, thorough optimisation of the in-house tissue dissociation protocol was not possible at the initial steps of this project. Hence, in this branch of the study (Chapter 4), immune cell yield was relatively low and biased towards T cells, with minimal if any rescue of B cells and myeloid cells. However, the impact here was minimal insofar as this aspect of the project was T cell specific and primarily functional, hence maximal numbers or recovery of all immune cell subsets was not essential. Furthermore, the collagenase was likely excessively damaging to some cell epitopes, meaning some markers could not be identified. For example, CD25 was not identified on skin cell samples and so was excluded from the Treg cell gating strategy.

scRNA-Seq is an exceptional research tool and has added a great amount of data to this study. However, like all techniques there are limits to its output; it reflects a snapshot of transcription and should not be interpreted as the absolute cellular RNA production, and certainly not protein translation. As such, some prominent genes which would be expected to be present in the immune cell subsets were absent; e.g. *CD4*, *IL6* and *IL10*.

5.4 Future directions

This study gave a global overview of the immune cell status within HS lesions before concentrating on the role of T cells, in particular IL-17⁺ T cells, in HS PBMC and skin. It has implicated subsets and proposed new research avenues. Identifying the specific initial triggers would significantly further the understanding of the underlying pathogenesis and instruct whether HS is primarily an autoimmune or autoinflammatory disease.

The recent evidence of cytosolic DAMPs generated in ORS stem cells driving inflammation in HS is intriguing (Orvain et al., 2020). Their findings that these DAMPS led to type I IFN production strongly suggests a role for pDC in HS pathogenesis. Hence it is surprising that the scRNA-Seq data presented within this thesis showed a significant absence of pDC in HS lesional skin compared with healthy skin. It would be of interest to confirm this with a new cohort, as well as investigate whether it is a similar case with clinically normal HS skin.

The inflammasome complex serves as a PRR and elicits activation of caspases and conversion of pro-IL-1 β to its active form IL-1 β . NLRP3 is the best characterised inflammasome and basal expression of NLRP3 is markedly increased upon PAMP or DAMP recognition. It has been implicated in numerous diseases including MS and CD (Zahid et al., 2019) as well as HS (Kelly et al., 2015; Witte-Handel et al., 2018). Having identified high expression of *IL1B*, *NLRP3* and *IL18* within cDC2, further studies of the NLRP3 inflammasome and its role in HS would be appropriate. Identifying the mechanisms involved through inhibiting the various signalling steps, as well as testing likely DAMPs and PAMPs, would reveal new insights. Pharmacological inhibition of the inflammasome is a rational target in treating HS and so could be attempted with new small molecule inhibitors (Coll et al., 2015).

Immunohistochemistry could add much needed details to localising the various immune cell subsets and their functional products within the HS lesion. This study has not conclusively shown where the innate cells, B cells and Th17 lineage cells are within the skin samples and it would be of interest to see if they co-localise to the hair follicle or elsewhere, or are dispersed throughout the tissue. The histology slides used here for H&E staining could be utilised for immunofluorescence and immunohistochemistry to give greater clarity.

Other immune cells, understudied in this thesis, likely contribute to HS inflammation and tissue damage. ILC and NK cells were shown to be increased in HS lesional skin, but there was a lack of appropriate markers in this study's cytometry panel. Upon a more thorough cytometry or histochemistry study, the scRNA-Seq data could be returned to for additional detail. Mast cells were also more abundant in HS skin although their role was unclear. They have been reported to produce IL-17 but no gene expression of *IL17* family cytokines were detected, although low level expression of the receptors *IL17RC*, *IL17RD* and *IL18R* was noted.

Neutrophils are prominent in HS but only limited studies were possible within this project. It is likely they exacerbate the disease not just through their infiltration and build-up of pus, but also through NET formation and accumulation of citrullinated

proteins. Further studies would be helpful but must be performed on fresh, unfrozen samples. For transcriptome analysis, it may be possible to perform cell sorting of neutrophils from freshly dissociated skin for bulk RNA-Seq analysis.

The contribution of non-immune cells to HS pathogenesis is substantial but was not investigated here. Fibroblasts have the highest expression of the IL-1 β receptor among skin cells (Witte-Handel et al., 2018). Keratinocytes in HS constitutively demonstrate an inflammatory profile, suggesting that they are primarily dysfunctional, and rather than enhancing a tissue protective response, contribute to chronic inflammation (Hotz et al., 2016). In psoriasis, keratinocytes are a primary target for IL-17 and in HS, an inflammatory loop involving IL-17 stimulation of keratinocytes induces chemokines, anti-microbial peptides and cytokines, including IL-1 β . Recently, IL-17C, produced by stimulated keratinocytes, has been implicated in the HS pathogenesis, with HS patients having significantly elevated IL-17C mRNA compared with healthy controls (Navrazhina et al., 2020). Upon stimulation, the IL-17C induces the production of IL-1 β , IL-8, CXCL1 and IL-36 γ , as well as elevating IL-17A and IL-17F production by Th17 cells (Ramirez-Carrozzi et al., 2011). This creates a feedback loop driving inflammation.

Corresponding to the CD45⁺ immune cell scRNA-Seq analysis within this study, there is the CD45⁻ cell dataset which should contribute important additional detail in the understanding of HS, building upon the research findings generated in this thesis.

Chapter 6

Appendix

6 Appendix

6.1 HS classifications

A					
Hurley Classifications					
Hurley stage 1	solitary or multiple isolated abscess formation without scarring or sinus tracts				
Hurley stage 2	recurrent abscesses, single or multiple widely separated lesions, with sinus tract formation				
Hurley stage 3	diffuse or broad involvement, with multiple interconnected sinus tracts and abscesses.				

B					
HS Severity Index					
score	# of sites	body surface area (%) *	# of lesions	drainage **	pain ***
0	0	0	0	0	0-1
1	1	1	1		
2	2	2-3	2-3	1	2-4
3	3	4-5	4-5	>1	5-7
4	≥4	≥5	≥5		8-10

* palm of hand = 1% body surface area

** dressing changes per hour

*** visual analog scale

composite scoring: mild (0-7), moderate (8-12), severe (13-19)

Table 6.1 The Hurley classification of HS (A) and the HS severity index (B).

Sartorius Classifications	
Right axilla Nodules & fistulae _____ Longest distance _____ Hurley III no/yes _____ Σ _____	Left axilla Nodules & fistulae _____ Longest distance _____ Hurley III no/yes _____ Σ _____
Right groin Nodules & fistulae _____ Longest distance _____ Hurley III no/yes _____ Σ _____	Left groin Nodules & fistulae _____ Longest distance _____ Hurley III no/yes _____ Σ _____
Right gluteal region Nodules & fistulae _____ Longest distance _____ Hurley III no/yes _____ Σ _____	Left gluteal region Nodules & fistulae _____ Longest distance _____ Hurley III no/yes _____ Σ _____
Other region Nodules & fistulae _____ Longest distance _____ Hurley III no/yes _____ Σ _____	Total Sum: _____
Patient report (not included in the score): Number of boils during latest month: _____ Soreness of most symptomatic lesion: _____ Visual analogue scale (0-10):	Legend Parameters points/parameter 1. number of regions? 3 points per region 3 2. number & severity of lesions? nodules 1 fistulae 6 3. longest distance between 2 relevant lesions? <5 cm 1 5-10 cm 3 > 10 cm 9 4. lesions clearly separated by normal skin? yes 0 no (Hurley III) 9

Table 6.2 The Sartorius System classifying severity of HS.

A	
HS PGA Classifications	
Stage 1	clear ; no nodules
Stage 2	minimal ; non-inflammatory nodules only
Stage 3	mild ; <5 inflammatory nodules or 1 abscess or draining fistula with no inflammatory nodules
Stage 4	moderate ; 0 abscesses or draining fistula and ≥5 inflammatory nodules or 1 abscess or draining fistula with ≥1 inflammatory nodule or 2-5 abscesses or draining fistulae with <10 inflammatory nodules
Stage 5	severe ; 2-5 abscesses or draining fistulae with ≥10 inflammatory nodules
Stage 6	very severe ; >5 abscesses or draining fistulae

B	
IHS4	
IHS4 (points) =	
number of nodules	x 1
number of abscesses	x 4
number of draining tunnels	x 4
Mild HS	≤ 3
Moderate HS	4 – 10
Severe HS	≥ 11

Table 6.3 The HS Physician’s Global Assessment (A) and the International Hidradenitis Suppurativa Severity Score System (B).

6.2 Quality of RNA sequencing data is within normal parameters

TCD code	AbbVie Code	Estimated cell #	Mean reads per cell	Median. genes per cell	Number of reads	Valid barcodes	Sequencing saturation	Q30 Bases in barcode	Q30 Bases in RNA read	Q30 Bases in Sample index	Q30 Bases in UMI
HS310	CD45neg1	2,316	72,747	1,156	168,482,585	97.90%	91.00%	97.10%	74.20%	93.90%	97.10%
HS312	CD45neg2	936	81,305	1,180	76,101,549	97.90%	90.90%	97.10%	71.70%	93.30%	97.00%
HS313	CD45neg3	2,368	60,178	972	142,503,743	98.20%	90.00%	97.20%	75.50%	93.50%	97.10%
HS408	CD45neg4	3,667	46,654	2,018	171,081,289	98.20%	71.20%	97.20%	77.10%	93.50%	97.30%
SVPH1	CD45neg5	3,464	67,648	1,871	234,335,326	98.20%	81.40%	97.20%	75.50%	92.00%	97.30%
SVPH2	CD45neg6	3,854	65,299	1,649	251,663,118	98.30%	83.90%	97.20%	75.90%	94.00%	97.30%
SVPH3	CD45neg7	3,463	49,146	1,692	170,193,019	98.30%	78.50%	97.20%	74.20%	94.10%	97.30%
HS412	CD45neg8	2,422	59,831	1,918	144,911,305	98.30%	77.20%	97.20%	78.30%	94.10%	97.30%
HS413	CD45neg9	2,995	39,443	1,283	118,134,700	98.10%	81.40%	97.20%	78.80%	94.20%	97.30%
HS310	CD45pos1	2,975	56,097	513	166,889,372	98.20%	91.40%	97.20%	73.00%	93.50%	97.10%
HS312	CD45pos2	3,972	21,160	529	84,049,299	98.10%	75.60%	97.00%	72.20%	92.00%	96.90%
HS313	CD45pos3	3,971	19,555	501	77,654,498	98.20%	73.40%	97.00%	72.00%	92.40%	96.90%
HS408	CD45pos4	3,788	62,064	971	235,101,860	98.10%	84.60%	97.20%	77.30%	94.10%	97.30%
SVPH1	CD45pos5	3,423	50,691	830	173,518,389	98.10%	85.10%	97.20%	78.70%	94.20%	97.20%
SVPH2	CD45pos6	3,474	50,796	868	176,466,505	98.20%	84.30%	97.20%	78.40%	93.70%	97.30%
SVPH3	CD45pos7	3,688	56,227	725	207,367,071	98.20%	88.70%	97.20%	79.80%	93.40%	97.30%
HS412	CD45pos8	3,379	44,410	514	150,063,309	98.30%	86.70%	97.20%	77.40%	94.20%	97.30%
HS413	CD45pos9	2,241	38,642	771	86,598,276	98.10%	80.90%	97.20%	78.20%	93.50%	97.30%

Table 6.4 Quality of RNA sequencing data is within normal parameters (1 of 2).

Data from AbbVie Genomics Research Center regarding the quality of the scRNA-Seq data.

TCD code	AbbVie Code	Reads mapped to genome	Reads mapped confidently to genome	Reads mapped confidently to intergenic regions	Reads mapped confidently to intronic regions	Reads mapped confidently to exonic regions	Reads mapped confidently to transcriptome	Reads mapped antisense to gene	Fraction reads in cells	Total genes detected	Median UMI counts per cell
HS310	CD45neg1	91.20%	89.30%	3.50%	20.10%	65.70%	61.80%	1.10%	95.20%	19,717	2,709
HS312	CD45neg2	90.00%	88.00%	4.70%	19.60%	63.70%	59.90%	1.10%	93.50%	17,930	2,768
HS313	CD45neg3	91.20%	88.90%	3.50%	17.10%	68.40%	64.30%	1.20%	93.60%	19,365	2,142
HS408	CD45neg4	92.00%	89.80%	4.80%	16.00%	69.10%	65.20%	1.10%	94.90%	21,763	6,237
SVPH1	CD45neg5	91.50%	89.30%	4.10%	14.60%	70.50%	66.80%	0.90%	95.60%	21,702	5,959
SVPH2	CD45neg6	91.60%	89.50%	3.60%	15.00%	71.00%	67.40%	0.90%	96.00%	21,375	4,670
SVPH3	CD45neg7	90.60%	88.40%	4.70%	13.80%	70.00%	66.30%	1.00%	96.20%	21,058	5,038
HS412	CD45neg8	92.30%	89.80%	2.80%	14.90%	72.10%	68.40%	0.90%	94.90%	20,512	6,425
HS413	CD45neg9	92.50%	90.40%	6.00%	16.90%	67.40%	63.80%	1.10%	93.20%	20,261	3,263
HS310	CD45pos1	90.40%	86.40%	3.20%	18.70%	64.50%	60.80%	0.90%	87.60%	17,440	1,218
HS312	CD45pos2	88.50%	84.50%	3.50%	18.40%	62.60%	57.50%	0.90%	86.60%	17,680	1,321
HS313	CD45pos3	88.90%	83.90%	2.70%	16.00%	65.10%	60.80%	0.70%	89.90%	17,347	1,309
HS408	CD45pos4	91.70%	89.20%	4.10%	21.30%	63.80%	60.30%	1.00%	94.20%	19,363	3,020
SVPH1	CD45pos5	92.70%	90.60%	4.60%	23.60%	62.40%	59.10%	0.90%	92.50%	19,219	2,355
SVPH2	CD45pos6	92.20%	90.20%	4.40%	23.70%	62.10%	58.80%	0.90%	93.90%	19,596	2,489
SVPH3	CD45pos7	92.80%	90.70%	5.50%	23.20%	62.00%	58.70%	1.00%	94.30%	19,360	2,100
HS412	CD45pos8	92.20%	87.80%	2.70%	15.20%	69.90%	66.10%	0.60%	86.30%	17,686	1,479
HS413	CD45pos9	91.60%	87.50%	4.20%	14.80%	68.50%	64.50%	0.80%	89.40%	17,808	2,129

Table 6.5 Quality of RNA sequencing data is within normal parameters (2 of 2).

Data from AbbVie Genomics Research Center regarding the quality of the scRNA-Seq data.

6.3 Differential gene expression reveals a distinct transcriptional profile for each identified cell cluster

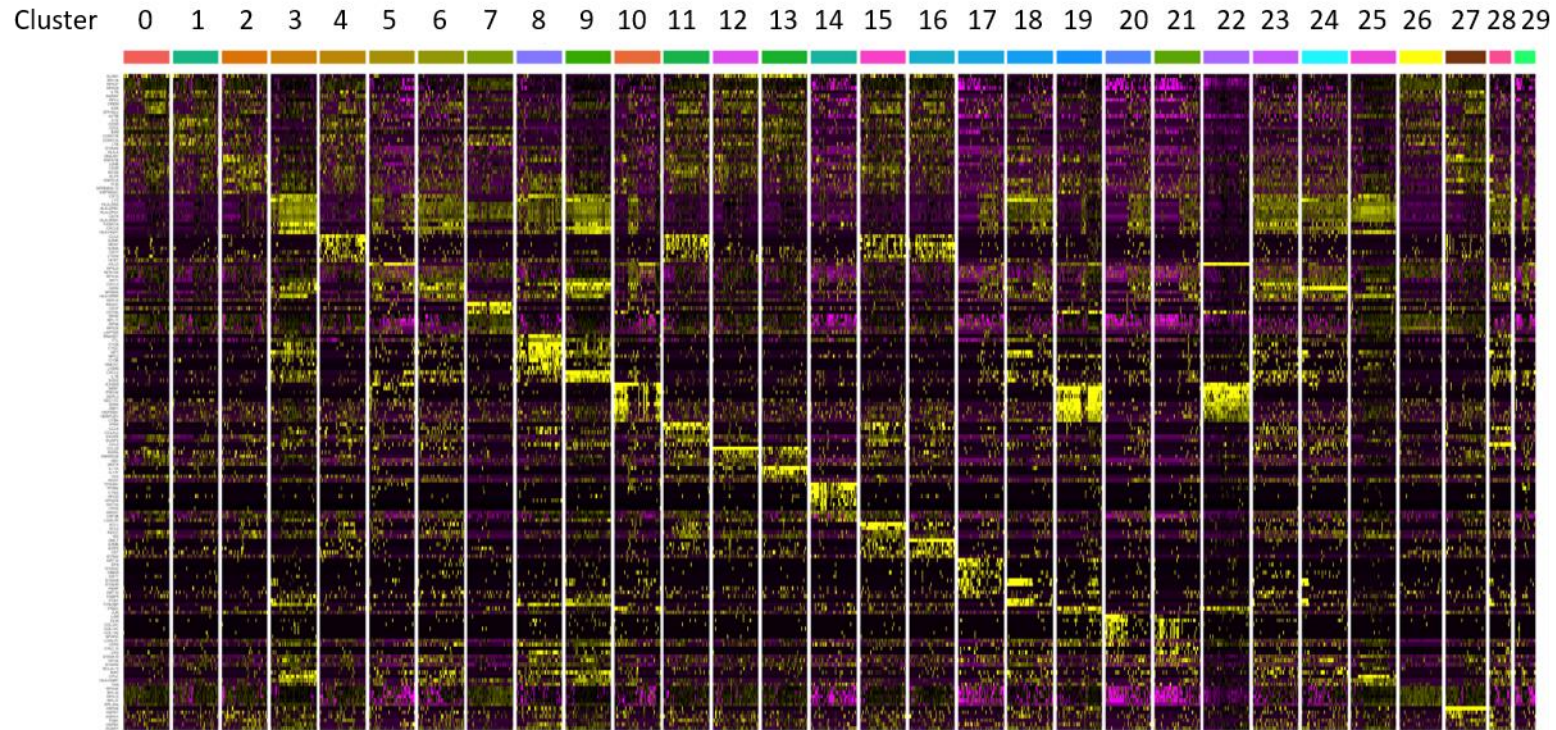


Figure 6.1 Differential gene expression reveals a distinct transcriptional profile for each identified cell cluster.

Cells isolated from the skin of healthy controls (Con; n=3) or HS lesional skin (HS; n=6) were purified based on CD45 expression, barcoded and their gene expression determined by single cell RNA sequencing (scRNA-Seq). Differential gene expression, generated through the statistical framework MAST, reveals a different gene expression pattern for each of the thirty cell clusters identified.

6.4 Cell cluster locations of genes markedly up- and down-regulated expressed in HS compared with healthy control skin

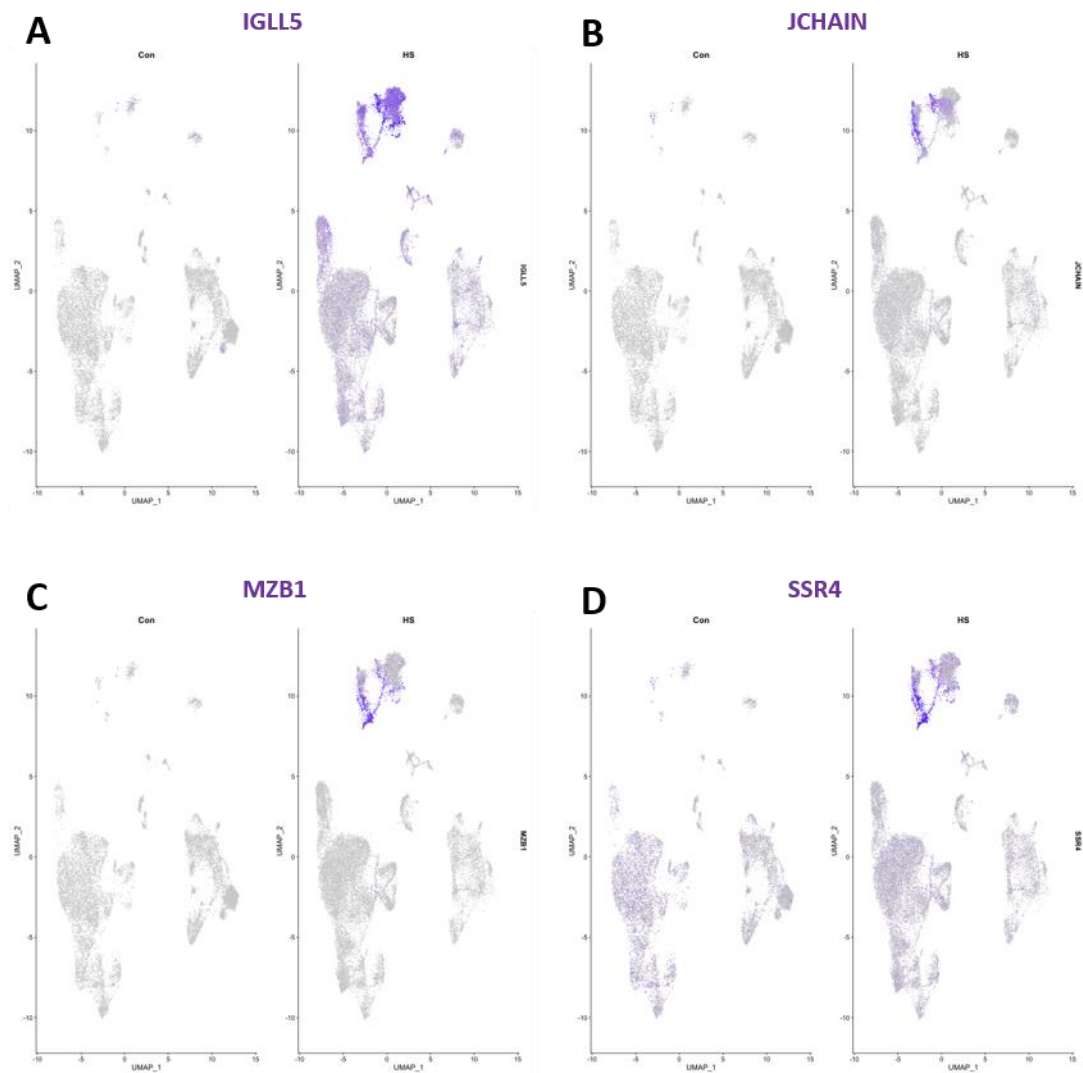


Figure 6.2 UMAP plots for markedly upregulated genes primarily in plasmablasts and plasma cells.

Cells isolated from the skin of healthy controls (Con; n=3) or HS lesional skin (HS; n=6) were purified based on CD45 expression, barcoded and their gene expression determined by scRNA-Seq. UMAP plots display gene expression for Con (left) and HS samples (right) for IGLL5 (A), JCHAIN (B), MZB1 (C) and SSR4 (D).

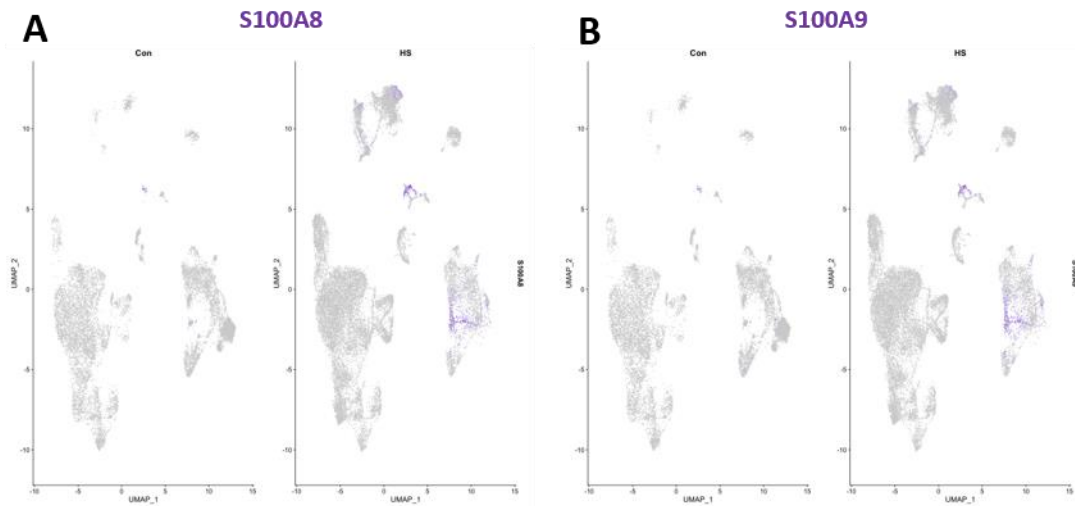


Figure 6.3 UMAP plots for markedly upregulated genes primarily in myeloid subsets. Cells isolated from the skin of healthy controls (Con; n=3) or HS lesional skin (HS; n=6) were purified based on CD45 expression, barcoded and their gene expression determined by scRNA-Seq. UMAP plots display gene expression for Con (left) and HS samples (right) for S100A8 (A) and S100A9 (B).

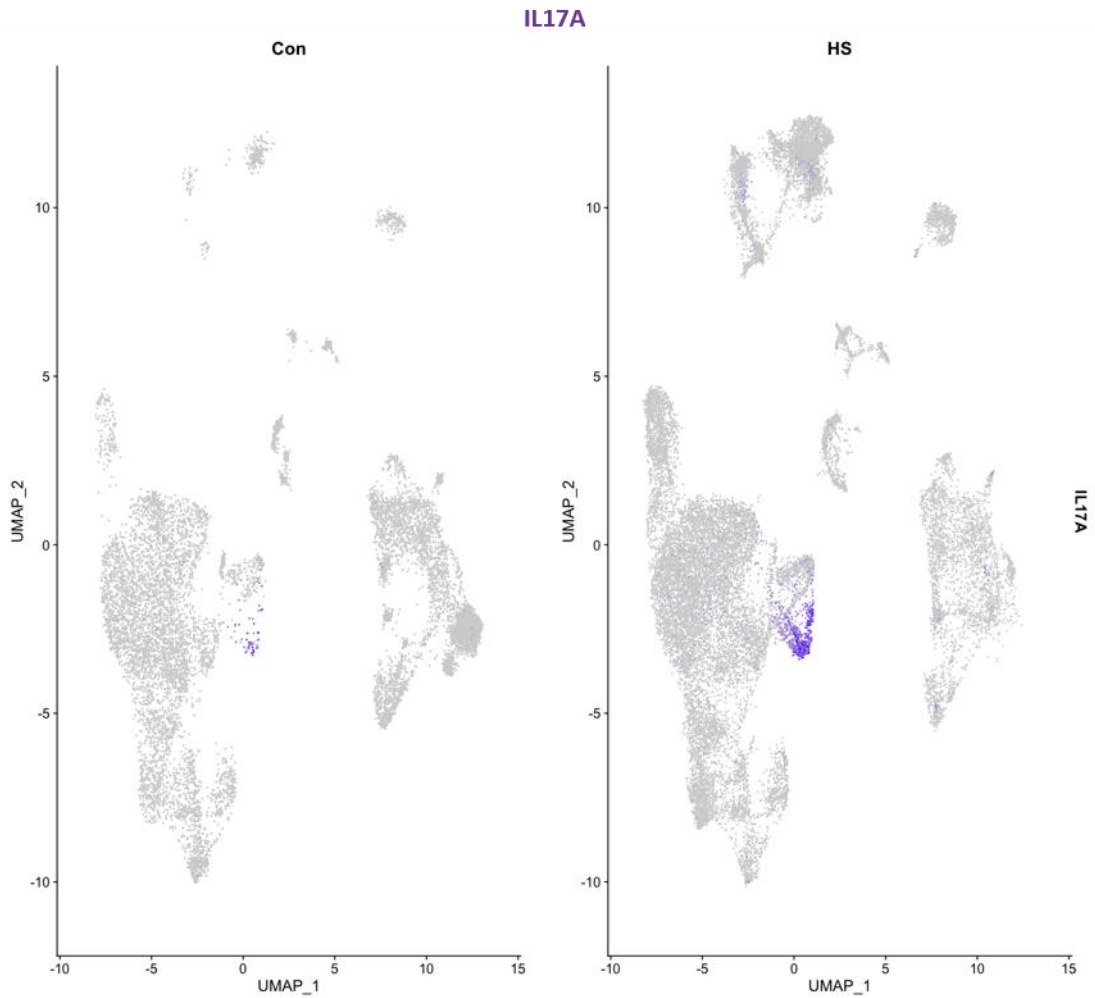


Figure 6.4 UMAP plot for markedly upregulated genes primarily in Th17 cells.

Cells isolated from the skin of healthy controls (Con; n=3) or HS lesional skin (HS; n=6) were purified based on CD45 expression, barcoded and their gene expression determined by scRNA-Seq. UMAP plots display gene expression for Con (left) and HS samples (right) for IL-17A.

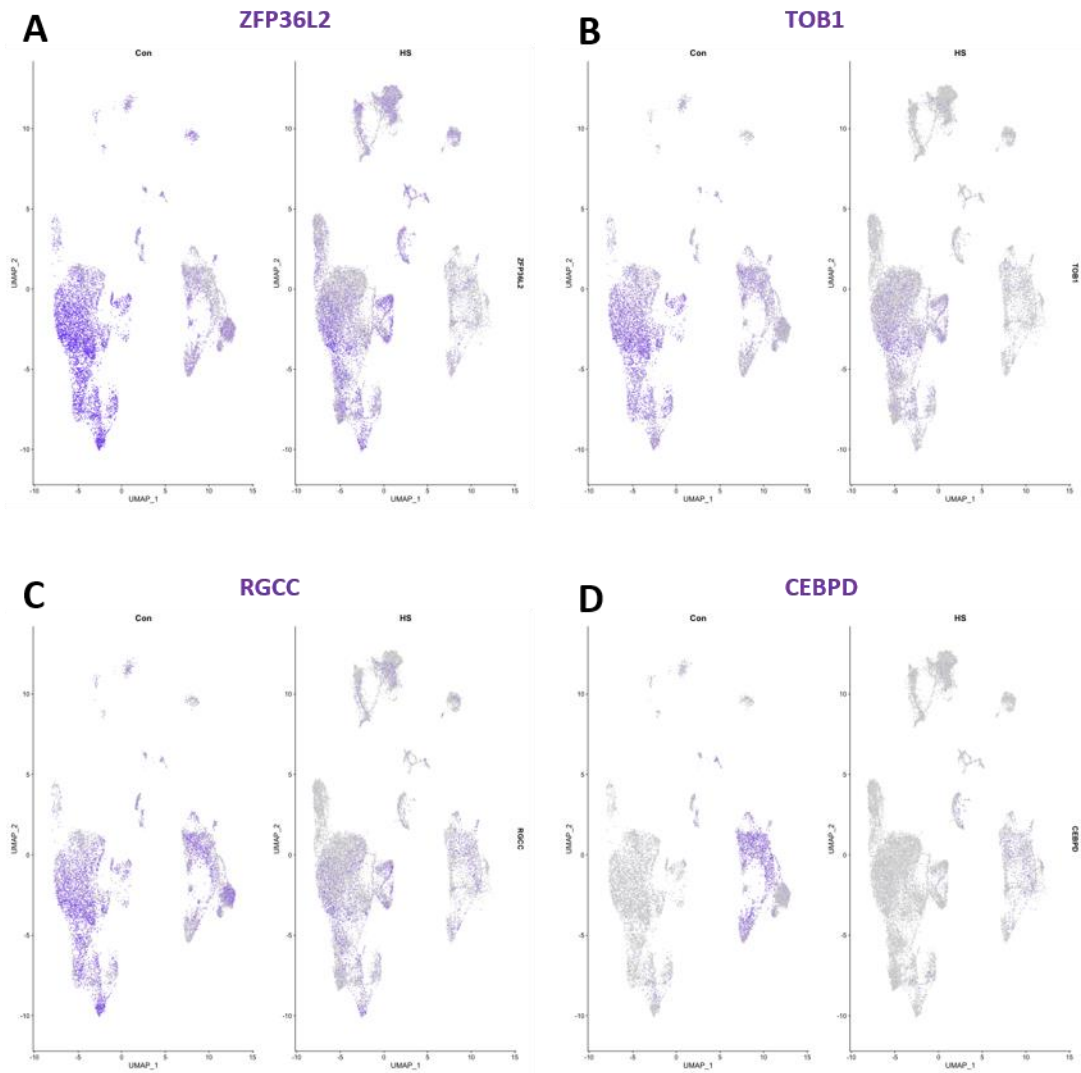


Figure 6.5 UMAP plot for markedly downregulated genes primarily in T cells and myeloid subsets.

Cells isolated from the skin of healthy controls (Con; n=3) or HS lesional skin (HS; n=6) were purified based on CD45 expression, barcoded and their gene expression determined by scRNA-Seq. UMAP plots display gene expression for Con (left) and HS samples (right) for CEBPD.

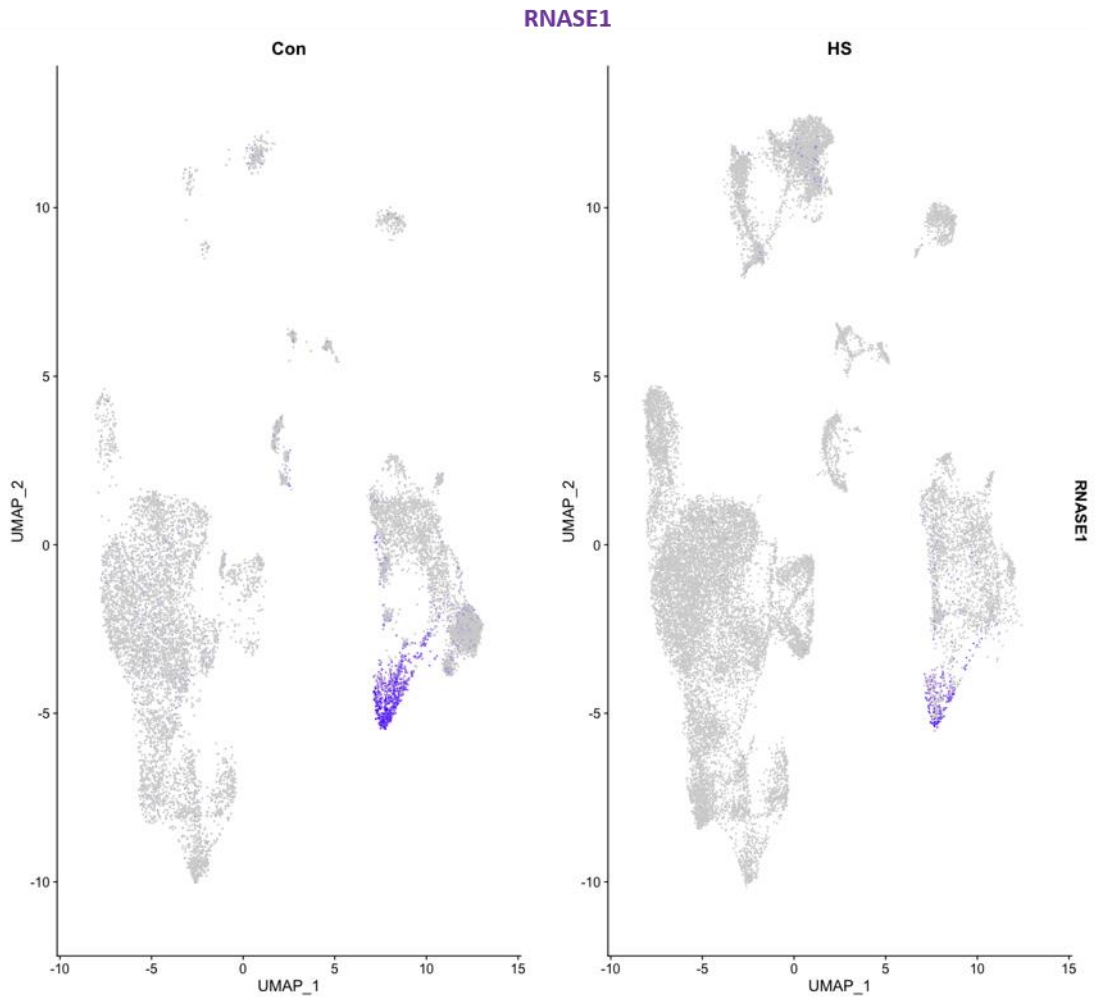


Figure 6.6 UMAP plot for markedly downregulated genes primarily in pDC.

Cells isolated from the skin of healthy controls (Con; n=3) or HS lesional skin (HS; n=6) were purified based on CD45 expression, barcoded and their gene expression determined by scRNA-Seq. UMAP plots display gene expression for Con (left) and HS samples (right) for RNASE1.

Chapter 7

Bibliography

7 Bibliography

- Afzali, B., Mitchell, P. J., Edozie, F. C., Povoleri, G. A., Dowson, S. E., Demandt, L., . . . Lombardi, G. (2013). CD161 expression characterizes a subpopulation of human regulatory T cells that produces IL-17 in a STAT3-dependent manner. *Eur J Immunol*, *43*(8), 2043-2054. doi:10.1002/eji.201243296
- Alavi, A., Farzanfar, D., Rogalska, T., Lowes, M. A., & Chavoshi, S. (2018). Quality of life and sexual health in patients with hidradenitis suppurativa. *Int J Womens Dermatol*, *4*(2), 74-79. doi:10.1016/j.ijwd.2017.10.007
- Alharbi, Z., Kauczok, J., & Pallua, N. (2012). A review of wide surgical excision of hidradenitis suppurativa. *BMC Dermatol*, *12*, 9. doi:10.1186/1471-5945-12-9
- Alikhan, A., Lynch, P. J., & Eisen, D. B. (2009). Hidradenitis suppurativa: a comprehensive review. *J Am Acad Dermatol*, *60*(4), 539-561; quiz 562-533. doi:10.1016/j.jaad.2008.11.911
- Almeida, F. F., & Belz, G. T. (2016). Innate lymphoid cells: models of plasticity for immune homeostasis and rapid responsiveness in protection. *Mucosal Immunol*, *9*(5), 1103-1112. doi:10.1038/mi.2016.64
- Annunziato, F., Cosmi, L., Santarlasci, V., Maggi, L., Liotta, F., Mazzinghi, B., . . . Romagnani, S. (2007). Phenotypic and functional features of human Th17 cells. *J Exp Med*, *204*(8), 1849-1861. doi:10.1084/jem.20070663
- Apetoh, L., Quintana, F. J., Pot, C., Joller, N., Xiao, S., Kumar, D., . . . Kuchroo, V. K. (2010). The aryl hydrocarbon receptor interacts with c-Maf to promote the differentiation of type 1 regulatory T cells induced by IL-27. *Nat Immunol*, *11*(9), 854-861. doi:10.1038/ni.1912
- Aran, D., Looney, A. P., Liu, L., Wu, E., Fong, V., Hsu, A., . . . Bhattacharya, M. (2019). Reference-based analysis of lung single-cell sequencing reveals a transitional profibrotic macrophage. *Nat Immunol*, *20*(2), 163-172. doi:10.1038/s41590-018-0276-y
- Basdeo, S. A., Cluxton, D., Sulaimani, J., Moran, B., Canavan, M., Orr, C., . . . Fletcher, J. M. (2017). Ex-Th17 (Nonclassical Th1) Cells Are Functionally Distinct from Classical Th1 and Th17 Cells and Are Not Constrained by Regulatory T Cells. *J Immunol*, *198*(6), 2249-2259. doi:10.4049/jimmunol.1600737
- Basdeo, S. A., Moran, B., Cluxton, D., Canavan, M., McCormick, J., Connolly, M., . . . Fletcher, J. M. (2015). Polyfunctional, Pathogenic CD161+ Th17 Lineage Cells Are Resistant to Regulatory T Cell-Mediated Suppression in the Context of Autoimmunity. *J Immunol*, *195*(2), 528-540. doi:10.4049/jimmunol.1402990
- Becht, E., McInnes, L., Healy, J., Dutertre, C. A., Kwok, I. W. H., Ng, L. G., . . . Newell, E. W. (2018). Dimensionality reduction for visualizing single-cell data using UMAP. *Nat Biotechnol*. doi:10.1038/nbt.4314
- Bernink, J. H., Ohne, Y., Teunissen, M. B. M., Wang, J., Wu, J., Krabbendam, L., . . . Humbles, A. A. (2019). c-Kit-positive ILC2s exhibit an ILC3-like signature that may contribute to IL-17-mediated pathologies. *Nat Immunol*, *20*(8), 992-1003. doi:10.1038/s41590-019-0423-0
- Blanco, R., Martinez-Taboada, V. M., Villa, I., Gonzalez-Vela, M. C., Fernandez-Llaca, H., Agudo, M., & Gonzalez-Lopez, M. A. (2009). Long-term successful adalimumab therapy in severe hidradenitis suppurativa. *Arch Dermatol*, *145*(5), 580-584. doi:10.1001/archdermatol.2009.49
- Blighe, K. R., S; Lewis, M. (2020). EnhancedVolcano: Publication-ready volcano plots with enhanced colouring and labeling. <https://github.com/kevinblighe/EnhancedVolcano>.
- Blok, J. L., Li, K., Brodmerkel, C., Horvatovich, P., Jonkman, M. F., & Horvath, B. (2016). Ustekinumab in hidradenitis suppurativa: clinical results and a search for potential biomarkers in serum. *Br J Dermatol*, *174*(4), 839-846. doi:10.1111/bjd.14338

- Blondel VD, G. J., Lambiotte R, Lefebvre E. (2008). Fast Unfolding of Communities in Large Networks. *Journal of Statistical Mechanics: Theory and Experiment*, 10.
- Boulouvar, S., Michelet, X., Duquette, D., Alvarez, D., Hogan, A. E., Dold, C., . . . Lynch, L. (2017). Adipose Type One Innate Lymphoid Cells Regulate Macrophage Homeostasis through Targeted Cytotoxicity. *Immunity*, 46(2), 273-286. doi:10.1016/j.immuni.2017.01.008
- Brand, S. (2009). Crohn's disease: Th1, Th17 or both? The change of a paradigm: new immunological and genetic insights implicate Th17 cells in the pathogenesis of Crohn's disease. *Gut*, 58(8), 1152-1167. doi:10.1136/gut.2008.163667
- Brembilla, N. C., Senra, L., & Boehncke, W. H. (2018). The IL-17 Family of Cytokines in Psoriasis: IL-17A and Beyond. *Front Immunol*, 9, 1682. doi:10.3389/fimmu.2018.01682
- Brinkmann, V., Reichard, U., Goosmann, C., Fauler, B., Uhlemann, Y., Weiss, D. S., . . . Zychlinsky, A. (2004). Neutrophil extracellular traps kill bacteria. *Science*, 303(5663), 1532-1535. doi:10.1126/science.1092385
- Buckland, K. (2020). Basophils.
- Byrd, A. S., Carmona-Rivera, C., O'Neil, L. J., Carlucci, P. M., Cisar, C., Rosenberg, A. Z., . . . Kaplan, M. J. (2019). Neutrophil extracellular traps, B cells, and type I interferons contribute to immune dysregulation in hidradenitis suppurativa. *Sci Transl Med*, 11(508). doi:10.1126/scitranslmed.aav5908
- Cai, Y., Shen, X., Ding, C., Qi, C., Li, K., Li, X., . . . Yan, J. (2011). Pivotal role of dermal IL-17-producing gammadelta T cells in skin inflammation. *Immunity*, 35(4), 596-610. doi:10.1016/j.immuni.2011.08.001
- Calao, M., Wilson, J. L., Spelman, L., Billot, L., Rubel, D., Watts, A. D., & Jemec, G. B. E. (2018). Hidradenitis Suppurativa (HS) prevalence, demographics and management pathways in Australia: A population-based cross-sectional study. *PLoS One*, 13(7), e0200683. doi:10.1371/journal.pone.0200683
- Canavan, M., Walsh, A. M., Bhargava, V., Wade, S. M., McGarry, T., Marzaioli, V., . . . Fearon, U. (2018). Enriched Cd141+ DCs in the joint are transcriptionally distinct, activated, and contribute to joint pathogenesis. *JCI Insight*, 3(23). doi:10.1172/jci.insight.95228
- Canoui-Poitrine, F., Revuz, J. E., Wolkenstein, P., Viallette, C., Gabison, G., Pouget, F., . . . Bastuji-Garin, S. (2009). Clinical characteristics of a series of 302 French patients with hidradenitis suppurativa, with an analysis of factors associated with disease severity. *J Am Acad Dermatol*, 61(1), 51-57. doi:10.1016/j.jaad.2009.02.013
- Caproni, M., Antiga, E., Volpi, W., Verdelli, A., Venegoni, L., Quaglino, P., . . . Marzano, A. V. (2015). The Treg/Th17 cell ratio is reduced in the skin lesions of patients with pyoderma gangrenosum. *Br J Dermatol*, 173(1), 275-278. doi:10.1111/bjd.13670
- Carmi-Levy, I., Homey, B., & Soumelis, V. (2011). A modular view of cytokine networks in atopic dermatitis. *Clin Rev Allergy Immunol*, 41(3), 245-253. doi:10.1007/s12016-010-8239-6
- Carolan, E., Tobin, L. M., Mangan, B. A., Corrigan, M., Gaoatswe, G., Byrne, G., . . . Hogan, A. E. (2015). Altered distribution and increased IL-17 production by mucosal-associated invariant T cells in adult and childhood obesity. *J Immunol*, 194(12), 5775-5780. doi:10.4049/jimmunol.1402945
- Cheuk, S., Schlums, H., Gallais Serezal, I., Martini, E., Chiang, S. C., Marquardt, N., . . . Eidsmo, L. (2017). CD49a Expression Defines Tissue-Resident CD8+ T Cells Poised for Cytotoxic Function in Human Skin. *Immunity*. doi:10.1016/j.immuni.2017.01.009
- Cheuk, S., Wiken, M., Blomqvist, L., Nysten, S., Talme, T., Stahle, M., & Eidsmo, L. (2014). Epidermal Th22 and Tc17 cells form a localized disease memory in clinically healed psoriasis. *J Immunol*, 192(7), 3111-3120. doi:10.4049/jimmunol.1302313
- Chiba, A., Murayama, G., & Miyake, S. (2018). Mucosal-Associated Invariant T Cells in Autoimmune Diseases. *Front Immunol*, 9, 1333. doi:10.3389/fimmu.2018.01333

- Chiricozzi, A., Guttman-Yassky, E., Suarez-Farinas, M., Nograles, K. E., Tian, S., Cardinale, I., . . . Krueger, J. G. (2011). Integrative responses to IL-17 and TNF-alpha in human keratinocytes account for key inflammatory pathogenic circuits in psoriasis. *J Invest Dermatol*, *131*(3), 677-687. doi:10.1038/jid.2010.340
- Church, J. M., Fazio, V. W., Lavery, I. C., Oakley, J. R., & Milsom, J. W. (1993). The differential diagnosis and comorbidity of hidradenitis suppurativa and perianal Crohn's disease. *Int J Colorectal Dis*, *8*(3), 117-119.
- Cibrian, D., Saiz, M. L., de la Fuente, H., Sanchez-Diaz, R., Moreno-Gonzalo, O., Jorge, I., . . . Sanchez-Madrid, F. (2016). CD69 controls the uptake of L-tryptophan through LAT1-CD98 and AhR-dependent secretion of IL-22 in psoriasis. *Nat Immunol*, *17*(8), 985-996. doi:10.1038/ni.3504
- Clark, A. K., Quinonez, R. L., Saric, S., & Sivamani, R. K. (2017). Hormonal therapies for hidradenitis suppurativa: Review. *Dermatol Online J*, *23*(10).
- Clark, R. A., Chong, B., Mirchandani, N., Brinster, N. K., Yamanaka, K., Dowgiert, R. K., & Kupper, T. S. (2006). The vast majority of CLA+ T cells are resident in normal skin. *J Immunol*, *176*(7), 4431-4439. doi:10.4049/jimmunol.176.7.4431
- Clark, R. A., Chong, B. F., Mirchandani, N., Yamanaka, K., Murphy, G. F., Dowgiert, R. K., & Kupper, T. S. (2006). A novel method for the isolation of skin resident T cells from normal and diseased human skin. *J Invest Dermatol*, *126*(5), 1059-1070. doi:10.1038/sj.jid.5700199
- Codarri, L., Gyulveszi, G., Tosevski, V., Hesske, L., Fontana, A., Magnenat, L., . . . Becher, B. (2011). RORgammat drives production of the cytokine GM-CSF in helper T cells, which is essential for the effector phase of autoimmune neuroinflammation. *Nat Immunol*, *12*(6), 560-567. doi:10.1038/ni.2027
- Cole, S., & Maroof, A. (2019). P089 Mucosal-associated invariant T (MAIT)-cell-derived IL-17A and IL-17F production is IL-23-independent and biased towards IL-17F. *Ann Rheum Dis*, *78*(Suppl 1), A38-A39. doi:10.1136/annrheumdis-2018-EWRR2019.78
- Coll, R. C., Robertson, A. A., Chae, J. J., Higgins, S. C., Muñoz-Planillo, R., Inserra, M. C., . . . O'Neill, L. A. (2015). A small-molecule inhibitor of the NLRP3 inflammasome for the treatment of inflammatory diseases. *Nat Med*, *21*(3), 248-255. doi:10.1038/nm.3806
- Conrad, C., Di Domizio, J., Mylonas, A., Belkhdja, C., Demaria, O., Navarini, A. A., . . . Gilliet, M. (2018). TNF blockade induces a dysregulated type I interferon response without autoimmunity in paradoxical psoriasis. *Nat Commun*, *9*(1), 25. doi:10.1038/s41467-017-02466-4
- Cook, A. D., & Hamilton, J. A. (2018). Investigational therapies targeting the granulocyte macrophage colony-stimulating factor receptor-alpha in rheumatoid arthritis: focus on mavrilimumab. *Ther Adv Musculoskelet Dis*, *10*(2), 29-38. doi:10.1177/1759720x17752036
- Coquet, J. M., Chakravarti, S., Kyparissoudis, K., McNab, F. W., Pitt, L. A., McKenzie, B. S., . . . Godfrey, D. I. (2008). Diverse cytokine production by NKT cell subsets and identification of an IL-17-producing CD4-NK1.1- NKT cell population. *Proc Natl Acad Sci U S A*, *105*(32), 11287-11292. doi:10.1073/pnas.0801631105
- Cosmi, L., De Palma, R., Santarlasci, V., Maggi, L., Capone, M., Frosali, F., . . . Annunziato, F. (2008). Human interleukin 17-producing cells originate from a CD161+CD4+ T cell precursor. *J Exp Med*, *205*(8), 1903-1916. doi:10.1084/jem.20080397
- Deckers, I. E., Janse, I. C., van der Zee, H. H., Nijsten, T., Boer, J., Horvath, B., & Prens, E. P. (2016). Hidradenitis suppurativa (HS) is associated with low socioeconomic status (SES): A cross-sectional reference study. *J Am Acad Dermatol*, *75*(4), 755-759.e751. doi:10.1016/j.jaad.2016.04.067

- Di Caprio, R., Balato, A., Caiazzo, G., Lembo, S., Raimondo, A., Fabbrocini, G., & Monfrecola, G. (2017). IL-36 cytokines are increased in acne and hidradenitis suppurativa. *Arch Dermatol Res*. doi:10.1007/s00403-017-1769-5
- Dias, J., Boulouis, C., Gorin, J. B., van den Biggelaar, R., Lal, K. G., Gibbs, A., . . . Leeansyah, E. (2018). The CD4(-)CD8(-) MAIT cell subpopulation is a functionally distinct subset developmentally related to the main CD8(+) MAIT cell pool. *Proc Natl Acad Sci U S A*, *115*(49), E11513-e11522. doi:10.1073/pnas.1812273115
- Doisne, J. M., Becourt, C., Amniai, L., Duarte, N., Le Luduec, J. B., Eberl, G., & Benlagha, K. (2009). Skin and peripheral lymph node invariant NKT cells are mainly retinoic acid receptor-related orphan receptor (gamma)t+ and respond preferentially under inflammatory conditions. *J Immunol*, *183*(3), 2142-2149. doi:10.4049/jimmunol.0901059
- Dominguez-Villar, M., & Hafler, D. A. (2018). Regulatory T cells in autoimmune disease. *Nat Immunol*, *19*(7), 665-673. doi:10.1038/s41590-018-0120-4
- Dowell, A. C., Cobby, E., Wen, K., Devall, A. J., During, V., Anderson, J., . . . Taylor, G. S. (2017). Interleukin-17-positive mast cells influence outcomes from BCG for patients with CIS: Data from a comprehensive characterisation of the immune microenvironment of urothelial bladder cancer. *PLoS One*, *12*(9), e0184841. doi:10.1371/journal.pone.0184841
- Dusseaux, M., Martin, E., Serriari, N., Peguillet, I., Premel, V., Louis, D., . . . Lantz, O. (2011). Human MAIT cells are xenobiotic-resistant, tissue-targeted, CD161hi IL-17-secreting T cells. *Blood*, *117*(4), 1250-1259. doi:10.1182/blood-2010-08-303339
- Esmann, S., & Jemec, G. B. (2016). Assessing the quality of life over longer periods. *J Eur Acad Dermatol Venereol*, *30*(1), 189-190. doi:10.1111/jdv.12700
- Eyerich, K., & Eyerich, S. (2015). Th22 cells in allergic disease. *Allergo J Int*, *24*(1), 1-7. doi:10.1007/s40629-015-0039-3
- Eyerich, S., Eyerich, K., Pennino, D., Carbone, T., Nasorri, F., Pallotta, S., . . . Cavani, A. (2009). Th22 cells represent a distinct human T cell subset involved in epidermal immunity and remodeling. *J Clin Invest*, *119*(12), 3573-3585. doi:10.1172/jci40202
- Fei, M., Bhatia, S., Oriss, T. B., Yarlagaadda, M., Khare, A., Akira, S., . . . Ray, A. (2011). TNF-alpha from inflammatory dendritic cells (DCs) regulates lung IL-17A/IL-5 levels and neutrophilia versus eosinophilia during persistent fungal infection. *Proc Natl Acad Sci U S A*, *108*(13), 5360-5365. doi:10.1073/pnas.1015476108
- Fletcher, J. M., Lonergan, R., Costelloe, L., Kinsella, K., Moran, B., O'Farrelly, C., . . . Mills, K. H. (2009). CD39+Foxp3+ regulatory T Cells suppress pathogenic Th17 cells and are impaired in multiple sclerosis. *J Immunol*, *183*(11), 7602-7610. doi:10.4049/jimmunol.0901881
- Fobelo Lozano, M. J., Serrano Gimenez, R., & Castro Fernandez, M. (2018). Emergence of Inflammatory Bowel Disease During Treatment with Secukinumab. *J Crohns Colitis*. doi:10.1093/ecco-jcc/jjy063
- Franco, C. B., Chen, C. C., Drukker, M., Weissman, I. L., & Galli, S. J. (2010). Distinguishing mast cell and granulocyte differentiation at the single-cell level. *Cell Stem Cell*, *6*(4), 361-368. doi:10.1016/j.stem.2010.02.013
- Fujino, S., Andoh, A., Bamba, S., Ogawa, A., Hata, K., Araki, Y., . . . Fujiyama, Y. (2003). Increased expression of interleukin 17 in inflammatory bowel disease. *Gut*, *52*(1), 65-70. doi:10.1136/gut.52.1.65
- Fujita, H., Nograles, K. E., Kikuchi, T., Gonzalez, J., Carucci, J. A., & Krueger, J. G. (2009). Human Langerhans cells induce distinct IL-22-producing CD4+ T cells lacking IL-17 production. *Proc Natl Acad Sci U S A*, *106*(51), 21795-21800. doi:10.1073/pnas.0911472106
- Gaffen, S. L. (2009). Structure and signalling in the IL-17 receptor family. *Nat Rev Immunol*, *9*(8), 556-567. doi:10.1038/nri2586

- Gao, X., Arpin, C., Marvel, J., Prokopiou, S. A., Gandrillon, O., & Crauste, F. (2016). IL-2 sensitivity and exogenous IL-2 concentration gradient tune the productive contact duration of CD8(+) T cell-APC: a multiscale modeling study. *BMC Syst Biol*, *10*(1), 77. doi:10.1186/s12918-016-0323-y
- Garg, A., Hundal, J., & Strunk, A. (2018). Overall and Subgroup Prevalence of Crohn Disease Among Patients With Hidradenitis Suppurativa: A Population-Based Analysis in the United States. *JAMA Dermatol*, *154*(7), 814-818. doi:10.1001/jamadermatol.2018.0878
- Garg, A., Kirby, J. S., Lavian, J., Lin, G., & Strunk, A. (2017). Sex- and Age-Adjusted Population Analysis of Prevalence Estimates for Hidradenitis Suppurativa in the United States. *JAMA Dermatol*, *153*(8), 760-764. doi:10.1001/jamadermatol.2017.0201
- Garg, A., Papagermanos, V., Midura, M., & Strunk, A. (2018). Incidence of hidradenitis suppurativa among tobacco smokers: a population-based retrospective analysis in the U.S.A. *Br J Dermatol*, *178*(3), 709-714. doi:10.1111/bjd.15939
- Gehad, A., Teague, J. E., Matos, T. R., Huang, V., Yang, C., Watanabe, R., . . . Clark, R. A. (2018). A primary role for human central memory cells in tissue immunosurveillance. *Blood Adv*, *2*(3), 292-298. doi:10.1182/bloodadvances.2017011346
- Giamarellos-Bourboulis, E. J., Platzer, M., Karagiannidis, I., Kanni, T., Nikolakis, G., Ulrich, J., . . . Huse, K. (2016). High Copy Numbers of beta-Defensin Cluster on 8p23.1, Confer Genetic Susceptibility, and Modulate the Physical Course of Hidradenitis Suppurativa/Acne Inversa. *J Invest Dermatol*, *136*(8), 1592-1598. doi:10.1016/j.jid.2016.04.021
- Giatrakos, S., Huse, K., Kanni, T., Tzanetakou, V., Kramer, M., Grech, I., . . . Giamarellos-Bourboulis, E. J. (2013). Haplotypes of IL-12Rbeta1 impact on the clinical phenotype of hidradenitis suppurativa. *Cytokine*, *62*(2), 297-301. doi:10.1016/j.cyto.2013.03.008
- Ginhoux, F., Tacke, F., Angeli, V., Bogunovic, M., Loubeau, M., Dai, X. M., . . . Merad, M. (2006). Langerhans cells arise from monocytes in vivo. *Nat Immunol*, *7*(3), 265-273. doi:10.1038/ni1307
- Giudici, F., Maggi, L., Santi, R., Cosmi, L., Annunziato, F., Nesi, G., . . . Tonelli, F. (2015). Perianal Crohn's disease and hidradenitis suppurativa: a possible common immunological scenario. *Clin Mol Allergy*, *13*(1), 12. doi:10.1186/s12948-015-0018-8
- Gkini, M. A., & Bewley, A. P. (2018). Development of hidradenitis suppurativa in a patient treated with ustekinumab for her psoriasis: A potential paradoxical reaction? *Dermatol Ther*, *31*(6), e12742. doi:10.1111/dth.12742
- Goepfert, A., Lehmann, S., Blank, J., Kolbinger, F., & Rondeau, J. M. (2020). Structural Analysis Reveals that the Cytokine IL-17F Forms a Homodimeric Complex with Receptor IL-17RC to Drive IL-17RA-Independent Signaling. *Immunity*, *52*(3), 499-512.e495. doi:10.1016/j.immuni.2020.02.004
- Gold, M. C., Napier, R. J., & Lewinsohn, D. M. (2015). MR1-restricted mucosal associated invariant T (MAIT) cells in the immune response to Mycobacterium tuberculosis. *Immunol Rev*, *264*(1), 154-166. doi:10.1111/imr.12271
- Gomez Perdiguero, E., Klapproth, K., Schulz, C., Busch, K., Azzoni, E., Crozet, L., . . . Rodewald, H. R. (2015). Tissue-resident macrophages originate from yolk-sac-derived erythromyeloid progenitors. *Nature*, *518*(7540), 547-551. doi:10.1038/nature13989
- Gracey, E., Qiayum, Z., Almaghlouth, I., Lawson, D., Karki, S., Avvaru, N., . . . Inman, R. D. (2016). IL-7 primes IL-17 in mucosal-associated invariant T (MAIT) cells, which contribute to the Th17-axis in ankylosing spondylitis. *Ann Rheum Dis*, *75*(12), 2124-2132. doi:10.1136/annrheumdis-2015-208902
- Grant, A., Gonzalez, T., Montgomery, M. O., Cardenas, V., & Kerdel, F. A. (2010). Infliximab therapy for patients with moderate to severe hidradenitis suppurativa: a randomized,

- double-blind, placebo-controlled crossover trial. *J Am Acad Dermatol*, 62(2), 205-217. doi:10.1016/j.jaad.2009.06.050
- Guggino, G., Ciccia, F., Di Liberto, D., Lo Pizzo, M., Ruscitti, P., Cipriani, P., . . . Triolo, G. (2016). Interleukin (IL)-9/IL-9R axis drives gammadelta T cells activation in psoriatic arthritis patients. *Clin Exp Immunol*, 186(3), 277-283. doi:10.1111/cei.12853
- Gutiérrez-Martínez, E., Planès, R., Anselmi, G., Reynolds, M., Menezes, S., Adiko, A. C., . . . Guermonprez, P. (2015). Cross-Presentation of Cell-Associated Antigens by MHC Class I in Dendritic Cell Subsets. *Front Immunol*, 6(363). doi:10.3389/fimmu.2015.00363
- Guttman-Yassky, E., & Krueger, J. G. (2018). IL-17C: A Unique Epithelial Cytokine with Potential for Targeting across the Spectrum of Atopic Dermatitis and Psoriasis. *J Invest Dermatol*, 138(7), 1467-1469. doi:10.1016/j.jid.2018.02.037
- Hafemeister, C., & Satija, R. (2019). Normalization and variance stabilization of single-cell RNA-seq data using regularized negative binomial regression. *Genome Biol*, 20(1), 296. doi:10.1186/s13059-019-1874-1
- Hana, A., Booken, D., Henrich, C., Gratchev, A., Maas-Szabowski, N., Goerdts, S., & Kurzen, H. (2007). Functional significance of non-neuronal acetylcholine in skin epithelia. *Life Sci*, 80(24-25), 2214-2220. doi:10.1016/j.lfs.2007.02.007
- Harrington, L. E., Hatton, R. D., Mangan, P. R., Turner, H., Murphy, T. L., Murphy, K. M., & Weaver, C. T. (2005). Interleukin 17-producing CD4+ effector T cells develop via a lineage distinct from the T helper type 1 and 2 lineages. *Nat Immunol*, 6(11), 1123-1132. doi:10.1038/ni1254
- Haygreen, E. (2020). NKT Cells: Invariant [Web blog]. (2020). Retrieved from <https://www.immunology.org/public-information/bitesized-immunology/cells/nkt-cells-invariant>
- Hessam, S., Sand, M., Gambichler, T., Skrygan, M., Ruddel, I., & Bechara, F. G. (2018). Interleukin-36 in hidradenitis suppurativa: evidence for a distinctive proinflammatory role and a key factor in the development of an inflammatory loop. *Br J Dermatol*, 178(3), 761-767. doi:10.1111/bjd.16019
- Higgins, R., Pink, A., Hunger, R., Yawalkar, N., & Navarini, A. A. (2017). Generalized Comedones, Acne, and Hidradenitis Suppurativa in a Patient with an FGFR2 Missense Mutation. *Front Med (Lausanne)*, 4, 16. doi:10.3389/fmed.2017.00016
- Ho, A. W., & Kupper, T. S. (2019). T cells and the skin: from protective immunity to inflammatory skin disorders. *Nat Rev Immunol*, 19(8), 490-502. doi:10.1038/s41577-019-0162-3
- Hoeffel, G., Wang, Y., Greter, M., See, P., Teo, P., Malleret, B., . . . Ginhoux, F. (2012). Adult Langerhans cells derive predominantly from embryonic fetal liver monocytes with a minor contribution of yolk sac-derived macrophages. *J Exp Med*, 209(6), 1167-1181. doi:10.1084/jem.20120340
- Hoffman, L. K., Ghias, M. H., & Lowes, M. A. (2017). Pathophysiology of hidradenitis suppurativa. *Semin Cutan Med Surg*, 36(2), 47-54. doi:10.12788/j.sder.2017.017
- Hotz, C., Boniotto, M., Guguin, A., Surenaud, M., Jean-Louis, F., Tisserand, P., . . . Hue, S. (2016). Intrinsic Defect in Keratinocyte Function Leads to Inflammation in Hidradenitis Suppurativa. *J Invest Dermatol*, 136(9), 1768-1780. doi:10.1016/j.jid.2016.04.036
- Hoxie, J. A., Matthews, D. M., Callahan, K. J., Cassel, D. L., & Cooper, R. A. (1986). Transient modulation and internalization of T4 antigen induced by phorbol esters. *J Immunol*, 137(4), 1194-1201.
- Hueber, W., Sands, B. E., Lewitzky, S., Vandemeulebroecke, M., Reinisch, W., Higgins, P. D., . . . Travis, S. P. (2012). Secukinumab, a human anti-IL-17A monoclonal antibody, for moderate to severe Crohn's disease: unexpected results of a randomised, double-blind placebo-controlled trial. *Gut*, 61(12), 1693-1700. doi:10.1136/gutjnl-2011-301668

- Hunger, R. E., Surovy, A. M., Hassan, A. S., Braathen, L. R., & Yawalkar, N. (2008). Toll-like receptor 2 is highly expressed in lesions of acne inversa and colocalizes with C-type lectin receptor. *Br J Dermatol*, *158*(4), 691-697. doi:10.1111/j.1365-2133.2007.08425.x
- Jain, N., Nguyen, H., Chambers, C., & Kang, J. (2010). Dual function of CTLA-4 in regulatory T cells and conventional T cells to prevent multiorgan autoimmunity. *Proc Natl Acad Sci U S A*, *107*(4), 1524-1528. doi:10.1073/pnas.0910341107
- Jemec, G. B. (2012). Clinical practice. Hidradenitis suppurativa. *N Engl J Med*, *366*(2), 158-164. doi:10.1056/NEJMcp1014163
- Jemec, G. B., Heidenheim, M., & Nielsen, N. H. (1996a). A case-control study of hidradenitis suppurativa in an STD population. *Acta Derm Venereol*, *76*(6), 482-483. doi:10.2340/0001555576482483
- Jemec, G. B., Heidenheim, M., & Nielsen, N. H. (1996b). Hidradenitis suppurativa--characteristics and consequences. *Clin Exp Dermatol*, *21*(6), 419-423.
- Johansen, C., Riis, J. L., Gedebjerg, A., Kragballe, K., & Iversen, L. (2011). Tumor necrosis factor alpha-mediated induction of interleukin 17C in human keratinocytes is controlled by nuclear factor kappaB. *J Biol Chem*, *286*(29), 25487-25494. doi:10.1074/jbc.M111.240671
- Johnston, A., Fritz, Y., Dawes, S. M., Diaconu, D., Al-Attar, P. M., Guzman, A. M., . . . Ward, N. L. (2013). Keratinocyte overexpression of IL-17C promotes psoriasiform skin inflammation. *J Immunol*, *190*(5), 2252-2262. doi:10.4049/jimmunol.1201505
- Kabashima, K., Honda, T., Ginhoux, F., & Egawa, G. (2019). The immunological anatomy of the skin. *Nat Rev Immunol*, *19*(1), 19-30. doi:10.1038/s41577-018-0084-5
- Kang, H., Wu, W. Y., Lo, B. K., Yu, M., Leung, G., Shapiro, J., & McElwee, K. J. (2010). Hair follicles from alopecia areata patients exhibit alterations in immune privilege-associated gene expression in advance of hair loss. *J Invest Dermatol*, *130*(11), 2677-2680. doi:10.1038/jid.2010.180
- Kashem, S. W., Haniffa, M., & Kaplan, D. H. (2017). Antigen-Presenting Cells in the Skin. *Annu Rev Immunol*, *35*, 469-499. doi:10.1146/annurev-immunol-051116-052215
- Katsanos, K. H., Christodoulou, D. K., & Tsianos, E. V. (2002). Axillary hidradenitis suppurativa successfully treated with infliximab in a Crohn's disease patient. *Am J Gastroenterol*, *97*(8), 2155-2156. doi:10.1111/j.1572-0241.2002.05950.x
- Keary, E., Hevey, D., & Tobin, A. M. (2019). A qualitative analysis of psychological distress in Hidradenitis Suppurativa. *Br J Dermatol*. doi:10.1111/bjd.18135
- Kelly, G., Hughes, R., McGarry, T., van den Born, M., Adamzik, K., Fitzgerald, R., . . . Kirby, B. (2015). Dysregulated cytokine expression in lesional and nonlesional skin in hidradenitis suppurativa. *Br J Dermatol*, *173*(6), 1431-1439. doi:10.1111/bjd.14075
- Kelly, M. E., Heneghan, H. M., McDermott, F. D., Nason, G. J., Freeman, C., Martin, S. T., & Winter, D. C. (2014). The role of loose seton in the management of anal fistula: a multicenter study of 200 patients. *Tech Coloproctol*, *18*(10), 915-919. doi:10.1007/s10151-014-1186-0
- Kimball, A. B., Jemec, G. B., Yang, M., Kageleiry, A., Signorovitch, J. E., Okun, M. M., . . . Sundaram, M. (2014). Assessing the validity, responsiveness and meaningfulness of the Hidradenitis Suppurativa Clinical Response (HiSCR) as the clinical endpoint for hidradenitis suppurativa treatment. *Br J Dermatol*, *171*(6), 1434-1442. doi:10.1111/bjd.13270
- Kimball, A. B., Kerdel, F., Adams, D., Mrowietz, U., Gelfand, J. M., Gniadecki, R., . . . Jemec, G. B. (2012). Adalimumab for the treatment of moderate to severe Hidradenitis suppurativa: a parallel randomized trial. *Ann Intern Med*, *157*(12), 846-855. doi:10.7326/0003-4819-157-12-201212180-00004

- Kimball, A. B., Okun, M. M., Williams, D. A., Gottlieb, A. B., Papp, K. A., Zouboulis, C. C., . . . Jemec, G. B. (2016). Two Phase 3 Trials of Adalimumab for Hidradenitis Suppurativa. *N Engl J Med*, *375*(5), 422-434. doi:10.1056/NEJMoa1504370
- Kjaersgaard Andersen, R., Ring, H. C., Kallenbach, K., Eriksen, J. O., & Jemec, G. B. E. (2019). Bacterial biofilm is associated with higher levels of regulatory T cells in unaffected hidradenitis suppurativa skin. *Exp Dermatol*, *28*(3), 312-316. doi:10.1111/exd.13885
- Klareskog, L., Malmstrom, V., Lundberg, K., Padyukov, L., & Alfredsson, L. (2011). Smoking, citrullination and genetic variability in the immunopathogenesis of rheumatoid arthritis. *Semin Immunol*, *23*(2), 92-98. doi:10.1016/j.smim.2011.01.014
- Klicznik, M. M., Morawski, P. A., Höllbacher, B., Varkhande, S. R., Motley, S. J., Kuri-Cervantes, L., . . . Gratz, I. K. (2019). Human CD4(+)CD103(+) cutaneous resident memory T cells are found in the circulation of healthy individuals. *Sci Immunol*, *4*(37). doi:10.1126/sciimmunol.aav8995
- Korsunsky, I., Millard, N., Fan, J., Slowikowski, K., Zhang, F., Wei, K., . . . Raychaudhuri, S. (2019). Fast, sensitive and accurate integration of single-cell data with Harmony. *Nat Methods*, *16*(12), 1289-1296. doi:10.1038/s41592-019-0619-0
- Krejci, J., Casneuf, T., Nijhof, I. S., Verbist, B., Bald, J., Plesner, T., . . . Sasser, A. K. (2016). Daratumumab depletes CD38+ immune regulatory cells, promotes T-cell expansion, and skews T-cell repertoire in multiple myeloma. *Blood*, *128*(3), 384-394. doi:10.1182/blood-2015-12-687749
- Krovi, S. H., & Gapin, L. (2018). Invariant Natural Killer T Cell Subsets-More Than Just Developmental Intermediates. *Front Immunol*, *9*, 1393. doi:10.3389/fimmu.2018.01393
- Kubo, A., Nagao, K., Yokouchi, M., Sasaki, H., & Amagai, M. (2009). External antigen uptake by Langerhans cells with reorganization of epidermal tight junction barriers. *J Exp Med*, *206*(13), 2937-2946. doi:10.1084/jem.20091527
- Kumar, B. V., Ma, W., Miron, M., Granot, T., Guyer, R. S., Carpenter, D. J., . . . Farber, D. L. (2017). Human Tissue-Resident Memory T Cells Are Defined by Core Transcriptional and Functional Signatures in Lymphoid and Mucosal Sites. *Cell Rep*, *20*(12), 2921-2934. doi:10.1016/j.celrep.2017.08.078
- Kurioka, A., Cosgrove, C., Simoni, Y., van Wilgenburg, B., Geremia, A., Björkander, S., . . . Klenerman, P. (2018). CD161 Defines a Functionally Distinct Subset of Pro-Inflammatory Natural Killer Cells. *Front Immunol*, *9*, 486. doi:10.3389/fimmu.2018.00486
- Laggner, U., Di Meglio, P., Perera, G. K., Hundhausen, C., Lacy, K. E., Ali, N., . . . Nestle, F. O. (2011). Identification of a novel proinflammatory human skin-homing Vgamma9Vdelta2 T cell subset with a potential role in psoriasis. *J Immunol*, *187*(5), 2783-2793. doi:10.4049/jimmunol.1100804
- Lajevardi, S. S., & Abeysinghe, J. (2015). Novel Technique for Management of Axillary Hidradenitis Suppurativa Using Setons. *Case Rep Surg*, *2015*, 369657. doi:10.1155/2015/369657
- Lalor, S. J., Dungan, L. S., Sutton, C. E., Basdeo, S. A., Fletcher, J. M., & Mills, K. H. (2011). Caspase-1-processed cytokines IL-1beta and IL-18 promote IL-17 production by gammadelta and CD4 T cells that mediate autoimmunity. *J Immunol*, *186*(10), 5738-5748. doi:10.4049/jimmunol.1003597
- Lam, L., Chin, L., Halder, R. C., Sagong, B., Famenini, S., Sayre, J., . . . Fiala, M. (2016). Epigenetic changes in T-cell and monocyte signatures and production of neurotoxic cytokines in ALS patients. *Faseb j*. doi:10.1096/fj.201600259RR
- Lande, R., Botti, E., Jandus, C., Dojcinovic, D., Fanelli, G., Conrad, C., . . . Frasca, L. (2014). The antimicrobial peptide LL37 is a T-cell autoantigen in psoriasis. *Nat Commun*, *5*, 5621. doi:10.1038/ncomms6621

- Langrish, C. L., Chen, Y., Blumenschein, W. M., Mattson, J., Basham, B., Sedgwick, J. D., . . . Cua, D. J. (2005). IL-23 drives a pathogenic T cell population that induces autoimmune inflammation. *J Exp Med*, *201*(2), 233-240. doi:10.1084/jem.20041257
- Lawand, M., Déchanet-Merville, J., & Dieu-Nosjean, M. C. (2017). Key Features of Gamma-Delta T-Cell Subsets in Human Diseases and Their Immunotherapeutic Implications. *Front Immunol*, *8*, 761. doi:10.3389/fimmu.2017.00761
- Lee, Y., Clinton, J., Yao, C., & Chang, S. H. (2019). Interleukin-17D Promotes Pathogenicity During Infection by Suppressing CD8 T Cell Activity. *Front Immunol*, *10*, 1172. doi:10.3389/fimmu.2019.01172
- Lee, Y. J., Holzapfel, K. L., Zhu, J., Jameson, S. C., & Hogquist, K. A. (2013). Steady-state production of IL-4 modulates immunity in mouse strains and is determined by lineage diversity of iNKT cells. *Nat Immunol*, *14*(11), 1146-1154. doi:10.1038/ni.2731
- Lexberg, M. H., Taubner, A., Albrecht, I., Lepenies, I., Richter, A., Kamradt, T., . . . Chang, H. D. (2010). IFN- γ and IL-12 synergize to convert in vivo generated Th17 into Th1/Th17 cells. *Eur J Immunol*, *40*(11), 3017-3027. doi:10.1002/eji.201040539
- Ley, K. (2017). M1 Means Kill; M2 Means Heal. *J Immunol*, *199*(7), 2191-2193. doi:10.4049/jimmunol.1701135
- Li, J., Reantragoon, R., Kostenko, L., Corbett, A. J., Varigos, G., & Carbone, F. R. (2017). The frequency of mucosal-associated invariant T cells is selectively increased in dermatitis herpetiformis. *Australas J Dermatol*, *58*(3), 200-204. doi:10.1111/ajd.12456
- Li, S., Joseph, C., Becourt, C., Klibi, J., Luce, S., Dubois-Laforgue, D., . . . Benlagha, K. (2014). Potential role of IL-17-producing iNKT cells in type 1 diabetes. *PLoS One*, *9*(4), e96151. doi:10.1371/journal.pone.0096151
- Li, T., Wen, H., Brayton, C., Das, P., Smithson, L. A., Fauq, A., . . . Wong, P. C. (2007). Epidermal growth factor receptor and notch pathways participate in the tumor suppressor function of gamma-secretase. *J Biol Chem*, *282*(44), 32264-32273. doi:10.1074/jbc.M703649200
- Lima, A. L., Karl, I., Giner, T., Poppe, H., Schmidt, M., Presser, D., . . . Bauer, B. (2015). Keratinocytes and neutrophils are important sources of proinflammatory molecules in hidradenitis suppurativa. *Br J Dermatol*. doi:10.1111/bjd.14214
- Lin, A. M., Rubin, C. J., Khandpur, R., Wang, J. Y., Riblett, M., Yalavarthi, S., . . . Bruce, A. T. (2011). Mast cells and neutrophils release IL-17 through extracellular trap formation in psoriasis. *J Immunol*, *187*(1), 490-500. doi:10.4049/jimmunol.1100123
- Liu, M., Davis, J. W., Idler, K. B., Mostafa, N. M., Okun, M. M., & Waring, J. F. (2016). Genetic analysis of NCSTN for potential association with hidradenitis suppurativa in familial and nonfamilial patients. *Br J Dermatol*, *175*(2), 414-416. doi:10.1111/bjd.14482
- Lun, A. T. L., Riesenfeld, S., Andrews, T., Dao, T. P., Gomes, T., & Marioni, J. C. (2019). EmptyDrops: distinguishing cells from empty droplets in droplet-based single-cell RNA sequencing data. *Genome Biol*, *20*(1), 63. doi:10.1186/s13059-019-1662-y
- Luna-Gomes, T., Bozza, P., & Bandeira-Melo, C. (2013). Eosinophil recruitment and activation: the role of lipid mediators. *Front Pharmacol*, *4*(27). doi:10.3389/fphar.2013.00027
- Lynch, L., Nowak, M., Varghese, B., Clark, J., Hogan, A. E., Toxavidis, V., . . . Exley, M. A. (2012). Adipose tissue invariant NKT cells protect against diet-induced obesity and metabolic disorder through regulatory cytokine production. *Immunity*, *37*(3), 574-587. doi:10.1016/j.immuni.2012.06.016
- Maarouf, M., Clark, A. K., Lee, D. E., & Shi, V. Y. (2017). Targeted treatments for hidradenitis suppurativa: a review of the current literature and ongoing clinical trials. *J Dermatolog Treat*, 1-9. doi:10.1080/09546634.2017.1395806

- Maeda, S., Osaga, S., Maeda, T., Takeda, N., Tamechika, S. Y., Naniwa, T., & Niimi, A. (2019). Circulating Th17.1 cells as candidate for the prediction of therapeutic response to abatacept in patients with rheumatoid arthritis: An exploratory research. *PLoS One*, *14*(11), e0215192. doi:10.1371/journal.pone.0215192
- Magnani, C. F., Alberigo, G., Bacchetta, R., Serafini, G., Andreani, M., Roncarolo, M. G., & Gregori, S. (2011). Killing of myeloid APCs via HLA class I, CD2 and CD226 defines a novel mechanism of suppression by human Tr1 cells. *Eur J Immunol*, *41*(6), 1652-1662. doi:10.1002/eji.201041120
- Malara, A., Hughes, R., Jennings, L., Sweeney, C. M., Lynch, M., Awdeh, F., . . . Kirby, B. (2018). Adipokines are dysregulated in patients with hidradenitis suppurativa. *Br J Dermatol*, *178*(3), 792-793. doi:10.1111/bjd.15904
- Marasca, C., Megna, M., Balato, A., Balato, N., Napolitano, M., & Fabbrocini, G. (2019). Secukinumab and hidradenitis suppurativa: Friends or foes? *JAAD Case Rep*, *5*(2), 184-187. doi:10.1016/j.jdcr.2018.12.002
- Margesson, L. J., & Danby, F. W. (2014). Hidradenitis suppurativa. *Best Pract Res Clin Obstet Gynaecol*, *28*(7), 1013-1027. doi:10.1016/j.bpobgyn.2014.07.012
- Martinez-Cingolani, C., Grandclaude, M., Jeanmougin, M., Jouve, M., Zollinger, R., & Soumelis, V. (2014). Human blood BDCA-1 dendritic cells differentiate into Langerhans-like cells with thymic stromal lymphopoietin and TGF-beta. *Blood*, *124*(15), 2411-2420. doi:10.1182/blood-2014-04-568311
- Martinez, F., Nos, P., Benlloch, S., & Ponce, J. (2001). Hidradenitis suppurativa and Crohn's disease: response to treatment with infliximab. *Inflamm Bowel Dis*, *7*(4), 323-326. doi:10.1097/00054725-200111000-00008
- Martorell, A., Garcia-Martinez, F. J., Jimenez-Gallo, D., Pascual, J. C., Pereyra-Rodriguez, J., Salgado, L., & Vilarrasa, E. (2015). An Update on Hidradenitis Suppurativa (Part I): Epidemiology, Clinical Aspects, and Definition of Disease Severity. *Actas Dermosifiliogr*, *106*(9), 703-715. doi:10.1016/j.ad.2015.06.004
- Marzano, A. V., Borghi, A., Stadnicki, A., Crosti, C., & Cugno, M. (2014). Cutaneous manifestations in patients with inflammatory bowel diseases: pathophysiology, clinical features, and therapy. *Inflamm Bowel Dis*, *20*(1), 213-227. doi:10.1097/01.MIB.0000436959.62286.f9
- Marzano, A. V., Cugno, M., Trevisan, V., Fanoni, D., Venegoni, L., Berti, E., & Crosti, C. (2010). Role of inflammatory cells, cytokines and matrix metalloproteinases in neutrophil-mediated skin diseases. *Clin Exp Immunol*, *162*(1), 100-107. doi:10.1111/j.1365-2249.2010.04201.x
- Marzuillo, P., Piccolo, V., Mascolo, M., Apicella, A., Argenziano, G., Della Vecchia, N., . . . La Manna, A. (2018). Patients affected by dent disease 2 could be predisposed to hidradenitis suppurativa. *J Eur Acad Dermatol Venereol*, *32*(8), e309-e311. doi:10.1111/jdv.14860
- Mashiko, S., Bouguermouh, S., Rubio, M., Baba, N., Bissonnette, R., & Sarfati, M. (2015). Human mast cells are major IL-22 producers in patients with psoriasis and atopic dermatitis. *J Allergy Clin Immunol*, *136*(2), 351-359.e351. doi:10.1016/j.jaci.2015.01.033
- Matusiak, L., Bieniek, A., & Szepietowski, J. C. (2009). Increased serum tumour necrosis factor-alpha in hidradenitis suppurativa patients: is there a basis for treatment with anti-tumour necrosis factor-alpha agents? *Acta Derm Venereol*, *89*(6), 601-603. doi:10.2340/00015555-0749
- Matusiak, L., Szczech, J., Bieniek, A., Nowicka-Suszko, D., & Szepietowski, J. C. (2017). Increased interleukin (IL)-17 serum levels in patients with hidradenitis suppurativa: Implications for treatment with anti-IL-17 agents. *J Am Acad Dermatol*, *76*(4), 670-675. doi:10.1016/j.jaad.2016.10.042

- Maya-Mendoza, A., Moudry, P., Merchut-Maya, J. M., Lee, M., Strauss, R., & Bartek, J. (2018). High speed of fork progression induces DNA replication stress and genomic instability. *Nature*, *559*(7713), 279-284. doi:10.1038/s41586-018-0261-5
- Mbongue, J. C., Nicholas, D. A., Torrez, T. W., Kim, N. S., Firek, A. F., & Langridge, W. H. (2015). The Role of Indoleamine 2, 3-Dioxygenase in Immune Suppression and Autoimmunity. *Vaccines (Basel)*, *3*(3), 703-729. doi:10.3390/vaccines3030703
- McGeachy, M. J., Cua, D. J., & Gaffen, S. L. (2019). The IL-17 Family of Cytokines in Health and Disease. *Immunity*, *50*(4), 892-906. doi:10.1016/j.immuni.2019.03.021
- McGinley, A. M., Sutton, C. E., Edwards, S. C., Leane, C. M., DeCoursey, J., Teijeiro, A., . . . Mills, K. H. G. (2020). Interleukin-17A Serves a Priming Role in Autoimmunity by Recruiting IL-1 β -Producing Myeloid Cells that Promote Pathogenic T Cells. *Immunity*, *52*(2), 342-356.e346. doi:10.1016/j.immuni.2020.01.002
- Melnik, B. C., & Plewig, G. (2013). Impaired Notch signalling: the unifying mechanism explaining the pathogenesis of hidradenitis suppurativa (acne inversa). *Br J Dermatol*, *168*(4), 876-878. doi:10.1111/bjd.12068
- Meng, W., Zhang, B., Schwartz, G. W., Rosenfeld, A. M., Ren, D., Thome, J. J. C., . . . Luning Prak, E. T. (2017). An atlas of B-cell clonal distribution in the human body. *Nat Biotechnol*, *35*(9), 879-884. doi:10.1038/nbt.3942
- Miller, I., Lynggaard, C. D., Lophaven, S., Zachariae, C., Dufour, D. N., & Jemec, G. B. (2011). A double-blind placebo-controlled randomized trial of adalimumab in the treatment of hidradenitis suppurativa. *Br J Dermatol*, *165*(2), 391-398. doi:10.1111/j.1365-2133.2011.10339.x
- Miller, I. M., Ellervik, C., Vinding, G. R., Zarchi, K., Ibler, K. S., Knudsen, K. M., & Jemec, G. B. (2014). Association of metabolic syndrome and hidradenitis suppurativa. *JAMA Dermatol*, *150*(12), 1273-1280. doi:10.1001/jamadermatol.2014.1165
- Miller, I. M., Ring, H. C., Prens, E. P., Rytgaard, H., Mogensen, U. B., Ellervik, C., & Jemec, G. B. (2016). Leukocyte Profile in Peripheral Blood and Neutrophil-Lymphocyte Ratio in Hidradenitis Suppurativa: A Comparative Cross-Sectional Study of 462 Cases. *Dermatology*, *232*(4), 511-519. doi:10.1159/000446021
- Mills, C. D., Kincaid, K., Alt, J. M., Heilman, M. J., & Hill, A. M. (2000). M-1/M-2 macrophages and the Th1/Th2 paradigm. *J Immunol*, *164*(12), 6166-6173. doi:10.4049/jimmunol.164.12.6166
- Miskinyte, S., Nassif, A., Merabtene, F., Ungeheuer, M. N., Join-Lambert, O., Jais, J. P., & Hovnanian, A. (2012). Nicastrin mutations in French families with hidradenitis suppurativa. *J Invest Dermatol*, *132*(6), 1728-1730. doi:10.1038/jid.2012.23
- Montgomery, J. R., White, T. W., Martin, B. L., Turner, M. L., & Holland, S. M. (2004). A novel connexin 26 gene mutation associated with features of the keratitis-ichthyosis-deafness syndrome and the follicular occlusion triad. *J Am Acad Dermatol*, *51*(3), 377-382. doi:10.1016/j.jaad.2003.12.042
- Moran, B., Gallagher, C., Tobin, A. M., & Fletcher, J. M. (2020). Enrichment of Polyfunctional IL-17-Producing T Cells in Paradoxical Psoriasis Skin Lesions. *J Invest Dermatol*, *140*(5), 1094-1097. doi:10.1016/j.jid.2019.10.010
- Moran, B., Sweeney, C. M., Hughes, R., Malara, A., Kirthi, S., Tobin, A. M., . . . Fletcher, J. M. (2017). Hidradenitis suppurativa is characterised by dysregulation of the Th17:Treg cell axis, which is corrected by anti-TNF therapy. *J Invest Dermatol*. doi:10.1016/j.jid.2017.05.033
- Moreira-Teixeira, L., Resende, M., Coffre, M., Devergne, O., Herbeuval, J. P., Hermine, O., . . . Leite-de-Moraes, M. C. (2011). Proinflammatory environment dictates the IL-17-

- producing capacity of human invariant NKT cells. *J Immunol*, 186(10), 5758-5765. doi:10.4049/jimmunol.1003043
- Moschen, A. R., Tilg, H., & Raine, T. (2019). IL-12, IL-23 and IL-17 in IBD: immunobiology and therapeutic targeting. *Nat Rev Gastroenterol Hepatol*, 16(3), 185-196. doi:10.1038/s41575-018-0084-8
- Murphy, K., Weaver, C., Mowat, A., Berg, L., Chaplin, D., Janeway, C. A., . . . Walport, M. (2016). *Janeway's Immunobiology* (9 ed.): Garland Science.
- Musilova, J., Moran, B., Sweeney, C. M., Malara, A., Zaborowski, A., Hughes, R., . . . Kirby, B. (2020). Enrichment of Plasma Cells in the Peripheral Blood and Skin of Patients with Hidradenitis Suppurativa. *J Invest Dermatol*, 140(5), 1091-1094.e1092. doi:10.1016/j.jid.2019.08.453
- Napier, R. J., Adams, E. J., Gold, M. C., & Lewinsohn, D. M. (2015). The Role of Mucosal Associated Invariant T Cells in Antimicrobial Immunity. *Front Immunol*, 6, 344. doi:10.3389/fimmu.2015.00344
- Napolitano, M., Megna, M., Timoshchuk, E. A., Patrino, C., Balato, N., Fabbrocini, G., & Monfrecola, G. (2017). Hidradenitis suppurativa: from pathogenesis to diagnosis and treatment. *Clin Cosmet Investig Dermatol*, 10, 105-115. doi:10.2147/ccid.S111019
- Navrazhina, K., Frew, J. W., & Krueger, J. G. (2020). Interleukin 17C is elevated in lesional tissue of hidradenitis suppurativa. *Br J Dermatol*, 182(4), 1045-1047. doi:10.1111/bjd.18556
- Nii, T., Kuzuya, K., Kabata, D., Matsui, T., Murata, A., Ohya, T., . . . Saeki, Y. (2019). Crosstalk between tumor necrosis factor-alpha signaling and aryl hydrocarbon receptor signaling in nuclear factor -kappa B activation: A possible molecular mechanism underlying the reduced efficacy of TNF-inhibitors in rheumatoid arthritis by smoking. *J Autoimmun*, 98, 95-102. doi:10.1016/j.jaut.2018.12.004
- Nistala, K., Adams, S., Cambrook, H., Ursu, S., Olivito, B., de Jager, W., . . . Wedderburn, L. R. (2010). Th17 plasticity in human autoimmune arthritis is driven by the inflammatory environment. *Proc Natl Acad Sci U S A*, 107(33), 14751-14756. doi:10.1073/pnas.1003852107
- Nogralas, K. E., Zaba, L. C., Guttman-Yassky, E., Fuentes-Duculan, J., Suarez-Farinas, M., Cardinale, I., . . . Krueger, J. G. (2008). Th17 cytokines interleukin (IL)-17 and IL-22 modulate distinct inflammatory and keratinocyte-response pathways. *Br J Dermatol*, 159(5), 1092-1102. doi:10.1111/j.1365-2133.2008.08769.x
- Nogralas, K. E., Zaba, L. C., Shemer, A., Fuentes-Duculan, J., Cardinale, I., Kikuchi, T., . . . Guttman-Yassky, E. (2009). IL-22-producing "T22" T cells account for upregulated IL-22 in atopic dermatitis despite reduced IL-17-producing TH17 T cells. *J Allergy Clin Immunol*, 123(6), 1244-1252.e1242. doi:10.1016/j.jaci.2009.03.041
- Nogueira, M., & Torres, T. (2019). Guselkumab for the treatment of psoriasis - evidence to date. *Drugs Context*, 8, 212594. doi:10.7573/dic.212594
- Nomura, T. (2020). Hidradenitis Suppurativa as a Potential Subtype of Autoinflammatory Keratinization Disease. *Front Immunol*, 11(847). doi:10.3389/fimmu.2020.00847
- Nomura, Y., Nomura, T., Sakai, K., Sasaki, K., Ohguchi, Y., Mizuno, O., . . . Shimizu, H. (2013). A novel splice site mutation in NCSTN underlies a Japanese family with hidradenitis suppurativa. *Br J Dermatol*, 168(1), 206-209. doi:10.1111/j.1365-2133.2012.11174.x
- Noordenbos, T., Blijdorp, I., Chen, S., Stap, J., Mul, E., Canete, J. D., . . . Baeten, D. (2016). Human mast cells capture, store, and release bioactive, exogenous IL-17A. *J Leukoc Biol*, 100(3), 453-462. doi:10.1189/jlb.3HI1215-542R
- Onderdijk, A. J., van der Zee, H. H., Esmann, S., Lophaven, S., Dufour, D. N., Jemec, G. B., & Boer, J. (2013). Depression in patients with hidradenitis suppurativa. *J Eur Acad Dermatol Venereol*, 27(4), 473-478. doi:10.1111/j.1468-3083.2012.04468.x

- Orvain, C., Lin, Y. L., Jean-Louis, F., Hocini, H., Hersant, B., Bennasser, Y., . . . Hue, S. (2020). Hair follicle stem cell replication stress drives IFI16/STING-dependent inflammation in hidradenitis suppurativa. *J Clin Invest*. doi:10.1172/jci131180
- Otsuka, M., Egawa, G., & Kabashima, K. (2018). Uncovering the Mysteries of Langerhans Cells, Inflammatory Dendritic Epidermal Cells, and Monocyte-Derived Langerhans Cell-Like Cells in the Epidermis. *Front Immunol*, *9*, 1768. doi:10.3389/fimmu.2018.01768
- Pan, Y., Lin, M. H., Tian, X., Cheng, H. T., Gridley, T., Shen, J., & Kopan, R. (2004). gamma-secretase functions through Notch signaling to maintain skin appendages but is not required for their patterning or initial morphogenesis. *Dev Cell*, *7*(5), 731-743. doi:10.1016/j.devcel.2004.09.014
- Panaccione, R., Sandborn, W. J., Gordon, G. L., Lee, S. D., Safdi, A., Sedghi, S., . . . Carcereri, R. (2015). Briakinumab for treatment of Crohn's disease: results of a randomized trial. *Inflamm Bowel Dis*, *21*(6), 1329-1340. doi:10.1097/mib.0000000000000366
- Papayannopoulos, V. (2018). Neutrophil extracellular traps in immunity and disease. *Nat Rev Immunol*, *18*(2), 134-147. doi:10.1038/nri.2017.105
- Papotto, P. H., Reinhardt, A., Prinz, I., & Silva-Santos, B. (2017). Innately versatile: gammadelta17 T cells in inflammatory and autoimmune diseases. *J Autoimmun*. doi:10.1016/j.jaut.2017.11.006
- Papp, K. A., Leonardi, C., Menter, A., Ortonne, J. P., Krueger, J. G., Kricorian, G., . . . Baumgartner, S. (2012). Brodalumab, an anti-interleukin-17-receptor antibody for psoriasis. *N Engl J Med*, *366*(13), 1181-1189. doi:10.1056/NEJMoa1109017
- Parkes, G. C., Whelan, K., & Lindsay, J. O. (2014). Smoking in inflammatory bowel disease: impact on disease course and insights into the aetiology of its effect. *J Crohns Colitis*, *8*(8), 717-725. doi:10.1016/j.crohns.2014.02.002
- Pasparakis, M., Haase, I., & Nestle, F. O. (2014). Mechanisms regulating skin immunity and inflammation. *Nat Rev Immunol*, *14*(5), 289-301. doi:10.1038/nri3646
- Pavon Blanco, A., Turner, M. A., Petrof, G., & Weinman, J. (2019). To what extent do disease severity and illness perceptions explain depression, anxiety and quality of life in hidradenitis suppurativa? *Br J Dermatol*, *180*(2), 338-345. doi:10.1111/bjd.17123
- Pereira, S. S., & Alvarez-Leite, J. I. (2014). Low-Grade Inflammation, Obesity, and Diabetes. *Curr Obes Rep*, *3*(4), 422-431. doi:10.1007/s13679-014-0124-9
- Perret, L. J., & Tait, C. P. (2014). Non-antibiotic properties of tetracyclines and their clinical application in dermatology. *Australas J Dermatol*, *55*(2), 111-118. doi:10.1111/ajd.12075
- Pesenacker, A. M., Bending, D., Ursu, S., Wu, Q., Nistala, K., & Wedderburn, L. R. (2013). CD161 defines the subset of FoxP3+ T cells capable of producing proinflammatory cytokines. *Blood*, *121*(14), 2647-2658. doi:10.1182/blood-2012-08-443473
- Piaserico, S., Sandini, E., Saldan, A., & Abate, D. (2014). Effects of TNF-alpha inhibitors on circulating Th17 cells in patients affected by severe psoriasis. *Drug Dev Res*, *75 Suppl 1*, S73-76. doi:10.1002/ddr.21202
- Pink, A. E., Simpson, M. A., Brice, G. W., Smith, C. H., Desai, N., Mortimer, P. S., . . . Trembath, R. C. (2011). PSENEN and NCSTN mutations in familial hidradenitis suppurativa (Acne Inversa). *J Invest Dermatol*, *131*(7), 1568-1570. doi:10.1038/jid.2011.42
- Pink, A. E., Simpson, M. A., Desai, N., Trembath, R. C., & Barker, J. N. (2013). gamma-Secretase mutations in hidradenitis suppurativa: new insights into disease pathogenesis. *J Invest Dermatol*, *133*(3), 601-607. doi:10.1038/jid.2012.372
- Prens, L. M., Rondags, A., Volkering, R. J., Janse, I. C., Politiek, K., Zuidema, Y. S., . . . Horvath, B. (2019). The refined Hurley classification: the interrater and intrarater reliability and face validity. *Br J Dermatol*. doi:10.1111/bjd.18235

- Prussick, L., Rothstein, B., Joshipura, D., Saraiya, A., Turkowski, Y., Abdat, R., . . . Rosmarin, D. (2019). Open-label, investigator-initiated, single-site exploratory trial evaluating secukinumab, an anti-interleukin-17A monoclonal antibody, for patients with moderate-to-severe hidradenitis suppurativa. *Br J Dermatol*. doi:10.1111/bjd.17822
- Qiu, S. L., Zhang, H., Tang, Q. Y., Bai, J., He, Z. Y., Zhang, J. Q., . . . Zhong, X. N. (2017). Neutrophil extracellular traps induced by cigarette smoke activate plasmacytoid dendritic cells. *Thorax*, 72(12), 1084-1093. doi:10.1136/thoraxjnl-2016-209887
- Quintana, F. J., Basso, A. S., Iglesias, A. H., Korn, T., Farez, M. F., Bettelli, E., . . . Weiner, H. L. (2008). Control of T(reg) and T(H)17 cell differentiation by the aryl hydrocarbon receptor. *Nature*, 453(7191), 65-71. doi:10.1038/nature06880
- Radek, K. A., Elias, P. M., Taupenot, L., Mahata, S. K., O'Connor, D. T., & Gallo, R. L. (2010). Neuroendocrine nicotinic receptor activation increases susceptibility to bacterial infections by suppressing antimicrobial peptide production. *Cell Host Microbe*, 7(4), 277-289. doi:10.1016/j.chom.2010.03.009
- Ramirez-Carrozzi, V., Sambandam, A., Luis, E., Lin, Z., Jeet, S., Lesch, J., . . . Pappu, R. (2011). IL-17C regulates the innate immune function of epithelial cells in an autocrine manner. *Nat Immunol*, 12(12), 1159-1166. doi:10.1038/ni.2156
- Raphael, I., Nalawade, S., Eagar, T. N., & Forsthuber, T. G. (2015). T cell subsets and their signature cytokines in autoimmune and inflammatory diseases. *Cytokine*, 74(1), 5-17. doi:10.1016/j.cyto.2014.09.011
- Reddy, S., Strunk, A., & Garg, A. (2019). Comparative Overall Comorbidity Burden Among Patients With Hidradenitis Suppurativa. *JAMA Dermatol*. doi:10.1001/jamadermatol.2019.0164
- Revuz, J. E., Canoui-Poitrine, F., Wolkenstein, P., Viallette, C., Gabison, G., Pouget, F., . . . Bastuji-Garin, S. (2008). Prevalence and factors associated with hidradenitis suppurativa: results from two case-control studies. *J Am Acad Dermatol*, 59(4), 596-601. doi:10.1016/j.jaad.2008.06.020
- Reynolds, J. M., Lee, Y. H., Shi, Y., Wang, X., Angkasekwina, P., Nallaparaju, K. C., . . . Dong, C. (2015). Interleukin-17B Antagonizes Interleukin-25-Mediated Mucosal Inflammation. *Immunity*, 42(4), 692-703. doi:10.1016/j.immuni.2015.03.008
- Ring, H. C., Bay, L., Nilsson, M., Kallenbach, K., Miller, I. M., Saunte, D. M., . . . Jemec, G. B. (2017). Bacterial biofilm in chronic lesions of hidradenitis suppurativa. *Br J Dermatol*, 176(4), 993-1000. doi:10.1111/bjd.15007
- Ring, H. C., Riis Mikkelsen, P., Miller, I. M., Jenssen, H., Fursted, K., Saunte, D. M., & Jemec, G. B. (2015). The bacteriology of hidradenitis suppurativa: a systematic review. *Exp Dermatol*, 24(10), 727-731. doi:10.1111/exd.12793
- Rodrigues, P. F., Alberti-Servera, L., Eremin, A., Grajales-Reyes, G. E., Ivanek, R., & Tussiwand, R. (2018). Distinct progenitor lineages contribute to the heterogeneity of plasmacytoid dendritic cells. *Nat Immunol*, 19(7), 711-722. doi:10.1038/s41590-018-0136-9
- Roederer, M., Nozzi, J. L., & Nason, M. C. (2011). SPICE: exploration and analysis of post-cytometric complex multivariate datasets. *Cytometry A*, 79(2), 167-174. doi:10.1002/cyto.a.21015
- Roghani, A. N., R. (2020). B Cells [Bitesized Immunology]. Retrieved from <https://www.immunology.org/public-information/bitesized-immunology/cells/b-cells>
- Romee, R., Foley, B., Lenvik, T., Wang, Y., Zhang, B., Ankarlo, D., . . . Miller, J. (2013). NK cell CD16 surface expression and function is regulated by a disintegrin and metalloprotease-17 (ADAM17). *Blood*, 121(18), 3599-3608. doi:10.1182/blood-2012-04-425397
- Ross, S. H., & Cantrell, D. A. (2018). Signaling and Function of Interleukin-2 in T Lymphocytes. *Annu Rev Immunol*, 36, 411-433. doi:10.1146/annurev-immunol-042617-053352

- Rudak, P. T., Choi, J., & Haeryfar, S. M. M. (2018). MAIT cell-mediated cytotoxicity: Roles in host defense and therapeutic potentials in infectious diseases and cancer. *J Leukoc Biol*, *104*(3), 473-486. doi:10.1002/jlb.4ri0118-023r
- Sabat, R., Jemec, G. B. E., Matusiak, L., Kimball, A. B., Prens, E., & Wolk, K. (2020). Hidradenitis suppurativa. *Nat Rev Dis Primers*, *6*(1), 18. doi:10.1038/s41572-020-0149-1
- Sack, U. (2017). CD64 expression by neutrophil granulocytes. *Cytometry B Clin Cytom*, *92*(3), 189-191. doi:10.1002/cyto.b.21216
- Saleem, M. D., Arnold, D. L., & Feldman, S. R. (2018). Hidradenitis and smoking. *Br J Dermatol*, *178*(3), 810-811. doi:10.1111/bjd.16214
- Salio, M., Awad, W., Veerapen, N., Gonzalez-Lopez, C., Kulicke, C., Waithe, D., . . . Cerundolo, V. (2020). Ligand-dependent downregulation of MR1 cell surface expression. *Proc Natl Acad Sci U S A*, *117*(19), 10465-10475. doi:10.1073/pnas.2003136117
- Sartorius, K., Emtestam, L., Jemec, G. B., & Lapins, J. (2009). Objective scoring of hidradenitis suppurativa reflecting the role of tobacco smoking and obesity. *Br J Dermatol*, *161*(4), 831-839. doi:10.1111/j.1365-2133.2009.09198.x
- Saunte, D. M. L., & Jemec, G. B. E. (2017). Hidradenitis Suppurativa: Advances in Diagnosis and Treatment. *Jama*, *318*(20), 2019-2032. doi:10.1001/jama.2017.16691
- Savva, A., Kanni, T., Damoraki, G., Kotsaki, A., Giatrakou, S., Grech, I., . . . Giamarellos-Bourboulis, E. J. (2013). Impact of Toll-like receptor-4 and tumour necrosis factor gene polymorphisms in patients with hidradenitis suppurativa. *Br J Dermatol*, *168*(2), 311-317. doi:10.1111/bjd.12105
- Schellekens, G. A., de Jong, B. A., van den Hoogen, F. H., van de Putte, L. B., & van Venrooij, W. J. (1998). Citrulline is an essential constituent of antigenic determinants recognized by rheumatoid arthritis-specific autoantibodies. *J Clin Invest*, *101*(1), 273-281. doi:10.1172/jci1316
- Schlapbach, C., Hanni, T., Yawalkar, N., & Hunger, R. E. (2011). Expression of the IL-23/Th17 pathway in lesions of hidradenitis suppurativa. *J Am Acad Dermatol*, *65*(4), 790-798. doi:10.1016/j.jaad.2010.07.010
- Shalom, G., Freud, T., Ben Yakov, G., Khoury, R., Dreiherr, J., Vardy, D. A., . . . Cohen, A. D. (2016). Hidradenitis Suppurativa and Inflammatory Bowel Disease: A Cross-Sectional Study of 3,207 Patients. *J Invest Dermatol*, *136*(8), 1716-1718. doi:10.1016/j.jid.2016.04.003
- Sharon-Guidetti, A., Ziv, Y., Kummer, E., Yogev, R., & Halevy, A. (2006). Granulocyte-macrophage colony-stimulating factor for perianal hidradenitis suppurativa: report of a case. *Dis Colon Rectum*, *49*(5), 682-684. doi:10.1007/s10350-005-0309-0
- Shi, Y., Liu, C. H., Roberts, A. I., Das, J., Xu, G., Ren, G., . . . Devadas, S. (2006). Granulocyte-macrophage colony-stimulating factor (GM-CSF) and T-cell responses: what we do and don't know. *Cell Res*, *16*(2), 126-133. doi:10.1038/sj.cr.7310017
- Soler, D. C., Sugiyama, H., Young, A. B., Massari, J. V., McCormick, T. S., & Cooper, K. D. (2013). Psoriasis patients exhibit impairment of the high potency CCR5(+) T regulatory cell subset. *Clin Immunol*, *149*(1), 111-118. doi:10.1016/j.clim.2013.06.007
- Solimani, F., Pollmann, R., Schmidt, T., Schmidt, A., Zheng, X., Savai, R., . . . Hertl, M. (2019). Therapeutic Targeting of Th17/Tc17 Cells Leads to Clinical Improvement of Lichen Planus. *Front Immunol*, *10*, 1808. doi:10.3389/fimmu.2019.01808
- Steinbach, K., Vincenti, I., & Merkler, D. (2018). Resident-Memory T Cells in Tissue-Restricted Immune Responses: For Better or Worse? *Front Immunol*, *9*, 2827. doi:10.3389/fimmu.2018.02827
- Stuart, T., Butler, A., Hoffman, P., Hafemeister, C., Papalexi, E., Mauck, W. M., 3rd, . . . Satija, R. (2019). Comprehensive Integration of Single-Cell Data. *Cell*, *177*(7), 1888-1902.e1821. doi:10.1016/j.cell.2019.05.031

- Su, Y., Huang, J., Zhao, X., Lu, H., Wang, W., Yang, X. O., . . . Dong, C. (2019). Interleukin-17 receptor D constitutes an alternative receptor for interleukin-17A important in psoriasis-like skin inflammation. *Sci Immunol*, 4(36). doi:10.1126/sciimmunol.aau9657
- Sugiyama, H., Gyulai, R., Toichi, E., Garaczi, E., Shimada, S., Stevens, S. R., . . . Cooper, K. D. (2005). Dysfunctional blood and target tissue CD4⁺CD25^{high} regulatory T cells in psoriasis: mechanism underlying unrestrained pathogenic effector T cell proliferation. *J Immunol*, 174(1), 164-173.
- Sutton, C. E., Lalor, S. J., Sweeney, C. M., Brereton, C. F., Lavelle, E. C., & Mills, K. H. (2009). Interleukin-1 and IL-23 induce innate IL-17 production from gammadelta T cells, amplifying Th17 responses and autoimmunity. *Immunity*, 31(2), 331-341. doi:10.1016/j.immuni.2009.08.001
- Takahashi, K., Yanagi, T., Kitamura, S., Hata, H., Imafuku, K., Iwami, D., . . . Shimizu, H. (2018). Successful treatment of hidradenitis suppurativa with rituximab for a patient with idiopathic carpotarsal osteolysis and chronic active antibody-mediated rejection. *J Dermatol*, 45(5), e116-e117. doi:10.1111/1346-8138.14144
- Tamassia, N., Arruda-Silva, F., Calzetti, F., Lonardi, S., Gasperini, S., Gardiman, E., . . . Cassatella, M. A. (2018). A Reappraisal on the Potential Ability of Human Neutrophils to Express and Produce IL-17 Family Members In Vitro: Failure to Reproducibly Detect It. *Front Immunol*, 9, 795. doi:10.3389/fimmu.2018.00795
- Tamoutounour, S., Williams, M., Montanana Sanchis, F., Liu, H., Terhorst, D., Malosse, C., . . . Henri, S. (2013). Origins and functional specialization of macrophages and of conventional and monocyte-derived dendritic cells in mouse skin. *Immunity*, 39(5), 925-938. doi:10.1016/j.immuni.2013.10.004
- Teunissen, M. B., Yeremenko, N. G., Baeten, D. L., Chielie, S., Spuls, P. I., de Rie, M. A., . . . Res, P. C. (2014). The IL-17A-producing CD8⁺ T-cell population in psoriatic lesional skin comprises mucosa-associated invariant T cells and conventional T cells. *J Invest Dermatol*, 134(12), 2898-2907. doi:10.1038/jid.2014.261
- Teunissen, M. B. M., Munneke, J. M., Bernink, J. H., Spuls, P. I., Res, P. C. M., Te Velde, A., . . . Mjosberg, J. (2014). Composition of innate lymphoid cell subsets in the human skin: enrichment of NCR(+) ILC3 in lesional skin and blood of psoriasis patients. *J Invest Dermatol*, 134(9), 2351-2360. doi:10.1038/jid.2014.146
- Thorlacius, L., Theut Riis, P., & Jemec, G. B. E. (2018). Severe hidradenitis suppurativa responding to treatment with secukinumab: a case report. *Br J Dermatol*, 179(1), 182-185. doi:10.1111/bjd.15769
- Tian, Y., Babor, M., Lane, J., Schulten, V., Patil, V. S., Seumois, G., . . . Peters, B. (2017). Unique phenotypes and clonal expansions of human CD4 effector memory T cells re-expressing CD45RA. *Nat Commun*, 8(1), 1473. doi:10.1038/s41467-017-01728-5
- Trifari, S., Kaplan, C. D., Tran, E. H., Crellin, N. K., & Spits, H. (2009). Identification of a human helper T cell population that has abundant production of interleukin 22 and is distinct from T(H)-17, T(H)1 and T(H)2 cells. *Nat Immunol*, 10(8), 864-871. doi:10.1038/ni.1770
- Tu, J. F., Pan, H. Y., Ying, X. H., Lou, J., Ji, J. S., & Zou, H. (2016). Mast Cells Comprise the Major of Interleukin 17-Producing Cells and Predict a Poor Prognosis in Hepatocellular Carcinoma. *Medicine (Baltimore)*, 95(13), e3220. doi:10.1097/md.0000000000003220
- Tzellos, T., Yang, H., Mu, F., Calimlim, B., & Signorovitch, J. (2019). Impact of hidradenitis suppurativa on work loss, indirect costs and income. *Br J Dermatol*, 181(1), 147-154. doi:10.1111/bjd.17101
- Ulgen, E., Ozisik, O., & Sezerman, O. U. (2019). pathfindR: An R Package for Comprehensive Identification of Enriched Pathways in Omics Data Through Active Subnetworks. *Frontiers in Genetics*, 10(858). doi:10.3389/fgene.2019.00858

- Vaidya, T., Vangipuram, R., & Alikhan, A. (2017). Examining the race-specific prevalence of hidradenitis suppurativa at a large academic center; results from a retrospective chart review. *Dermatol Online J*, 23(6).
- van der Zee, H. H., de Rooter, L., Boer, J., van den Broecke, D. G., den Hollander, J. C., Laman, J. D., & Prens, E. P. (2012). Alterations in leucocyte subsets and histomorphology in normal-appearing perilesional skin and early and chronic hidradenitis suppurativa lesions. *Br J Dermatol*, 166(1), 98-106. doi:10.1111/j.1365-2133.2011.10643.x
- van der Zee, H. H., de Rooter, L., van den Broecke, D. G., Dik, W. A., Laman, J. D., & Prens, E. P. (2011). Elevated levels of tumour necrosis factor (TNF)-alpha, interleukin (IL)-1beta and IL-10 in hidradenitis suppurativa skin: a rationale for targeting TNF-alpha and IL-1beta. *Br J Dermatol*, 164(6), 1292-1298. doi:10.1111/j.1365-2133.2011.10254.x
- van der Zee, H. H., van der Woude, C. J., Florencia, E. F., & Prens, E. P. (2010). Hidradenitis suppurativa and inflammatory bowel disease: are they associated? Results of a pilot study. *Br J Dermatol*, 162(1), 195-197. doi:10.1111/j.1365-2133.2009.09430.x
- van Dijk, D., Sharma, R., Nainys, J., Yim, K., Kathail, P., Carr, A. J., . . . Pe'er, D. (2018). Recovering Gene Interactions from Single-Cell Data Using Data Diffusion. *Cell*, 174(3), 716-729. doi:10.1016/j.cell.2018.05.061
- van Rappard, D. C., Leenarts, M. F., Meijerink-van 't Oost, L., & Mekkes, J. R. (2012). Comparing treatment outcome of infliximab and adalimumab in patients with severe hidradenitis suppurativa. *J Dermatolog Treat*, 23(4), 284-289. doi:10.3109/09546634.2011.571657
- Vazquez, B. G., Alikhan, A., Weaver, A. L., Wetter, D. A., & Davis, M. D. (2013). Incidence of hidradenitis suppurativa and associated factors: a population-based study of Olmsted County, Minnesota. *J Invest Dermatol*, 133(1), 97-103. doi:10.1038/jid.2012.255
- Veldhoen, M., Hirota, K., Westendorf, A. M., Buer, J., Dumoutier, L., Renault, J. C., & Stockinger, B. (2008). The aryl hydrocarbon receptor links TH17-cell-mediated autoimmunity to environmental toxins. *Nature*, 453(7191), 106-109. doi:10.1038/nature06881
- Venken, K., Jacques, P., Mortier, C., Labadia, M. E., Decruy, T., Coudens, J., . . . Elewaut, D. (2019). RORgamma inhibition selectively targets IL-17 producing iNKT and gammadelta-T cells enriched in Spondyloarthritis patients. *Nat Commun*, 10(1), 9. doi:10.1038/s41467-018-07911-6
- Villanova, F., Flutter, B., Tosi, I., Gryns, K., Sreeneebus, H., Perera, G. K., . . . Nestle, F. O. (2014). Characterization of innate lymphoid cells in human skin and blood demonstrates increase of NKp44+ ILC3 in psoriasis. *J Invest Dermatol*, 134(4), 984-991. doi:10.1038/jid.2013.477
- Vivier, E., Artis, D., Colonna, M., Diefenbach, A., Di Santo, J. P., Eberl, G., . . . Spits, H. (2018). Innate Lymphoid Cells: 10 Years On. *Cell*, 174(5), 1054-1066. doi:10.1016/j.cell.2018.07.017
- Vlassova, N., Kuhn, D., & Okoye, G. A. (2015). Hidradenitis suppurativa disproportionately affects African Americans: a single-center retrospective analysis. *Acta Derm Venereol*, 95(8), 990-991. doi:10.2340/00015555-2176
- Vossen, A., Ardon, C. B., van der Zee, H. H., Lubberts, E., & Prens, E. P. (2019). The anti-inflammatory potency of biologics targeting tumour necrosis factor-alpha, interleukin (IL)-17A, IL-12/23 and CD20 in hidradenitis suppurativa: an ex vivo study. *Br J Dermatol*, 181(2), 314-323. doi:10.1111/bjd.17641
- Vossen, A., van der Zee, H. H., & Prens, E. P. (2018). Hidradenitis Suppurativa: A Systematic Review Integrating Inflammatory Pathways Into a Cohesive Pathogenic Model. *Front Immunol*, 9, 2965. doi:10.3389/fimmu.2018.02965

- Wang, B., Yang, W., Wen, W., Sun, J., Su, B., Liu, B., . . . Zhang, X. (2010). Gamma-secretase gene mutations in familial acne inversa. *Science*, 330(6007), 1065. doi:10.1126/science.1196284
- Watanabe, R., Gehad, A., Yang, C., Scott, L. L., Teague, J. E., Schlapbach, C., . . . Clark, R. A. (2015). Human skin is protected by four functionally and phenotypically discrete populations of resident and recirculating memory T cells. *Sci Transl Med*, 7(279), 279ra239. doi:10.1126/scitranslmed.3010302
- Weisberg, S. P., McCann, D., Desai, M., Rosenbaum, M., Leibel, R. L., & Ferrante, A. W., Jr. (2003). Obesity is associated with macrophage accumulation in adipose tissue. *J Clin Invest*, 112(12), 1796-1808. doi:10.1172/jci19246
- Wertenteil, S., Strunk, A., & Garg, A. (2018). Association of Low Socioeconomic Status With Hidradenitis Suppurativa in the United States. *JAMA Dermatol*, 154(9), 1086-1088. doi:10.1001/jamadermatol.2018.2117
- Wissinger, E. (2020). CD8+ T cells.
- Witte-Handel, E., Wolk, K., Tsaousi, A., Irmer, M. L., Mossner, R., Shomroni, O., . . . Sabat, R. (2019). The IL-1 Pathway Is Hyperactive in Hidradenitis Suppurativa and Contributes to Skin Infiltration and Destruction. *J Invest Dermatol*, 139(6), 1294-1305. doi:10.1016/j.jid.2018.11.018
- Wolk, K., Warszawska, K., Hoeflich, C., Witte, E., Schneider-Burrus, S., Witte, K., . . . Sabat, R. (2011). Deficiency of IL-22 contributes to a chronic inflammatory disease: pathogenetic mechanisms in acne inversa. *J Immunol*, 186(2), 1228-1239. doi:10.4049/jimmunol.0903907
- Wright, J. F., Bennett, F., Li, B., Brooks, J., Luxenberg, D. P., Whitters, M. J., . . . Carreno, B. M. (2008). The human IL-17F/IL-17A heterodimeric cytokine signals through the IL-17RA/IL-17RC receptor complex. *J Immunol*, 181(4), 2799-2805. doi:10.4049/jimmunol.181.4.2799
- Wu, Y., Ma, Y., Xu, T., Zhang, Q. Z., Bai, J., Wang, J., . . . Zhao, K. Q. (2018). Nicotine Enhances Staphylococcus epidermidis Biofilm Formation by Altering the Bacterial Autolysis, Extracellular DNA Releasing, and Polysaccharide Intercellular Adhesin Production. *Front Microbiol*, 9, 2575. doi:10.3389/fmicb.2018.02575
- Xu, M., & Dong, C. (2017). IL-25 in allergic inflammation. *Immunol Rev*, 278(1), 185-191. doi:10.1111/imr.12558
- Xu, M., Lu, H., Lee, Y. H., Wu, Y., Liu, K., Shi, Y., . . . Dong, C. (2018). An Interleukin-25-Mediated Autoregulatory Circuit in Keratinocytes Plays a Pivotal Role in Psoriatic Skin Inflammation. *Immunity*, 48(4), 787-798.e784. doi:10.1016/j.immuni.2018.03.019
- Yamaguchi, Y., Fujio, K., Shoda, H., Okamoto, A., Tsuno, N. H., Takahashi, K., & Yamamoto, K. (2007). IL-17B and IL-17C are associated with TNF-alpha production and contribute to the exacerbation of inflammatory arthritis. *J Immunol*, 179(10), 7128-7136. doi:10.4049/jimmunol.179.10.7128
- Yan, X., Tu, H., Liu, Y., Chen, T., & Cao, J. (2020). Interleukin-17D Aggravates Sepsis by Inhibiting Macrophage Phagocytosis. *Crit Care Med*, 48(1), e58-e65. doi:10.1097/ccm.0000000000004070
- Yang, D., Chen, X., Wang, J., Lou, Q., Lou, Y., Li, L., . . . Qian, Y. (2019). Dysregulated Lung Commensal Bacteria Drive Interleukin-17B Production to Promote Pulmonary Fibrosis through Their Outer Membrane Vesicles. *Immunity*, 50(3), 692-706.e697. doi:10.1016/j.immuni.2019.02.001
- Yao, Z., Spriggs, M. K., Derry, J. M., Strockbine, L., Park, L. S., VandenBos, T., . . . Armitage, R. J. (1997). Molecular characterization of the human interleukin (IL)-17 receptor. *Cytokine*, 9(11), 794-800. doi:10.1006/cyto.1997.0240

- Zahid, A., Li, B., Kombe, A. J. K., Jin, T., & Tao, J. (2019). Pharmacological Inhibitors of the NLRP3 Inflammasome. *Front Immunol*, *10*, 2538. doi:10.3389/fimmu.2019.02538
- Zhang, Y., Siegel, A. M., Sun, G., Dimaggio, T., Freeman, A. F., & Milner, J. D. (2019). Human T(H)9 differentiation is dependent on signal transducer and activator of transcription (STAT) 3 to restrain STAT1-mediated inhibition. *J Allergy Clin Immunol*, *143*(3), 1108-1118.e1104. doi:10.1016/j.jaci.2018.06.036
- Zheng, Y., Sun, L., Jiang, T., Zhang, D., He, D., & Nie, H. (2014). TNFalpha promotes Th17 cell differentiation through IL-6 and IL-1beta produced by monocytes in rheumatoid arthritis. *J Immunol Res*, *2014*, 385352. doi:10.1155/2014/385352
- Zielinski, C. E., Mele, F., Aschenbrenner, D., Jarrossay, D., Ronchi, F., Gattorno, M., . . . Sallusto, F. (2012). Pathogen-induced human TH17 cells produce IFN- γ or IL-10 and are regulated by IL-1 β . *Nature*, *484*(7395), 514-518. doi:10.1038/nature10957
- Zimmermann, J., Radbruch, A., & Chang, H. D. (2015). A Ca²⁺ concentration of 1.5 mM, as present in IMDM but not in RPMI, is critical for maximal response of Th cells to PMA/ionomycin. *Eur J Immunol*, *45*(4), 1270-1273. doi:10.1002/eji.201445247
- Zouboulis, C. C., Desai, N., Emtestam, L., Hunger, R. E., Ioannides, D., Juhasz, I., . . . Jemec, G. B. (2015). European S1 guideline for the treatment of hidradenitis suppurativa/acne inversa. *J Eur Acad Dermatol Venereol*, *29*(4), 619-644. doi:10.1111/jdv.12966
- Zouboulis, C. C., Tzellos, T., Kyrgidis, A., Jemec, G. B. E., Bechara, F. G., Giamarellos-Bourboulis, E. J., . . . Sabat, R. (2017). Development and validation of the International Hidradenitis Suppurativa Severity Score System (IHS4), a novel dynamic scoring system to assess HS severity. *Br J Dermatol*, *177*(5), 1401-1409. doi:10.1111/bjd.15748